

FINAL REPORT

EXTERNAL CORROSION DIRECT ASSESSMENT FOR UNIQUE THREATS TO UNDERGROUND PIPELINES

CONTRACT NO. DTPH56-06-T-0012

**PREPARED FOR
PIPELINE AND HAZARDOUS MATERIALS SAFETY ADMINISTRATION
US DEPARTMENT OF TRANSPORTATION
WASHINGTON, DC**

**PREPARED BY
CC TECHNOLOGIES, INC., A DNV COMPANY
MARK YUNOVICH, MS, MBA, NACE CORROSION SPECIALIST
STEVEN WATERS, BS**

NOVEMBER 2007

TABLE OF CONTENTS

TABLE OF CONTENTS	2
LIST OF FIGURES.....	6
LIST OF TABLES.....	11
INTRODUCTION.....	15
BACKGROUND	16
AC corrosion.....	16
High CP effects.....	18
Stray current interference	19
OBJECTIVES AND DELIVERABLES.....	20
WORK PLAN.....	21
Task 1 – Laboratory Analysis of AC corrosion and High CP effects.....	21
Task 1.1 – AC Corrosion	21
Task 1.1.1 – Literature survey and state-of-the-art	21
Task 1.1.2 – Computational modeling.....	22
Task 1.1.3 – Laboratory experiments.....	23
Task 1.2 – Effects of high CP potentials.....	23
Task 1.2.1 – Literature survey and state-of-the-art	23
Task 1.2.1 – Computational modeling.....	24
Task 1.2.3 – Laboratory experiments.....	24
Task 2 – Large-scale experimental studies.....	24
Task 2.1 – Experimental setup	25
Task 2.2 – Data collection	25
Task 3 – Field verification	25
Task 3.1 – Verification of AC corrosion laboratory results	26
Task 3.2 – Verification of high CP effects laboratory results	26
Task 3.3 – Verification of stray current interference laboratory results	26
Task 4 – Guidelines for ECDA	26

Task 5 – Reporting and public submission of results	26
RESULTS AND DISCUSSION	28
Task 1 – Laboratory Analysis of AC corrosion and High CP effects	28
Literature-survey: State-of-the-Art.....	28
AC-enhanced corrosion.....	28
<i>Historic notes</i>	28
<i>Threat criteria: current density vs. AC voltage</i>	30
<i>Cathodic Protection</i>	32
Summary of Literature Review on AC corrosion.....	33
Overprotection effects on underground coated structures.....	34
<i>Hazards of Overprotection</i>	34
<i>Coating Disbondment</i>	34
<i>Cathodic disbondment caused by alkalinization at high CP</i>	34
<i>Cathodic disbondment caused by hydrogen evolution at high CP</i>	35
<i>Limits for Cathodic Protection</i>	36
<i>Potential Limits</i>	36
<i>Current Limits</i>	38
<i>Special case: Pipe collapse under repair sleeves</i>	40
<i>Blowout</i>	42
<i>Cracking</i>	43
Summary of Literature Review on Overprotection	43
Experimental modeling.....	44
Numerical modeling.....	44
<i>Finite Element Modeling and Regression Analysis – ‘forward’ model</i>	44
<i>Reverse model</i>	46
<i>Conclusions</i>	49
<i>AC corrosion</i>	49
Laboratory experiments.....	50

Setup	50
DCVG – baseline readings.....	55
Case 1: Anode positioned at $x=6, y=9; i = 0.931 \text{ mA DC}$	55
Case 2: Anode positioned at $x=6, y=9; i = 0.118 \text{ mA DC}$	55
Case 3: Anode positioned at $x=1, y=9; i = 1.217 \text{ mA DC}$	56
DC interference experiments	69
Case 4: Anode positioned at $x=1, y=9; i = 1.217 \text{ mA DC}$	69
Case 5: Anode positioned at $x=1, y=9; i = 1.217 \text{ mA DC}$; Interference voltage of 30.63V applied through 2 additional anodes positioned at $x=1, y=1$ and $x=21, y=9$	69
Case 6: Anode positioned at $x=1, y=9; i = 1.217 \text{ mA DC}$; Interference voltage of 30.63V applied through 2 additional anodes positioned at the clay/sand boundary ($x=11, y=1$ and $x=11, y=9$).....	69
Case 7: Anode positioned at $x=1, y=9; i = 1.217 \text{ mA DC}$; Interference voltage of 30.63V applied through 2 additional anodes positioned at the clay/sand boundary and very near the pipe ($x=11, y=3$ and $x=11, y=7$).	71
Case 8: Anode positioned at $x=1, y=9; i = 1.217 \text{ mA DC}$; Interference voltage of 30.63V applied through 2 additional anodes positioned at the clay/sand boundary and as near the pipe as possible ($x=11, y=3-4$ and $x=11, y=6-7$). 71	71
Case 9: Anode positioned at $x=1, y=9; i = 1.217 \text{ mA DC}$; Interference voltage of 30.63V applied through 2 additional anodes positioned in line with defect 1 and as near the pipe as possible ($x=7, y=3-4$ and $x=7, y=6-7$).	71
Conclusions.....	84
DC and AC CIS measurements	84
DC measurements	84
DC interference measurements.....	86
Conclusions.....	97
AC measurements.....	97
AC current modeling.....	99
Conclusions.....	100

Task 2 – Large-scale experimental studies and Task 3 – Field verification	101
Setup construction and configuration	101
<i>CIS</i>	114
<i>Baseline readings</i>	114
<i>CIS under interference</i>	115
<i>Conclusions</i>	123
<i>Dynamic (field) vs. static (laboratory) stray current interference measurements</i>	124
<i>DCVG</i>	124
<i>Baseline readings</i>	124
<i>DCVG readings under interference</i>	127
<i>Conclusions</i>	142
<i>Pipeline Current Mapper</i>	142
AC Close Interval Survey as a means of AC Monitoring	144
<i>Conclusions</i>	153
<i>Field vs. laboratory findings</i>	153
GENERAL CONCLUSIONS	155
Experimental work	155
Unique conditions	158
AC corrosion	158
High CP (overprotection).....	159
ECDA methods under stray current interference.....	161
DCVG	161
CIS	162
PCM	162
APPENDIX A.....	163
NACE International Document	163

LIST OF FIGURES

Figure 1.	Summary of cathodic potential limits established by different standards and key literature.	39
Figure 2.	Pictures showing local collapse of API 5LX52 pipelines under the sleeve repair on a 600 mm diameter, 7.1 mm thickness gas pipeline ²⁸	41
Figure 3.	Illustration of hydrogen accumulation under Type B sleeve at high-CP conditions.....	42
Figure 4.	Illustration of collapse under sleeve after pipeline break and blow out. ...	43
Figure 5.	Predicted flaw size vs. DCVG signal strength (CP3D model). Cases for several soil resistivities are shown.....	47
Figure 6.	Predicted flaw size vs: soil resistivity (top), depth of cover (middle), IR drop away from the anomaly (bottom).	49
Figure 7.	Schematic of the test configuration.....	50
Figure 8.	Pipe segments showing the external coating and electric lead.....	51
Figure 9.	The pipe assembly inside the cell; the reference electrode is fed through the hole in the lid.....	52
Figure 10.	General view of the experimental cell and the pipe assembly.	53
Figure 11.	Small cell filled with clay and sand.....	54
Figure 12.	Small-cell experimental setup.....	54
Figure 13.	Contour plot of DCVG measurements near anode, $i = 0.931$ mA DC with anode positioned at $x=6, y=9$	57
Figure 14.	Contour plot of DCVG measurements near Defect 1 (Case 1).	58
Figure 15.	Contour plot of DCVG measurements near Defect 2 (Case 1).	59
Figure 16.	Contour plot of DCVG measurements near Defect 3 (Case 1).	60
Figure 17.	Contour plot of DCVG measurements near anode, $i = 0.118$ mA DC with anode positioned at $x=6, y=9$	61

Figure 18.	Contour plot of DCVG measurements near Defect 1 (Case 2).	62
Figure 19.	Contour plot of DCVG measurements near Defect 2 (Case 2).	63
Figure 20.	Contour plot of DCVG measurements near Defect 3 (Case 2).	64
Figure 21.	Contour plot of measurements near anode, $i = 1.217$ mA DC with anode positioned near $x=1, y=9$	65
Figure 22.	Contour plot of measurements near Defect 1 (Case 3).....	66
Figure 23.	Contour plot of measurements near anode Defect 2 (Case 3).....	67
Figure 24.	Contour plot of measurements near Defect 3 (Case 3).....	68
Figure 25.	Layout of buried pipe in 'sandbox' – colored anodes show where interference anodes were positioned for the various cases	70
Figure 26.	Contour plot of measurements (Case 4 – repeat of baseline conditions). 72	
Figure 27.	Contour plot of measurements (Case 4 – repeat of baseline conditions). 73	
Figure 28.	Contour plot of measurements (Case 4 – repeat of baseline conditions). 74	
Figure 29.	Contour plot of measurements (Case 5).	75
Figure 30.	Contour plot of measurements (Case 6).	76
Figure 31.	Contour plot of measurements (Case 6).	77
Figure 32.	Contour plot of measurements (Case 6).	78
Figure 33.	Contour plot of measurements (Case 7).	79
Figure 34.	Contour plot of measurements (Case 8).	80
Figure 35.	Contour plot of measurements (Case 8).	81
Figure 36.	Contour plot of measurements (Case 8).	82
Figure 37.	Contour plot of measurements (Case 9).	83
Figure 38.	DC CIS profile in clay/sand.	85

Figure 39.	CIS profile (Experiment 1).....	87
Figure 40.	CIS profile (Experiment 2).....	88
Figure 41.	CIS profile (Experiment 3).....	89
Figure 42.	CIS profile (Experiment 4).....	90
Figure 43.	CIS profile (Experiment 5).....	91
Figure 44.	CIS profile (Experiment 6).....	92
Figure 45.	CIS profile (Experiment 7).....	93
Figure 46.	CIS profile (Experiment 8).....	94
Figure 47.	CIS profile (Experiment 9).....	95
Figure 48.	CIS profile (Experiment 10).....	96
Figure 49.	AC CIS profile in sand/clay. Red points denote locations of Defects.	99
Figure 50.	Pipeline sections (20" diameter, left, 8" diameter, right) with end caps..	102
Figure 51.	Single centrally positioned 10 sq. inch defect in 20 inch pipeline section.	102
Figure 52.	Single centrally positioned 10 sq. inch defect in 8 inch pipeline section.	103
Figure 53.	Examples of offset 10 sq. inch defects in 8 inch (above) and 20 inch (below) pipeline sections.....	103
Figure 54.	Examples of centrally positioned 1 sq. inch defects in 8 inch (above) and 20 inch (below) pipeline sections.	104
Figure 55.	Examples of distributed defects (10 individual 1 sq. inch defects) on 20 inch (top) and 8 inch (bottom) sections.	105
Figure 56.	Example of a reference electrode (platinized niobium wire encased in epoxy with an outer metal casing).	106
Figure 57.	Example of magnesium (left) and copper (right) electrodes.....	106

Figure 58.	Reference electrode (left), magnesium electrode (upper right) and copper electrode (bottom right) strapped to the 20 inch pipeline section prior to installation.....	107
Figure 59.	Reference electrode (left) attached next to an off-center 10 sq. inch defect on 8 inch pipeline section; magnesium electrode (right, lower) and copper electrode (right, upper) placed in between two adjacent pipeline sections.	107
Figure 60.	Installation of cable leads.....	108
Figure 61.	Installation of first 9 sections (20 inch line on the left, 8 inch line on the right). Note bare pipeline sections indicated by arrows.....	109
Figure 62.	Section of bare pipeline inserted between two 8 inch pipeline sections.	110
Figure 63.	Drainage pipe installed prior to laying of the 8 inch pipeline sections in sand backfill (left); pipeline sections in partially filled trench (right). Upright corrugated stack houses a sump pump to remove drained water.....	110
Figure 64.	Completed site (red flags show coating holiday locations).....	111
Figure 65.	Panel with electrical connections to all large-scale setup components..	112
Figure 66.	CIS profile of 8 inch pipeline segments (potentials are in mV against copper/copper sulfate reference electrode).	114
Figure 67.	CIS profile of 20 inch pipeline segments (potentials are in mV against copper/copper sulfate reference electrode).	115
Figure 68.	CIS profile (1V interference at three different frequencies). Gray shading – 4 ft depth of cover in soil; yellow shading – 2 ft depth of cover in soil; no shading – 4 ft depth of cover in sand. Allegro meter.....	117
Figure 69.	CIS profile (5V interference at three different frequencies). Gray shading – 4 ft depth of cover in soil; yellow shading – 2 ft depth of cover in soil; no shading – 4 ft depth of cover in sand. Allegro meter.....	118
Figure 70.	Distribution of potential difference between native potentials and potentials measured under AC interference (1V, different frequencies). Allegro meter.....	119

Figure 71.	Distribution of potential difference between native potentials and potentials measured under AC interference (5V, different frequencies). Allegro meter.....	119
Figure 72.	CIS profile (5V interference at two different frequencies). Gray shading – 4 ft depth of cover in soil; yellow shading – 2 ft depth of cover in soil; no shading – 4 ft depth of cover in sand. Fluke meter.	121
Figure 73.	Distribution of potential difference between native potentials and potentials measured under AC interference (1V, different frequencies). Fluke meter.	122
Figure 74.	Percent of measurements affected by interference by more than 10 mV. Allegro meter.	123
Figure 75.	Percent of measurements affected by interference by more than 10 mV. Fluke meter.	123
Figure 76.	Schematic of calculation of absolute distance to anomaly.	128
Figure 77.	Effect of dynamic stray current interference on measurement accuracy for 1 sq.in. indications (all positions). Interference calculated as current SNR.	134
Figure 78.	Effect of dynamic stray current interference on measurement accuracy for 10 sq.in. indications (all positions). Interference calculated as current SNR.	135
Figure 79.	Effect of dynamic stray current interference on measurement accuracy for 6 o'clock positions (all indication sizes). Interference calculated as current SNR.	136
Figure 80.	Effect of dynamic stray current interference on measurement accuracy for 12 o'clock positions (all indication sizes) Interference calculated as current SNR.	137
Figure 81.	Effect of dynamic stray current interference on measurement accuracy for 1 sq.in. indications (all positions). Interference calculated as voltage SNR.	138
Figure 82.	Effect of dynamic stray current interference on measurement accuracy for 10 sq.in. indications (all positions). Interference calculated as voltage SNR.	139

Figure 83.	Effect of dynamic stray current interference on measurement accuracy for 6 o'clock positions (all indication sizes). Interference calculated as voltage SNR.	140
Figure 84.	Effect of dynamic stray current interference on measurement accuracy for 12 o'clock positions (all indication sizes) Interference calculated as voltage SNR.	141
Figure 85.	PCM data with and without interference.	143
Figure 86.	Dependence of current density and spread resistance on defect diameter in soil (top graph) and sand (bottom graph). AC voltage is fixed at 5V.	146
Figure 87.	AC current density vs. soil resistivity (AC voltage fixed at 5V).	147
Figure 88.	AC current density vs. AC voltage (soil resistivity fixed at 5,000 ohm-cm).	148
Figure 89.	AC current density vs. distance (first pipeline segment, all sections connected).	149
Figure 90.	AC current density vs. distance for all surveyed combinations.	150
Figure 91.	AC current density vs. effective defect size.	151
Figure 92.	Actual current density vs. calculated current density.	151
Figure 93.	Actual current density vs. calculated current density.	152

LIST OF TABLES

Table 1.	Design current density for coated pipe ($J F_C$) for steel in soils with various pipeline coating to be used in the design of CP systems for operating temperatures $\leq 30^\circ\text{C}$ according to the ISO standard ²⁴	40
Table 2.	Corresponding data for Figure 13 with (+) representing the position of the anode.....	57
Table 3.	Corresponding data for Figure 14 with (*) representing defect and (+) representing anode.....	58

Table 4.	Corresponding data for Figure 15 with (*) representing defect and (+) representing anode.....	59
Table 5.	Corresponding data for Figure 16 with (*) representing defect and (+) representing anode.....	60
Table 6.	Corresponding data for Figure 17 with (+) representing the anode.....	61
Table 7.	Corresponding data for Figure 18 with (*) representing defect and (+) representing anode.....	62
Table 8.	Corresponding data for Figure 19 with (*) representing defect and (+) representing anode.....	63
Table 9.	Corresponding data for Figure 20 with (*) representing defect and (+) representing anode.....	64
Table 10.	Corresponding data for Figure 21 with (+) representing the anode.....	65
Table 11.	Corresponding data for Figure 22 with (*) representing defect and (+) representing anode.....	66
Table 12.	Corresponding data for Figure 23 with (*) representing defect and (+) representing anode.....	67
Table 13.	Corresponding data for Figure 24 with (*) representing defect and (+) representing anode.....	68
Table 14.	Corresponding data for Figure 26 with (*) representing a defect and (+) representing an anode.....	72
Table 15.	Corresponding data for Figure 27with (*) representing a defect and (+) representing an anode.....	73
Table 16.	Corresponding data for Figure 28 with (*) representing a defect and (+) representing an anode.....	74
Table 17.	Corresponding data for Figure 29 with (*) representing a defect and (+) representing an anode.....	75
Table 18.	Corresponding data for Figure 30 with (*) representing a defect and (+) representing an anode.....	76

Table 19.	Corresponding data for Figure 31 with (*) representing a defect and (+) representing an anode.....	77
Table 20.	Corresponding data for Figure 32 with (*) representing a defect and (+) representing an anode.....	78
Table 21.	Corresponding data for Figure 33with (*) representing a defect and (+) representing an anode.....	79
Table 22.	Corresponding data for Figure 34 with (*) representing a defect and (+) representing an anode.....	80
Table 23.	Corresponding data for Figure 35 with (*) representing a defect and (+) representing an anode.....	81
Table 24.	Corresponding data for Figure 36 with (*) representing a defect and (+) representing an anode.....	82
Table 25.	Corresponding data for Figure 37with (*) representing a defect and (+) representing an anode.....	83
Table 26.	Current distribution (Experiments 1-5, measurements in mA).	91
Table 27.	'On' and 'Off' potentials (Experiments 1-5, measurements in V).....	91
Table 28.	Current distribution (Experiments 6-10, measurements in mA).	96
Table 29.	'On' and 'Off' potentials (Experiments 6-10, measurements in V).....	96
Table 30.	Estimated and measured AC current density.....	99
Table 31.	Input values used in PRCI model.....	100
Table 32.	Model output.	100
Table 33.	Summary of tested interference levels.....	116
Table 34.	DCVG-based defect assessment (location).....	125
Table 35.	DCVG-based defect assessment (defect size per NACE RP0502)	126
Table 36.	Anomalies (pipe sections) assessed under dynamic stray current interference.....	127

Table 37.	Distance off from original indication location, ft. Interference is calculated as current SNR.	130
Table 38.	Severity category, based on %IR under the influence of interference (current-based SNR).....	131
Table 39.	Distance off from original indication location, ft. Interference calculated as voltage SNR.....	132
Table 40.	Severity category, based on %IR under the influence of interference (voltage-based SNR).	133
Table 41.	Soil resistivity for the three pipeline segments.	145
Table 42.	Defect size and orientation.	149

INTRODUCTION

External corrosion direct assessment process (ECDA) implemented in accordance with the NACE Recommended Practice RP0502-02 relies on above ground DA techniques to prioritize locations at risk for corrosion. Two special cases warrant special consideration.

1. In situations when the ECDA process has to be conducted in areas with AC and DC (static and dynamic) stray current activity, the stray currents (SC) will likely greatly affect any voltage or current-based measurements used in the indirect assessment step of ECDA. The ECDA potential/voltage measurement techniques are subject to IR-drop errors (observed to reach magnitudes in excess of 5V) due to the flow of both CP current and stray current in the soil. These IR-drops must be considered before this type of data can be accurately related to existing protection criteria. Given that the traditional ECDA methods, such as CIS, DCVG, and PCM, rely on the measurements directly impacted by the SC, the principal problem is to establish the conditions under which the ECDA techniques are compromised to such extent that the survey results become invalid. The accuracy and reliability of the common ECDA tools under varying conditions of stray (static and dynamic DC and AC) requires an assessment; it is expected that the limitations are dependent on both the level of stray current activity and the conditions of the external coating on the buried pipeline.
2. As a further complication, some corrosion-related concerns are not specifically addressed by the ECDA process in its present form. The pipelines have been documented to suffer from AC corrosion; further, a recent research project (co-funded by DOT and PRCI) investigated the risks of excessively high CP potentials to both external coating and linepipe steels. Whereas the threats from these adverse influences have been acknowledged, they are not currently being explicitly addressed in the indirect assessment step of the ECDA process (no procedure to account for AC corrosion threat exists). Although neither NACE International nor the Code of Federal Regulations presently offer any quantitative criteria for either AC corrosion or high CP-related risks, there are published data which tentatively set the upper limits on the AC discharge current density and CP potentials/CP current density

BACKGROUND

AC corrosion

The phenomenon of alternating current (AC)-enhanced corrosion has been considered by many authors since the early 1900s. However, for many years, corrosion experts did not regard corrosion due to alternating currents on metallic structures as a very important phenomenon. AC corrosion was not well understood for two reasons: (1) the electrochemical phenomena of corrosion are normally attributed to direct current; and (2) the instruments normally used to measure the electric parameters in direct currents can not correctly detect the presence of AC current with frequencies between 50 and 100 Hz. The body of recent (post 1980) literature indicates that AC-corrosion or AC-enhanced corrosion (ACEC) is a bona fide effect (reported corrosion rates up to 20 mpy, with pitting rate considerably higher). Probabilistically, higher AC current densities are likely to result in accelerated corrosion of steel. There is an inverse relationship between the impact of AC current and its frequency; however, there appears to be a tacit agreement that at prevailing commercial current frequencies (such as 50 or 60Hz) corrosion is possible, even on the cathodically protected pipelines.

Multiple publications exist that discuss what constitutes the limiting AC current density below which AC corrosion would not be considered a factor. Most agree that $>100 \text{ A/m}^2$ ACEC is likely and, furthermore, some indicate that CP is not effective in mitigating ACEC at current densities greater than 100 A/m^2 . The majority of the studies indicated that ACEC is possible at current densities >20 to 30 A/m^2 . For example, Draft European Standard ("Evaluation of AC corrosion likelihood of buried pipelines. Application to cathodically protected pipelines", CEN TC 219, No. 329, December 2004) offers the following guidelines:

The pipeline is considered protected from AC corrosion if the RMS AC. current density is lower than 30 A/m^2 .

In practice, the evaluation of AC corrosion likelihood is done on a broader basis:

- current density lower than 30 A/m^2 : no or low likelihood,
- current density between 30 and 100 A/m^2 : medium likelihood,
- current density higher than 100 A/m^2 : very high likelihood.

Similarly, German standard (DIN 50925 Korrosion der Metalle; Nachweis der Wirksamkeit des kathodischen Korrosionsschutzes erdverlegter Anlagen, 1992) adopts a value of 30 A/m^2 ; "Handbook of cathodic corrosion protection" by Baeckmann and Schwenk (W. von Baeckmann, W. Schwenk, (eds.) Handbuch des Kathodischen

Korrosionsschutzes, Wiley-VCH, Weinheim, 1999) cites a value of 20 A/m². However, a recent study sponsored by PRCI and conducted by CC Technologies (Mark Yunovich and Neil G. Thompson, "AC Corrosion", PRCI Catalog No. Catalog No. L52098, September 2003) indicated that AC current density discharge on the order of 20 A/m² can produce significant corrosion.

The publications point out that AC mitigation on the basis of AC voltage is misleading. At present in the U.S., AC mitigation is mostly driven by the safety considerations. The primary focus of these efforts is to reduce the induced AC voltage below the 15V to assure the compliance with the NACE Standard RP0177 "Mitigation of Alternating Current and Lightning Effects on Metallic Structures and Corrosion Control Systems". On the other hand, in Germany, the same threshold is 65V (Technical Recommendation No. 7, "Measures for the installation and operation of pipelines in the vicinity of three-phase high-voltage systems and single-line traction systems", Verlags-und Wirtschaftsgesellschaft der Elektrizitätswerke mbH- WVEW, Frankfurt Main, 1985). Considering that the primary factor in determining the possibility for the presence of AC corrosion is the AC current density, monitoring the current density rather than an AC voltage is crucial to assessing the AC current-related hazards to a buried pipeline.

It is a very important departure from the prevailing practices of measuring (and mitigating) the AC voltages on the buried pipelines, notwithstanding the fact that the reduction of AC potentials is expected to reduce the AC current magnitude as well. Field data shows that a relatively small-sized defect (6 to 13 cm²) in the coating on the pipe in a relatively low-resistivity soil could have AC current density in excess of 100 A/m², while the AC voltage could be as low as 6V. Similarly, the above-referenced Draft European Standard suggests that to reduce the AC corrosion likelihood on a buried pipeline, the pipeline AC voltage should not exceed at any time 10 V over the entire pipeline or 4 V where the local soil resistivity measured along the pipeline is less than 25 ohm·m.

A number of publications in the past two years offered additional insight with regard to the field manifestations of the ACEC, suggested mechanisms of attack, and discussed possible acceptance criteria (e.g. L. Nielsen et al, "AC-induced corrosion in pipelines: detection, characterization, and mitigation", Paper No. 04211, NACE International, 2004; Mark Yunovich, "AC corrosion: Mechanism and proposed model", Paper IPC04-0574, Proceedings of IPC 2004 International Pipeline Conference, October 2004, Calgary, Canada). NACE International has created a Task Group (TG 327) to create the state-of-the-art report on AC corrosion (Mark Yunovich, Chairman).

High CP effects

The concerns over the adverse effects of overprotection are related to the impact of high potentials on linepipe steels (hydrogen-related damage, HRD) and external coatings (cathodic disbondment, CD). According to the Office of Pipeline Safety (Office of Pipeline Safety, Department of Transportation, <http://ops.dot.gov/IA98.htm>), several reported pipeline failures may have been the result of a combination of high cathodic protection (CP) levels and “hard spots” in the linepipe steel. The cathodic protection criteria outlined in the NACE Recommended Practice RP0169 (NACE Recommended Practice for External Corrosion on Underground or Submerged Metallic Piping, NACE RP0169-96, NACE International, Houston, TX) are being currently reviewed by the NACE Task Group TG 285. There are a number of issues with the currently employed criteria; e.g., in the case of an aging pipeline (i.e., a pipe with a large population of the external coating defects), meeting the “-850 mV off-potential” criterion, even if possible, may create conditions of locally excessive cathodic protection potentials (“overprotection”). Further, RP0169 does not offer any specific guidance on the upper CP limit. The document does point out the fact that excessive polarized potentials on externally coated pipelines should be avoided to minimize cathodic disbondment of the coating. Also it includes a precautionary note regarding polarized potentials that result in excessive generation of hydrogen. In the latter case, the NACE Recommended Practice states that these excessive potentials should be avoided in all metals, particularly high-strength steels.

The ISO 15589-1 (INTERNATIONAL ISO STANDARD 15589-1 First edition, Petroleum and natural gas industries - Cathodic protection of pipeline -transportation systems) establishes maximum and minimum cathodic potential limits, as a general guidance. The general criterion given in the ISO Standard is to polarize a buried pipeline to potentials which are more negative than -850 mV and less negative than -1,200 mV (CSE). The limit of -1,200 mV is recommended to prevent cathodic disbondment.

Whether or not CD is caused by the chemical action of high pH or the physical action of gaseous hydrogen, there appears to be no danger of corrosion in the disbonded region in the short term, unless CP current is shielded by the coating or the CD region extends dramatically leading to lower polarization levels and insufficient CP conditions. That is, even if CP may lead to CD, the general opinion is that if the coatings fail, they do so without threat to pipeline integrity due to the existing protection afforded by CP (the high pH environment which passivates carbon steel and causes formation of carbonate salts and the imposed CP current). Worthingham et al (R. Worthingham, M. Cetiner, “Long Term Performance of Fusion Bond Epoxy Coated Pipelines”, IPC04-0570, October, 2004) examined pipelines with FBE blistering and disbondment; the results revealed no

correlation between the cathodic protection potential (on and off) and the extent of disbondment.

The reliance on the potential values alone may lead to underestimation of the hazards of overprotection. CC Technologies has completed a DOT-sponsored research on the subject of effect of high CP potentials on pipelines (DTRS56-03-T-0004, Mark Yunovich, Principal Investigator), the results by show that, at high CP currents, the change in polarized potential is relatively minor, compared to a significant (ten-fold) increase in applied CP current density. The study concluded that the CP off-potentials, being a derivative of the applied current density, environmental characteristics, and material properties, serves merely as a convenient metric to assess the danger of the overprotection and not as the primary cause of the possible damage caused by overprotection. Therefore, heavy reliance on the potential measurements alone may lead to errors in the assessment of the actual threat of overprotection. The research recommended that the use of the polarized off-potentials as the sole criterion for the assessment of the hazards of hydrogen-related damage should be discouraged.

Stray current interference

The impact of stray currents (including long-line and telluric) on underground pipelines is well documented, both from the standpoint of corrosion and the SC interference with the above-ground potential measurements. Some of the past projects funded by various industry groups, such as PRCI, NGA, ESEERCO, established approaches for SC monitoring and provided guidelines on how to compensate for the IR drop. The issue of dynamic DC currents in urban environments was also investigated. The prior research work identified the major SC monitoring methods, which included potential surveys (close interval surveys and time-dependent surveys), line current surveys (using calibrated spans, clamp-on meters, and electromagnetic surveys), and beta correlation technique. All of these methods suffer from the same major limitation – the inability to accurately compensate for the SC effect or to relate the measurements to the corrosion conditions on the surveyed structure. Thus, each method is severely handicapped for the purposes of prioritization of pipeline locations from the standpoint of ECDA.

The research conducted by CC Technologies indicated that the resolution of some of the above-ground techniques, particularly PCM, may be insufficient for all but larger holidays. If the measurements are attempted in presence of the SC activity, one can assume that the validity of the data is going to suffer even further.

Several recent, state-of-the art research projects conducted by CC Technologies, which were both laboratory- and field-based, served as the foundation for multiple aspects of the proposed project. During the prior research, the impact of the high CP potentials on

some of the common external coatings and linepipe steels was quantified; also, extensive analysis of AC corrosion has led to suggesting the mechanism of the phenomenon and indicated possible metrics for the assessment of associated risks. There is an added advantage of the CC Technologies' personnel's involvement in and familiarity with the results of the above-referenced projects, particularly in the extensive research in the area of AC corrosion and high CP effects on pipelines. This advantage translated into a more focused approach to achieving the primary objective and provided a significant head-start for the research effort.

OBJECTIVES AND DELIVERABLES

There is a need to address the threats, which either currently are unaccounted for by the ECDA process or are associated with the process' existing deficiencies. While adverse effects of AC current and CP overprotection are left out of the ECDA scope, there is presently sufficient evidence that these phenomena affect the pipelines and may pose considerable integrity risks and thus should be included in ECDA assessment. The research focused on two primary objectives:

1. The threats, which may be categorized as unique (uncommon threats not currently evaluated via the ECDA process), are nonetheless common to many underground pipelines and include 1) AC corrosion and 2) possible disbondment of the external coatings and hydrogen-related damage (HRD) to pipeline body due to excessive CP. The first objective of the proposed research is to complement ECDA protocol by including assessment of threats posed by alternating current and excessive cathodic protection. The above-referenced phenomena are typically regarded in terms of current density and rely on voltage-based measurements for above ground detection. Therefore, no new techniques are necessary to make the assessment; however, a set of guidelines is required for using the existing methods, which would include metrics and criteria to for prioritization of the AC corrosion and high CP risks.
2. The pipelines subjected to stray corrosion current are potentially at risk for misinterpretation of the ECDA results due to SC interference; the limits on the signal-to-noise ratio for the common ECDA techniques, such as CIS, AC/DCVG, and PCM need to be established. These techniques use voltage/current measurements and thus directly affected by stray currents, which give rise to voltage/current gradients. Present compensation methods (e.g., logging and averaging potential values over time at a stationary position) are insufficient for most cases. The second objective of the proposed research is to establish the limitations to applicability to the ECDA indirect assessment techniques under

stray current conditions. The guidelines will enable a pipeline operator to make an informed decision with regard to the applicability of each technique, given the level of SC interference – whether the measurements are corrupted beyond salvaging, or only defects of certain size could be detected, or whether the stray currents should be mitigated prior to indirect assessment (if applicable).

WORK PLAN

The research included laboratory (Task 1, Task 2,) and field work (Task 3). Most ECDA above-ground indirect inspection techniques rely on potential measurements; Task 1 laboratory work focused on defining the ranges for the critical parameters affecting the AC and DC potentials on a buried pipe which were used to assess the AC corrosion and high CP threats. As a part of laboratory studies, an extensive literature search was conducted to 1) establish the state-of-the-art in AC corrosion/high CP threat assessment; 2) determine the most promising approach to evaluating/monitoring of the risks; and 3) identify the best *metrics*, which, in turn, define the proper assessment techniques. In Task 2, to evaluate the effects of stray currents, a large-scale laboratory experimental site was constructed, which enabled simulation of various field conditions (different levels of SC, varying degrees of CP polarization, various configurations of coating defects on a buried pipeline). Task 3 field-based activities provided a major input by generating the empirical data using the approach to AC corrosion and high CP threat assessment developed in Task 1. Task 3 also provided a means to verify the limitations to the accuracy and resolution of standard ECDA at-grade techniques established during Task 2. Each Task and included sub-Tasks are described below. Task 4 consisted of preparing the guidelines for the AC corrosion and high CP threat assessment and for indirect inspection techniques' applicability in presence of stray currents. Task 5 activities consisted of reporting (quarterly reports) and presenting of the results (interim and final Peer Reviews).

Task 1 – Laboratory Analysis of AC corrosion and High CP effects

Task 1 included literature survey, followed by computational modeling and experimental work to define the threat of AC corrosion/effects of high CP potentials and use state-of-the-art metrics for determining the likelihood of AC corrosion on a buried pipeline via above-ground methods.

Task 1.1 – AC Corrosion

Task 1.1 focused on AC corrosion threats and consisted of several sub-Tasks.

Task 1.1.1 – Literature survey and state-of-the-art

Task 1 started with a literature survey and establishing the state-of-the-art with respect to AC corrosion to 1) establish the state-of-the-art in AC corrosion; 2) determine the most promising approach to evaluating/monitoring of the risks (information on the acceptance criteria were evaluated); and 3) identify the best *metrics*, which define the proper assessment techniques. Field portion of the proposed project endeavored to verify the selected criteria. The success was expected to be dependent on the existence of detrimental conditions on the surveyed pipelines.

As a part of state-of-the-art activities and in conjunction with the efforts of Task Group (TG) 327 of NACE International, a draft document entitled “State-of-the-Art on AC corrosion” was developed. At the time of the report, the document was being prepared to be ready for balloting and comments by the NACE membership.

Task 1.1.2 – Computational modeling

Current state-of-the-art suggests that the threat of AC corrosion should be estimated based on the current density, rather than potential measurements. However, the above-ground potential measurements (such as an AC potential CIS) are easy to perform and therefore should not be dismissed out of hand. Task 1.2 was planned to consist of computational modeling using several existing approaches: 1) PRCI-developed software (AC Predictive and Mitigation Techniques (Software and Documentation), PRCI Catalog No. L51835), which includes comprehensive electromagnetic coupling equations with an interface formatted to enable both steady state and fault induced voltages and currents; 2) *forward* and *reverse* models which use soil property data (such as soil resistivity, depth of cover) and steel surface characteristics (coating defect size and location, polarization characteristics) to compute the expected potential distribution at grade level (*forward* model) or attempt to solve the inverse case of establishing the steel surface conditions, given the at-grade potential distribution (*reverse* model).

There are several models, which use either finite element analysis (FEA) or boundary element method (BEM), or a combination of FEA and BEM. The models were planned to be used to establish whether at-grade measurements (such as measurements of AC potentials) can be used to establish the AC conditions at the steel surface and which additional measurements would be required in the laboratory and field to make this determination.

Once the work has begun, the research team has encountered a number of significant challenges. The available reverse models were not adequate for establishing the critical driving factors for AC corrosion. The FEA forward model, which was being developed for the concurrently run PHMSA-sponsored project (Guidelines for

Interpretation of Close Interval Surveys for External Corrosion Direct Assessment (ECDA), contract No. DTPH56-06-T-0012), while performing adequately for the purposes of modeling DC potentials was not producing desired results for the AC corrosion process.

As described in the state-of-the-art, AC corrosion is a complex phenomenon; in order to model the process, incorporation of the polarization relationship linking AC current and potential shift into the model was essential. However, the model experienced considerable problems with convergence of the numerical solution when the polarization relationship was incorporated.

In the interest of maximizing the project funds and in order to achieve the overall objectives of the project, it was decided to limit the modeling to the assessment of the PRCI-developed software. The NACE draft document on the State-of-the-Art on AC corrosion included considerable information and extended discussion of the proposed AC corrosion mechanism.

Task 1.1.3 – Laboratory experiments

Once the broad trends linking between the grade-level measurements and steel surface conditions have been established, the relationships between the at-grade measurable values and the AC current density on the buried pipe sections were verified in the laboratory experiments, using small and large(r)-scale (soil-box) experiments. Limited bench-top laboratory experiments were carried out using clay and sand environments on small-diameter pipe sections. Coated sections were tested in two different soils; different size defects were to be evaluated; circumferential position of the defect (e.g., top vs. bottom location) was investigated also. The experiments are also planned to be carried out using the large-scale experimental site setup during Task 3 activities. The experiments were planned to concentrate on the verification of the output of the model, so that the assessment methods can be employed in the field.

Task 1.2 – Effects of high CP potentials

Task 1.1 focused on high CP threats and consisted of several sub-Tasks. Task 2 drew on the recently completed DOT-funded project on the effects of high CP potentials on coatings and steels (DOT CONTRACT NO. DTRS56-03-T-0004). The primary goal was to establish whether above-ground techniques can be utilized to determine and prioritize the locations at risk to high CP damage.

Task 1.2.1 – Literature survey and state-of-the-art

Task 1 started with a literature survey and establishing the state-of-the-art with respect to high CP to 1) establish the state-of-the-art regarding cathodic overprotection; 2)

determine the most promising approach to evaluating/monitoring of the risks; and 3) identify the best *metrics*, which define the proper assessment techniques. The results of a current project funded by NGA (“ECDA indication criteria sensitive to specific pipeline conditions”), which attempts to link the above-ground survey results to the pipe/interface conditions through development of a reverse model, are expected to provide additional insight. Field portion of the proposed project endeavored to verify the selected criteria. The success was expected to be dependent on the existence of detrimental conditions on the surveyed pipelines.

Task 1.2.1 – Computational modeling

Similarly to AC corrosion threat assessment, the publications suggest that the threat of overprotection should be estimated based on the current density, rather than potential measurements. Nonetheless, the first and primary metric used by pipeline operators to raise the issue of the risk of high CP is the existence of high negative on/off potentials (typically discovered through CIS). The modeling was planned to use forward and reverse models and follow the same path as described in Task 1.1.2, i.e., attempted to establish the trends linking the on/off potential profile to the conditions at steel interface for different soil properties and pipeline conditions, particularly the relationship between the at-grade off-potentials and CP current density at the anomaly site.

Task 1.2.3 – Laboratory experiments

Once the broad trends linking between the grade-level measurements and pipeline surface conditions have been established using the models, the practical range for the values of the critical parametric affecting the relationships was verified in the laboratory experiments, using soil-box experiments. Coated pipeline sections were tested in two different soil environments (clay and sand).

Task 2 – Large-scale experimental studies

Task 2 focused on establishing the limitations and accuracy of the common above-ground ECDA methods under the conditions of static and dynamic stray currents. The evaluation of the techniques was performed to establish the basis for classifying the SC conditions falling into three basic categories:

1. ECDA techniques provide reliable results and may be used.
2. ECDA techniques are capable of discerning of large-sized coatings defects only and may be used with limitations.
3. Common ECDA techniques are significantly affected by the SC and should not be used, unless the SC activity is mitigated below a certain threshold value.

Task 2.1 – Experimental setup

Task 2.1 consisted of setting up a large-scale experimental setup. The setup a total of 38 sections of buried pipe with two different commonly used coatings – fusion bonded epoxy (20 inch diameter) and a two-layer coating with FBE base layer (8 inch diameter). The setup versatility allowed determination the accuracy and limitations of the ECDA techniques when used in the presence of stray currents, using a ‘life-size’ model. The setup was made considerably more sophisticated and versatile than originally planned. The site was utilized as an alternative to the originally planned Task 3 activities (see below).

Task 2.2 – Data collection

It was expected that the reliability of the results of the ECDA techniques could be contingent on a combination of variables, such as the defect size/orientation, the soil conditions, and the magnitude/frequency characteristics of the stray current signal. The experiments used the defects of a known size exposed to the controlled conditions simulating a variety of SC regimes. Several defect configurations were tested (e.g., a single large defect, a cluster of smaller sized defects, different circumferential orientation); the effect of soil conditions (e.g., soil resistivity, depth of cover) were evaluated as well.

Task 3 – Field verification

The objectives of Task 3 were to confirm the findings of Task 1 and Task 2 on actual transmission pipelines. The investigations were planned to be carried on the natural gas pipelines on the SoCal system. As was noted in the proposal, the success of such verification would be contingent on the existence of detrimental conditions; thus direct examinations may provide only limited support. Based on the significant amount of data provided by SoCal, it became evident that the evidence of AC current activity or excessive CP potentials on the SoCal system was scarce. Therefore, the research team decided to conduct Task 3 activities of the field work on the large-scale experimental site in consultations with CC Technologies Field Services, which performs ECDA work on hundreds of miles of buried transmission and distribution pipelines annually. The focus of the field work was two-pronged; 1) confirmation of the threat assessment metrics identified in Task 1 and Task 2 and 2) confirmation of the laboratory results with respect to correlating at-grade measurements to conditions at the buried pipeline surface by a) carrying out at-grade measurements using methods/techniques identified during Task 1, b) processing the values, and c) matching the results to actual conditions at the anomaly site during direct examination step of ECDA.

Task 3.1 – Verification of AC corrosion laboratory results

Task 3.2 – Verification of high CP effects laboratory results

The objective of Task 3.1. and .3.2, which were carried out concurrently, was to verify the metrics/acceptance criteria for the assessment of underground pipeline integrity threats from AC current and high CP potentials, respectively. The threat evaluated with above-ground techniques using the correlation/trends established during modeling (Task 2) was assessed by conducting documented pipe conditions using known configuration of the buried sections at the CC Technologies large-scale experimental setup. In this manner, not only the laboratory/modeling-based trends were checked, but the validity of the risk criteria (selected on the basis of literature survey and state-of-the-art) could be confirmed.

Task 3.3 – Verification of stray current interference laboratory results

The activities of Task 3.3. were carried out concurrently with Tasks 3.1. and 3.2 Efforts established the basis for categorizing the SC conditions from the standpoint of feasibility of the ECDA process.

Task 4 – Guidelines for ECDA

Upon completion of the laboratory and field components of the proposed research effort, the findings were summarized into a three sets of guidelines for the pipeline operators. The guidelines, the primary deliverable of the project, describe the proposed procedures, explain the meaning of the measurements and provide instructions regarding the following:

- Augmented indirect assessment (as a part of ECDA protocol) to assess the pipeline integrity threats from AC corrosion
- Augmented indirect assessment (as a part of ECDA protocol) to assess the pipeline integrity threats from CP overprotection (high negative CP potentials)
- Use and limitations of common above-ground ECDA techniques in presence of stray current activity.

The guidelines were prepared in the format suitable for inclusion in the NACE International RP0502.

Task 5 – Reporting and public submission of results

Task 5 consisted of generating and submitting quarterly update reports, discussing the results and the Peer Review meeting (2 meetings are anticipated), and presenting the project results at a public forum (presentation at the 2008 NACE International convention in New Orleans is planned). As noted above, the literature survey results

were incorporated in the NACE International Draft document “State-of-the-Art on AC Corrosion”.

RESULTS AND DISCUSSION

Task 1 – Laboratory Analysis of AC corrosion and High CP effects

Literature-survey: State-of-the-Art

The literature survey focused on two areas: corrosion caused by AC currents and hazards of overprotection to buried coated pipelines.

In addition to the extensive in-house archives, the following commercial literature databases were used to identify the publications on the above two subjects:

- Corrosion Abstracts_1966-2006/Apr
- TEME-Technology & Management_1989-2006/May
- CA SEARCH(R)_1967-2006
- Ei EnCompassLit(TM)_1965-2006/
- Ei Compendex(R)_1970-2006/Apr
- Energy SciTec_1974-2006/Apr
- TULSA (Petroleum Abs)_1965-2006/Apr
- Civil Engineering Abstracts._1966-2006/Apr
- FLUIDEX_1972-2006/Apr
- Pascal_1973-2006/Apr
- SciSearch(R) Cited Ref Sci_1990-2006/Apr
- MetalBase_1965-20060508
- ICONDA-Intl Construction_1976-2006/Apr
- Inside Conferences_1993-2006/May 09
- JICST-EPlus_1985-2006/Feb
- ChemEng & Biotec Abs_1970-2006/Apr
- Wilson Appl. Sci & Tech Abs_1983-2006/Apr
- INSPEC_1898-2006/Apr
- World Surface Coatings Abs_1976-2006/May
- ANTE: Abstracts in New Tech & Engineer_1966-2006/
- GEOBASE(TM)_1980-2006/Apr
- Ei EnCompassPat(TM)_1964-2006

The discussion below highlights the primary factors affecting AC corrosion of underground pipelines and hazards of overprotection.

AC-enhanced corrosion

Historic notes

The phenomenon of alternating current (AC)-enhanced corrosion has been considered by many authors since the early 1900s. However, the mechanism(s) of AC corrosion is still not completely understood. The body of recent (post 1980) literature indicates that

AC-corrosion or AC-enhanced corrosion (ACEC) is a bona fide effect (reported corrosion rates up to 20 mpy, with pitting rate considerably higher); there appears to be a tacit agreement that at prevailing commercial current frequencies (such as 50 or 60Hz) corrosion is possible, even on the cathodically protected pipelines.

Alternating current (AC)-enhanced corrosion on cathodically protected pipelines is not a well-understood phenomenon, despite discussion about the phenomenon dating back to the late 19th century. For many years, corrosion experts did not consider enhanced corrosion attributed to alternating currents on metallic structures very important. In 1891, Mengarini concluded that corrosion (“chemical decomposition”) by alternating current is (1) less than the equivalent direct current, (2) it is proportional to the AC current, (3) there exists a threshold AC current density below which no “decomposition of electrolyte” occurs, and (4) extent of corrosion decreases with the increased AC frequency.^[1] In 1916, McCollum et al published a research paper that concluded that iron does not suffer from attack when a limiting frequency of the current (somewhere between 15 and 60Hz) is reached.^[2] AC corrosion was not well understood for two reasons: (1) the electrochemical phenomena of corrosion is normally attributed to direct current; and (2) the instruments normally used to measure the electric parameters in direct currents cannot correctly detect the presence of AC current with frequencies between 50 and 100 Hz.^[3] Recently, there has been an increasing concern for AC corrosion mitigation since alternating currents interference has shown to effect cathodically protected equipment and increase safety concerns (i.e. high AC touch and step voltages). Factors that contribute to AC interference on pipelines include (1) growing number of high voltage power lines; (2) AC operated high-speed traction systems; (3) high isolation resistance of modern pipeline coatings, and (4) coating integrity.^[3,4]

In 1986, a corrosion failure on a high-pressure gas in Germany was attributed to AC corrosion. This failure initiated field and laboratory investigations that indicated that induced AC-enhanced corrosion can occur on coated steel pipelines even when

¹ G. Mengarini, *Electrical World*, Vol. 16 (6), August 1891, p.96.

² B. McCollum, G. Ahlborn, “Influence of frequency of alternating or infrequently reversed current on electrolytic corrosion”, *Technologic papers of the Bureau of Standards*, No. 72, August 15, 1916.

³ Lucio Diabiase, “Corrosion due to alternating current on metallic buried pipelines: background and perspectives,” *Committee on the Study of Pipe Corrosion and Protection, CEOCOR, 5th International Congress, Bruxelles, 2000.*

⁴ Summary, *ibid.*

protection criteria are met. In addition, the investigations ascertained that above a minimum AC current density, typically accepted levels of cathodic protection would not control AC-enhanced corrosion. The German AC corrosion investigators conclusions can be summarized as follows:^[5]

- AC induced corrosion does not occur at AC current densities less than 20 A/m²;
- AC corrosion is unpredictable for AC current densities between 20 to 100 A/m²;
- AC corrosion occurs at current densities greater than 100 A/m²; and
- The highest corrosion rates occur at holidays with a surface area between 1 and 3 cm².

Threat criteria: current density vs. AC voltage

Whereas many authors have concluded that there is a threshold AC current density below which AC corrosion is not a factor, the magnitude of the threshold is being debated. Chin et al studied mild steel exposed to a passivating sodium sulfate solution and observed that at 2000 A/m² passive layer appeared to be completely destroyed.⁶ In addition to the 20 A/m² referenced above, the literature suggests that densities in excess of 30 A/m² may be detrimental to buried steel structures.⁷

On the basis of laboratory tests, Pourbaix et al concluded that AC corrosion is not related to any particular critical AC current density value.⁸ In 1978, Jones published the results of a study of low alloy and carbon steel in sodium chloride solution, which observed an increase of corrosion rate of 4 to 6 times when the specimens in deaerated conditions were exposed to a 60Hz current with a density of 300 A/m², but found no

⁵ G. Helm, T. Helm, H. Heinzen, W. Schwenk, "Investigation of corrosion of cathodically protected steel subjected to alternating currents", 3R International, Vol. 32, 1993, p. 246

⁶ D.-T. Chin, T.-W. Fu, "Corrosion by alternating current: A study of the anodic polarization of mild steel in Na₂SO₄ solution", Corrosion, Vol. 35 (11), November 1979, p. 514

⁷ F. Stadler, "AC corrosion of cathodically protected pipelines. Guidelines for risk assessment and mitigation measures, Annex N.5-4," CEOCOR, 5th International Congress, Bruxelles 2000.

⁸ A. Pourbaix, P. Carpentiers, R. Gregoor, "Detection and assessment of alternating current corrosion", Materials Performance, Vol. 38 (3), March 2000, p. 34-39

acceleration of corrosion under aerated conditions.⁹ German standard¹⁰, DIN 50925, adopts a value of 30 A/m²; “Handbook of cathodic corrosion protection” by Baeckmann and Schwenk¹¹ cites a value of 20 A/m².

A European Standard¹² offers the following guidelines:

The pipeline is considered protected from AC corrosion if the RMS AC. current density is lower than 30 A/m².

In practice, the evaluation of AC corrosion likelihood is done on a broader basis:

- current density lower than 30 A/m² : no or low likelihood,
- current density between 30 and 100 A/m² : medium likelihood,
- current density higher than 100 A/m² : very high likelihood.

Recent experimental studies by Yunovich and Thompson¹³ concluded that AC current density discharge in the order of 20 A/m² can produce significant enhanced corrosion (higher rates of penetration and general attack). Further, the authors stated that there likely was not a theoretical ‘safe’ AC current density, i.e., a threshold below which AC does not enhance corrosion; however, a practical one may exist for which the increase in corrosion due to AC is not appreciably greater than the free-corrosion rate for a particular soil condition.

The conclusions of the doctoral thesis by Goidanich¹⁴ are similar in nature; the findings suggest that the current density of 10 A/m² may be hazardous, as it has increased corrosion rate by two-fold in a simulated soil solution compared to the AC-free conditions.

⁹ D. Jones, “Effect of alternating current on corrosion of low alloy and carbon steels”, Corrosion, Vol. 24 (12), December 1978, p. 428

¹⁰ DIN 50925 Korrosion der Metalle; Nachweis der Wirksamkeit des kathodischen Korrosionsschutzes erdverlegter Anlagen, 1992

¹¹ W. von Baeckmann, W. Schwenk, (eds.) Handbuch des Kathodischen Korrosionsschutzes, Wiley-VCH, Weinheim, 1999.

¹² “Evaluation of AC corrosion likelihood of buried pipelines. Application to cathodically protected pipelines”, CEN TC 219, No. 329, December 2004

¹³ Yunovich, M. and Thompson, N.G., “AC Corrosion: Corrosion Rate and Mitigation Requirements”, Corrosion NACEExpo 2004, New Orleans, Louisiana, April 2004, Paper No. 04206

¹⁴ Goidanich, S, “Influence of alternating current on metals (sic) corrosion”, PhD thesis, Politecnico di Milano, 2005

Wakelin and Gummow¹⁵ suggest that by knowing the soil resistivity and the pipeline's AC voltage, and by assuming the worst-case of a 1 cm² holiday, the risk of AC corrosion can be determined using a simple formula to calculate AC current density. For the case of a 1 cm² holiday on a pipe in 1000 ohm-cm soil, where the induced AC voltage on the pipeline is 10 V, the AC current density at the holiday would be 225 A/m²; for the above-referenced density of 100 A/m², the AC voltage would be 4.4V.

This suggests that assessment of AC corrosion threat (and for that matter, AC mitigation) on the basis of AC voltage may be misleading. At present in the U.S., AC mitigation is mostly driven by the safety considerations. The primary focus of these efforts is to reduce the induced AC voltage below the 15V to assure the compliance with the NACE Standard RP0177 "Mitigation of Alternating Current and Lightning Effects on Metallic Structures and Corrosion Control Systems". On the other hand, in Germany, the same threshold is 65V.¹⁶ The above-referenced Draft European Standard suggests that to reduce the AC corrosion likelihood on a buried pipeline, the pipeline AC voltage should not exceed at any time •10 V over the entire pipeline or 4 V where the local soil resistivity measured along the pipeline is less than 25 ohm•m.

Considering that the primary factor in determining the possibility for the presence of AC corrosion is the AC current density, monitoring the current density rather than an AC voltage is crucial to assessing the AC current-related hazards to a buried pipeline.

It is a very important departure from the prevailing practices of measuring (and mitigating) the AC voltages on the buried pipelines, notwithstanding the fact that the reduction of AC potentials is expected to reduce the AC current magnitude as well.

Cathodic Protection

The prevailing thought was that applying cathodic protection in accordance with industry standards could adequately control the AC-enhanced corrosion. However, multiple failures of pipelines under cathodic protection, primarily in Europe, have been attributed to AC corrosion. Additionally, case studies based on the investigations of failures of pipelines in the US have been presented recently.¹⁷ The 1986 German investigation of

¹⁵ R. Wakelin, R. Gummow, S. Segall, "AC corrosion-case histories, test procedures, and mitigation," CORROSION/98, March 1998, NACE.

¹⁶ Technical Recommendation No. 7, "Measures for the installation and operation of pipelines in the vicinity of three-phase high-voltage systems and single-line traction systems", Verlags-und Wirtschaftsgesellschaft der Elektrizitätswerke mbH- WVEW, Frankfurt Main, 1985.

¹⁷ R. Floyd, "Testing and Mitigation of AC Corrosion on 8" Line: A Field Study", NACEExpo/04, Paper No. 04210, NACE, Houston, TX, 2004.

an AC corrosion failure reported high pitting rate despite cathodic protection current density of 1.5 to 2 A/m² and on-potentials of -1.8 to -2.0V (CSE)¹⁸. The literature survey by Gummow references the follow-up investigation to the failure; it was found that increasing the CP current density to 5 A/m² reduced corrosion rate at 50 A/m² AC by a factor of two.¹⁵ The survey¹⁵ also cites another German work which demonstrated that AC corrosion could be mitigated at CP current densities of 4 A/m²; another quoted publication shows that even at 10 A/m² of DC current density, AC corrosion remained considerable at AC densities of 100 to 200 A/m².

The German standard requires limiting current density while maintaining about 1 A/m² of DC current density on coated pipelines¹⁰. Hosokawa et al quotes a study, which found that AC corrosion could be mitigated to corrosion rate of 0.4 mpy if AC density is below 70 A/m², but the AC-related attack remains probable if the AC density is over the threshold value.¹⁹

Summary of Literature Review on AC corrosion

The body of literature indicates that AC-corrosion or AC-enhanced corrosion is a bona fide phenomenon. Probabilistically, higher AC current densities are likely to result in accelerated corrosion of steel. There is an inverse relationship between the impact of AC current and its frequency; however, there appears to be a tacit agreement that at prevailing commercial current frequencies (such as 50 or 60Hz) corrosion is possible, even on the cathodically protected pipelines. General corrosion rates due to AC corrosion are not necessarily 'abnormally' high (much higher, naturally occurring rates of an existing pipeline which have been reported), but the rates are certainly multiples of the 'prevailing' corrosion rates of steel in soil in absence of AC.

The published data possesses a great deal of scatter; testing environments were not necessarily representative of conditions existing on buried pipelines, or the results are only applicable to a specific situation. Testing procedures needed to address AC-enhanced corrosion are relatively complicated, which has limited the necessary research to establish the mechanism. To address the issue of the AC impact on underground steel pipelines and define the criteria for its mitigation more research is required. Currently ongoing research, sponsored by PRCI, is dedicated to defining the

¹⁸ W. Prinz et al, "Alternating current corrosion of cathodically protected pipelines", 1992 International Gas Research conference, Orlando, Florida., November 16-19, 1992.

¹⁹ Y. Hosokawa, F. Kajiyama, Y. Nakamura, "New CP criteria for elimination the risks of AC corrosion and overprotection on cathodically protected pipelines", Corrosion 2002, Paper No. 02111, NACE.

necessary protection criteria; however, the critical element – field-based measurements of AC-enhanced corrosion threat, and the foundations on which to base the conclusions, are lacking. In other words, the work that is encompassed by the present project is important and necessary to address this question.

During the project activities, NACE International's TG327 produced a draft document on the State-of the-art with regard to AC Corrosion. A draft copy of this document is attached in Appendix A. The document is expected to be submitted for balloting and review in early January 2007.

Overprotection effects on underground coated structures

The literature review aimed to address several critical questions:

- What are the hazards of the overprotection to buried pipelines?
- Do these hazards represent an immediate threat to the pipeline integrity?
- What is known about the factors affecting the impact of overprotection and the mechanisms of the effect?
- Could any general guidance be offered given the current state of knowledge?

Hazards of Overprotection

It is generally considered that the two possible hazards of overprotection are (1) damages to external coating (cathodic disbonding, (CD)) and (2) to the pipeline body (hydrogen-related damage, (HRD)). Given that the current project is concerned with the above-ground methods to detect external corrosion sites where the external coating is compromised, the literature review concentrated on the effects of overprotection on coating damage, leaving the HRD-related effects out.

Coating Disbondment

Coating damage due to high CP potentials (overprotection) tends to be attributed to two causes:

1. Formation of a high pH environment at the coating/steel interface, which weakens the chemical bonds leading to the loss of adhesion and cathodic disbondment.
2. Evolution of gaseous hydrogen at the coating/steel interface, which may exacerbate coating disbondment.

Cathodic disbondment caused by alkalinization at high CP

Whereas the excessive CP may lead to CD, the general opinion is that if the coatings fail, they do so without creating an immediate hazard to the pipeline due to the existing

protection by both the high pH environment (which passivates carbon steel and causes formation of carbonate salts) and the imposed CP current. Worthingham et al²⁰ examined pipelines with FBE blistering and disbondment; the results revealed no correlation between the cathodic protection potential (ON and OFF) and the extent of disbondment. The authors suggested that as long as cathodic protection is operating in the pipeline, blistering and disbondment of FBE coating does not present an immediate integrity threat to the pipeline. Fraser et al²¹ demonstrated (by using Electrochemical Impedance Spectroscopy (EIS)) that CP was able to reach the surface underneath an extensively blistered FBE coating on a section of a 21-year-old pipeline.

The same behavior is expected from some other types of coatings such as asphalt and coal tar enamel which are regarded as “CP-compatible”, although there are no known published laboratory or field accounts. The CP-compatible coatings do not block CP current from reaching the underlying pipeline surface after “failing” (i.e., are not typically associated with shielding). The failure of the permeable coatings under CP is therefore not considered immediately hazardous.

Additionally, an increased area of a holiday in a coating would lead to a reduction in electrical resistance of the holiday and thus facilitate CP current pick-up at the disbonded site (note that some coatings, like those with polyethylene are known to shield the CP current under disbondment). However, if disbondment progresses and extends to a large area, it is likely to put a strain on the CP system and lead to insufficient cathodic polarization levels thus creating conditions which may be harmful. Further, increased disbondment may expose steel regions that are more susceptible to hydrogen-related damage than the surrounding matrix (see later discussion).

Cathodic disbondment caused by hydrogen evolution at high CP

No publications were found that specifically addressed cathodic disbondment due to the physical effect of gaseous hydrogen generation at high CP potentials. This may be the result of experimental difficulties to differentiate between the competing effects of alkalization and hydrogen evolution, at the metal/coating interface.

²⁰ Worthingham, R.; Cetiner, M.; Long Term Performance of Fusion Bond Epoxy Coated Pipelines, IPC04-0570, Proceedings of the International Pipeline Conference, October, 2004.

²¹ Fraser, K.; Miroslav, K.; Jack, T; Worthingham, R.; A permeable coating model for predicting the environment at the pipe surface under CP-compatible coatings, IPC04-0368, Proceedings of the International Pipeline Conference, October, 2004.

Hydrogen is generated during cathodic protection at potentials more negative than the water reduction potential, which depends on pH as seen in equation 1 (the potential is referenced to the Cu/CuSO₄ reference electrode). At the pH values higher than 12.5 (which can be routinely found adjacent to a coating holiday on an adequately cathodically protected pipe), the pipe-to-soil potential should be more negative than -1,060 mV (CSE) for the water reduction to occur.

Experimental work by Yunovich and Tossey,²² which examined different types of external pipeline coatings (FBE, liquid epoxy and a three layer system) under varying different levels of cathodic protection) in three soil environments indicated that, under sufficiently high imposed CP current, hydrogen evolution could occur. The results from this study revealed that cathodic disbondment of all the tested coatings (all coatings have shown varying degrees of disbondment) increased with the applied cathodic current density in the range from 2 to 200 mA/ft² (2.15 to 215.3 μA/cm²), with the most damage skewed towards the high levels of imposed current. The off potentials were in the range from -0.9 V to -1.2 V (CSE). However, the results did not distinguish between the effect of pH and hydrogen.

Whether or not CD is caused by the chemical action of high pH or the physical action of gaseous hydrogen, there appears to be no danger of corrosion in the disbonded region in the short term, unless CP current is shielded by the coating or the CD region extends dramatically leading to lower polarization levels and insufficient CP conditions.

Different coatings respond differently to the same high CP potentials (i.e., exhibit different propensity to disbondment). Furthermore, it has been demonstrated that the surface preparation/surface contamination is crucial to the coatings' performance²³; therefore, the coatings of the older vintage may behave differently from the more recent applications.

Limits for Cathodic Protection

Potential Limits

The NACE Recommended Practice RP0169 stipulates a negative (cathodic) pipe-to-soil potential of at least 850 mV (CSE) for an adequate corrosion protection of underground steel and cast iron piping systems. Voltage-drops other than those across the structure-

²² Yunovich, M.; Tossey, B.; Effect of high CP potential on pipelines, reports 3189-01R, August, 2004.

²³ M.A. Kazemi et al, "Fusion Bonded Epoxy Pipe Coating: Preparation and Application make a Big difference", Journal of Protective Coatings and Linings, May 1992.

to-electrolyte boundary must be considered for a valid interpretation of this voltage measurement according to the RP0169 (i.e., the measured polarized potential should be an instant-off potential).

The RP in paragraph 6.2.2.2 indicates that in some situations, such as the presence of sulfide and bacteria, the criteria of -850 mV (or a minimum cathodic polarization of 100 mV) may not be sufficient. ISO 15589-1 Standard²⁴ requires a cathodic protection potential more negative than -950 mV (CSE) when anaerobic bacteria are present to control external corrosion.

The NACE recommended practice cited above does not include any specific limit to avoid consequences of overprotection. Also, it does not include specific potential requirements to account for sulfides, bacterial activity, high temperature, acid environments and galvanic coupling, although it mentions that the general criteria of -850 mV may not be enough. The document does point out the fact that excessive polarized potentials on externally coated pipelines should be avoided to minimize cathodic disbondment of the coating. Also it includes a precautionary note regarding polarized potentials that result in excessive generation of hydrogen. In the latter case, the NACE Recommended Practice states that these excessive potentials should be avoided in all metals, particularly high-strength steels.

The ISO 15589-1²⁴ establishes maximum and minimum cathodic potential limits, as a general guidance. The general criterion given in the ISO Standard is to polarize a buried pipeline to potentials which are more negative than -850 mV and less negative than -1,200 mV (CSE). The limit of -1,200 mV is recommended to prevent cathodic disbondment.

These values are consistent with general guidelines used in Peabody²⁵ "Control of Pipeline Corrosion"; the book refers, as a rule of thumb, to the use of an instant-off potential not more negative than -1,100 mV (CSE) to avoid coating disbondment.

Figure 1 summarizes the most relevant cathodic potential criteria; the figure includes criteria that also address concerns for the HRD. However, a 'one-size-fits-all' approach may not be appropriate for a specific application (a particular pipeline). For example, if conditions exist where an increased efficiency of hydrogen absorption may be expected

²⁴ INTERNATIONAL ISO STANDARD 15589-1 First edition Petroleum and natural gas industries - Cathodic protection of pipeline -transportation systems - Part 1: On-land pipelines.

²⁵ Peabody's Control of Pipeline Corrosion, Peabody, A.W., Second Edition, NACE International Corrosion Society, Houston, TX, 2001, p. 28.

or where a higher amount of hydrogen can be absorbed inside of the metal, additional consideration of the risks and benefits of applying a specific CP criterion is indicated.

It should be also emphasized that the reliance on the potential values alone may lead to underestimation of the hazards of overprotection. Thus, the results by Yunovich and Tossey²² show that, at high CP currents, the change in polarized potential is relatively minor, compared to a significant (ten-fold) increase in applied CP current density. Therefore, when considering the limits for CP, both potential and current limits should be taken into account.

An earlier work by Barlo and Fessler²⁶ suggested that there is a practical upper (most negative) limit on “true” (i.e., OFF-) potentials that exists on actual pipelines. The authors contend that the limit is approximately -1,150 mV (CSE) and its existence is associated with the potentials falling into the range of hydrogen evolution and the buildup of alkaline environment. Whether or not the potentials on the pipelines may indeed be bound by the quoted value is subject to debate; however, the work’s conclusions are consistent with the notion that monitoring CP current may be preferable to monitoring potentials when it comes to determining the hazards of overprotection.

Current Limits

In the ISO²⁴ standard, current density requirements are also presented as a general guideline for the design of CP systems. For the design of cathodic protection systems, this standard considers three levels of cathodic current densities for the various stages of live of the installation:

1. A high initial current density required to rapidly generate highly alkaline conditions at the protected metal surface and thereby promote the formation of calcareous deposits over a period of several months, reducing the current density requirements.
2. A mean current density which satisfy the long-term demand under stable conditions (up to 40 years).
3. A final current density because calcareous deposits are imperfect and do not provide sufficient protection.

²⁶ T.J. Barlo, RR. Fessler, “Interpretation of True Pipe-to-Soil Potentials on Coated Lines with Holidays”, Corrosion/83, Paper No. 292, NACE, Houston, TX, 1983.

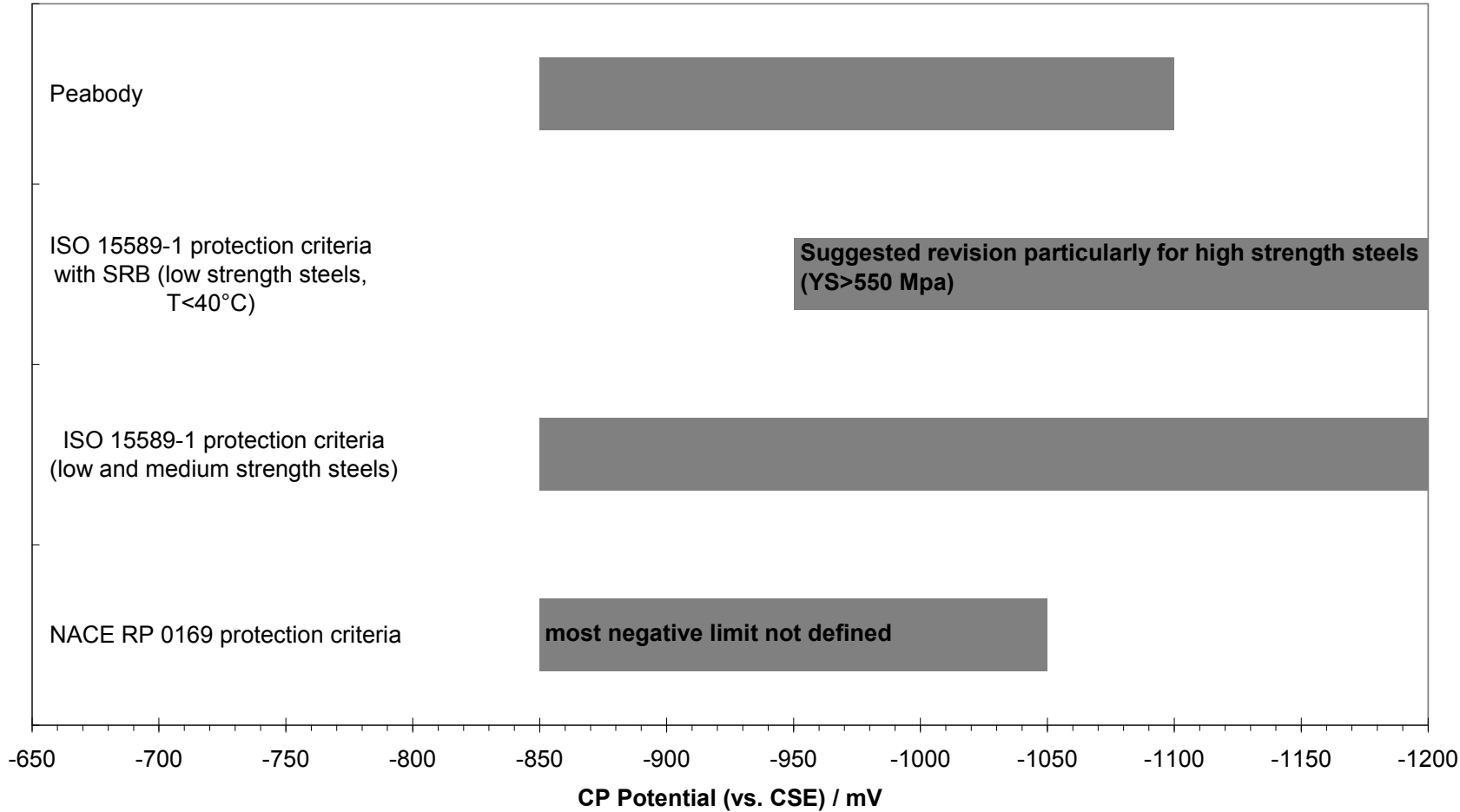


Figure 1. Summary of cathodic potential limits established by different standards and key literature.

The current requirements established in the ISO Standard²⁴ are as follows. The total current demand (I_{TOT} , in mA/m²) is defined as the product of the design electric current density for bare metal (J , in mA/m²), a coating breakdown factor (F_C , dimensionless), the outer radius of the pipe (r , in meters) and the pipeline length (L , in meters). The coating breakdown factor depends on the type of coating and design life as it is shown in **Error! Not a valid bookmark self-reference..**

Table 1. Design current density for coated pipe ($J F_C$) for steel in soils with various pipeline coating to be used in the design of CP systems for operating temperatures $\leq 30^\circ\text{C}$ according to the ISO standard²⁴

Pipeline coating	Design current density (mA/ft ²)		
	10-year design life	20-year design life	30-year design life
Asphalt/coal-tar-enamel Cold-applied tape	0.037	0.056	0.074
Fusion-bonded epoxy Liquid epoxy	0.037	0.056	0.084
3-layer epoxy-polyethylene 3-layer epoxy-polypropylene	0.007	0.009	0.037
<p>For a design life of more than 30 years, correspondingly greater factors should be used. It is assumed that pipeline construction and operation is carried out in such a manner that coating damage is minimized. For pipelines operating at elevated temperatures, the current density values shall be increased 25% for each 10°C rise in operating temperature above 30 °C. Alternative design current values may be used if reliable and properly documented. Current density requirements also depend upon oxygen content and resistivity of the soil.</p>			

Note: Consideration should be given to risk of the coating becoming disbonded during service life and the resulting possibility for corrosion due to shielding of the CP current.

Special case: Pipe collapse under repair sleeves

Full-encirclement steel sleeves are commonly used for onshore pipelines as a temporary or permanent repair of pipe anomalies. A typical sleeve consists of two half shells that are placed around the carrier pipe at the damaged area and after positioning, welded lengthwise. Depending on the type and severity of defect, the sleeves can be installed with or without circumferential fillet welding of the sleeve to the pipe (Type A and Type B sleeves, respectively).

Carrier pipe collapses (partial and full) under sleeve repairs have been objects of technical discussions²⁷ and investigations²⁸. These failures have been associated with various phenomena:

- (1) hydrogen gas accumulation in the annular space between the sleeve and the carrier pipe due to excessive cathodic protection (CP) – associated with Type B sleeves
- (2) abrupt de-pressurization in gas pipelines due to blow-outs (see example in Figure 2).
- (3) hydrogen stress cracking in hard spots under the sleeve repair due to corrosion (Type A sleeves);

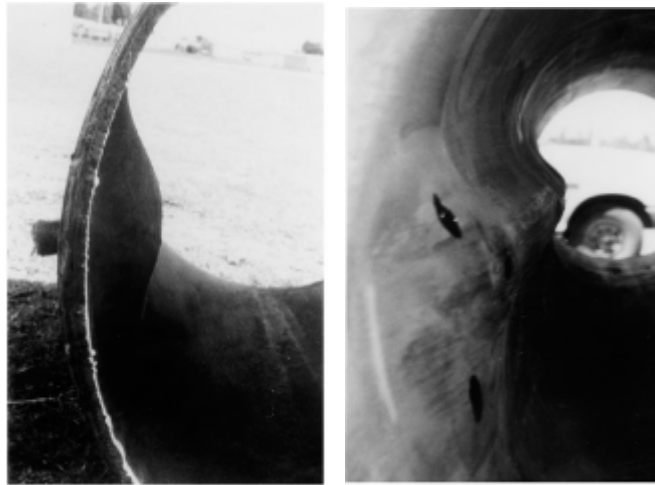


Figure 2. Pictures showing local collapse of API 5LX52 pipelines under the sleeve repair on a 600 mm diameter, 7.1 mm thickness gas pipeline²⁸.

At protection potentials more positive than -0.9 V (CSE), oxygen reduction is the predominant reaction; between -0.9 and -1.1 V, the rate of hydrogen production is comparable to that of oxygen reduction; at potentials between -1.0 to -1.2 V hydrogen production dominates the cathodic process. Formation of atomic hydrogen and its subsequent absorption in the steel leads to the next steps of diffusion through the metal and recombination of the atomic hydrogen (the form in which the hydrogen travels through the metal) into molecular, gaseous hydrogen either at ‘trap’ sites inside metal (inclusions), on the other side of the pipeline wall, or at other voids (which leads to the formation of hydrogen blisters).

²⁷ CCT private communications with pipeline operators

²⁸ Otegui J.L.1; Urquiza S.; Rivas A.; Trunzo A., Local collapse of gas pipelines under sleeve repairs, *The International Journal of Pressure Vessels and Piping*, Volume 77, Number 9, 1 August 2000 , pp. 555-566(12).

In the case of a sleeved pipe, diffusing hydrogen emerging in the sealed chamber formed between the sleeve and the carrier pipe will recombine forming hydrogen gas with a consequent pressure increase in the annular space (see Figure 3). Depending on the pressure differential between the operating pressure of the transport medium (P_2) and the pressure in the annular space under the sleeve (P_1), the carrier pipe can collapse. As is well-known, one of the proposed mechanisms of hydrogen cracking involves the development of extremely high hydrogen pressures (fugacity) at trap sites that exceeds the yield strength of the steel.

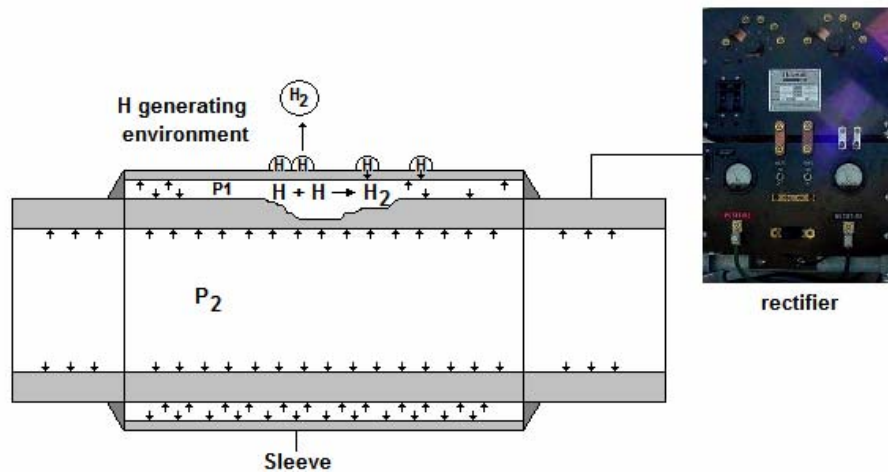


Figure 3. Illustration of hydrogen accumulation under Type B sleeve at high-CP conditions.

It is also feasible that excessive hydrogen pressure can lead to failure of Type A sleeves because of the failure of the epoxy seals at the ends of the sleeve. The ingress of the soil electrolyte under the sleeve will cause further corrosion of the repaired anomaly (or can cause cracking of a hard spot under the sleeve), as the sleeve will likely shield CP currents from the carrier pipe underneath.

Blowout

Blow outs that cause large gas losses and abrupt de-pressurization in gas pipelines²⁸ have also been linked to local collapses of pipe walls under full encirclement sleeve reinforcements (see Figure 4). The pressure in the annular space between the sleeve and the carrier pipe may not necessarily be exerted by hydrogen; it can be the result of a through wall penetration due to corrosion or a crack (see below) wherein the sleeve is acting as the main pressure boundary.

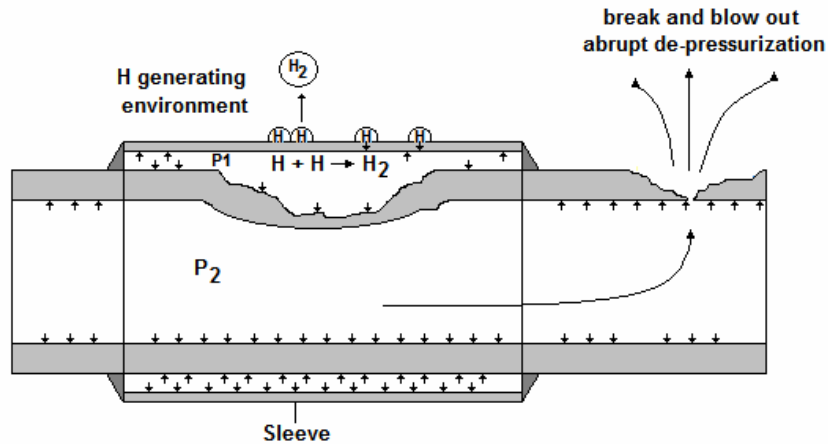


Figure 4. Illustration of collapse under sleeve after pipeline break and blow out.

Cracking

In pipelines with hard spots exceeding 35HRC²⁹, hydrogen absorption should be prevented. If a hard spot is found on an in-service pipe, one common repair method is to cover it with a protective metal sleeve. Failures of hard spots covered by Type A sleeves have been reported²⁷; the root cause of these failures was determined to be hydrogen-related cracking of the hard spot. If the fast-setting material often used in Type A repair sleeve fails and active corrosion initiates in the annulus, hydrogen stress cracking in the hard spot could eventually occur. If the gas in the pipeline leaks through the crack into the annular space, the pressure drop in the main line can cause a collapse under the sleeve (similar to the conditions illustrated in Figure 4).

Summary of Literature Review on Overprotection

The findings of the extended literature can be summarized as follows:

Coating damage at cathodically protected locations may not be an immediate threat to pipeline integrity because corrosion is mitigated. However, extensive areas of disbondment may be detrimental because of 1) increased current demand from the CP system (affecting current attenuation), 2) the possibility of corrosion occurring under disbonded coatings that CP might not protect, 3) inputting more hydrogen into the metal because of increased total current, and 4) exposing a hard spot that may be susceptible to hydrogen damage.

²⁹ Groeneveld, T.P., NG-18 Report No. 37, 1972 and American Gas Association Catalog No. L30174, 1979 in INGAA Report on Integrity Characteristics of Vintage Pipelines prepared by Clark, E.B; Leis, B.N.; and Eiber, R.J., 2004

Excessive CP can accelerate hydrogen flux through the steel, which can potentially cause partial or complete collapse of the carrier pipe inside a full encirclement repair sleeve, as suggested by several accounts. Under certain conditions, pipelines with hard spots can be susceptible of hydrogen-related cracking.

As a general guideline, CP current density of 2 mA/ft² may be offered as a target upper limit for cathodic protection. The current density can be monitored through the use of Coupon Test Stations. The cathodic current criteria are preferred to the potential-based criteria when evaluating the overprotection conditions. Cathodic current densities specified in the ISO Standard 15589-1 are similar.

As a general guideline, polarized potentials more positive than -1,200 mV (CSE) can be used as an upper-limit criterion to minimize cathodic disbondment and hydrogen-related damage to the steel.

Experimental modeling

Numerical modeling

Finite Element Modeling and Regression Analysis – ‘forward’ model

The distribution of potentials on and around a cathodically protected underground pipeline was modeled using finite element analysis (FEA). The modeling was done in conjunction with PHMSA-sponsored project contract No. DTPH56-06-T-0012.

FEA is a numerical technique for solving complex problems when no analytical methods are available. It involves subdividing a complex geometry into a number of simpler elements and nodes, which are referred to as a “mesh”. Physical properties are related to the elements and nodes by established mathematical equations. The equations governing each element are combined for all of the elements in the model to produce a series of simultaneous equations that is solved by a computer. FEA allows the potential and current distributions under a wide variety of conditions to be calculated quickly, despite the cumbersome mathematics involved. FEA can be used to quickly and efficiently calculate the expected ON and OFF potentials for a given combination of pipe dimensions, soil resistivity, defect size and location, and polarization behavior. By defining a matrix of parameters that are typical of conditions seen in the field, one can efficiently simulate a wide range of situations. The data produced can be analyzed statistically to identify the sensitivity of the various parameters to the measured ON and OFF potentials. If the mathematical relationships amongst the parameters can be described by an equation then there is a better understanding

of cathodic protection. The mathematical relationships can be determined by regression analysis. If the regression analysis is well-correlated, then the equation can be used to infer defect sizes and coating conditions from the measurable parameters. In effect, one can develop a useful mathematical tool to assist field crews in prioritizing dig sites.

The software used for the analysis was COSMOS/M from the Structural Research and Analysis Corporation (Version 2.8). The regression analysis performed was a multi-variable linear regression of the various parameters, to the calculated surface potential. No effort was made to derive a formal physically based equation. However, it was considered that there may be parameters correlated with each other. Some terms were multiplied together to produce combined terms, and these were also included in the analysis. The normalization scheme was also applied to the combined terms. The goal of the preliminary analysis was to identify which terms had a statistically significant effect on the regression equation.

Once the data were normalized, a preliminary regression analysis was performed. The correlation of each regression coefficient was calculated using established methods which are built-in functions of the Minitab software used for the analysis. The correlation statistics were used to determine which of the parameters are statistically significant, that is, which of the parameters can be mathematically shown to be relevant. These parameters were also ranked based on their significance. Once the key parameters were identified using the regression of the normalized parameters, a second regression was performed using the non-normalized data. In effect, the first regression is used to determine which parameters are relevant for the second regression. By normalizing, the second regression is not biased by the unequal ranges in the parameters.

The result of the second regression analysis was that six different terms were identified as being statistically significant;

1. Depth to Center x Resistivity. This is a combined term that includes the depth from the surface level to the centerline of the pipe times the resistivity of the soil.
2. Diameter x Resistivity. This is a combined term that includes the diameter of the pipe times the soil resistivity.
3. Defect Potential. This is the defect potential that is prescribed, effectively the OFF-potential.

4. Soil Resistivity. This is expected to have a significant effect on all of the calculated values.
5. Potential Difference. This is the difference between the prescribed defect (OFF-) potential and the prescribed coating potential.
6. Defect Size. This term was simply based on the number of nodes used to define the defect. As discussed above it does not scale linearly with defect area, due to current density and symmetry effects.

The results suggest that numerical model adequately described most of the first order effects between defect geometry, soil related parameters, and CP potentials. On the basis of the model-generated values, a regression analysis-derived relationship of the pipe/soil characteristics and ON potentials was established. The regression equation indicates that the impedance (soil resistivity and defect geometry) dominates the relationship.

However, the relationship between the at-grade potential measurements and the actual at-pipeline depth conditions is complex. On a real-life “macro” system, such as a buried pipeline, the modeling assumption that the holidays represent isolated breaches in an otherwise perfect external coating is not going to be universally applicable. There are variations of soil chemistries and soil particle sizes, which can be considerable even over a short distance along the pipe; these differences can affect not only the impedance characteristics of soil, but polarization behavior of the steel exposed through holidays. The effect is greater in the high resistance soils. Given that the potential gradients are so highly localized near the defects, it is not reasonable to assume a simple mathematical relationship amongst depth of cover, soil resistivity and potential difference. In effect, the IR-drop calculations cannot assume a linear relation, and any conclusions drawn from a simple inspection of the data must be made with caution. The IR-drop arguments are inherently valid, but do not describe the *complete relationship* of the various parameters that affect the ON and OFF potentials.

Reverse model

The reverse model output was evaluated using the results generated by the University of Florida CP3D model (Riemer and Orazem^{30, 31}). The model

³⁰ D. Riemer and M. E. Orazem, “Development of Mathematical Models for Cathodic Protection of Multiple Pipelines in a Right-of-Way,” Proceedings of the 1998 International Gas Research Conference, San Diego, November 8-11, 1998.

evaluated the capability of the common ECDA techniques to size the holidays on the surveyed pipe.

The graph in Figure 5 shows the correlation between the flaw (holiday) size and the DCVG signal strength.

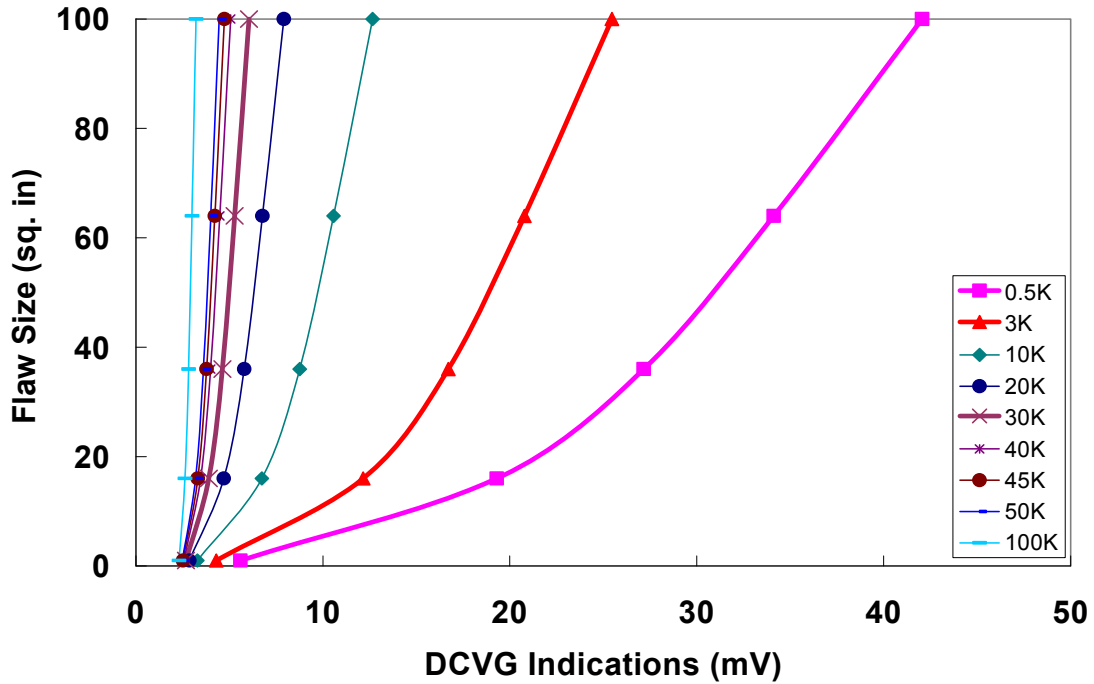
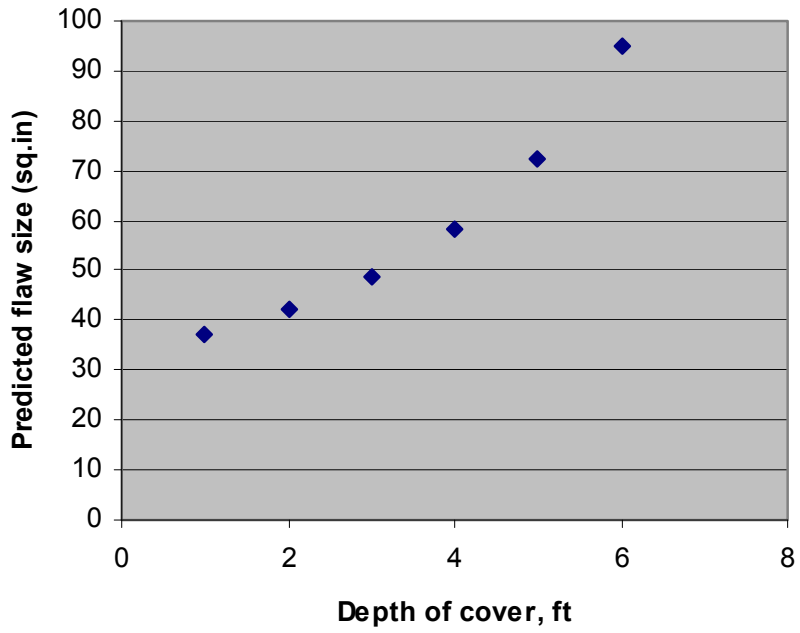
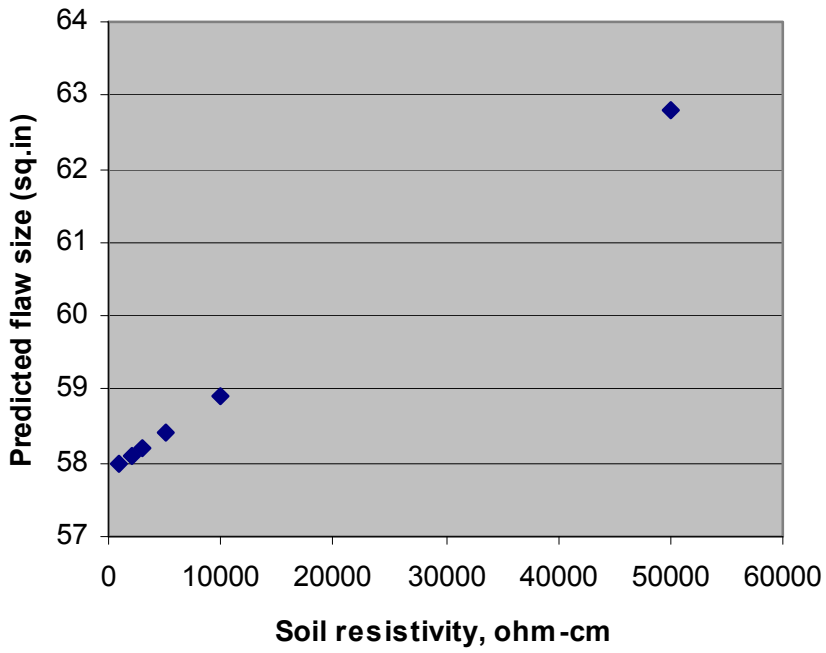


Figure 5. Predicted flaw size vs. DCVG signal strength (CP3D model). Cases for several soil resistivities are shown.

The model suggests that for a fixed input voltage for a DCVG measurement, the larger indications are likely to produce a larger response during measurements (for the same soil resistance conditions). Similarly, the higher the soil resistance, the lower the DCVG signal for the same size flaw in the coating. This is consistent with the forward model observations.

Similar trends are shown for the predictive results based on the CIS parameters (ON, OFF potentials and the IR drop). Some of the trends are presented in Figure 6.

³¹ D. P. Riemer and M. E. Orazem, "Models for Cathodic Protection of Multiple Pipelines with Coating Holidays," Cathodic Protection: Theory and Applications, M. E. Orazem, editor, NACE International, Houston, Texas, 1999.



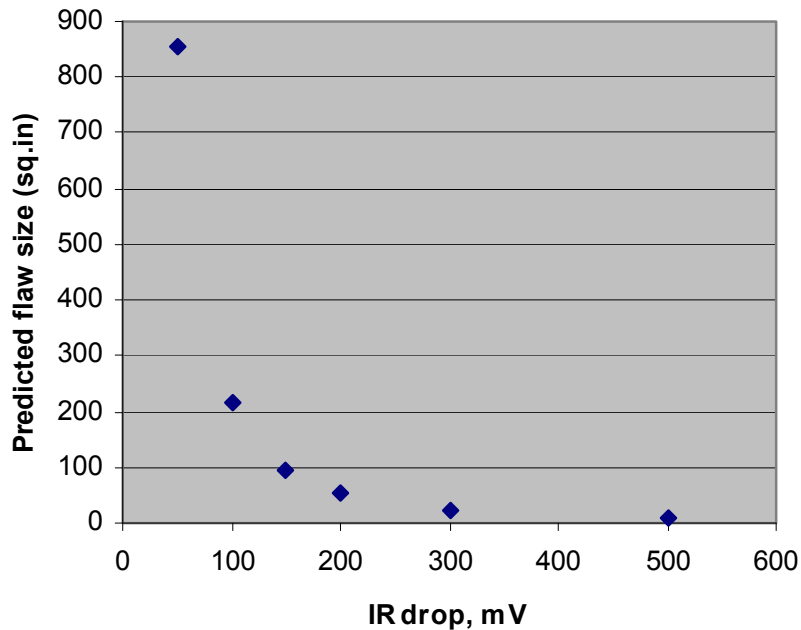


Figure 6. Predicted flaw size vs: soil resistivity (top), depth of cover (middle), IR drop away from the anomaly (bottom).

The trends show that for the same depth of cover and potential distribution, the holiday size scales linearly with soil resistivity (the greater the soil resistivity, the greater the defect to maintain the same IR drop). However, the soil resistivity effect, according to the model, is modest.

Likewise, as the depth of cover increases (as so does the overall impedance – keeping the soil resistivity the same), so does the defect size. In keeping with the same logic, the greater the IR drop, the smaller the defect size with all the other parameters remaining the same.

Conclusions

Both forward and reverse model outputs point to the same factors that define the potential distribution on top of the grade – specifically, soil-related variables (soil resistivity, depth of cover) and pipe-related characteristics (flaw size and defect potential).

AC corrosion

The approach to AC corrosion-related modeling was different. As noted earlier, the available sophisticated numerical models were found not to be suitable for evaluating the effects of AC current on at grade distribution of AC voltages. The software commercially offered by PRCI (AC Predictive and Mitigation

Techniques, Catalog No. L51835) was evaluated with regard to predicting AC current density at the coating flaw. The input values were provided by the results of the laboratory-based experiments. The modeling results are therefore discussed later in the report (see page 99).

Laboratory experiments

The laboratory experiments focused on modeling the major effects identified by the numerical simulation, such as soil resistivity and its effects on polarization and measured potential distribution.

Setup

Laboratory-based modeling used a small (sized approximately 20 by 12 by 12 inches) cell. The cell accommodates an assembly made of several segments of 2 inch diameter steel pipe coated with liquid epoxy coating. The total length of the assembly is approximately 16 inches. The assembly included three sections with an intentionally introduced defect (6 mm diameter). Each of the sections was electrically isolated from each other. A 'dummy' section was inserted between the first and the second sections to provide axial separation.

The schematic of the assembly is shown in Figure 7; the construction of the segments is illustrated in Figure 8.

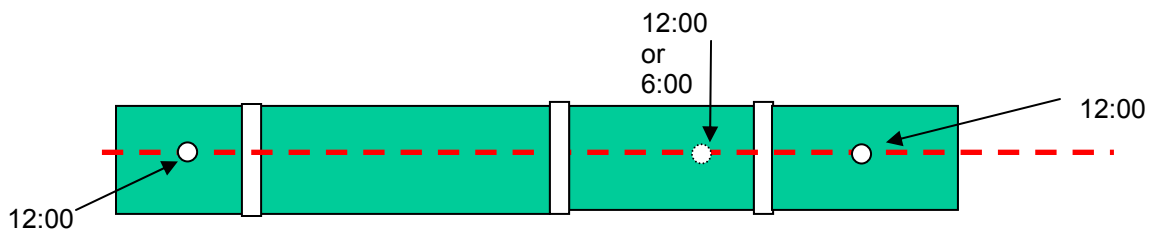


Figure 7. Schematic of the test configuration

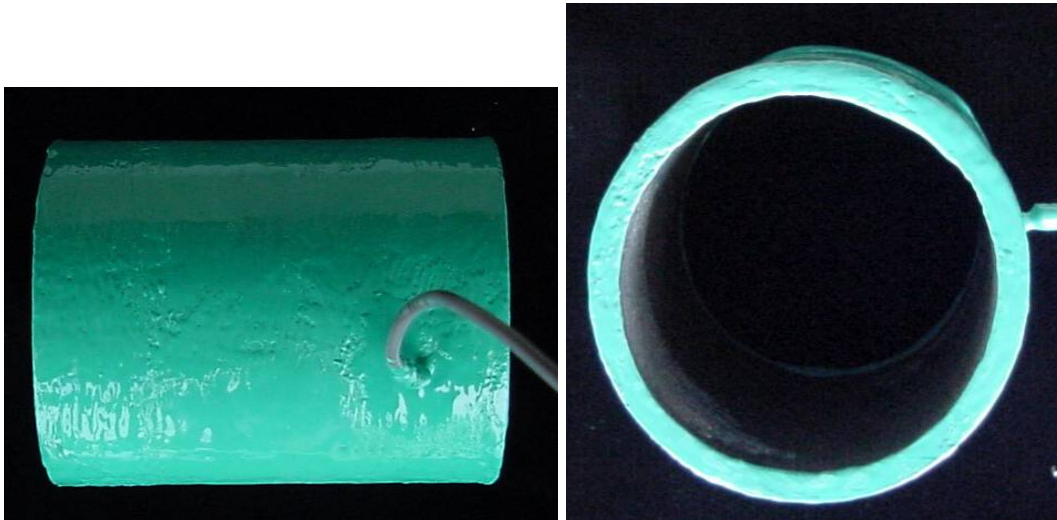


Figure 8. Pipe segments showing the external coating and electric lead.

Defect 1 was located at approximately 7 inches from the left edge of the cell at 12:00 o'clock position; Defect 2 was located approximately 15 inches from the left edge at either 12:00 o'clock or 6 o'clock position; Defect 3 was located approximately 2 inches further to the right at 12:00 o'clock position.

The size of the cell allows testing of various depths of cover, investigating the effect of the inclined pipe position, and researching the impact of different types of soil when the pipeline traverses two different soil strata.

The photographs of the pipe segments, the actual cell with the pipeline assembly are shown in Figure 9 and Figure 10. The cell was covered with a lid with a network of approximately 280 equally spaced holes, such that a reference electrode position can be consistent. In addition to the pencil-shaped copper/copper sulfate reference electrodes, the potentials of the defects could be measured with the help of platinized niobium wires placed in close proximity to the defect surface. The platinized wire maintains a relatively stable potential and thus can be used a pseudo-reference electrode. The potential of the wire can be then measured against the standard CSE and convert the potential values measured with regard to Pt to the CSE scale.

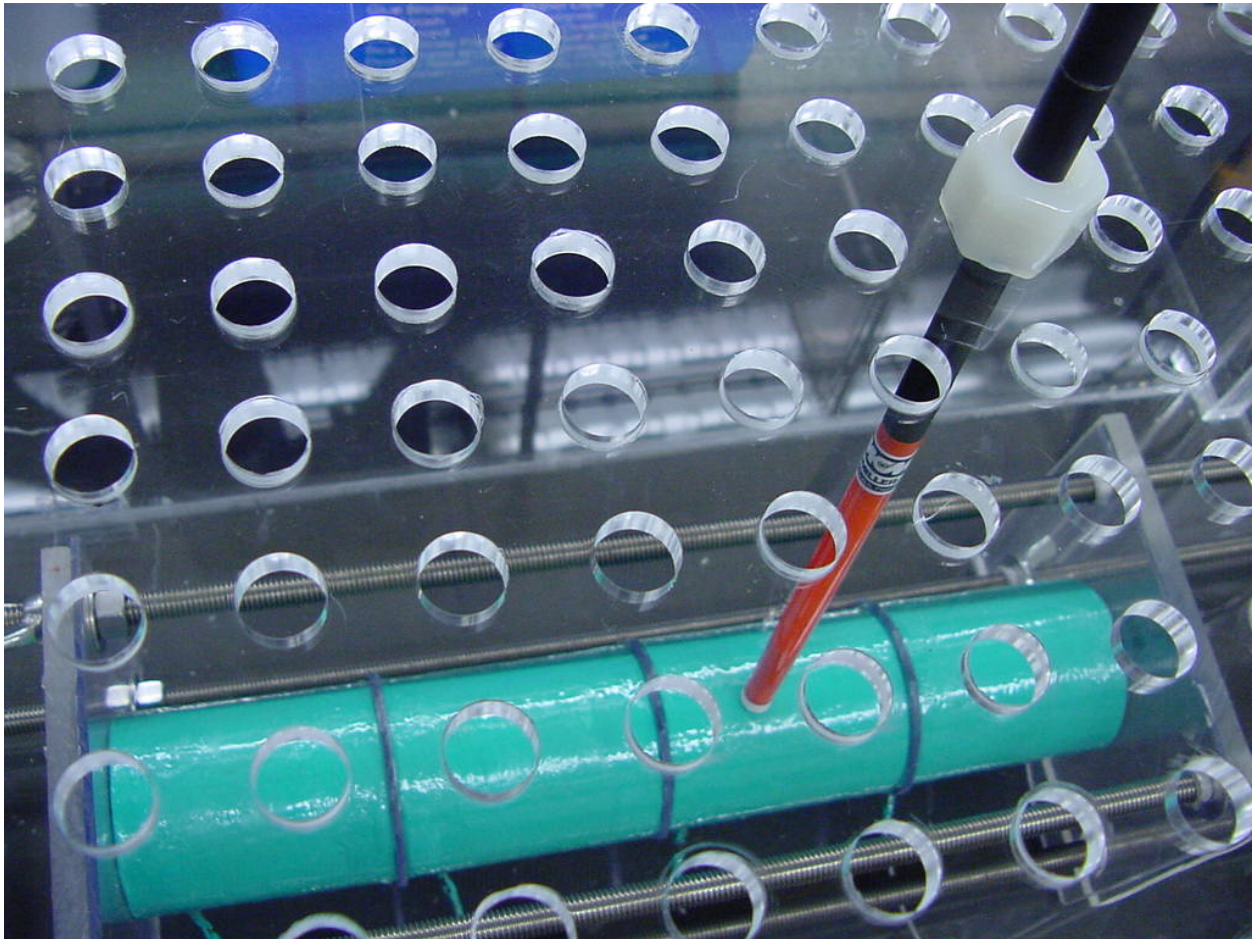


Figure 9. The pipe assembly inside the cell; the reference electrode is fed through the hole in the lid.

This configuration of the cell and the pipe assembly also permits flexibility in the approach to polarizing the pipeline segments to different potentials in order to simulate the conditions occurring on actual pipelines on a smaller scale, but with realistic parameters. The polarization was accomplished via the use of a potentiostat and variable resistors to adjust the currents to each of the segments.

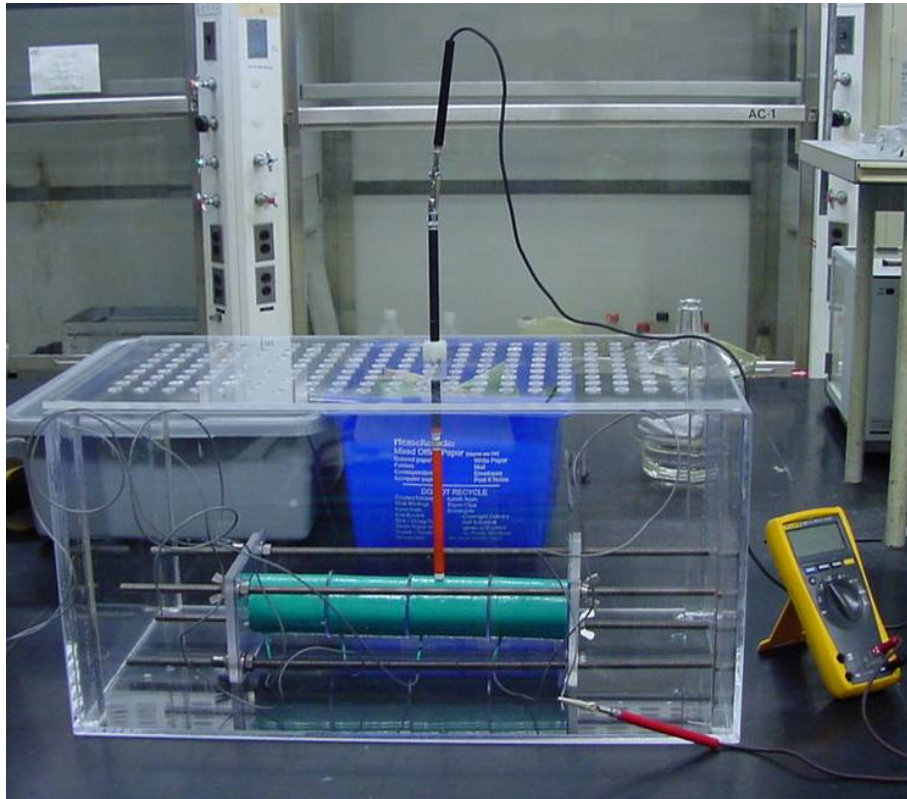


Figure 10. General view of the experimental cell and the pipe assembly.

The experimental work started with preliminary runs in the cell filled with tap water. After the water-based tests, the cell was filled with sand and clay, such that each type of soil occupied approximately half of the volume. Defect 1 was located in clay, and Defects 2 and 3 (at the 6:00 and 12:00 position, respectively) were backfilled with sand. Both sand and clay were moistened with water. The depth of cover for the pipe assembly was approximately 2 inches. The photographs in Figure 11 and Figure 12 depict the setup.

The resistivity of sand was considerably higher than that of clay (approximately 74,000 ohm-cm for sand and 90 ohm-cm for clay). The CP anode was located closer to Defect 1, in the sand portion of the cell.

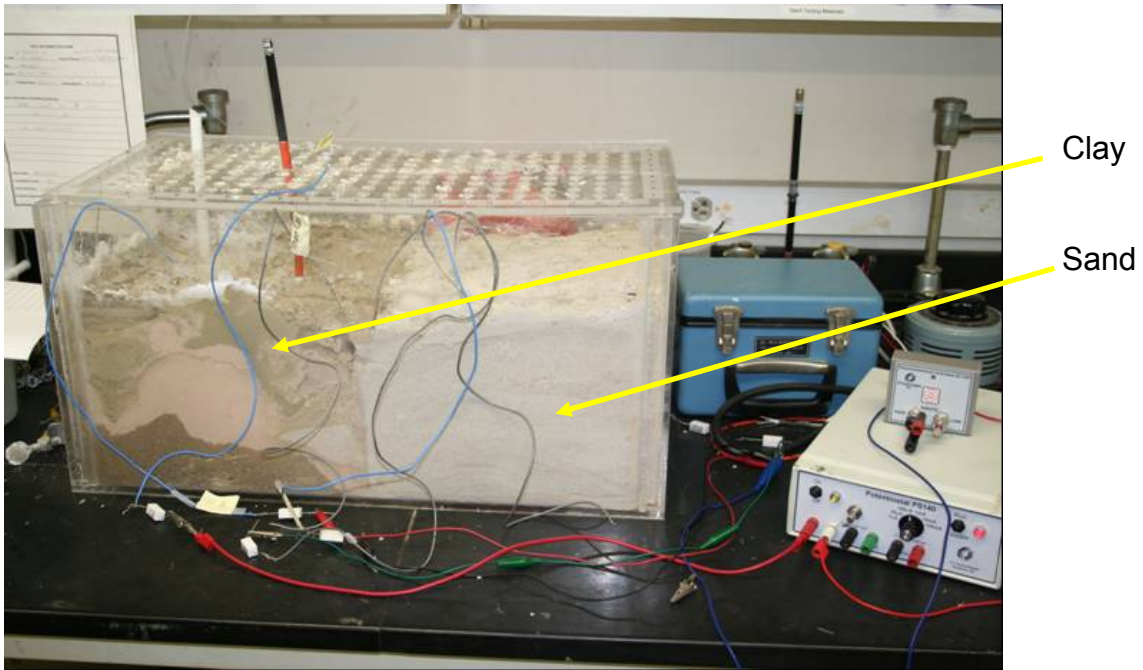


Figure 11. Small cell filled with clay and sand.

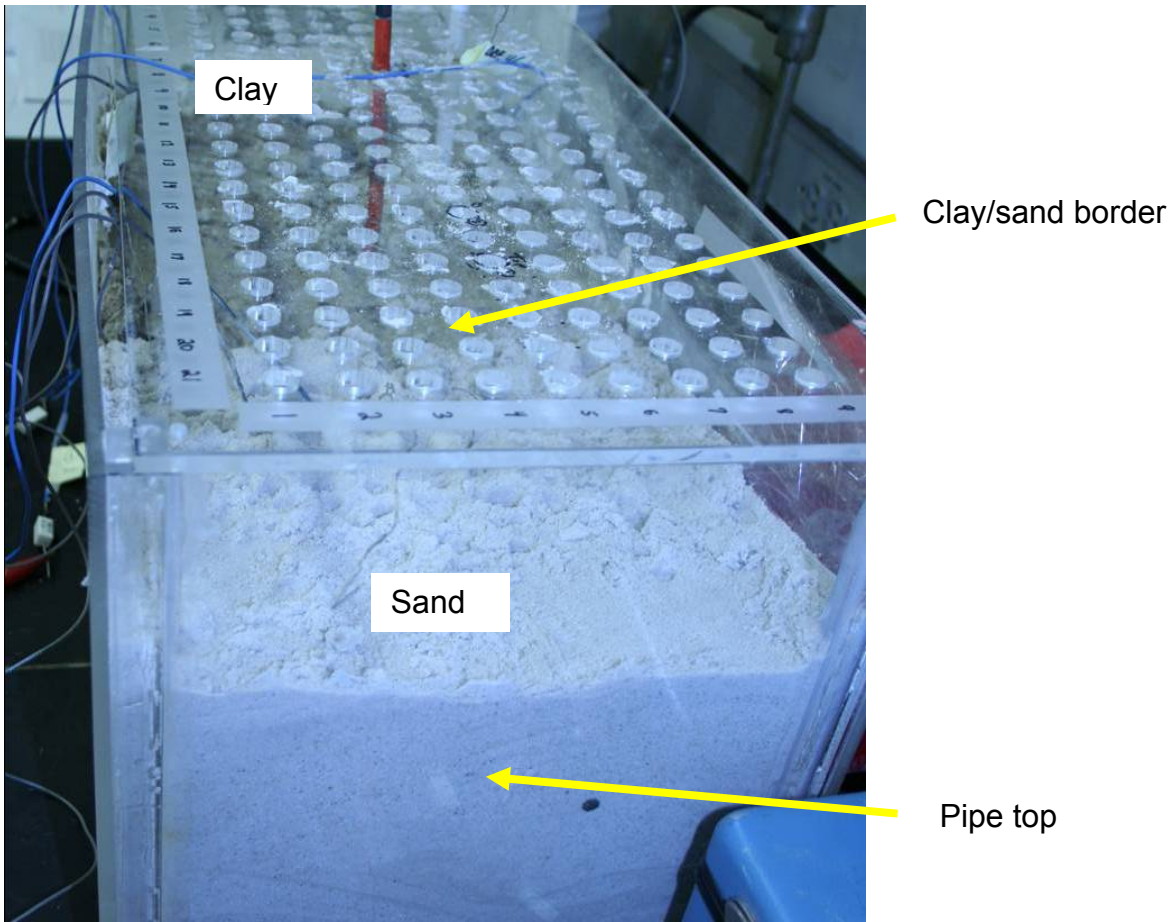


Figure 12. Small-cell experimental setup.

When all three Defects were switched in (i.e. were connected electrically for some of the measurements), given the differences in the specific resistance between sand and clay, the distribution of current to the Defects varied, with Defect 2 (6 o'clock position, closer to the clay/sand border), receiving most of the current.

DCVG – baseline readings

Direct Current Voltage Gradient (DCVG) measurements on this much-reduced scale were initially performed to establish the baseline readings for the specific defect configuration. The following is a description of the experiments performed.

Case 1: Anode positioned at $x=6$, $y=9$; $i = 0.931$ mA DC

Figures 2-5 illustrate the results obtained for the above conditions. 'On' and 'off' potentials were measured using Cu-CuSO₄ electrodes. Figure 2 shows the variation in equipotential field lines associated with the anode. Given the width of the field, the relatively small distance between the anode and the pipe assembly illustrates the limitations of the small cell regarding achieving 'remote earth'. This result should be considered when interpreting Figures 3-5. The resolution of defects may be limited as interference from the anode will affect the DCVG measurements. Figure 3 indicates relatively ambiguous location of the defect nearest the anode. Though a change in sign of the on-off potentials is observed on either side of the defect in the x-direction, there is no significant change in readings from $x=8$ to $x=13$. Resolution in the y-direction is again limited by a lack of significant change in measurements from $y=4$ to $y=1$. It would appear that the defect is located somewhere between $y=6$ and $y=1$, though it is difficult to interpret much further. Figure 4 shows very good resolution of Defect 2 in the x-direction (this is indicated by the change in sign of the on-off measurement on either side of the defect in the x-direction) as well as relatively good resolution in the y-direction. This defect is the most identifiable within this group of measurements. Figure 5 accurately depicts Defect 3 in terms of changing magnitude of the measurements in both the transverse and longitudinal directions.

Case 2: Anode positioned at $x=6$, $y=9$; $i = 0.118$ mA DC

Figures 6-9 depict the results obtained for the above conditions. All conditions are the same as for the case 1 measurements, with the exception of the current which has been reduced by approximately 1 order of magnitude in an attempt to enable better resolution of the defects with DCVG. However, decreasing the current resulted in increasing uncertainty of defect locations. From the data in

Table 5, it appears that a defect likely exists somewhere between $x=7$ and $x=8$ and between $y=6$ and $y=4$. This is indeed fairly accurate. The problem, however, is that these differences in readings are so slight (1/10 of 1 mV) that they could quite easily be seen as 'noise' in the data. Defect 2 is not clearly resolved. The measurements in the x-direction actually indicate a large defect spanning from $x=15$ to $x=20$ (as determined by the change in sign of the potential measurements). This is likely a result of Defect 3 being in proximity to Defect 2. The y-location of the defect is also unclear. The detection of Defect 3 is very similar to case 1. Changes in magnitude in both the x and y directions seem to indicate the presence of a defect, though the resolution in both directions is arguably less clear due to very small changes in magnitude at positions immediately surrounding the defect.

Case 3: Anode positioned at $x=1$, $y=9$; $i = 1.217$ mA DC

Figures 10-13 depict the results obtained for the above conditions. Upon inspection of results from cases 1 and 2, it was observed that more definitive results could be seen at a higher current. Thus the purpose of this series of measurements was to investigate the effects of the position of the anode. The anode was moved to the most remote location possible within the geometric confines of the soil box to try to obtain the "remote earth" relationship between the anode and the pipe. Investigation of Defect 1 yielded the same x-direction results as case 1 but a slightly larger change in magnitude of the measurements in the y-direction. This can be seen by comparing Table 10 with Table 2. Defect 2 again exhibits smeared resolution in the x-direction (similar to cases 1 and 2) but also shows enhanced resolution in the y-direction. Investigation of defect 3, like Defect 2, shows uncertain x-location of the defect but clearly depicts the y-location of the defect.

From the above results it the effects of current and anode location can be seen. Larger currents and increased distance between the anode and the pipe result in an increase in accuracy of defect detection. In all cases, resolution of Defects 2 and 3 in the x-direction presents a challenge. The defects seem to combine to create data which appear to indicate one larger defect. Increasing the distance between the anode and the pipe appears to improve this resolution.

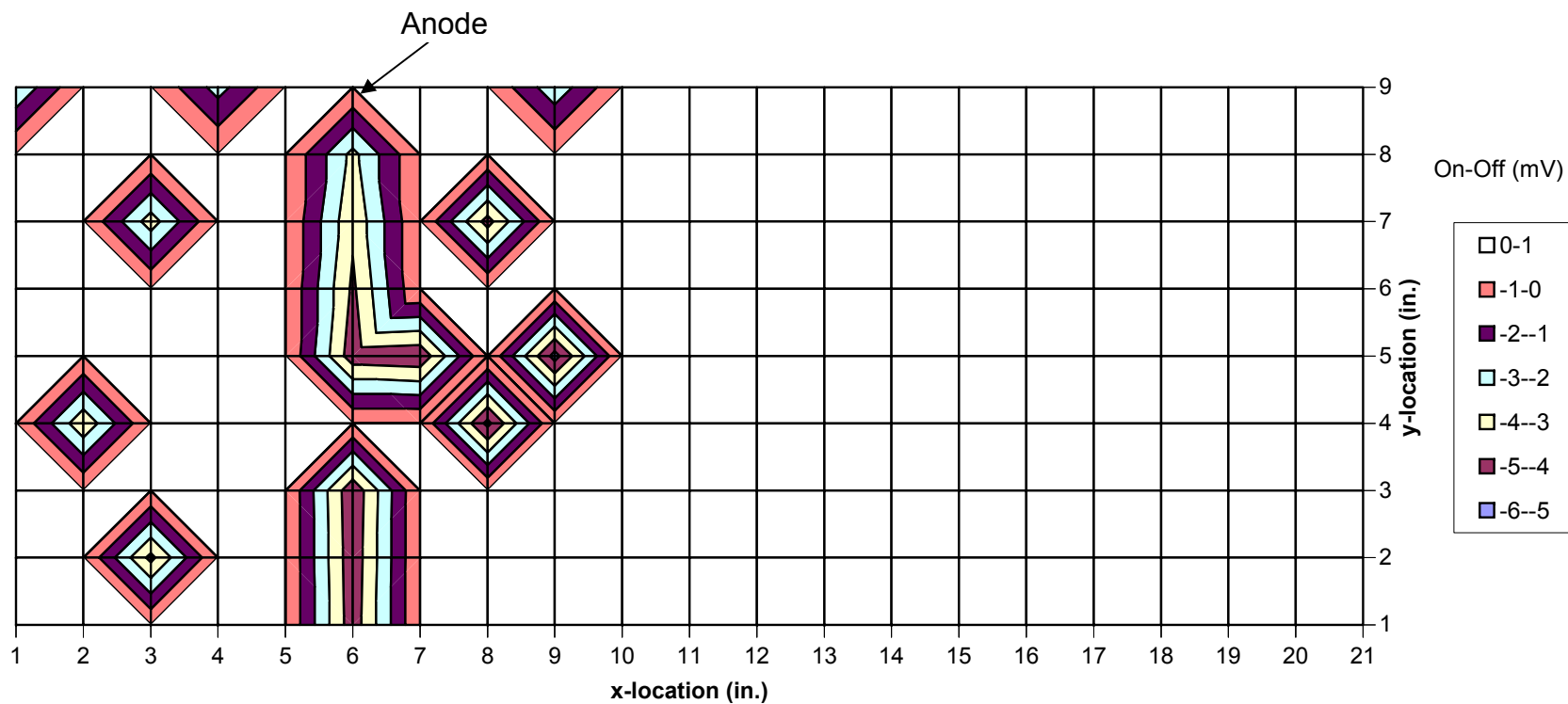


Figure 13. Contour plot of DCVG measurements near anode, $i = 0.931$ mA DC with anode positioned at $x=6, y=9$.

Table 2. Corresponding data for Figure 13 with (+) representing the position of the anode.

	1	2	3	4	5	6	7	8	9	10	11	12	13	14	15	16	17	18	19	20	21
9	-2.9			-2.4		+			-2.7												
8						-3.3															
7			-3.5			-3.8		-4.4													
6						-4.2															
5						-4.6	-4.8		-5.4												
4		-3.8						-5.3													
3						-4.8															
2			-4.3			-4.7															
1						-4.6															

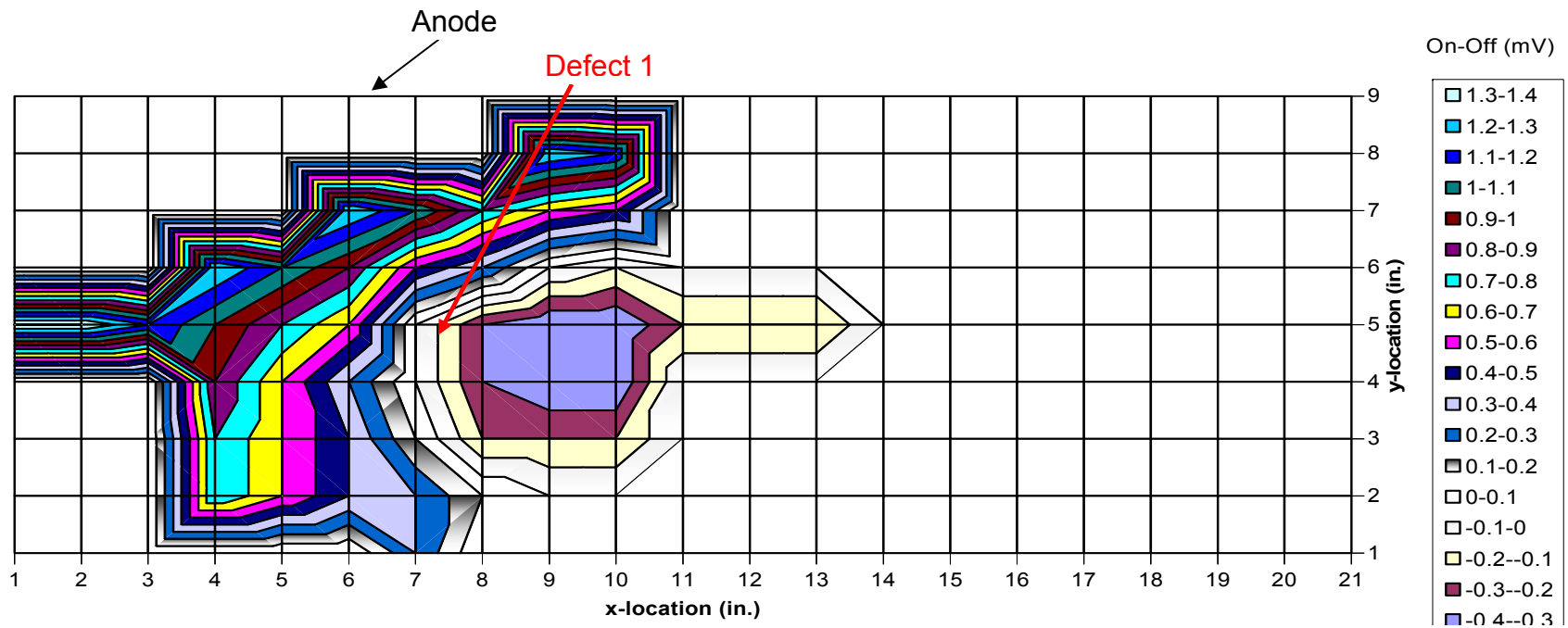


Figure 14. Contour plot of DCVG measurements near Defect 1 (Case 1).

Table 3. Corresponding data for Figure 14 with (*) representing defect and (+) representing anode.

	1	2	3	4	5	6	7	8	9	10	11	12	13	14	15	16	17	18	19	20	21
9						+															
8									1.3	1.2											
7						1.3	1.1	0.8	0.6	0.5											
6				1.3	1.1	0.9	0.5	0.3	0	-0.1											
5	1.4	1.4	1.2	1	0.8	0.6	*	-0.3	-0.4	-0.4	-0.2	-0.2	-0.2								
4				0.9	0.6	0.3	0	-0.3	-0.4	-0.4											
3				0.8	0.6	0.4	0.1	-0.2	-0.2	-0.2											
2				0.8	0.6	0.4	0.3	0.1	0	0											
1							0.3														

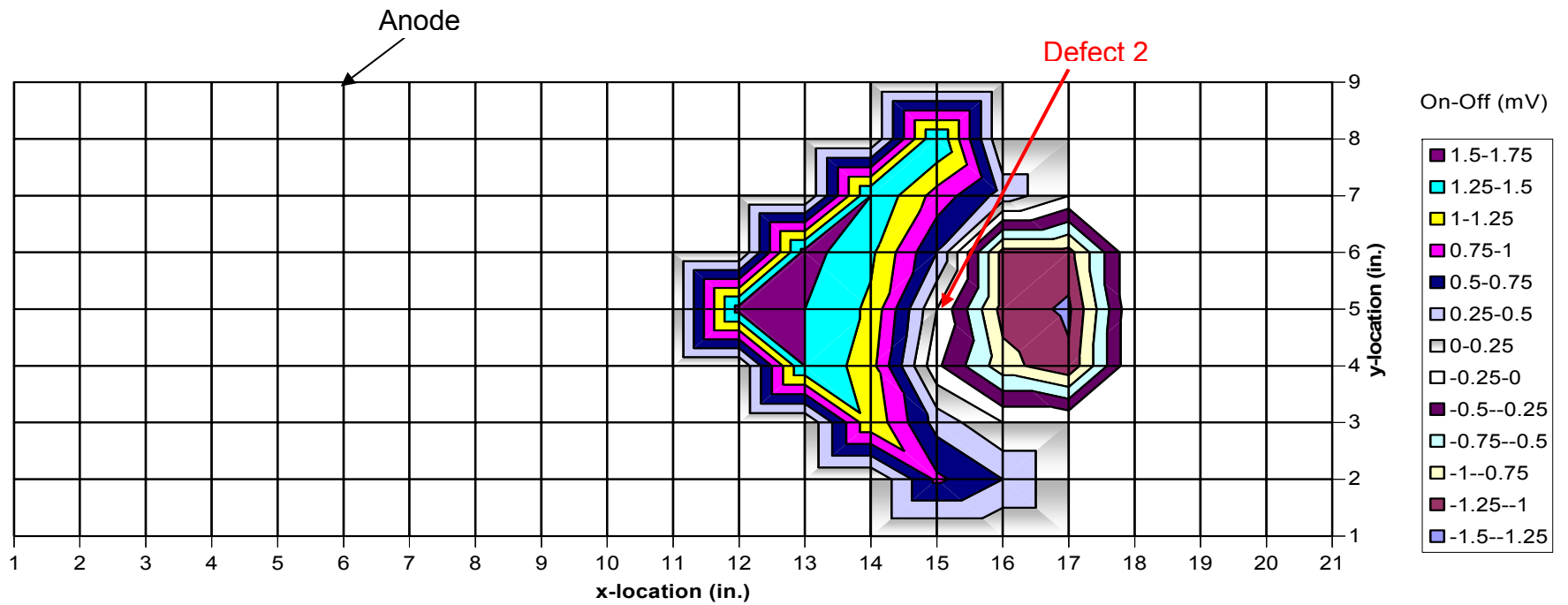


Figure 15. Contour plot of DCVG measurements near Defect 2 (Case 1).

Table 4. Corresponding data for Figure 15 with (*) representing defect and (+) representing anode.

	1	2	3	4	5	6	7	8	9	10	11	12	13	14	15	16	17	18	19	20	21
9						+															
8															1.5						
7														1.5	0.9	0.4					
6													1.6	1.3	0.5	-1.1	-1.1				
5												1.6	1.5	1.2	*	-1.1	-1.3				
4													1.5	1.1	-0.2	-0.9	-1.2				
3														1.2	0.4	0					
2															0.8	0.5					
1																					

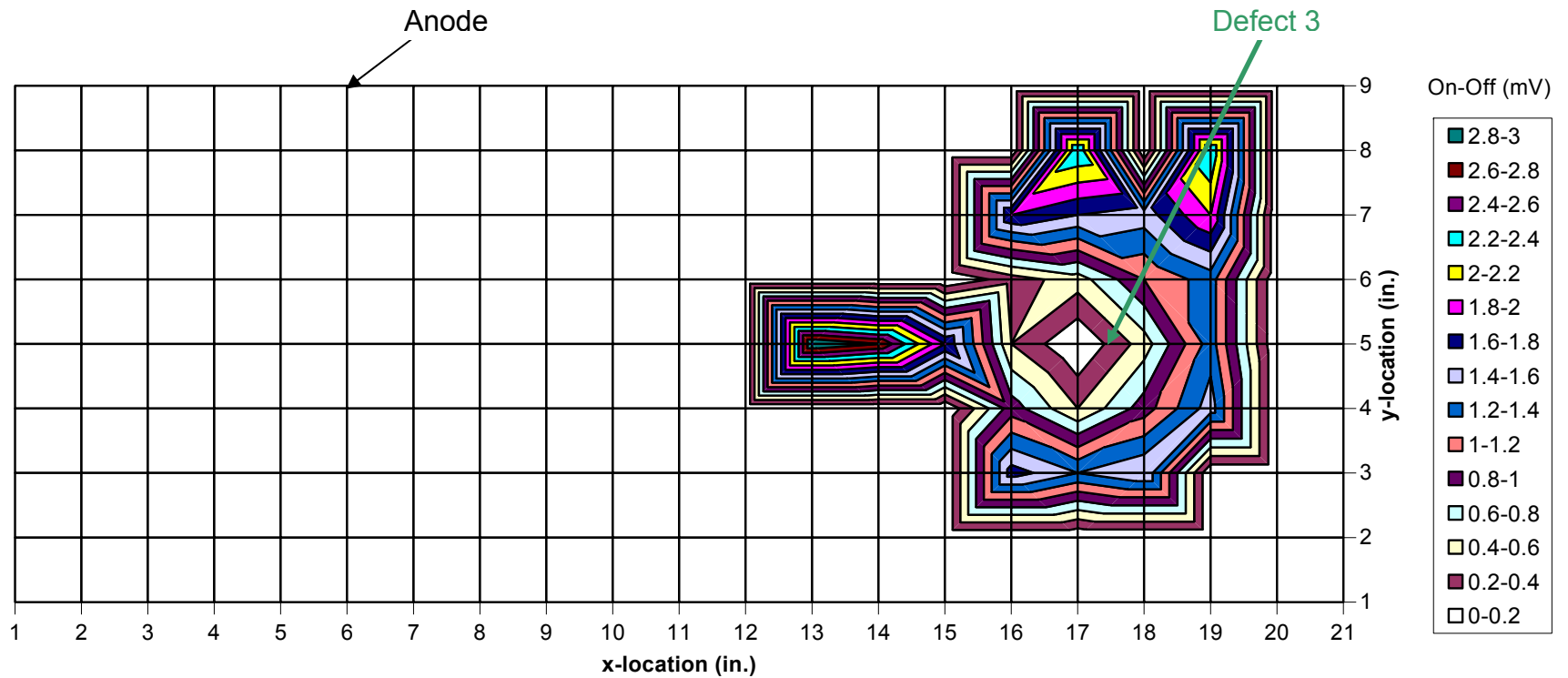


Figure 16. Contour plot of DCVG measurements near Defect 3 (Case 1).

Table 5. Corresponding data for Figure 16 with (*) representing defect and (+) representing anode.

	1	2	3	4	5	6	7	8	9	10	11	12	13	14	15	16	17	18	19	20	21
9						+															
8																	2.4		2.4		
7																1.8	1.6	1.5	2		
6																0.3	0.5	1	1.3		
5												3	2.8	1.8	0.4	*	0.5	1.3			
4																0.9	0.4	0.9	1.5		
3																1.7	1.4	1.6			
2																					
1																					

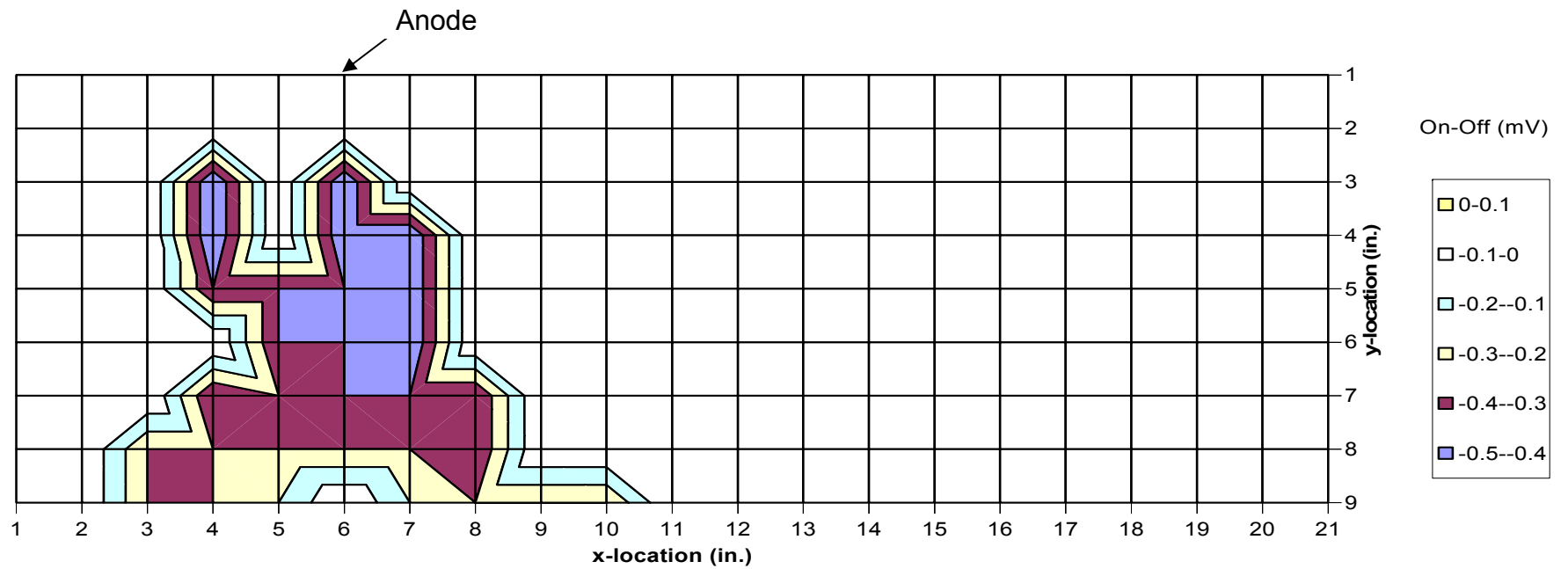


Figure 17. Contour plot of DCVG measurements near anode, $i = 0.118$ mA DC with anode positioned at $x=6, y=9$.

Table 6. Corresponding data for Figure 17 with (+) representing the anode.

	1	2	3	4	5	6	7	8	9	10	11	12	13	14	15	16	17	18	19	20	21
9			-0.3	-0.3	-0.2	+	-0.2	-0.3	-0.3	-0.3											
8			-0.3	-0.3	-0.3	-0.3	-0.3	-0.4													
7				-0.4	-0.3	-0.4	-0.4	-0.4													
6					-0.4	-0.4	-0.5														
5				-0.4	-0.4	-0.4	-0.5														
4				-0.5		-0.5	-0.5														
3				-0.5		-0.5															
2																					
1																					

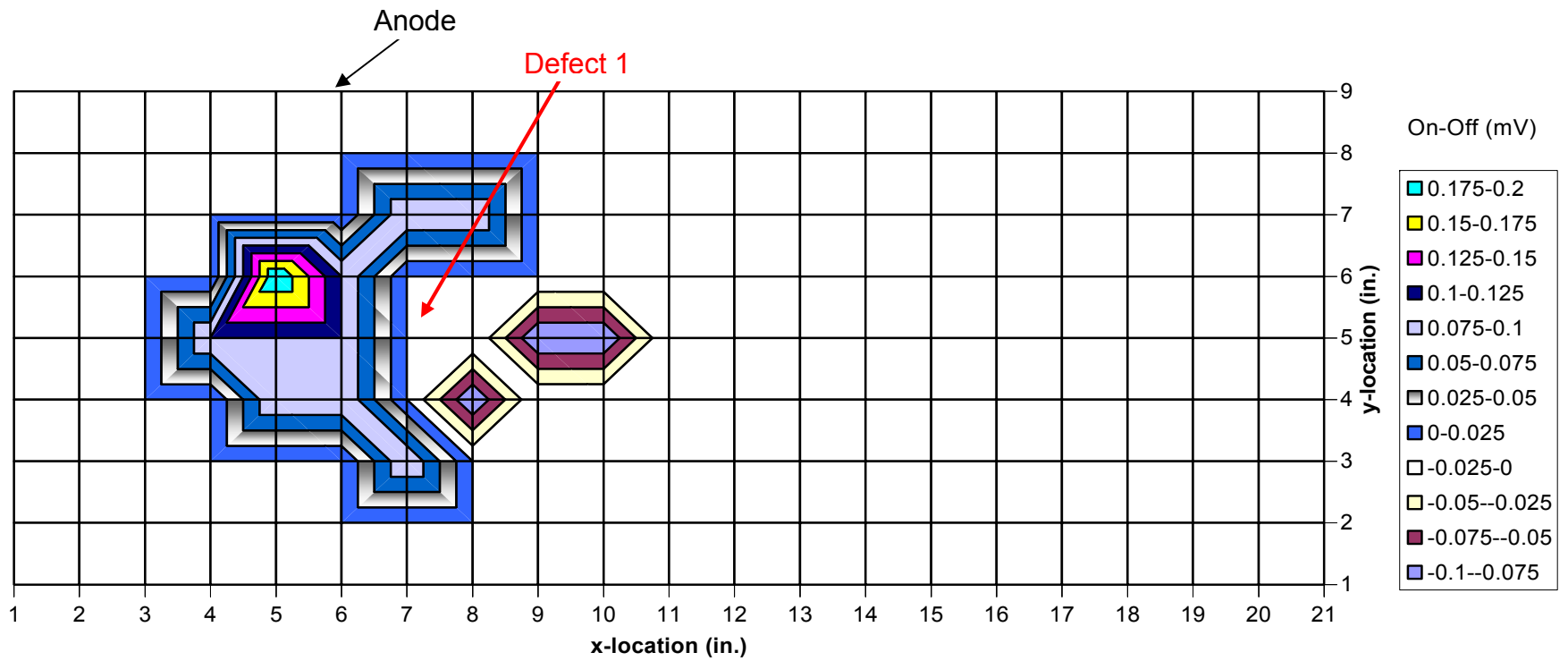


Figure 18. Contour plot of DCVG measurements near Defect 1 (Case 2).

Table 7. Corresponding data for Figure 18 with (*) representing defect and (+) representing anode

	1	2	3	4	5	6	7	8	9	10	11	12	13	14	15	16	17	18	19	20	21
9						+															
8																					
7							0.1	0.1													
6					0.2	0.1	0	0	0												
5				0.1	0.1	0.1	*	0	-0.1	-0.1											
4					0.1	0.1	0	-0.1	0												
3						0	0.1	0	0												
2																					
1																					

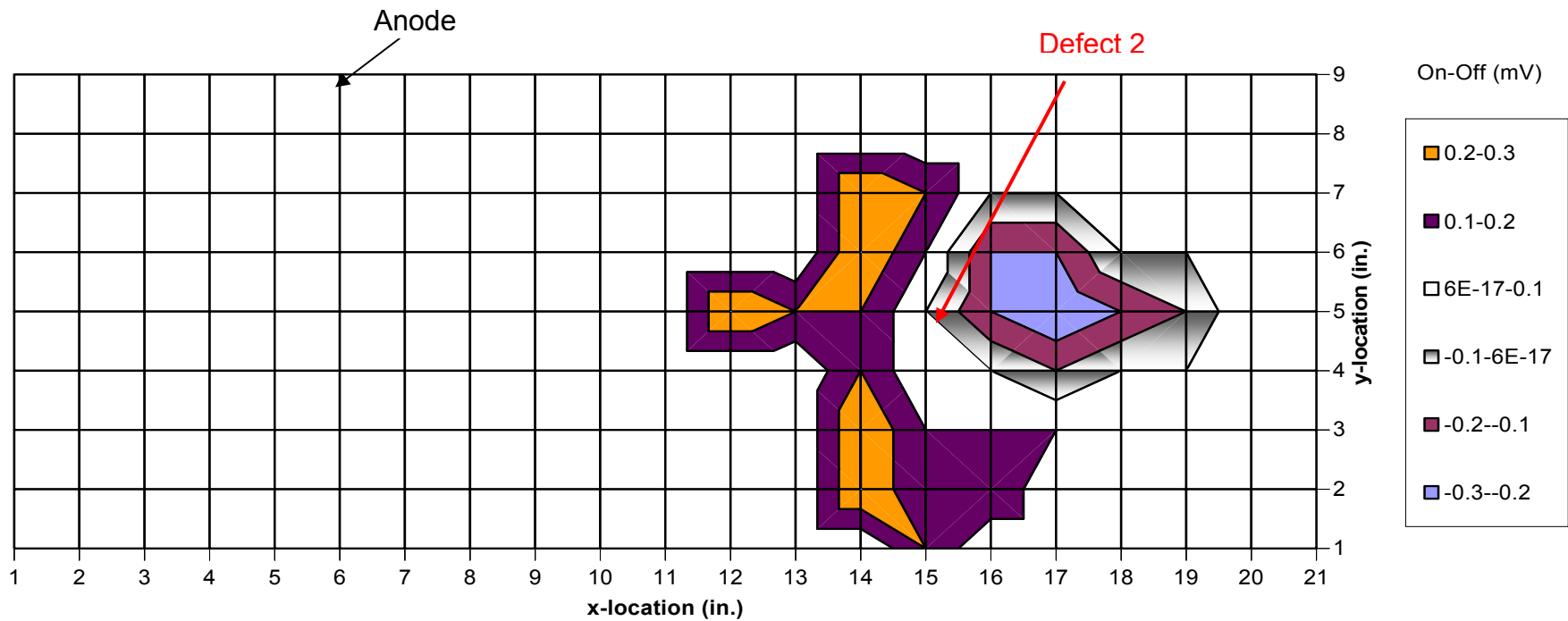


Figure 19. Contour plot of DCVG measurements near Defect 2 (Case 2).

Table 8. Corresponding data for Figure 19 with (*) representing defect and (+) representing anode.

	1	2	3	4	5	6	7	8	9	10	11	12	13	14	15	16	17	18	19	20	21
9						+															
8																					
7														0.3	0.2		0				
6														0.3	0.1	-0.2	-0.2				
5												0.3	0.2	0.2	*	-0.2	-0.3	-0.2	-0.1	0.1	0.1
4														0.2	0	0	-0.1				
3														0.3	0.1	0.1	0.1				
2														0.3	0.1	0.2					
1															0.2						

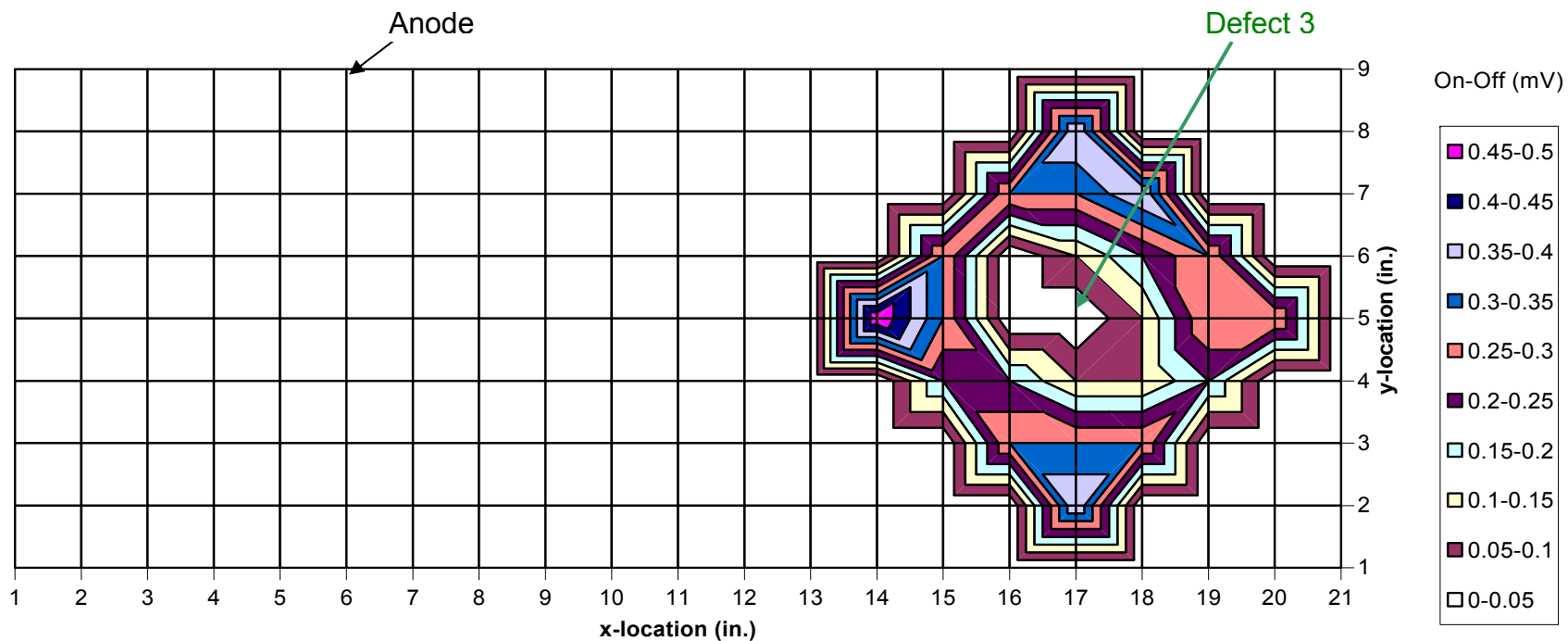


Figure 20. Contour plot of DCVG measurements near Defect 3 (Case 2).

Table 9. Corresponding data for Figure 20 with (*) representing defect and (+) representing anode.

	1	2	3	4	5	6	7	8	9	10	11	12	13	14	15	16	17	18	19	20	21
9						+															
8																	0.4				
7																0.3	0.3	0.4			
6															0.3	0	0.1	0.2	0.3		
5														0.5	0.3	0	*	0.1	0.3	0.3	
4															0.2	0.2	0.1	0.1	0.2		
3																0.3	0.3	0.3			
2																	0.4				
1																					

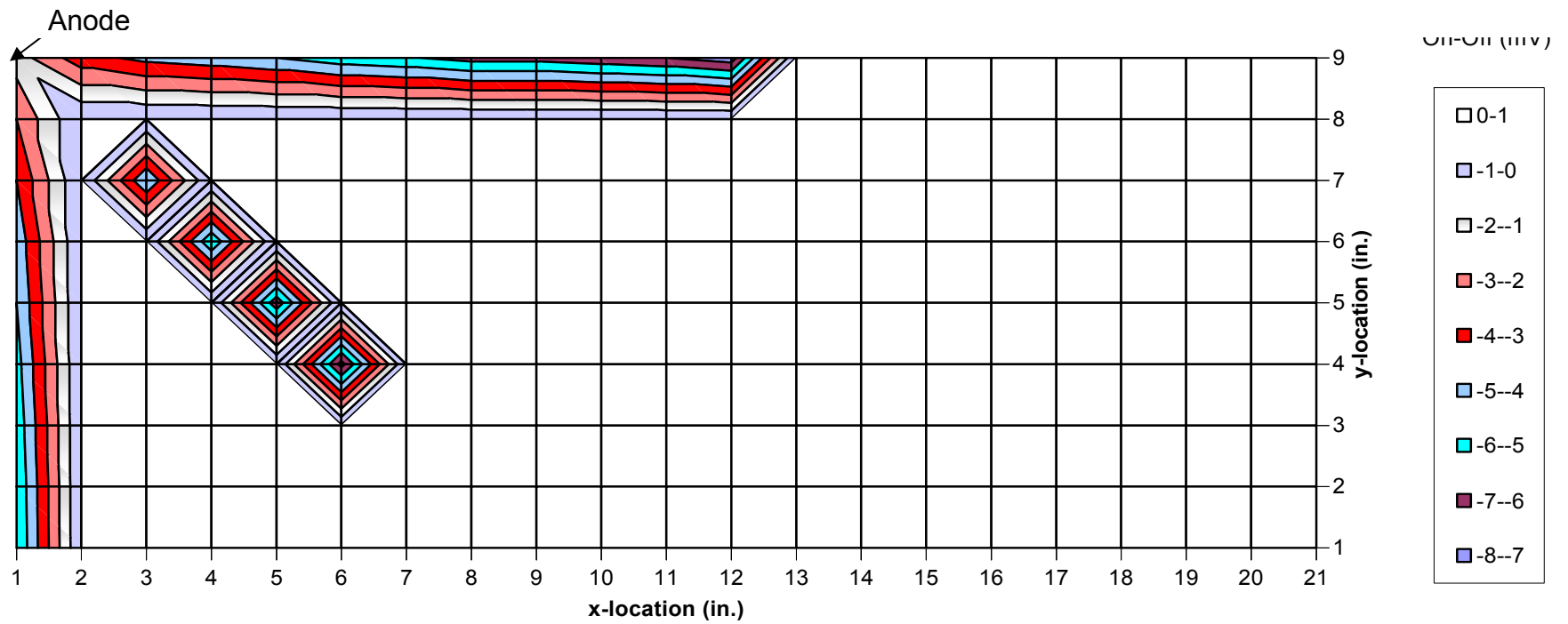


Figure 21. Contour plot of measurements near anode, $i = 1.217$ mA DC with anode positioned near $x=1, y=9$.

Table 10. Corresponding data for Figure 21 with (+) representing the anode.

+	1	2	3	4	5	6	7	8	9	10	11	12	13	14	15	16	17	18	19	20	21
9	-1.5	-3.6	-4.3	-4.6	-5	-5.6	-5.9	-6.4	-6.4	-6.7	-7	-7.6									
8	-3																				
7	-4		-5																		
6	-4.7			-5.9																	
5	-5				-6.7																
4	-5.4					-7.4															
3	-5.7																				
2	-5.9																				
1	-6																				

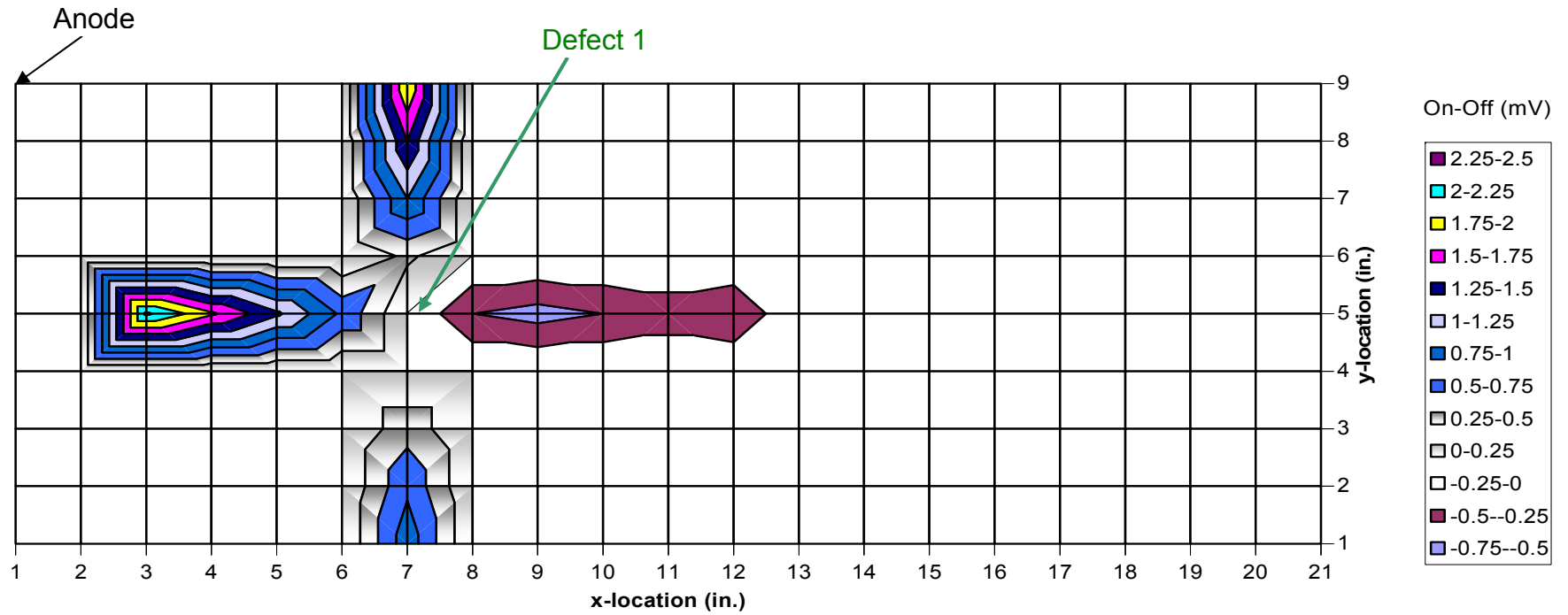


Figure 22. Contour plot of measurements near Defect 1 (Case 3).

Table 11. Corresponding data for Figure 22 with (*) representing defect and (+) representing anode.

+	1	2	3	4	5	6	7	8	9	10	11	12	13	14	15	16	17	18	19	20	21
9							2														
8							1.5														
7							1														
6							0.3														
5			2.3	1.8	1.3	0.7	*	-0.5	-0.6	-0.5	-0.4	-0.5									
4							0														
3							0.4														
2							0.7														
1							0.9														

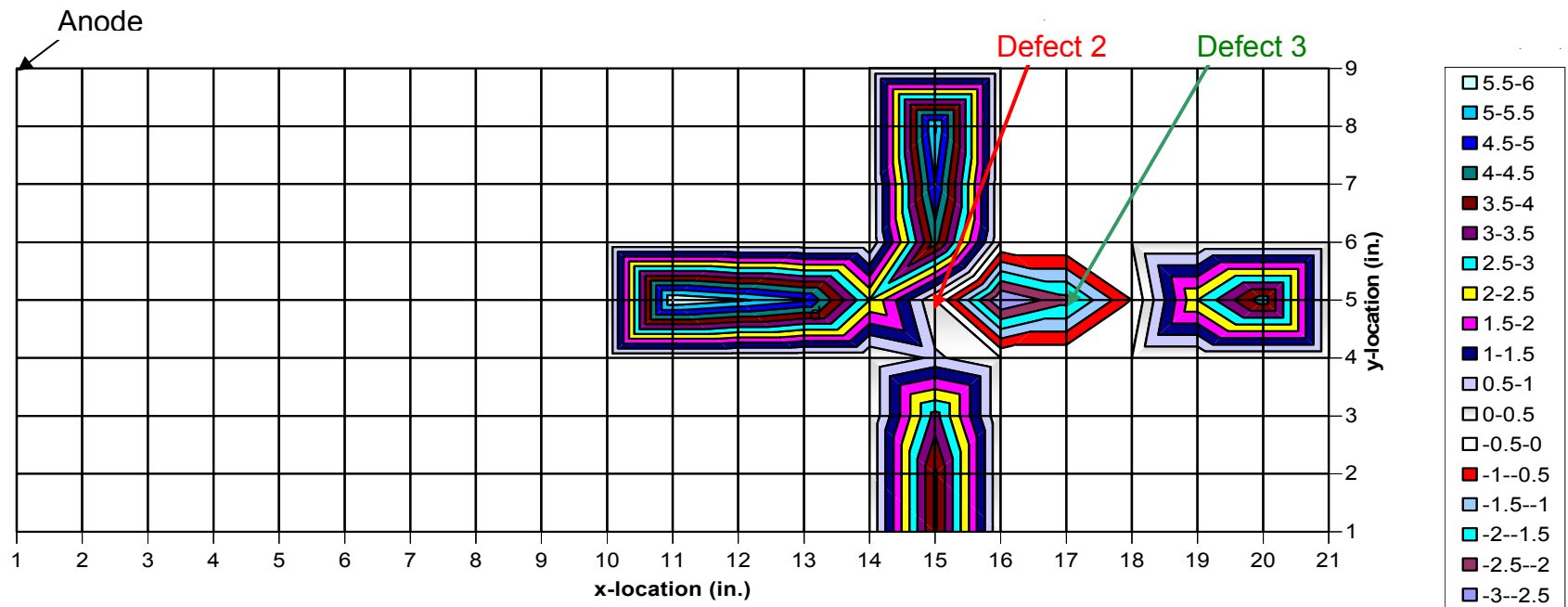


Figure 23. Contour plot of measurements near anode Defect 2 (Case 3).

Table 12. Corresponding data for Figure 23 with (*) representing defect and (+) representing anode.

+	1	2	3	4	5	6	7	8	9	10	11	12	13	14	15	16	17	18	19	20	21
9																					
8															5.5						
7															5						
6															4.2						
5										6	5.6	5.1	2.5	*	-3	-2.2	-0.5	2.5	4.3		
4															0.6						
3															3.2						
2															4.1						
1															4.1						

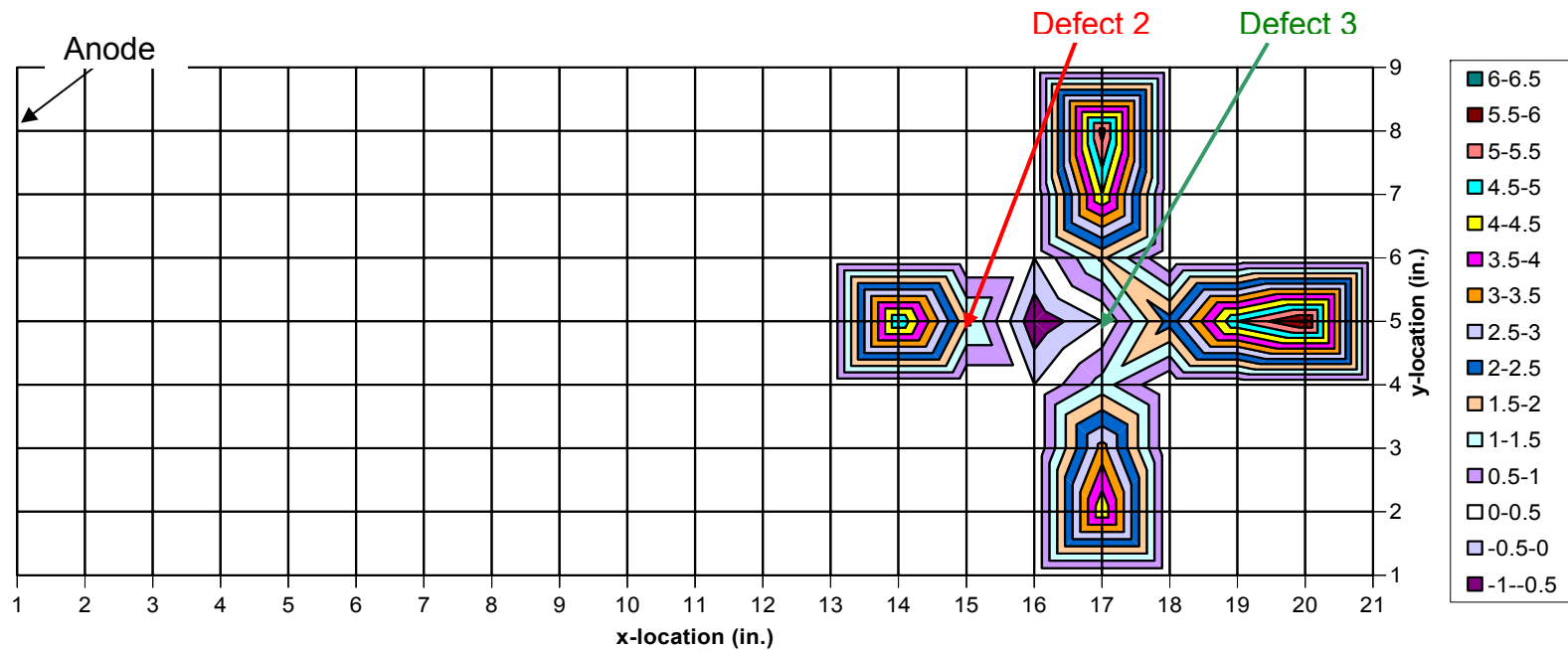


Figure 24. Contour plot of measurements near Defect 3 (Case 3).

Table 13. Corresponding data for Figure 24 with (*) representing defect and (+) representing anode.

+	1	2	3	4	5	6	7	8	9	10	11	12	13	14	15	16	17	18	19	20	21
9																					
8																	5.7				
7																	4.5				
6																	1.6				
5														5	1.6	-	*	2.2	5	6.1	
4																	1.2				
3																	3.2				
2																	4.4				
1																					

DC interference experiments

Further measurements were performed within the small-cell experimental set-up to examine the effect of the introduction of an interference current (representative of stray currents) on the accuracy of coating defect detection using DCVG. Figure 25 illustrates the layout of the DCVG setup components for all studied configurations.

The following is a brief description of the experiments performed.

Case 4: Anode positioned at $x=1, y=9$; $i = 1.217 \text{ mA DC}$

Previous results have shown that larger currents and increased distance between the anode and the pipe results in an increase in the accuracy of defect detection. Case 4 is merely a repeat of the “best-case” scenario (Case 3,) in order to re-establish baseline values for the experiment as it is possible, and in fact probable, that differences in experimental conditions (e.g. soil dampness, ambient temperature, etc.) could affect the baseline measurements. This allows for an accurate investigation of the effect of interference currents (to follow). Figure 26, Figure 27, and Figure 28 depict the results obtained for this condition.

Case 5: Anode positioned at $x=1, y=9$; $i = 1.217 \text{ mA DC}$; Interference voltage of 30.63V applied through 2 additional anodes positioned at $x=1, y=1$ and $x=21, y=9$.

Figure 29 illustrates the result obtained for the above condition. In this case, an interference voltage (30.63V) was introduced into the small-cell experimental set-up to determine its effect on defect detection accuracy. The anodes through which this interference was input were positioned at the corners of the cell. Comparison of Figure 26 and Figure 29 shows practically no difference in results obtained. The interference anodes were moved closer to the pipe in subsequent cases in an effort to cause the pipe to pick up some stray current.

Case 6: Anode positioned at $x=1, y=9$; $i = 1.217 \text{ mA DC}$; Interference voltage of 30.63V applied through 2 additional anodes positioned at the clay/sand boundary ($x=11, y=1$ and $x=11, y=9$).

Figure 30, Figure 31, and Figure 32 show the results obtained for the above condition. Similarly to Case 5 above, introducing stray current in this manner appeared to have virtually no effect on the ability to detect defects on the pipe. Considering that the interference was not strong enough (and/or near enough to the pipe) to affect the DCVG measurements, the interference anodes were moved nearer the pipe in Case 7

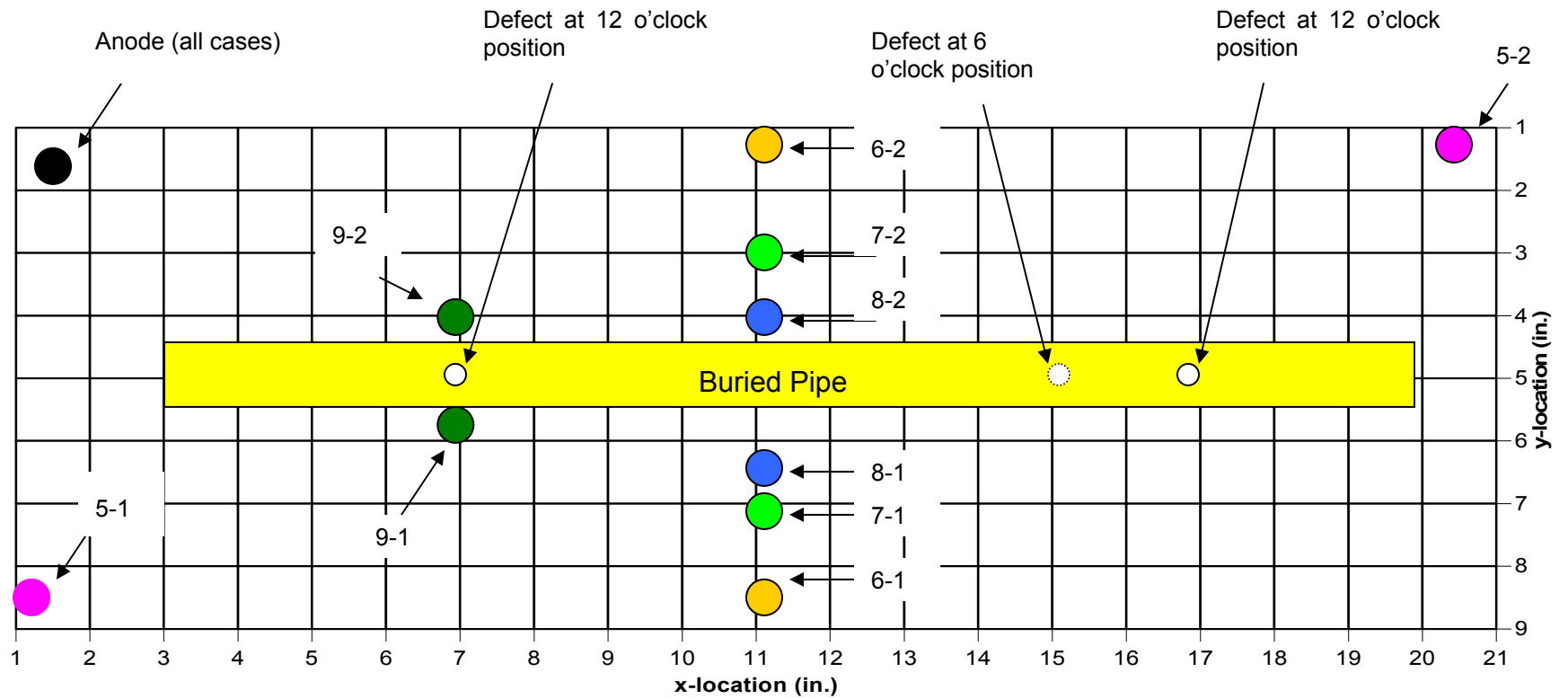


Figure 25. Layout of buried pipe in 'sandbox' – colored anodes show where interference anodes were positioned for the various cases

Case 7: Anode positioned at $x=1$, $y=9$; $i = 1.217$ mA DC; Interference voltage of 30.63V applied through 2 additional anodes positioned at the clay/sand boundary and very near the pipe ($x=11$, $y=3$ and $x=11$, $y=7$).

Again, no difference in the DCVG results is apparent. This is illustrated in Figure 33. The interference anodes were moved as near the pipe as possible in Case 8.

Case 8: Anode positioned at $x=1$, $y=9$; $i = 1.217$ mA DC; Interference voltage of 30.63V applied through 2 additional anodes positioned at the clay/sand boundary and as near the pipe as possible ($x=11$, $y=3-4$ and $x=11$, $y=6-7$).

Figure 34, Figure 35, and Figure 36 depict the results obtained for the above conditions. It is once again found that the introduced interference results in practically no change from previous results.

Case 9: Anode positioned at $x=1$, $y=9$; $i = 1.217$ mA DC; Interference voltage of 30.63V applied through 2 additional anodes positioned in line with defect 1 and as near the pipe as possible ($x=7$, $y=3-4$ and $x=7$, $y=6-7$).

As a final test, the interference anodes were positioned in line with one of the defects (defect 1) and as near the pipe as possible. Measurements again indicate that the interference current has no effect on the DCVG profile, as evidenced by Figure 37.

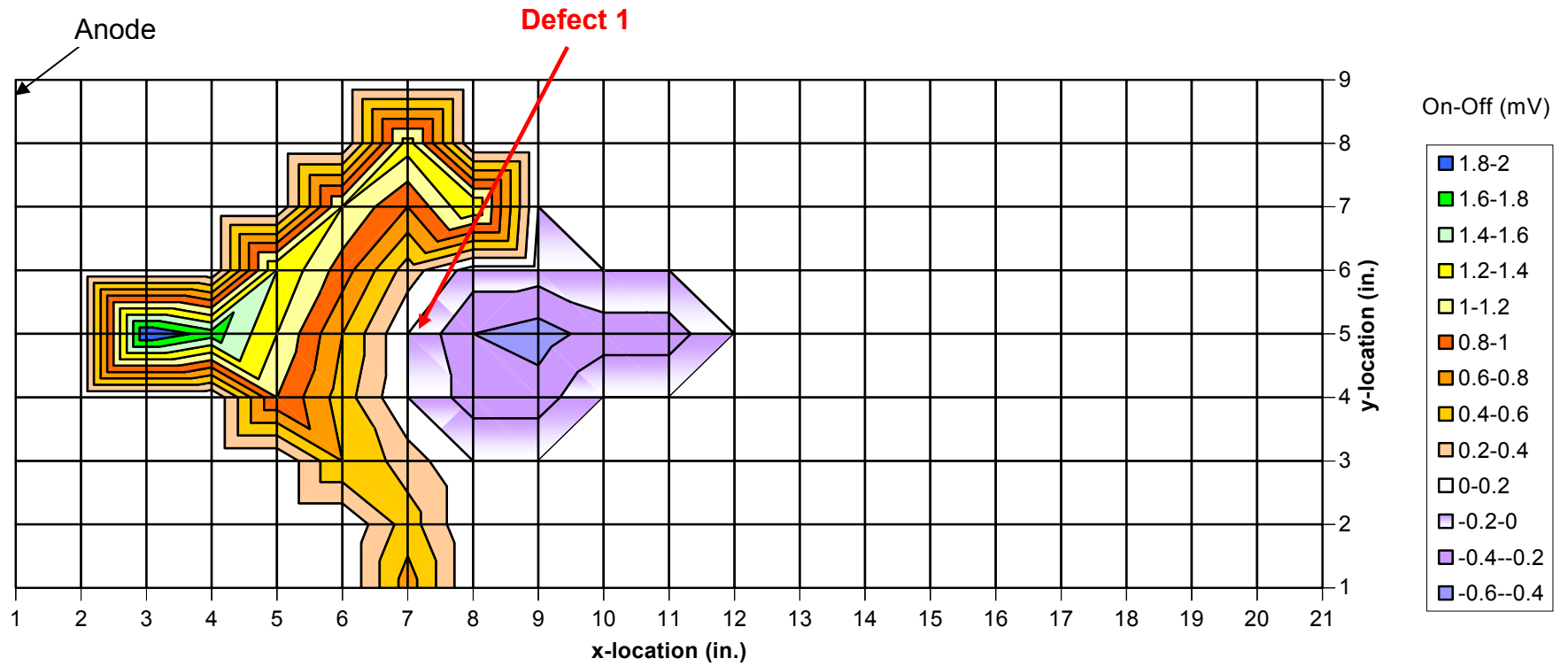


Figure 26. Contour plot of measurements (Case 4 – repeat of baseline conditions).

Table 14. Corresponding data for Figure 26 with (*) representing a defect and (+) representing an anode

	1	2	3	4	5	6	7	8	9	10	11	12	13	14	15	16	17	18	19	20	21
9	+																				
8							1.3														
7						1.2	0.8	1.4													
6					1.4	0.9	0.3	-0.1	-0.1												
5			2	1.7	1.2	0.6	*	-0.4	-0.5	-0.3	-0.3										
4					1.0	0.5	0	-0.3	-0.3												
3						0.6	0.3	0													
2							0.5														
1							0.7														

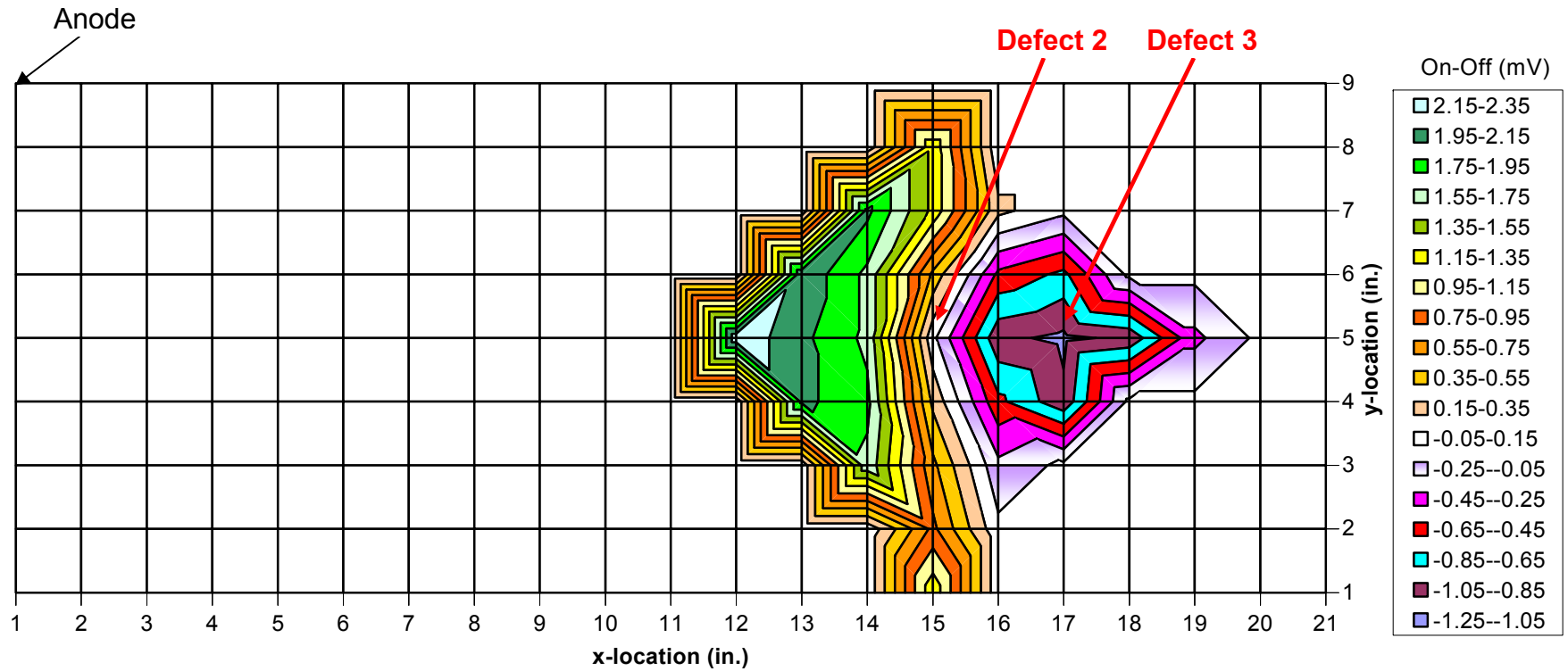


Figure 27. Contour plot of measurements (Case 4 – repeat of baseline conditions).

Table 15. Corresponding data for Figure 27 with (*) representing a defect and (+) representing an anode

	1	2	3	4	5	6	7	8	9	10	11	12	13	14	15	16	17	18	19	20	21
9	+																				
8															1.3						
7														2.0	1.3	0.2					
6													2.1	1.7	0.5	-0.5	-0.7				
5											2.3	2.0	1.7	*	-1.0	-1.1	-1	-0.3			
4												2.0	1.8	0.3	-0.6	-1.0					
3													1.7	0.6	-0.2						
2															0.8						
1															1.3						

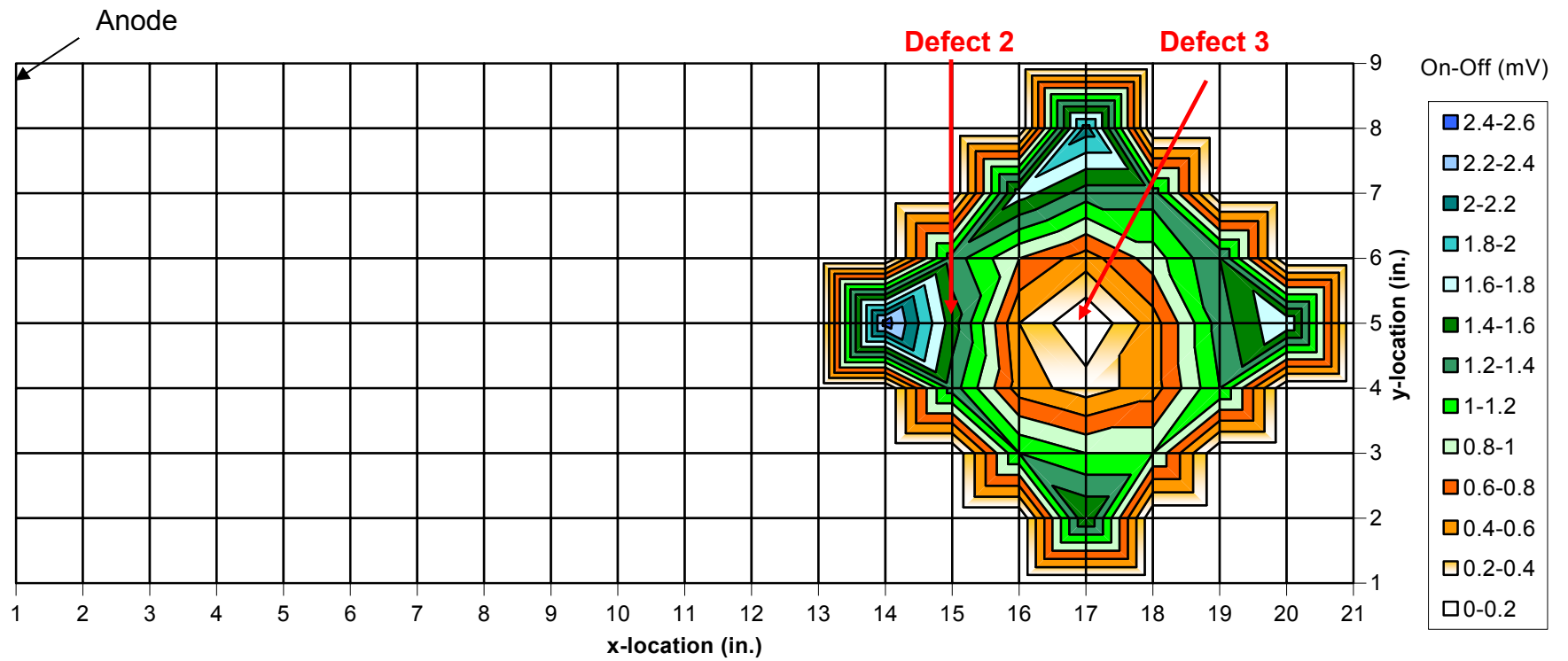


Figure 28. Contour plot of measurements (Case 4 – repeat of baseline conditions).

Table 16. Corresponding data for Figure 28 with (*) representing a defect and (+) representing an anode

	1	2	3	4	5	6	7	8	9	10	11	12	13	14	15	16	17	18	19	20	21
9	+																				
8																	2.1				
7																1.7	1.3	1.3			
6															1.3	0.8	0.5	0.9	1.4		
5														2.5	1.5	0.4	*	0.5	1.3	1.8	
4															1.3	0.5	0.3	0.5	1.2		
3																1.2	1.0	1.0			
2																	1.6				
1																					

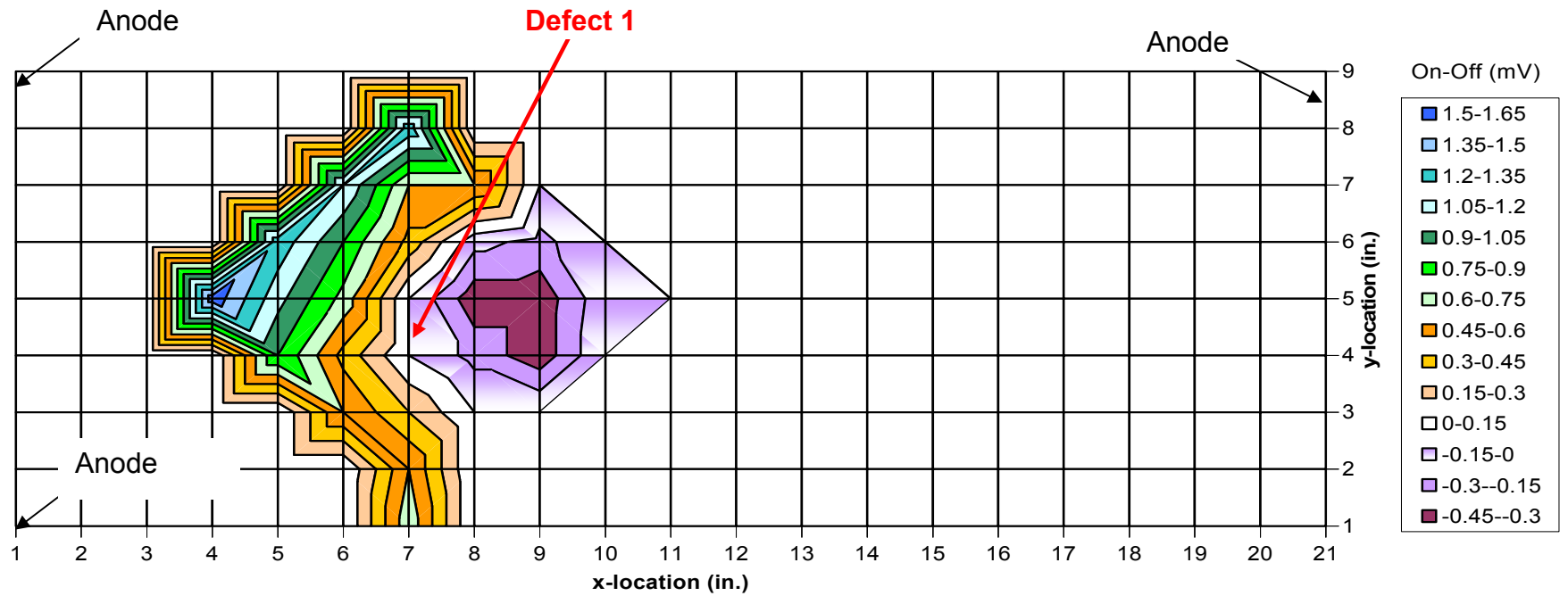


Figure 29. Contour plot of measurements (Case 5).

Table 17. Corresponding data for Figure 29 with (*) representing a defect and (+) representing an anode.

	1	2	3	4	5	6	7	8	9	10	11	12	13	14	15	16	17	18	19	20	21	
9	+																					+
8							1.3															
7						1.2	0.6	0.6														
6					1.3	0.9	0.4	-0.1	-0.2													
5				1.6	1.1	0.7	*	-0.4	-0.4	-0.04												
4					0.9	0.4	0	-0.2	-0.4													
3						0.6	0.3	0														
2							0.6															
1	+						0.7															

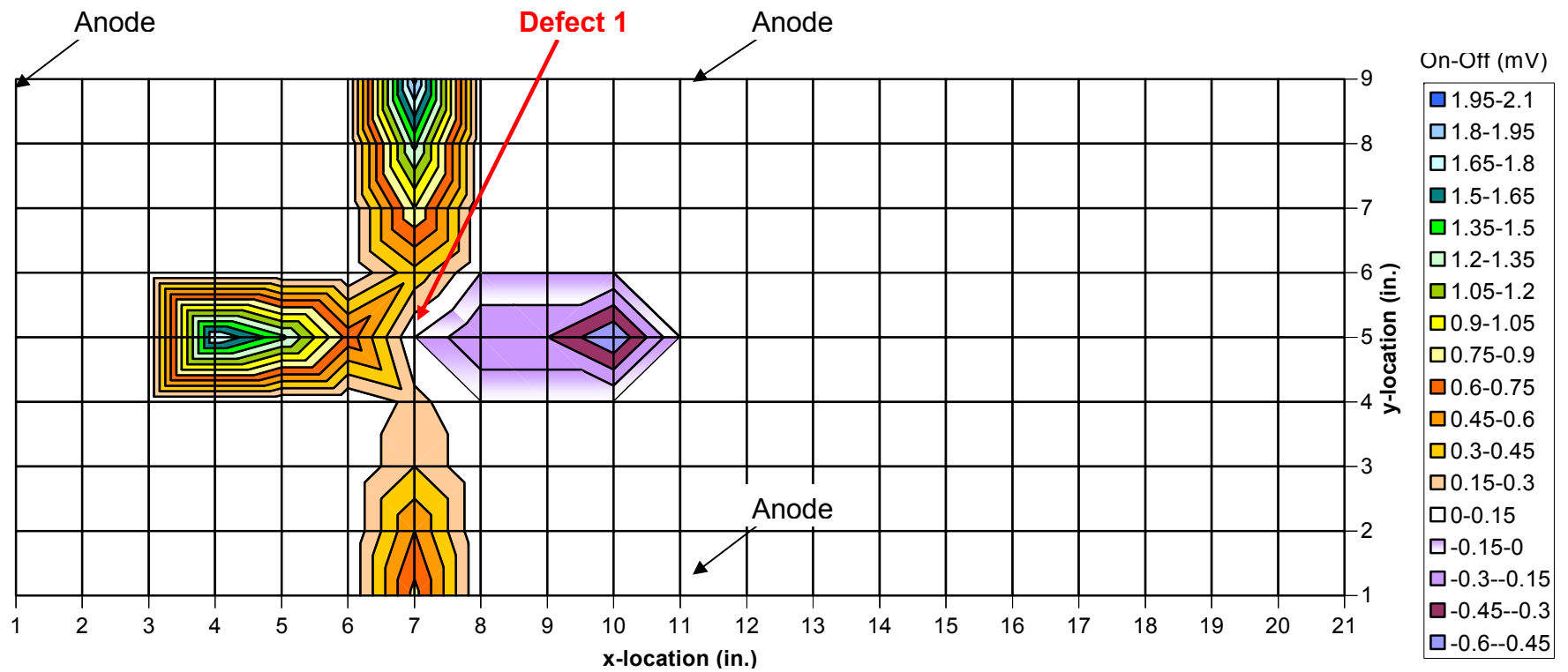


Figure 30. Contour plot of measurements (Case 6).

Table 18. Corresponding data for Figure 30 with (*) representing a defect and (+) representing an anode.

	1	2	3	4	5	6	7	8	9	10	11	12	13	14	15	16	17	18	19	20	21
9	+						2.0				+										
8							1.4														
7							0.9														
6							0.4														
5				1.8	1.4	0.7	*	-0.3	-0.3	-0.6											
4							0.2														
3							0.3														
2							0.6														
1							0.8				+										

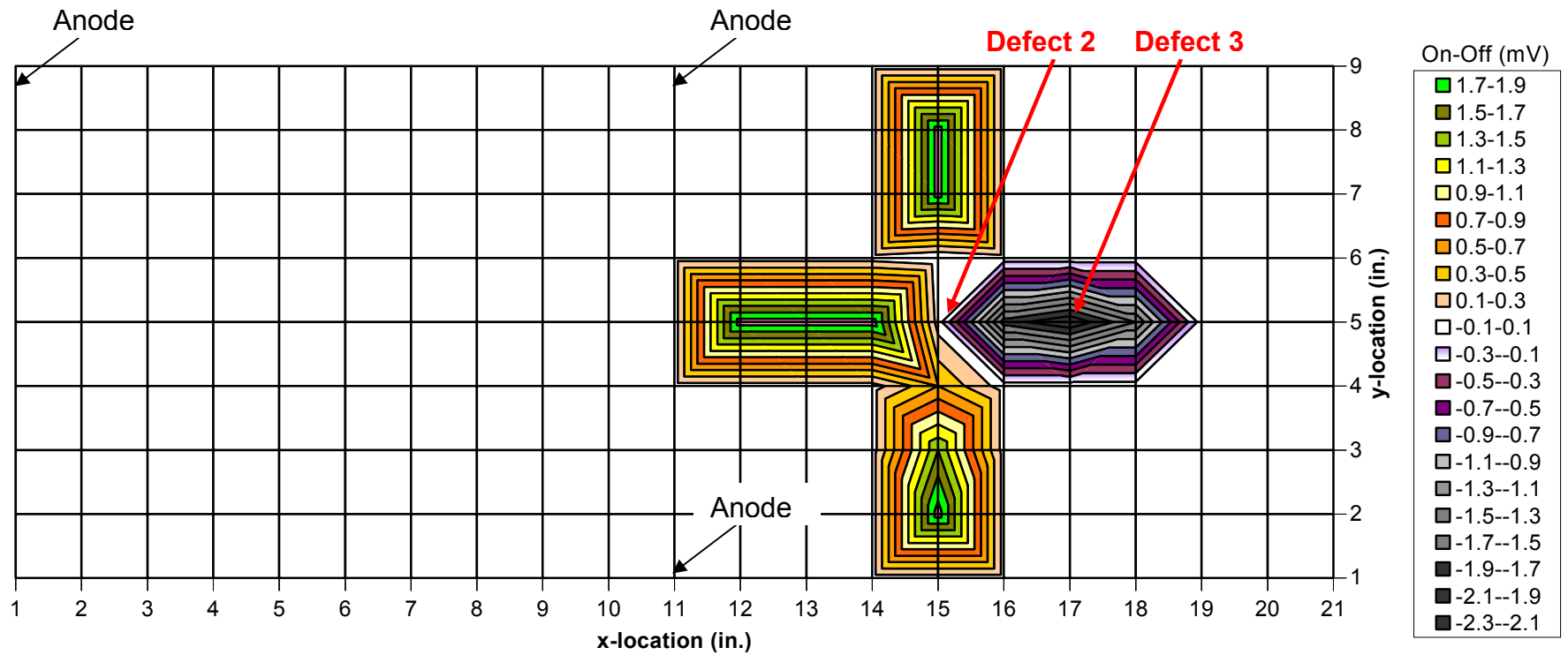


Figure 31. Contour plot of measurements (Case 6).

Table 19. Corresponding data for Figure 31 with (*) representing a defect and (+) representing an anode.

	1	2	3	4	5	6	7	8	9	10	11	12	13	14	15	16	17	18	19	20	21
9	+										+										
8															3.0						
7															2.5						
6															-0.1						
5												4.1	3.4	2.6	*	-1.8	-2.1	-1.5	0		
4															0.5						
3															1.5						
2															2.0						
1											+										

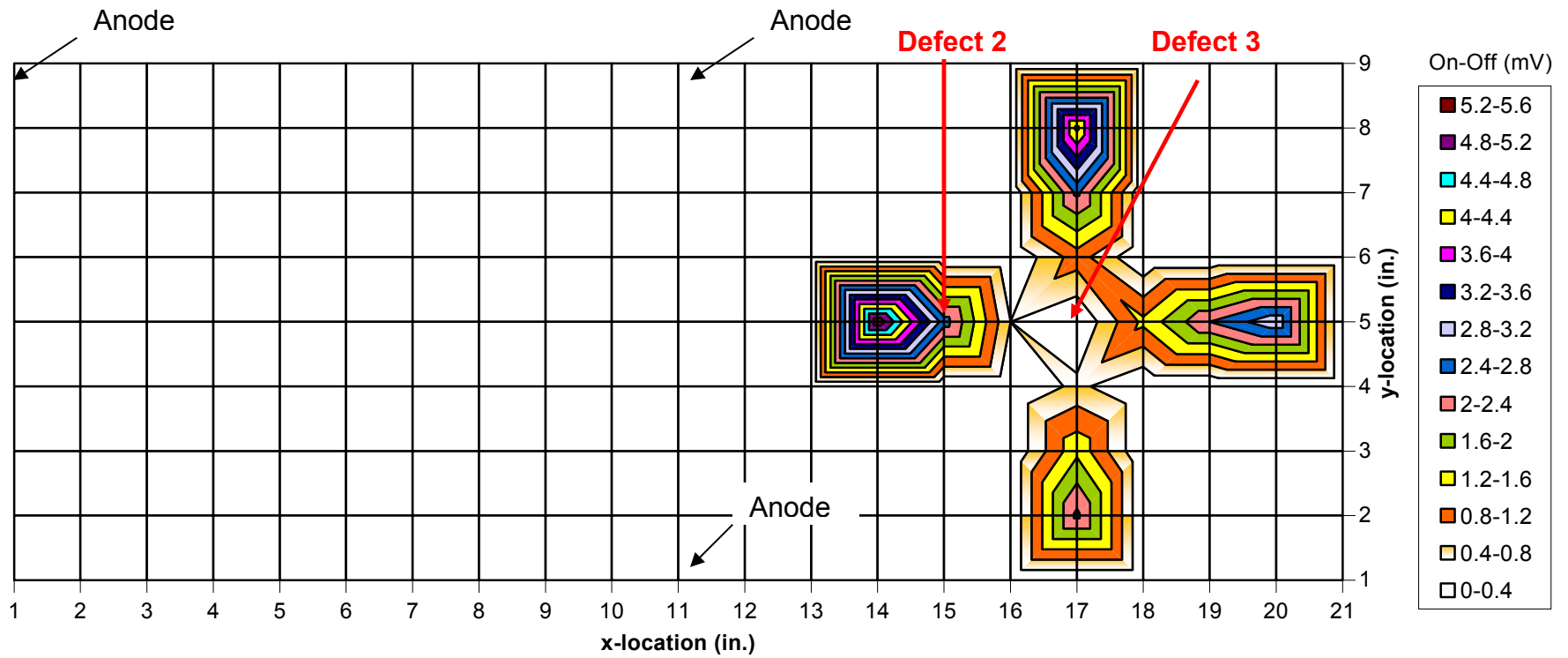


Figure 32. Contour plot of measurements (Case 6).

Table 20. Corresponding data for Figure 32 with (*) representing a defect and (+) representing an anode.

	1	2	3	4	5	6	7	8	9	10	11	12	13	14	15	16	17	18	19	20	21
9	+										+										
8																		4.5			
7																		2.5			
6																		1.0			
5														5.5	2.6	0.4	*	1.3	2.4	3.1	
4																		0.5			
3																		1.5			
2																		2.5			
1											+										

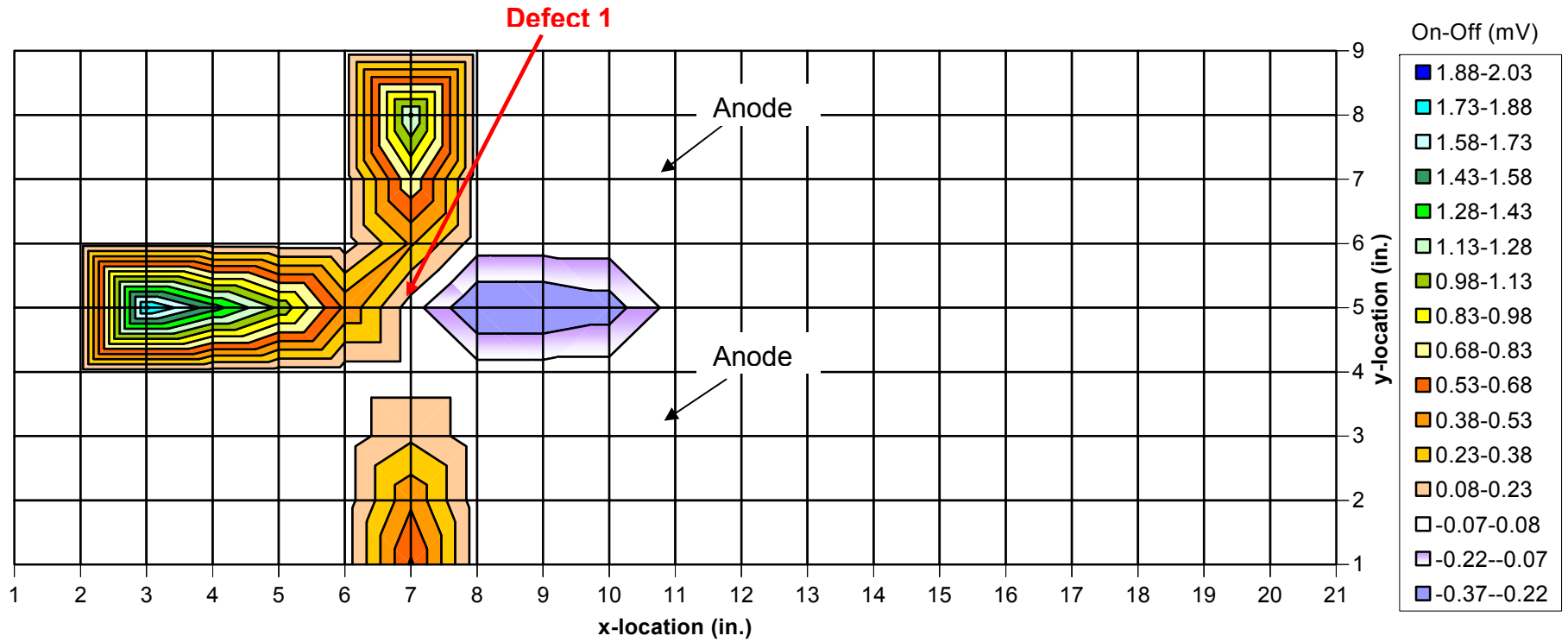


Figure 33. Contour plot of measurements (Case 7).

Table 21. Corresponding data for Figure 33 with (*) representing a defect and (+) representing an anode

	1	2	3	4	5	6	7	8	9	10	11	12	13	14	15	16	17	18	19	20	21	
9	+																					
8							1.3															
7							0.8															
6							0.4				+											
5			1.9	1.5	1.1	0.5	*	-0.4	-0.4	-0.3												
4							0															
3							0.2				+											
2							0.5															
1							0.7															

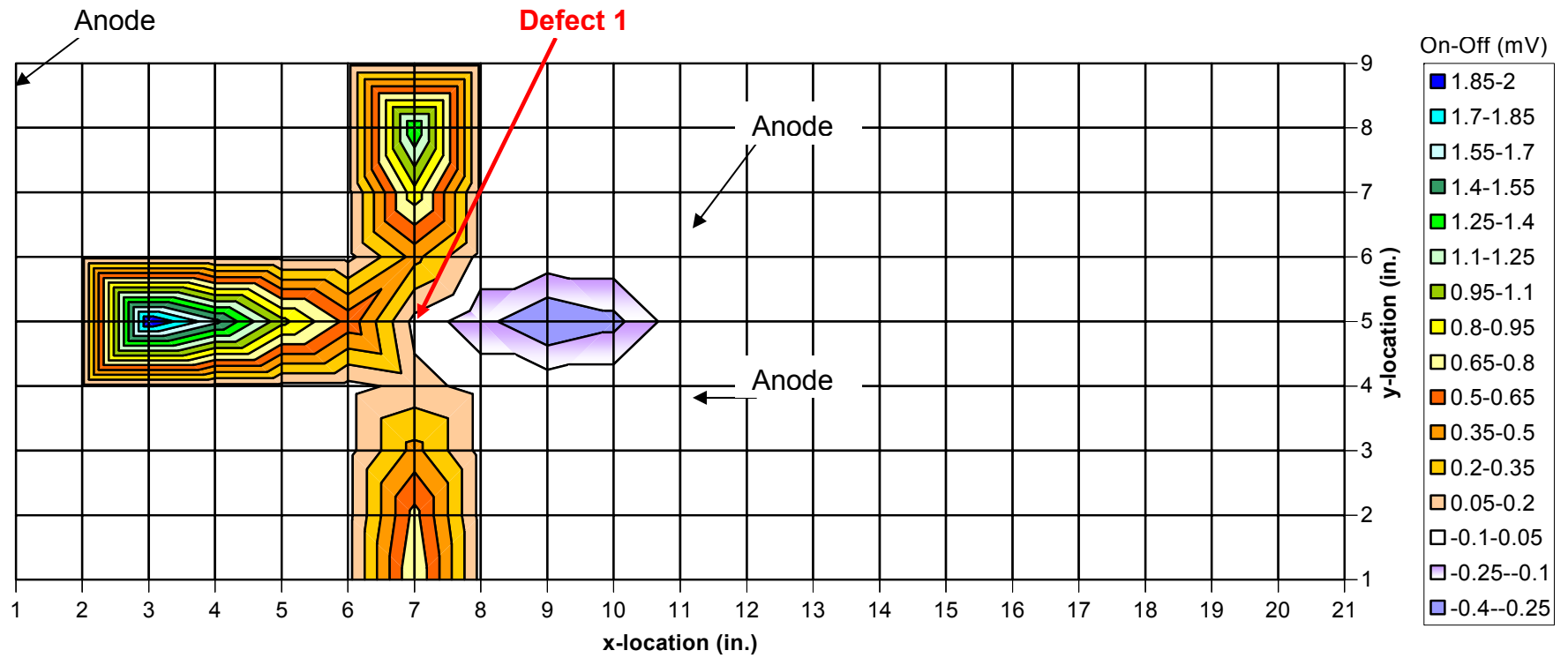


Figure 34. Contour plot of measurements (Case 8).

Table 22. Corresponding data for Figure 34 with (*) representing a defect and (+) representing an anode

	1	2	3	4	5	6	7	8	9	10	11	12	13	14	15	16	17	18	19	20	21
9	+																				
8							1.4														
7							0.9														
6							0.4				+										
5			2	1.6	1	0.6	*	-0.2	-0.4	-0.3											
4							0.1														
3							0.4				+										
2							0.7														
1							0.8														

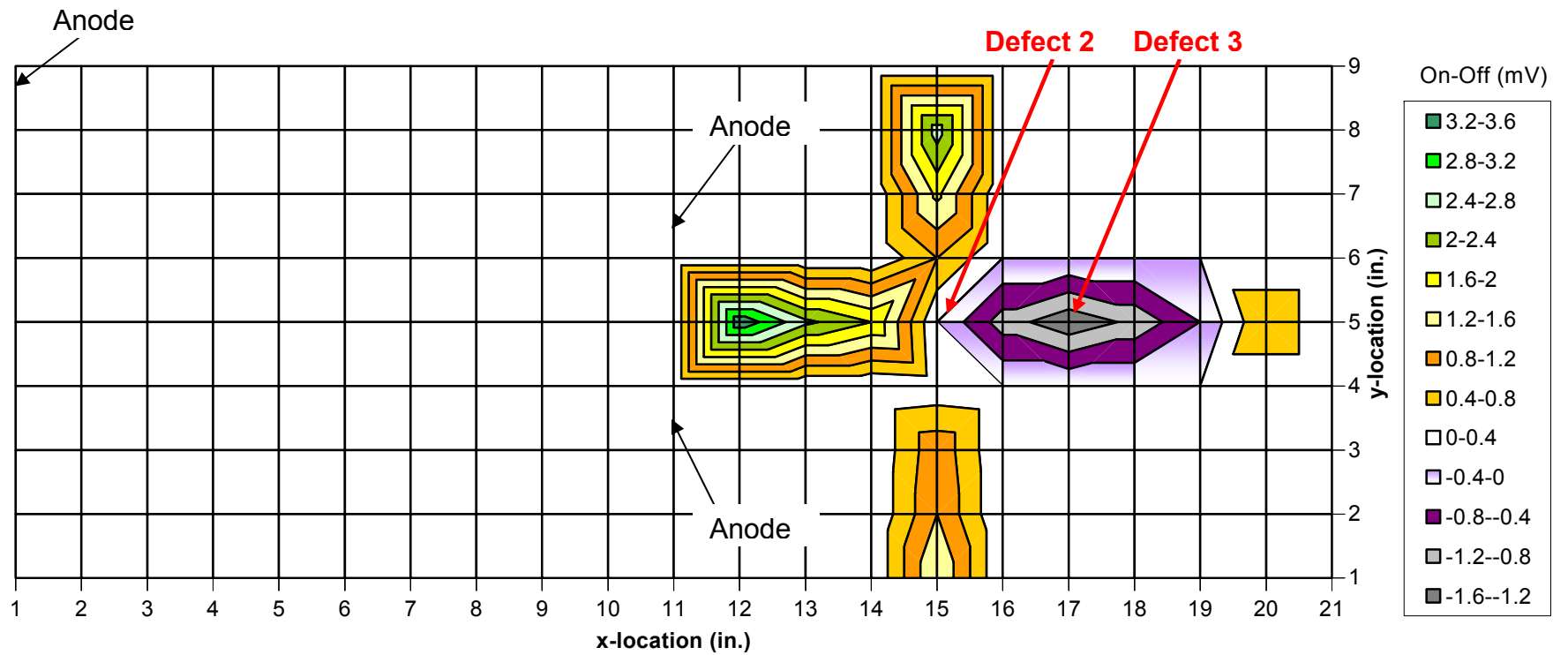


Figure 35. Contour plot of measurements (Case 8).

Table 23. Corresponding data for Figure 35 with (*) representing a defect and (+) representing an anode.

	1	2	3	4	5	6	7	8	9	10	11	12	13	14	15	16	17	18	19	20	21
9	+																				
8															2.6						
7															1.7						
6											+				0.8						
5												3.5	2.5	2.0	*	-1.0	-1.5	-1.1	-0.4	0.8	
4															0.1						
3											+				1.1						
2															1.2						
1															1.6						

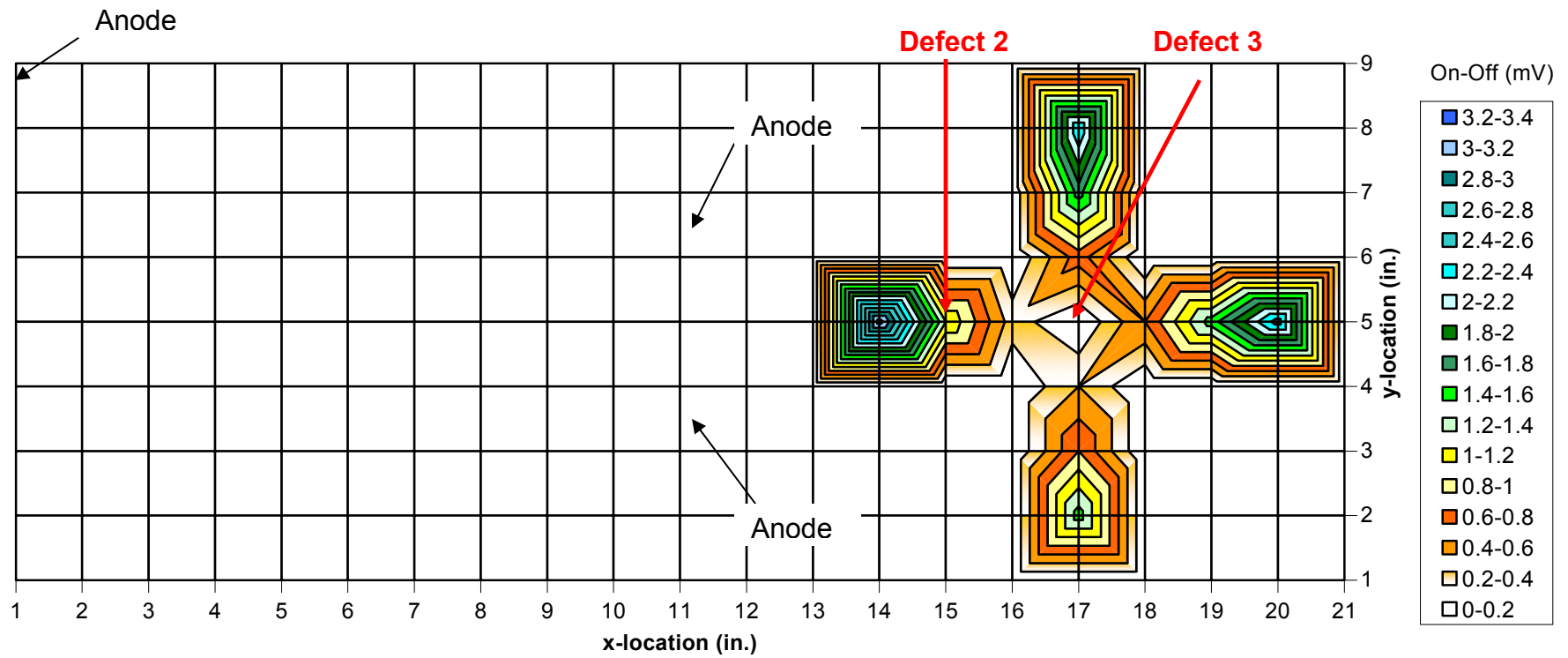


Figure 36. Contour plot of measurements (Case 8).

Table 24. Corresponding data for Figure 36 with (*) representing a defect and (+) representing an anode

	1	2	3	4	5	6	7	8	9	10	11	12	13	14	15	16	17	18	19	20	21
9	+																				
8																	2.4				
7																	1.7				
6											+						0.7				
5														3.3	1.2	0.3	*	0.6	1.5	2.5	
4																	0.4				
3											+						0.8				
2																	1.5				
1																					

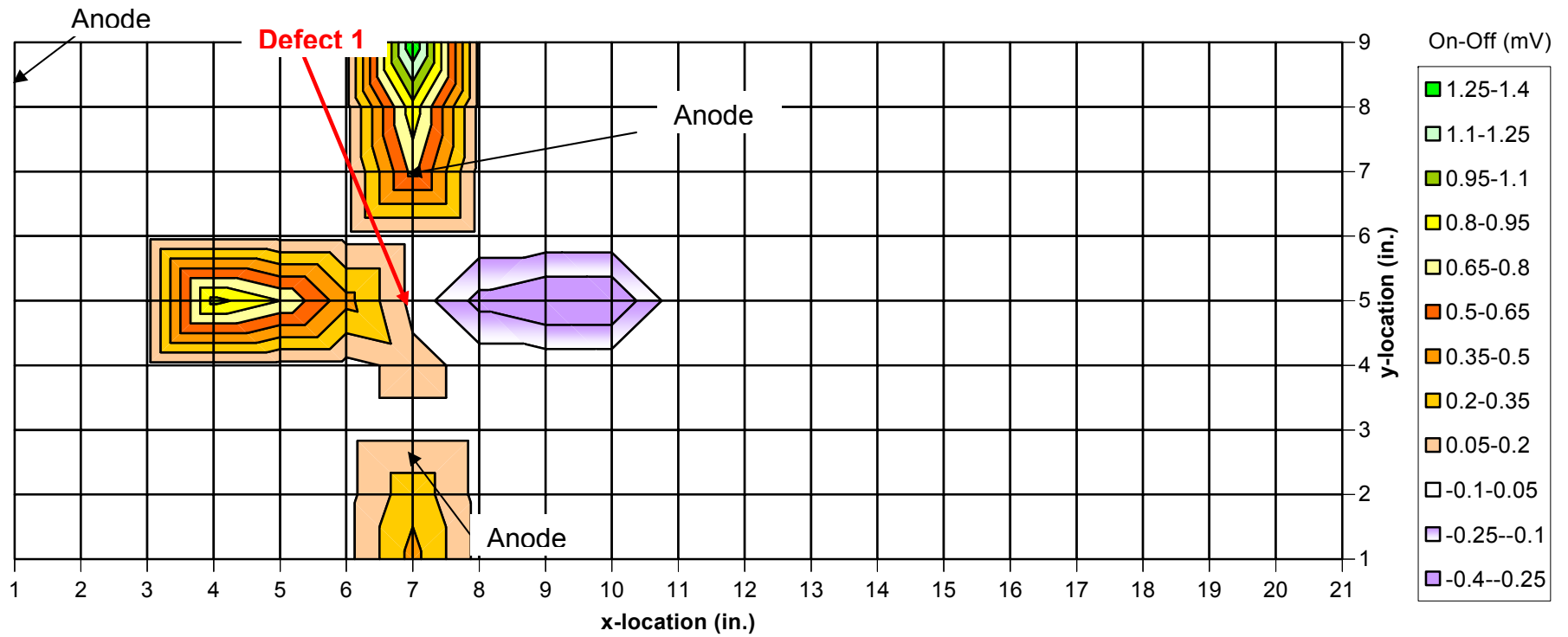


Figure 37. Contour plot of measurements (Case 9).

Table 25. Corresponding data for Figure 37 with (*) representing a defect and (+) representing an anode.

	1	2	3	4	5	6	7	8	9	10	11	12	13	14	15	16	17	18	19	20	21
9	+						1.4														
8							0.9														
7							0.7														
6							0	<-- +													
5				1.0	0.8	0.4	*	-0.3	-0.4	-0.4											
4							0.1	<---+													
3							0														
2							0.3														
1							0.4														

Conclusions

Experimental results show that DCVG measurements can locate defects in the pipe with the same degree of accuracy both whether static (DC) interference currents are present or not. In other words, DCVG appears to be a robust detection tool which, under tested conditions, was capable of identifying the presence of coating defects. The effect of *dynamic* stray current interference (AC currents of varying frequencies) was tested on the large-scale outdoor facility.

DC and AC CIS measurements

In addition to the DCVG measurements, close interval survey (CIS) readings were obtained on the pipe assembly described above. The measurements included readings for DC and AC potential/voltage, when the pipe was under either cathodic protection (CP) or simulated AC interference, respectively.

DC measurements

The DC readings included both ON and OFF potential values (the latter one collected when the CP system was electrically interrupted to eliminate the ohmic drop contribution). The OFF potentials were collected in two ways – (1) with all three Defects interrupted from the CP anode while still forming an electric circuit, and (2) the individual Defect was completely electrically isolated from the CP anode and the other defects at the time of the measurement.

The results varied depending on how the measurements are taken. The difference in resistance paths from the CP anode to the defects resulted in different polarization (OFF) potentials. Consider the graph shown in Figure 38.

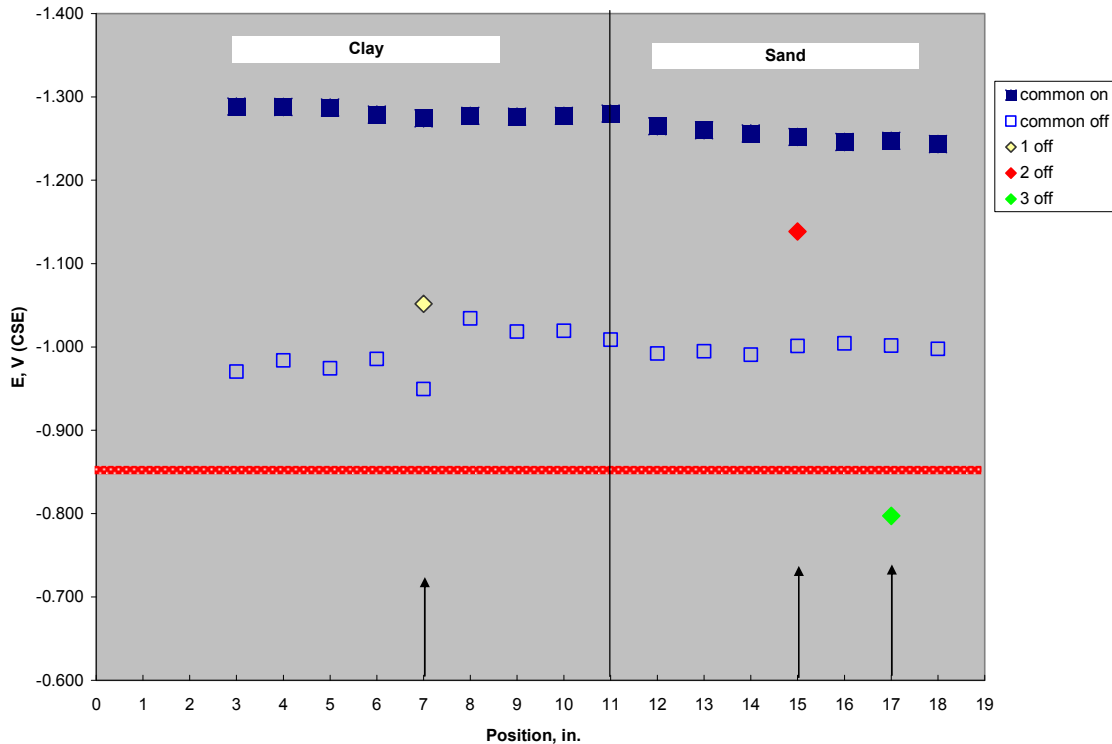


Figure 38. DC CIS profile in clay/sand.

The graph shows the ON/OFF potential profile for the case when all three defects were connected and only the CP anode circuit was interrupted (“Common ON”) and also shows the three individual OFF potentials for each of the Defects. Upward facing arrows denote the location of the Defects.

As can be seen, the “Common OFF” profile suggests that the pipeline appears to be within the compliance with RP0169 criterion of -850mV (CSE) indicated by the red horizontal line. However, when the OFF potentials are measured for each individual Defect, it becomes apparent that the “Common OFF” value is the weighted average of all three Defect OFF potentials (as it would be on a real pipeline). The “Common OFF” values are closer to the OFF potential for Defect 1; Defect 2 is actually polarized to higher potentials and Defect 3 has rather positive polarization potential, which is out of compliance with the CP criterion.

Each measured potential value of the CIS ON/OFF (“Common”) profile could be represented as:

$$E = \frac{\sum E_i g_i}{\sum g_i}$$

where E_i and g_i are the potentials of each individual defects in the coating and conductivity of the measurement path between the reference electrode and the defect, respectively.

Therefore, the defect with the least resistive path (Defect 2 in this case, which has the most negative CP potential) will be weighed the most heavily (i.e., its contribution to the measured E value will be the largest).

The results underscore a very important point when it comes to interpreting the CIS profiles. In this particular case, the potential of Defect 3 is out of compliance with CP protection criteria, which is not reflected in the “Common OFF” chart. On the other hand, the potential of Defect 2 is rather negative (in excess of -1,100 mV CSE), which, had it been on a real pipeline would have put the location at danger for overprotection. This condition was not revealed by the “Common OFF” values either.

Therefore, it is important not to rely solely on CIS profiles when assessing the CP effectiveness. If a pipeline traverses soils with drastically different properties, or if there is reason to believe that the coating condition (or coating type) changes at some point, further investigations are indicated. The locations with higher impedance (due to soil properties or defect geometry) may not be reflected in the collected CIS data.

DC interference measurements

A series of experiments were performed within the small-cell experimental set-up to examine the effect of the introduction of an interference current (representative of stray currents) on the accuracy of the close-interval survey (CIS) inspection technique.

Note that in all experiments described below, measurements labeled as *common* represent the set of measurements which would be obtained in a field survey. For these measurements, all sections of the pipe are electrically connected. Data series labeled 1, 2, and 3 represent the on/off potentials of the respective individual defect when electrically isolated from the other sections of pipe.

Experiment 1: Baseline

Figure 39 shows the baseline CIS profile, a reference for subsequent experiments. All defects show OFF potentials more negative than -850mV when measured against the common, indicating that all defects are adequately cathodically protected. When the defects are electrically isolated and measured

individually, however, it becomes evident that defects 2 and 3 are not protected. Experiments 2-5 show how these readings are affected by static stray currents.

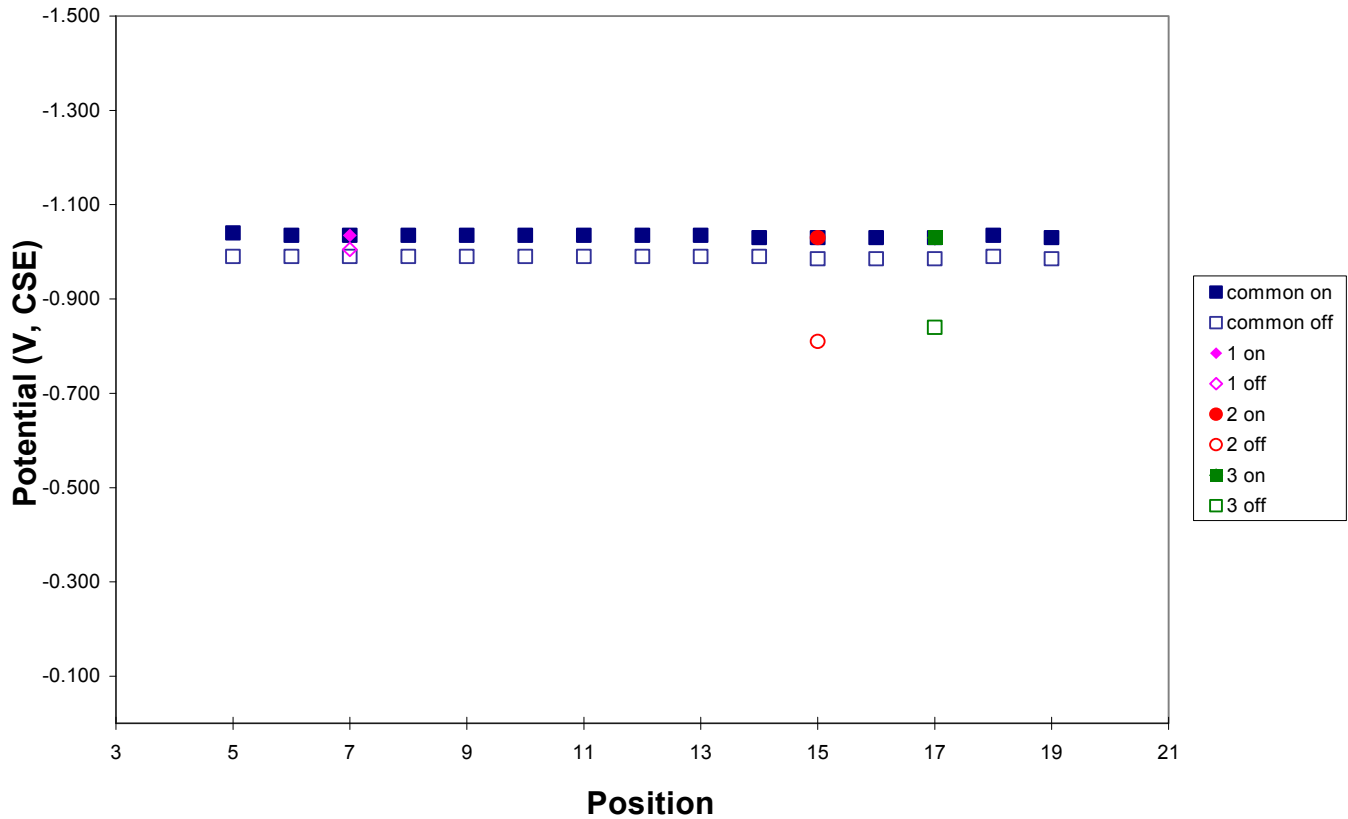


Figure 39. CIS profile (Experiment 1).

Experiment 2: 3.840V interference

Figure 40 shows the measured CIS profile with 3.840V of interference introduced into the small-cell experimental set-up through anodes positioned in opposite corners of the cell. As in the baseline reading, defect 1 is cathodically protected. Defects 2 and 3 once again appear to be protected when measured against the common, though electrical isolation gives measurements indicative of the contrary.

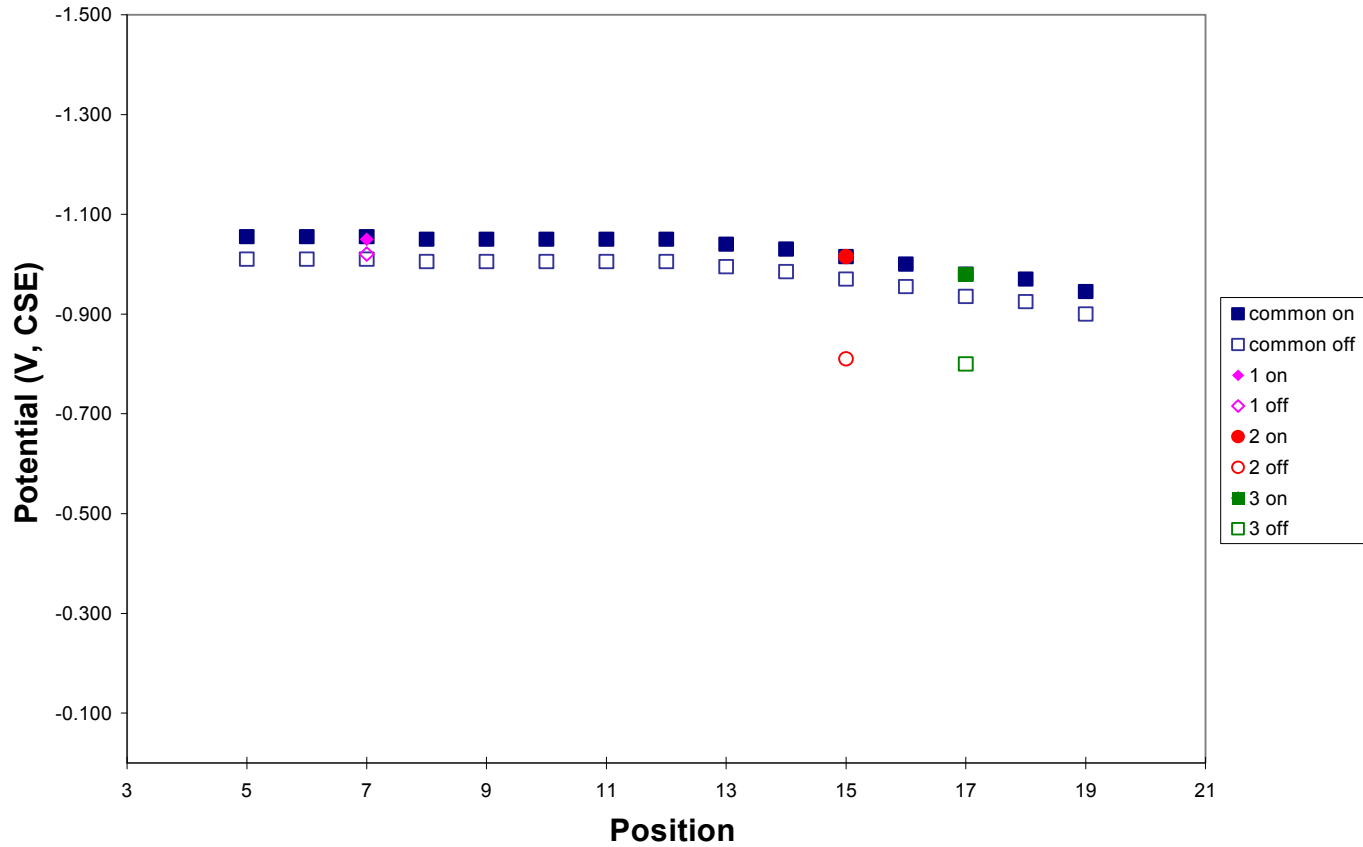


Figure 40. CIS profile (Experiment 2).

Experiment 3: 7.750V interference

Figure 41 depicts the measured CIS profile with 7.750V of interference present in the cell. The results are similar to those of experiment 2. One notices that defects 2 and 3 are discharging, while defect 1 is picking up current.

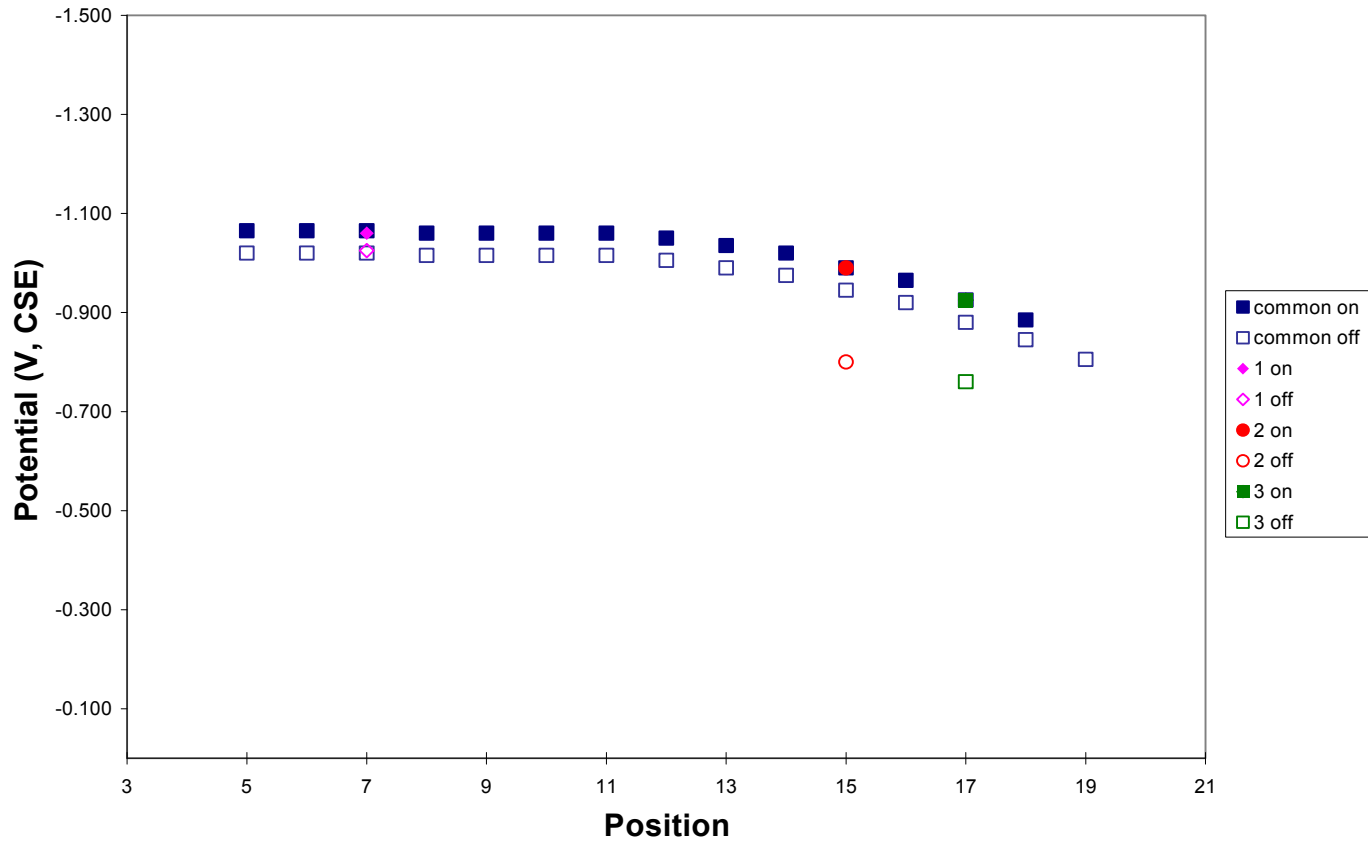


Figure 41. CIS profile (Experiment 3).

Experiment 4: 15.50V interference

Figure 42 shows the CIS profile measured with 15.50V of interference. Defect 1 appears to be, and in fact is, protected. Defect 2 appears cathodically protected when measured against the common (-900mV, see table 1). After electrically isolating this defect, however, it is seen that it is not protected (-790mV). Defect 3 is not protected.

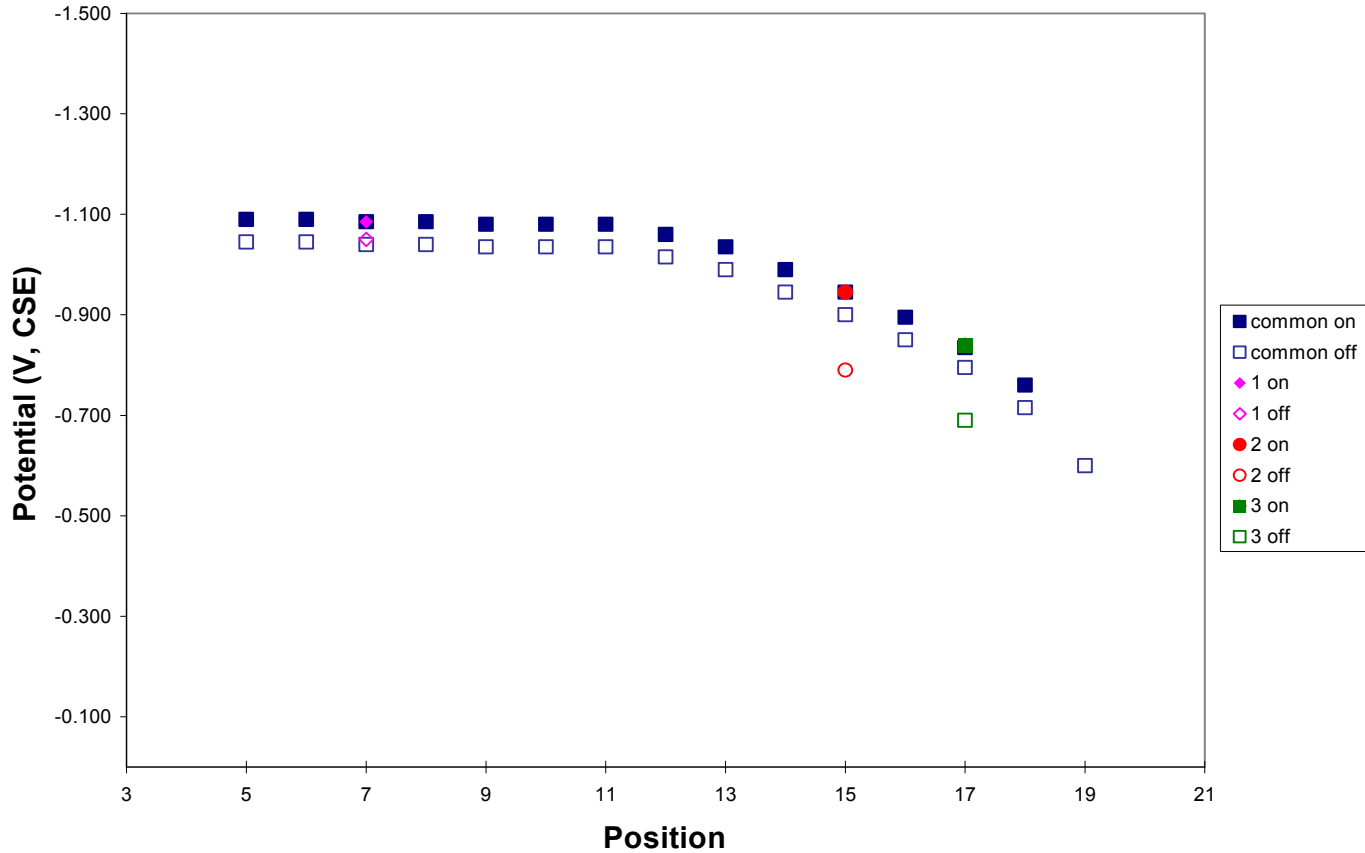


Figure 42. CIS profile (Experiment 4).

Experiment 5: 30.69V interference

The CIS profile measured with 30.69V of interference in the set-up is shown in Figure 43. Defect 1 has picked-up about 100mV, while defect 3 has discharged several hundred mV. Defect 1 is still cathodically protected, though at -1080mV it is approaching hydrogen evolution should much more interference be present. Defect 2 is not cathodically protected, and neither is defect 3.

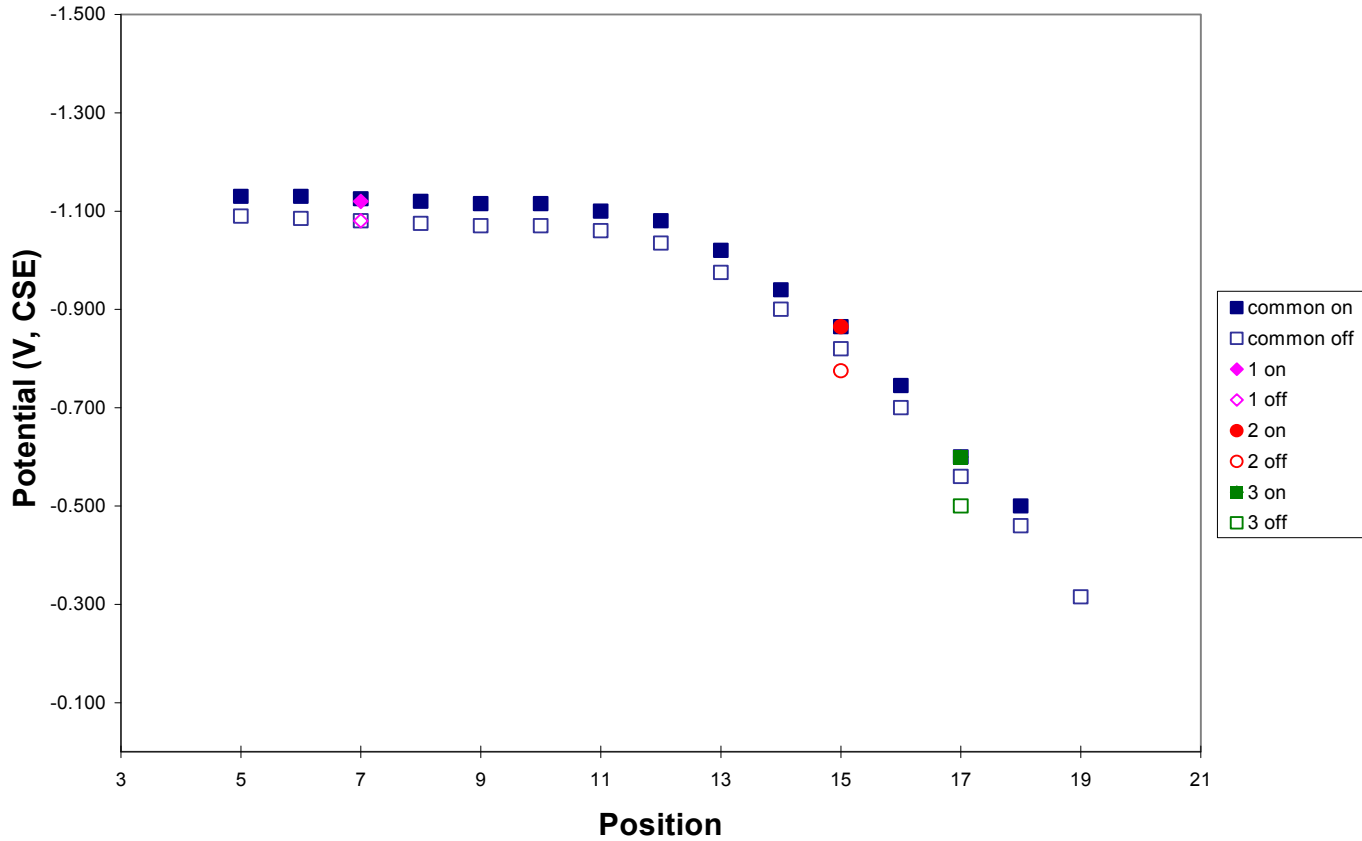


Figure 43. CIS profile (Experiment 5).

Table 1 and Table 2 summarize the results of Experiments 1-5.

Table 26. Current distribution (Experiments 1-5, measurements in mA).

Location	Interference				
	None	3.840V	7.75V	15.50V	30.69V
Defect 1	0.09	0.10	0.11	0.12	0.13
Defect 2	0.01	0.01	0.01	0.01	0.00
Defect 3	0.06	0.05	0.05	0.04	0.03
Σ Defects 1-3	0.16	0.16	0.16	0.16	0.16

Table 27. 'On' and 'Off' potentials (Experiments 1-5, measurements in V).

Location	Interference									
	None		3.840V		7.75V		15.50V		30.69V	
	On	Off	On	Off	On	Off	On	Off	On	Off
Defect 1										
Electrically Isolated	-1.035	-1.005	-1.050	-1.020	-1.060	-1.025	-1.085	-1.050	-1.120	-1.080
Common	-1.035	-0.990	-1.055	-1.010	-1.065	-1.020	-1.085	-1.040	-1.125	-1.080

Defect 2										
Electrically Isolated	-1.030	-0.810	-1.015	-0.810	-0.990	-0.800	-0.945	-0.790	-0.865	-0.775
Common	-1.030	-0.985	-1.015	-0.970	-0.990	-0.945	-0.945	-0.900	-0.865	-0.820
Defect 3										
Electrically Isolated	-1.030	-0.840	-0.980	-0.800	-0.925	-0.760	-0.840	-0.690	-0.600	-0.500
Common	-1.030	-0.985	-0.980	-0.935	-0.925	-0.880	-0.835	-0.795	-0.600	-0.560

Experiment 6: Baseline reading

Another baseline reading was taken for experiments 7-10 as these experiments were performed with slightly different soil saturation than experiments 1-5 (due to a lapse in time). Again the purpose of this series of measurements is simply to serve as a reference for future CIS profiles. These measurements closely mirror those of experiment 1, as expected, and the CIS profile is illustrated in Figure 44.

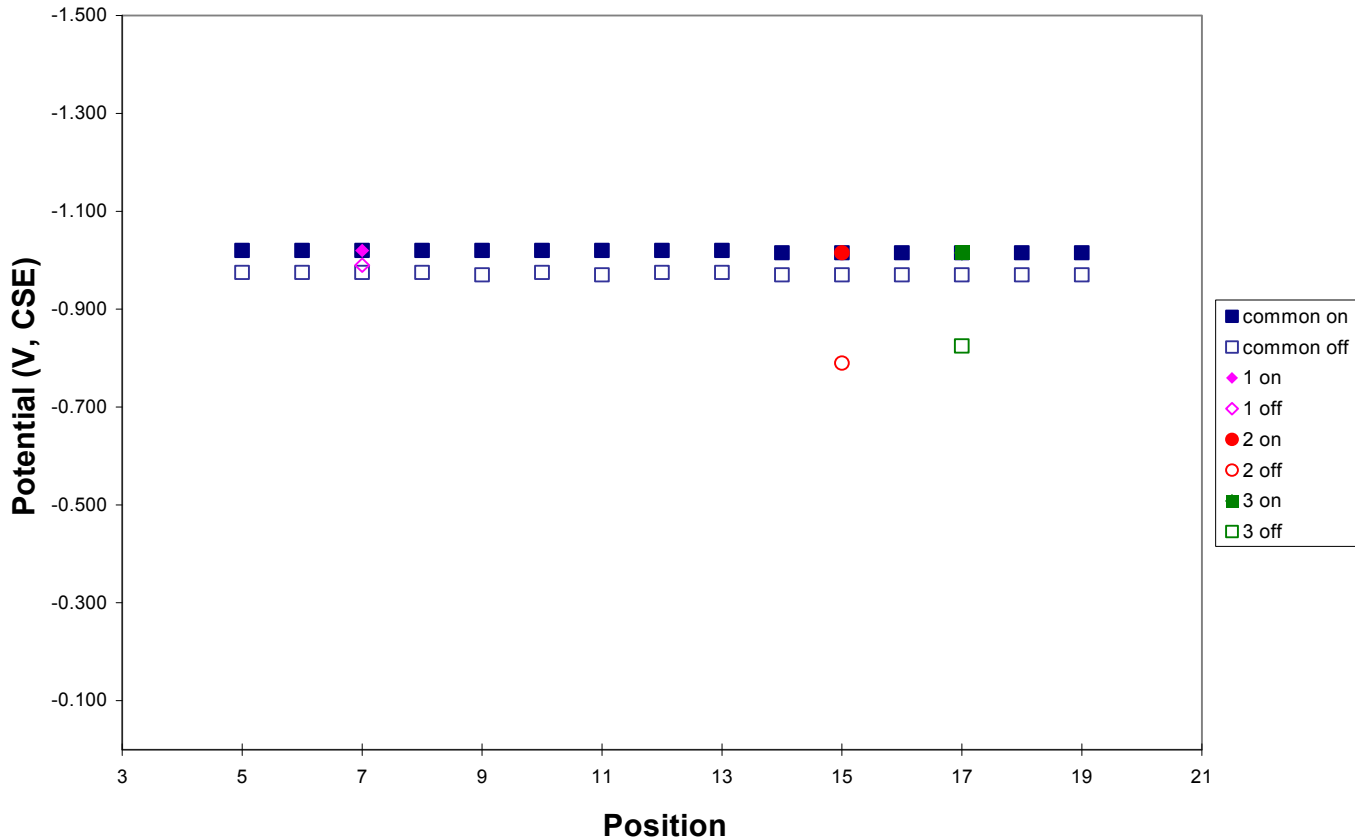


Figure 44. CIS profile (Experiment 6).

Experiment 7: 3.840V interference (reverse polarity)

Figure 45 shows the measured CIS profile with 3.840V of (reverse) interference introduced into the small-cell experimental set-up through anodes positioned in opposite corners of the cell. The polarity of this interference is opposite that of experiment 2. In this experiment, even with such a small interference, it immediately becomes evident that the effect of the interference is opposite that of experiment 2. Namely, defect 1 is discharging, while defects 2 and 3 are picking up. As with experiments 1, 2, and 6, defect 1 is cathodically protected and defect 2 appears protected when measured against the common, though electrical isolation shows that it is not. Defect 3 has actually picked-up to the point that it is now protected (-855mV, see table 2), but before the interference was introduced it was not protected.

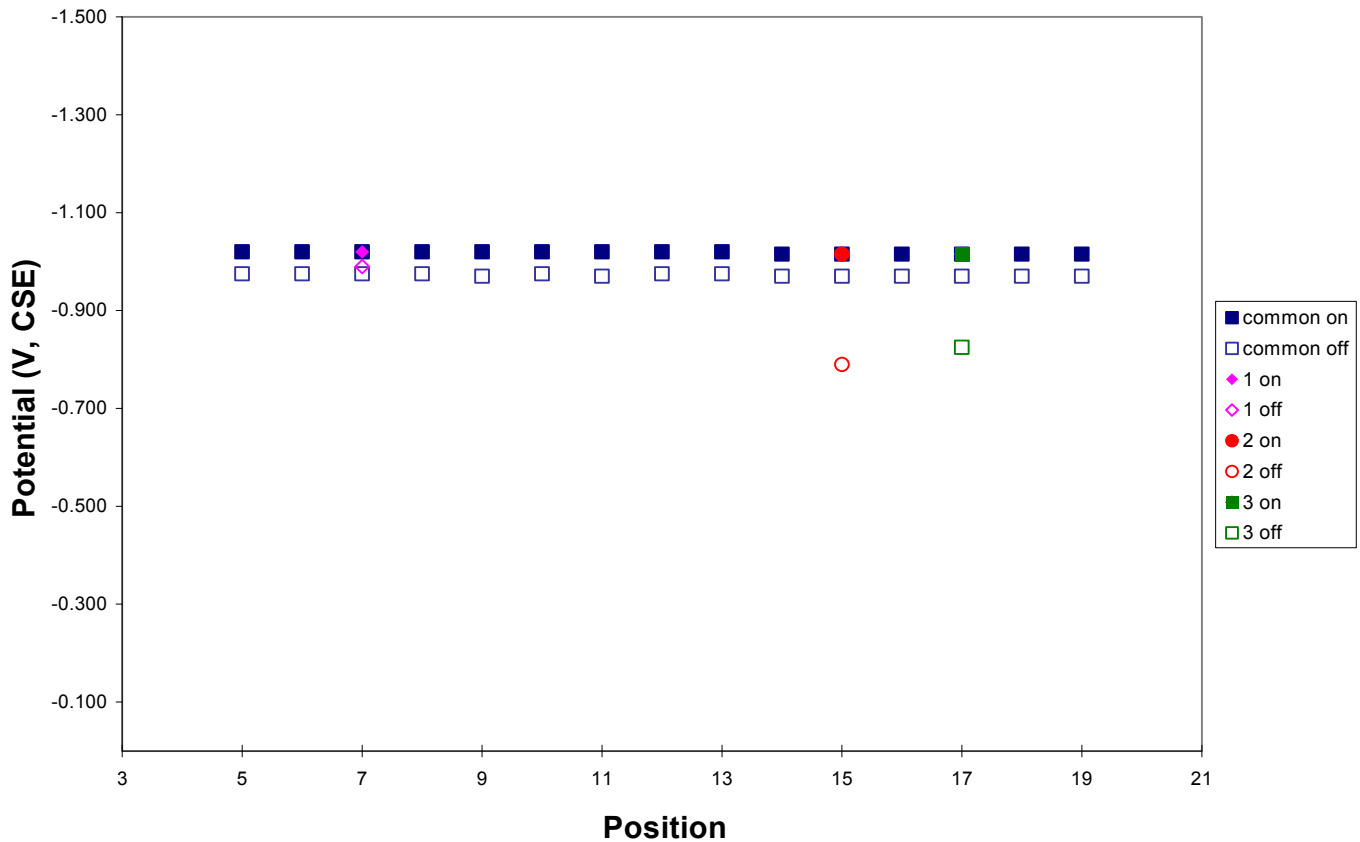


Figure 45. CIS profile (Experiment 7).

Experiment 8: 7.750V interference (reverse polarity)

All things in experiment 8 are the same as those in experiment 7 except for the interference voltage which has been doubled. The results are consistent with expected. Defect 1 has discharged slightly more and defects 2 and 3 have

picked-up again. Defect 3, however, is picking up noticeably more than defect 2 (see table 2). The CIS profile for experiment 8 is presented in Figure 46.

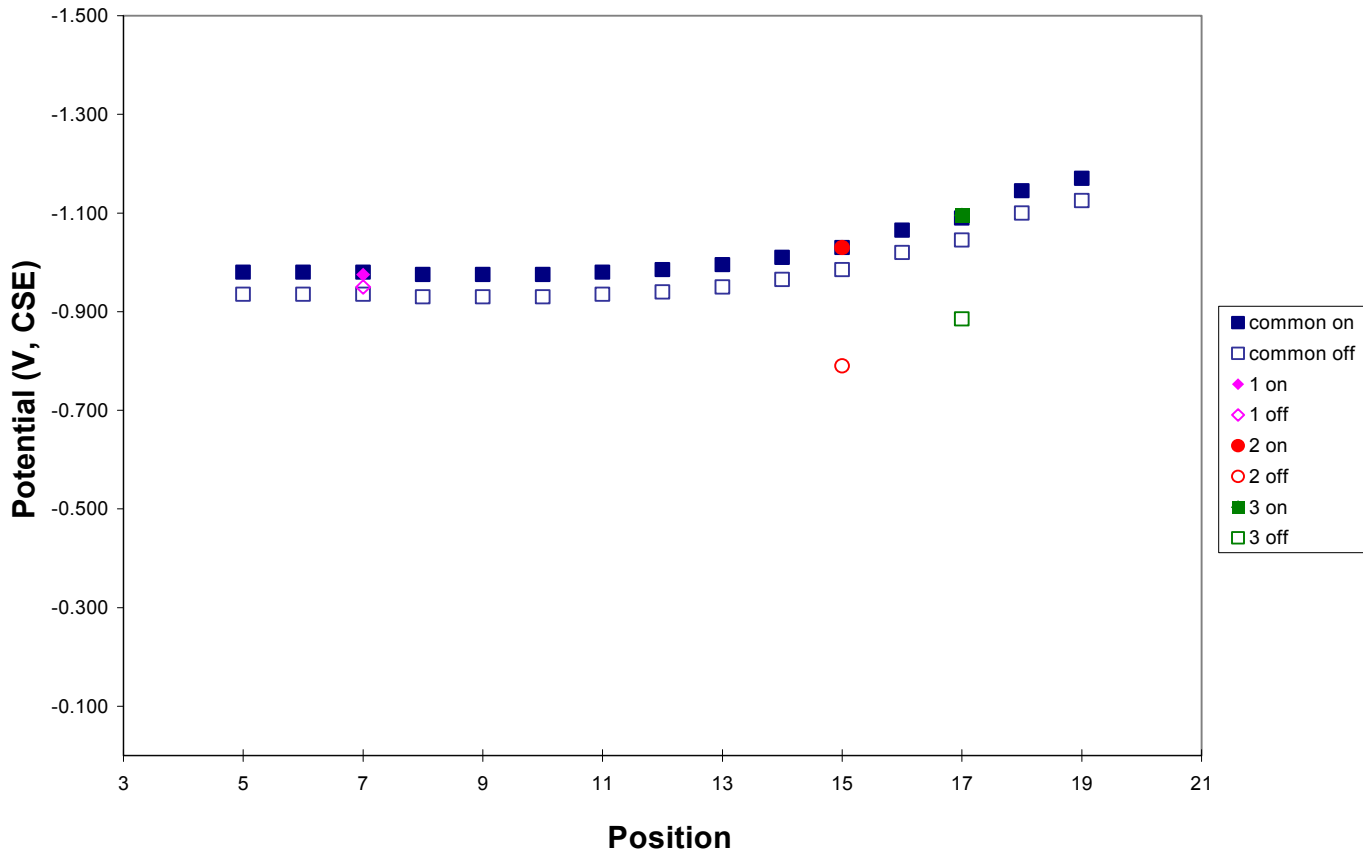


Figure 46. CIS profile (Experiment 8).

Experiment 9: 15.50V interference (reverse polarity)

Figure 47 shows the CIS profile of measurements performed with a 15.50V (reverse polarity) interference voltage. The results are once again consistent with those expected. Defect 1 continues to discharge, and defects 2 and 3 continue to pick-up, with defect 3 picking-up much more than defect 2. Defect 3 has picked-up so much, in fact, that the common measurement indicates an off potential more negative than -1100mV, a measurement seeming to indicate hydrogen evolution may be present at this defect. Electrical isolation of the defect produces a measured off potential of -955mV, a measurement signifying adequate, but not excessive, cathodic protection.

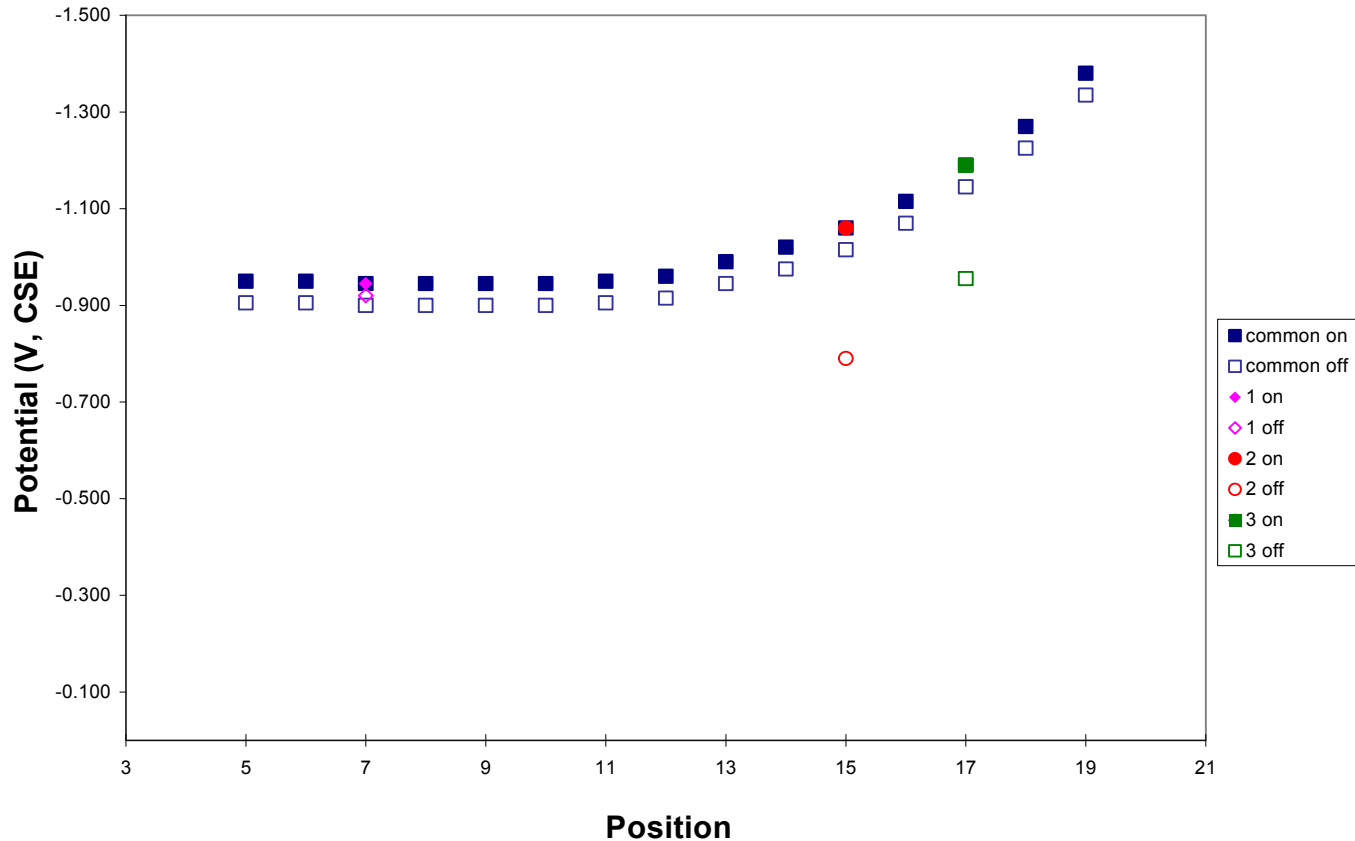


Figure 47. CIS profile (Experiment 9).

Experiment 10: 30.69V interference (reverse polarity)

Figure 48 illustrates the CIS profile measured with 30.69V of (reverse polarity) interference present. Defect 1 has discharged to the extent that the common measurement now indicates it is no longer cathodically protected (-830mV, see table 2), when in fact it still is (-860mV). As with experiments 6-9, defect 2 appears protected when measured against the common when in fact it is not. Similar to experiment 9, defect 3 appears to be a location where hydrogen evolution is occurring (-1320mV). Electrical isolation, however, shows the defect to be adequately, but not excessively, cathodically protected.

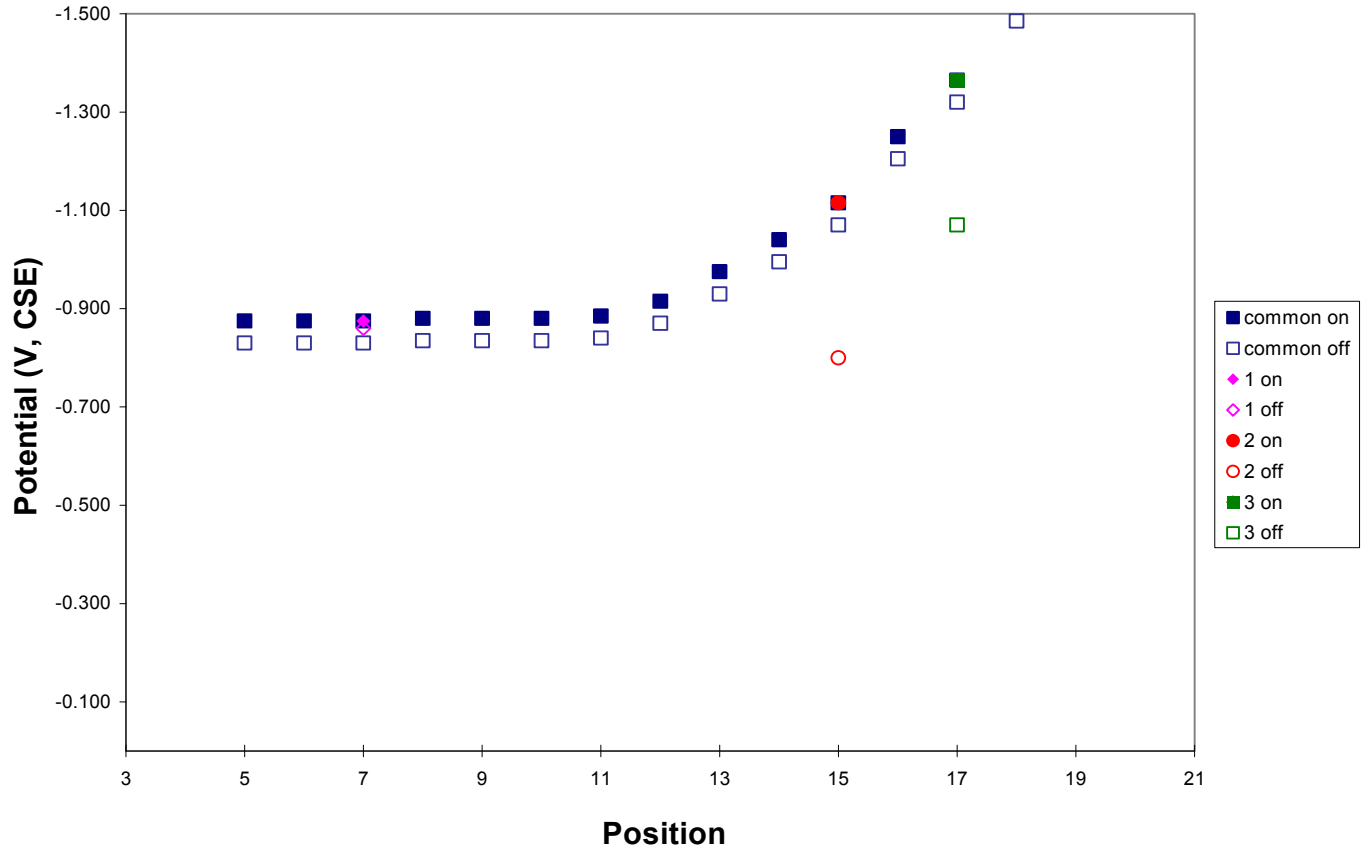


Figure 48. CIS profile (Experiment 10).

Table 28 and Table 29 summarize the results of Experiments 1-5.

Table 28. Current distribution (Experiments 6-10, measurements in mA).

Location	Interference				
	None	3.840V	7.75V	15.50V	30.68V
Defect 1	0.10	0.09	0.08	0.07	0.05
Defect 2	0.01	0.01	0.01	0.01	0.01
Defect 3	0.05	0.06	0.06	0.07	0.09
Σ Defects 1-3	0.16	0.16	0.16	0.16	0.15

Table 29. 'On' and 'Off' potentials (Experiments 6-10, measurements in V).

Location	Interference									
	None		3.840V		7.75V		15.50V		30.68V	
	On	Off	On	Off	On	Off	On	Off	On	Off
Defect 1										
Electrically Isolated	-1.020	-0.990	-0.995	-0.965	-0.975	-0.950	-0.945	-0.920	-0.875	-0.860

Common	-1.020	-0.975	-1.000	-0.955	-0.980	-0.935	-0.945	-0.900	-0.875	-0.830
Defect 2										
Electrically Isolated	-1.015	-0.790	-1.020	-0.785	-1.030	-0.790	-1.060	-0.790	-1.115	-0.800
Common	-1.015	-0.970	-1.020	-0.975	-1.030	-0.985	-1.060	-1.015	-1.115	-1.070
Defect 3										
Electrically Isolated	-1.015	-0.825	-1.050	-0.855	-1.095	-0.885	-1.190	-0.955	-1.365	-1.070
Common	-1.015	-0.970	-1.050	-1.005	-1.090	-1.045	-1.190	-1.145	-1.365	-1.320

Conclusions

Experimental results show that stray currents present in the soils do in fact alter the actual (with pipe sections electrically isolated) and observed (all sections of pipe electrically connected) OFF potentials along the pipe. The nature of the measurements, that is, the factors defining the measured potential, is the same whether or not interference is present.

In other words, the impedance of the measured structure defines the magnitude of the measured potential and influences the distribution of the CP and stray currents. The existence of static DC current that is picked up and discharged by the structure may not be apparent to the surveyor. It can be argued that the 31V interference is likely to manifest itself on any at-grade reference electrode-to-reference electrode measurements. However, following the impedance arguments, it is the current picked up/discharged by the holidays that determines the extent of polarization caused by the stray current. In this regard, the value of 30V should not be dismissed as an 'obvious' one; in fact, if the resistance of soil is low, a considerably lower interference voltage can lead to the same effect.

The experiments clearly illustrate that stray currents can lead to inaccurate CIS survey data, which in turn affects the ability to accurately discern the condition of the pipeline coating. For example, a location may show an OFF potential more negative than 1300 mV (which would suggest considerable overprotection) when measured in the presence of a 30.68V interference, when in reality the OFF potential at that location is -1070mV and the defect is not over-protected to the extent that damage is occurring.

AC measurements

Given that AC corrosion is fast becoming more and more recognized as a phenomenon occurring on underground pipelines, one commonly employed

technique of assessing the problem is conducting AC CIS measurements (AC voltage on the pipe is measured).

The AC voltage can be used to make an approximate calculation of the current density expected for a defect of a known (or assumed size). The formula uses “leakage” resistance to convert the voltage into current density:

$$i = \frac{8V_{AC}}{\rho\pi d}$$

where:

i = AC current density

V_{AC} = AC voltage of pipeline to remote earth

ρ = soil resistivity

d = diameter of a circular holiday having an area equal to that of the actual holiday

Strictly speaking, if the defect is small in size, the resistance of the “pore” will be non-trivial and should be considered. However, for this discussion it can be left out.

Given that the holiday size is the same for all the Defects, the primary driving factors determining the AC current density are the measured voltage and the specific soil resistivity.

Shown in Figure 49 is the AC CIS profile. The AC voltage was set at approximately 4.5 volts. Using the AC voltage and the soil resistivity values (approximately 90 ohm-cm for clay and 74,000 ohm-cm for sand), estimates of the AC current density can be made.

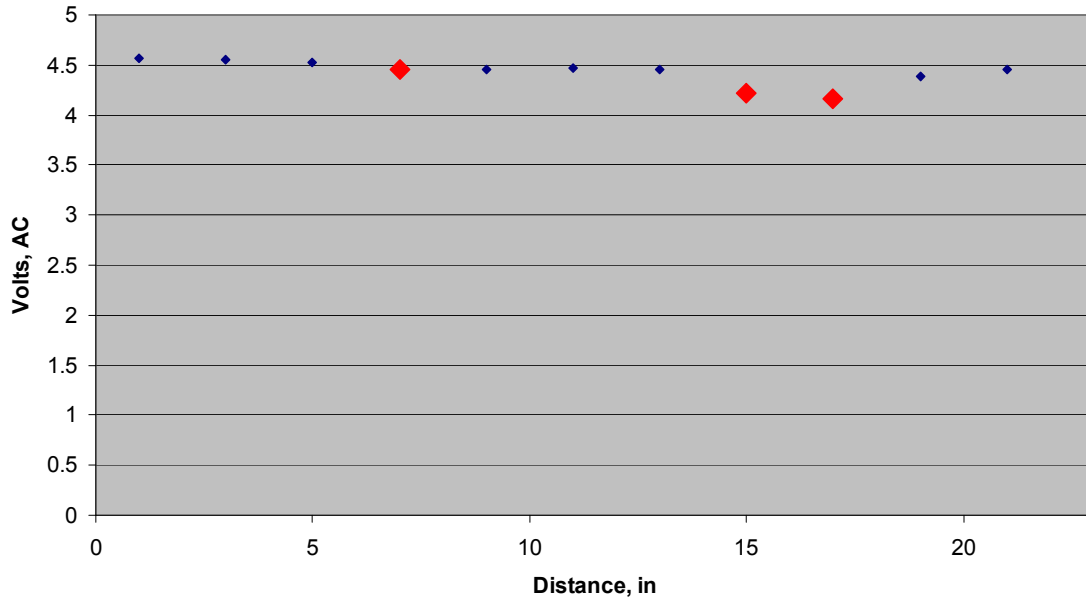


Figure 49. AC CIS profile in sand/clay. Red points denote locations of Defects.

Due to the configuration of the pipe assembly, however, currents to individual Defects could be measured directly and compared with the estimates.

The following Table summarizes the results, which have been converted to current density.

Table 30. Estimated and measured AC current density

	AC density, A/m ²		Error
	Estimated	Measured	
Defect 1	2103	2045	3%
Defect 2	2.4	1.1	55%
Defect 3	2.39	24.7	-938%

AC current modeling

The PRCI model, according to the software provider’s description, includes comprehensive electromagnetic coupling equations with an interface format to enable both steady state and fault induced voltages and currents to be calculated. The program was not expressly made for predicting AC currents and because its inner logic could not be modified (it estimates coating condition by multiplying the soil resistivity by a certain coefficient), a number of assumptions had to be made to accommodate the requirements.

The seed values were obtained in one of the laboratory tests (AC voltage of 3.5V) and are summarized in Table 31:

Table 31. Input values used in PRCI model.

	Holiday Location	AC current, measured, (mA)	Impedance, ohm
Defect 1 (clay)	4"	53.18	65.8
Defect 3 (sand)	14"	0.3	11666.7

Due to the small size of the laboratory cell, in order to be able to use the software to predict currents, a scaling factor had to be calculated (1200:1). Next several software runs were made assuming various coating conditions (excellent, good, fair) to determine the current estimates at the defect location (calculated as the induced current magnitude for a section of pipeline with a given length). The results are shown in Table 32.

Table 32. Model output.

Coating condition	Current, mA	
	Defect 1	Defect 3
Fair	2.08	0.58
Good	2.17	0.58
Excellent	3.75	0.5
Superior	9.92	0.42
Flawless	11.08	0.25

When treated with the above caveats in mind, the results are consistent with the laboratory measurements and other models. The defect located in the low resistivity soil discharges more current than the one in high resistivity soil for all coating conditions. However, as the coating condition degrades, the current at Defect 1 becomes smaller, because now there are more holidays present in the coating. For Defect 3, it is the soil resistivity that dominates the impedance of the holiday; therefore, the trend for the AC current is to only slightly increase as the coating quality changes from flawless to fair. Even when the coating is uniformly poor for both soils (with the high and the low resistivity), the soil resistivity at Defect 3 restricts the current flow and Defect 1 is forced to act as a current drain.

Conclusions

The experiments show that the knowledge of soil resistivity is absolutely critical if one attempts to estimate AC current densities using AC voltage measurements. The two adjacent soils (sand and clay) can have two drastically different resistivities. As the calculation demonstrates, in clay, margin of error between the estimated and the calculated values was minimal. In the sand, the difference

becomes dramatically different. However, in case of Defect 2, even with the 55% error, the estimated current density falls in the same “Low AC hazard” category as the measured one. In case of Defect 3, the error is not only much greater, but the calculation errs on the side of underestimation of the AC current density. The actual measured density, which is more than 10 times greater, has been demonstrated to cause accelerated corrosion of buried steel.

The results suggest that the use of AC CIS for assessing the AC corrosion hazard even when the soil resistivity is known may lead to erroneous conclusions in high resistivity soils. The likely reason for such a difference is that the AC voltage measurements are subject to the same considerations as those involving the DC potentials. That is, each measured value may represent multiple ‘sites’ on the buried pipeline; depending on the impedance associated with each particular site, the AC voltage may be skewed more towards the voltage of some of the sites.

The software package made commercially available by PRCI has been demonstrated to be able to make approximate estimates of AC current in a span of pipeline of known length. Using certain known input parameters (such as soil resistivity) and estimated values of coating quality and ‘typical’ holiday size, it is possible to make ‘degree of magnitude’ estimates of AC current density and relate it to AC corrosion likelihood.

Task 2 – Large-scale experimental studies and Task 3 – Field verification

As discussed in the Work Scope, due to the scarcity of specific conditions related to AC and DC interference, a decision has been made to combine the activities of Tasks 2 and 3 using the large-scale experimental setup constructed during Task 2. The detailed description of the site follows.

Setup construction and configuration

The setup incorporated a total of 38 sections of coated pipeline. There are two parallel lines of two pipelines – both consisting of 19 sections each. Pipeline 1 has an internal diameter of 20 inches and an external FBE coating; pipeline 2 has an internal diameter of 8 inches and a dual-coat FBE system. The total length of the sections for either diameter is approximately 60 feet. The sections have plastic end caps on both ends; the caps are wrapped with Canusa® shrink sleeves to ensure water-proofing of the inside surfaces for long-term testing. The appearance of the sections is illustrated in Figure 50.



Figure 50. Pipeline sections (20" diameter, left, 8" diameter, right) with end caps.

Each section contains intentionally introduced single defect (with the exception of the first section for each pipeline which has multiple random defects). The defects range both in size (1 inch vs. 10 inch area), circumferential position (12:00, 3:00, and 6:00 clock), and lateral spacing (2.5 to 5 feet). Some defects are centrally located and some are placed off to one end in order to arrive at the desired spacing between the holidays. In addition, several sections of both pipelines contain distributed defects (a cluster of ten 1 square inch defects). The examples of defects are shown in Figure 51 through

Figure 55.

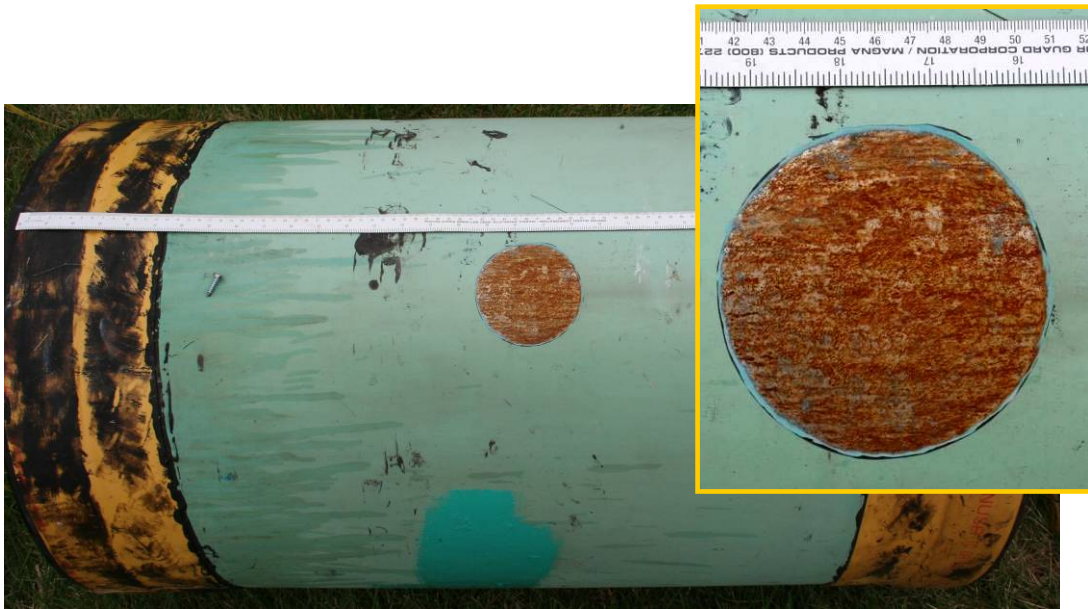


Figure 51. Single centrally positioned 10 sq. inch defect in pipeline section.



Figure 52. Single centrally positioned 10 sq. inch defect in 8 inch pipeline section.





Figure 53. Examples of offset 10 sq. inch defects in 8 inch (above) and 20 inch (below) pipeline sections.

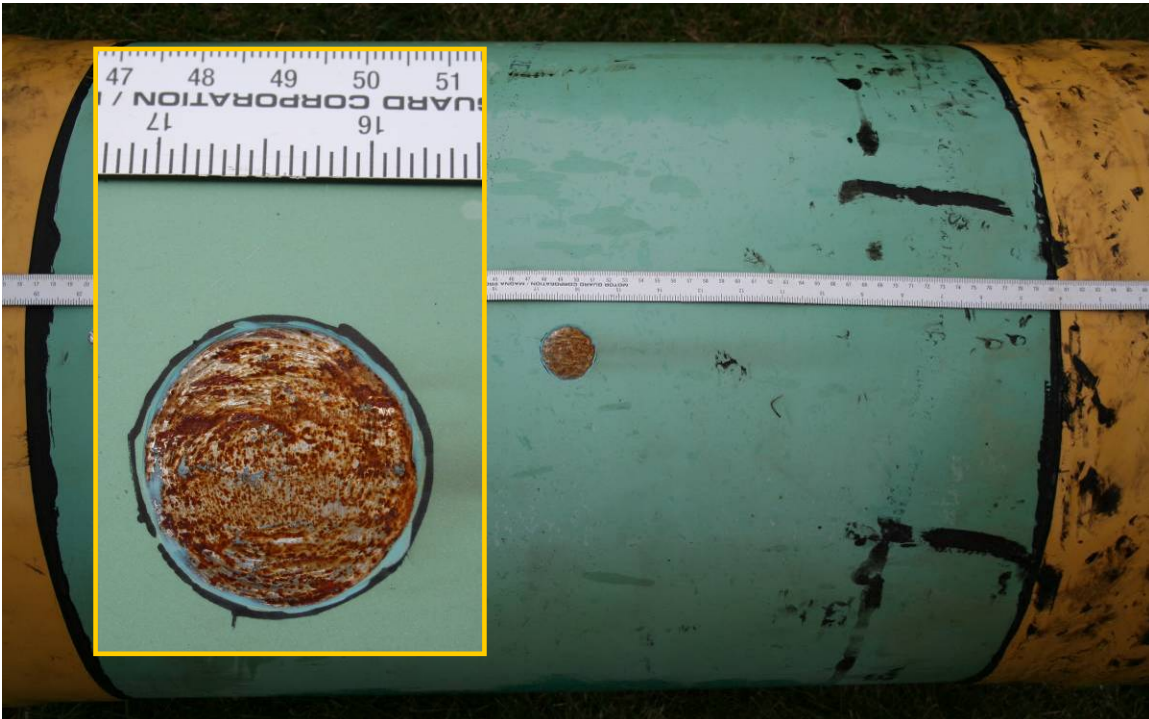




Figure 54. Examples of centrally positioned 1 sq. inch defects in 8 inch (above) and 20 inch (below) pipeline sections.

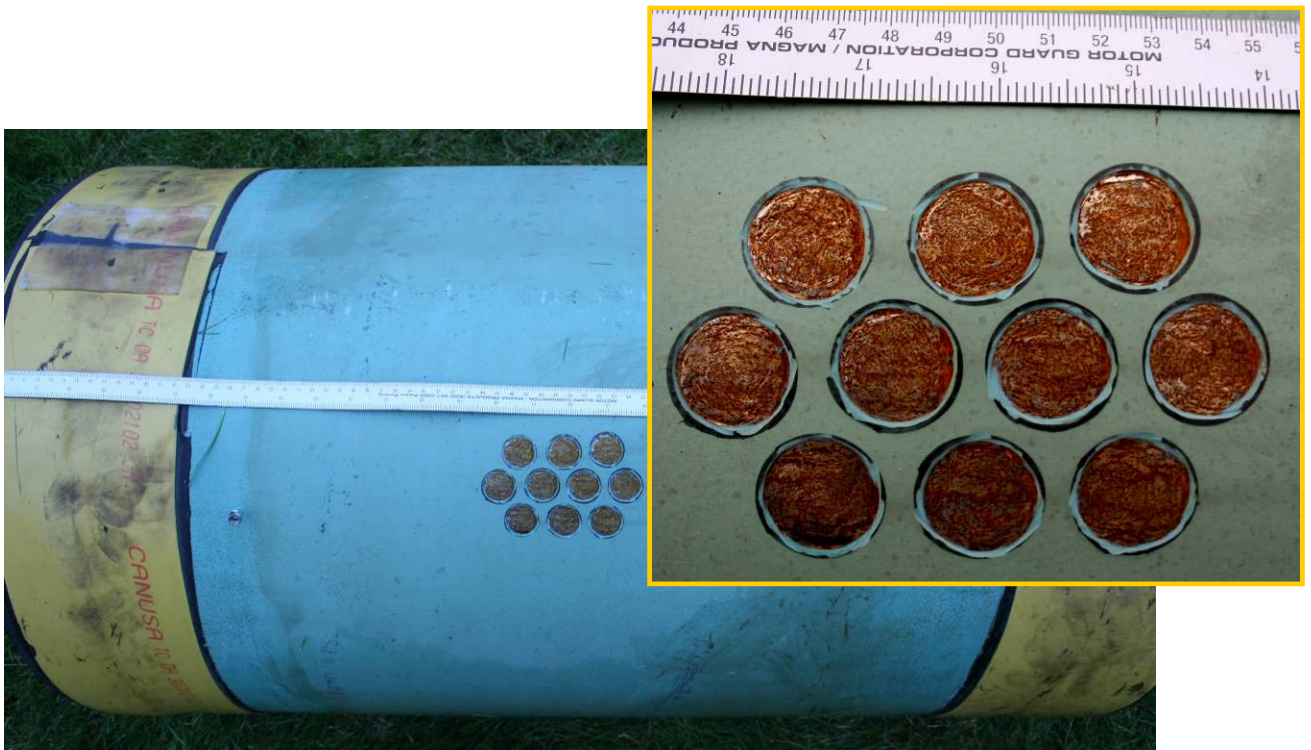




Figure 55. Examples of distributed defects (10 individual 1 sq. inch defects) on 20 inch (top) and 8 inch (bottom) sections.

To measure the potentials at the defects, nine of the sections are outfitted with permanent reference electrodes manufactured from platinized niobium wire. The wire is encased in epoxy and affixed to the surface of the pipe section in the vicinity of the defect (less than 1 inch of distance). In this manner, the measurements of potentials at the grade level can be correlated with the (almost) in-situ readings. In addition, the outer metal casing of the reference electrode assembly can be used as a counter electrode, so that in-situ polarization measurements could be performed, if necessary.

An example of a reference electrode is shown in Figure 56.

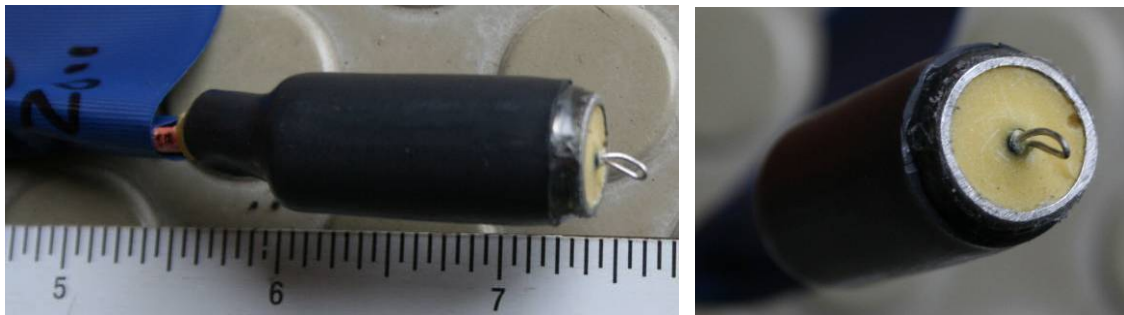


Figure 56. Example of a reference electrode (platinized niobium wire encased in epoxy with an outer metal casing).

In addition, to facilitate different polarization levels of defects in the coating, eight of the sections have pencil-type electrodes manufactured from magnesium and copper placed next to them. This permits, if desired, to polarize the defects in

either negative or positive direction to arrive at the desired target potential value (see Figure 57 for illustration).

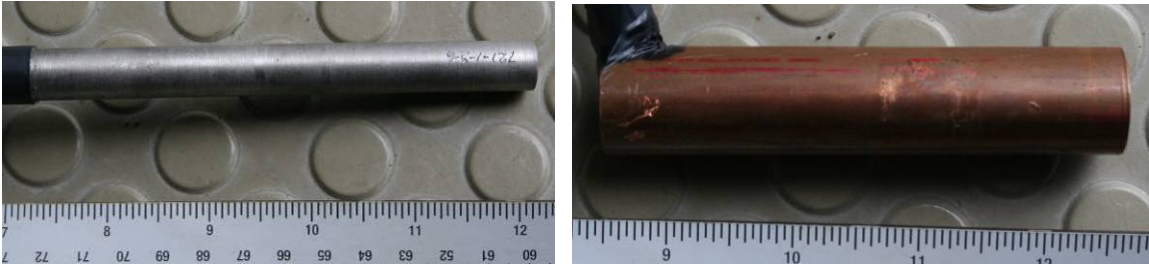


Figure 57. Example of magnesium (left) and copper (right) electrodes.

Figure 58 shows the reference electrode and magnesium and copper electrodes in place prior to backfilling the pipeline. Most of the magnesium and copper electrodes were placed in between the pipeline sections, as opposed to the immediate proximity of a defect (see Figure 59).



Figure 58. Reference electrode (left), magnesium electrode (upper right) and copper electrode (bottom right) strapped to the 20 inch pipeline section prior to installation.



Figure 59. Reference electrode (left) attached next to an off-center 10 sq. inch defect on 8 inch pipeline section; magnesium electrode (right, lower) and copper electrode (right, upper) placed in between two adjacent pipeline sections.

The sections are configured such that they could be either electrically isolated from each other or connected into a single network. Each section has a single coated wire lead (rated for underground service) cad-welded to it. The sequence of cable installation is illustrated in Figure 60.

Ten (10) sections of each pipe are buried under 4 feet of soil cover; five (5) sections are buried under 2 feet of soil, and remaining four (4) sections are buried under 4 feet of sand (to test higher resistivity soil conditions). The site installation is illustrated in Figure 61 through Figure 63. Six-inch wide sections of 16 and 8 inch diameter bare pipelines are interspersed between the coated sections (4 sections for each pipe diameter); each has a lead and can be connected to the coated sections (see Figure 62). Each sand-filled section has a sump pump to remove collected water.



Figure 60. Installation of cable leads.





Figure 61. Installation of first 9 sections (20 inch line on the left, 8 inch line on the right). Note bare pipeline sections indicated by arrows.



Figure 62. Section of bare pipeline inserted between two 8 inch pipeline sections.



Figure 63. Drainage pipe installed prior to laying of the 8 inch pipeline sections in sand backfill (left); pipeline sections in partially filled trench (right). Upright corrugated stack houses a sump pump to remove drained water.

The pipeline sections can be cathodically protected using four sacrificial CP magnesium anodes. The intent was to achieve different levels of polarization and to make the setup flexible so that multiple configurations of the pipeline sections and potential distributions can be studied.

The potential measurements at grade can be augmented by the measurements taken using five Coupon Test Stations placed in the vicinity of the coating defects (5 CTSs are placed next to each of the pipeline section strings). The overall view of the completed setup is shown in Figure 64.



Figure 64. Completed site (red flags show coating holiday locations).

The lead wires from all underground components (pipe sections, coupon test stations, sacrificial anodes, counter electrodes, etc.) were routed through buried plastic conduit and terminated in a board mounted next to the site. The board setup allows imposition of stray currents on the pipeline sections; by varying the stray current activity and comparing the ECDA results to the actual configuration of the experimental setup (with regard to the size, distribution and location of the coating defects), the limitations of the common, potential-based ECDA techniques were ascertained for each chosen level of stray currents.

The panel with the segments' outline and electrical connections is shown in Figure 65.

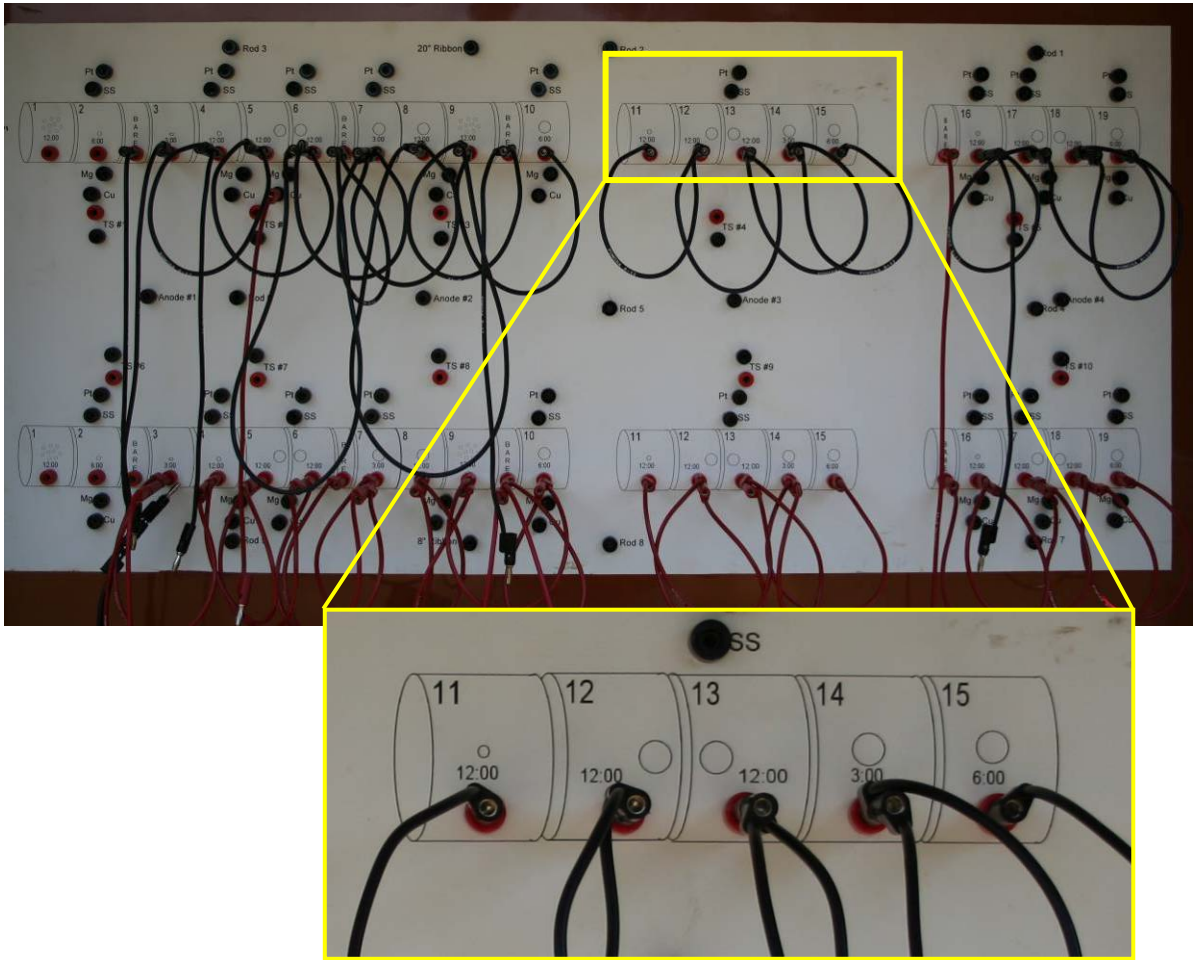
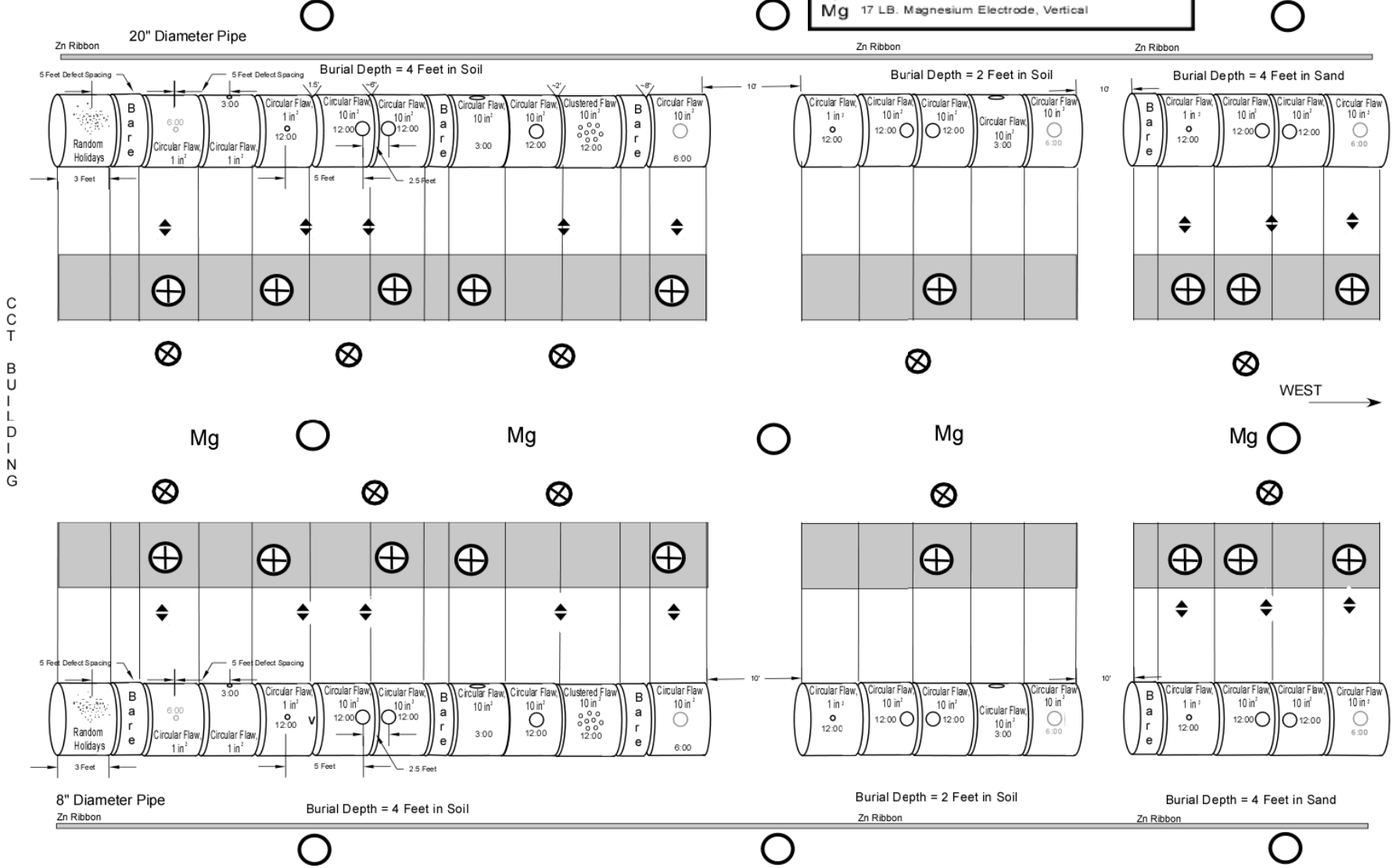
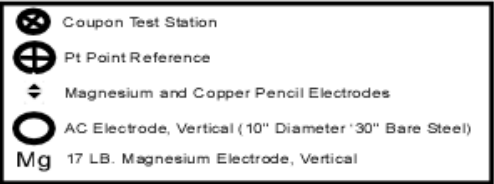


Figure 65. Panel with electrical connections to all large-scale setup components.



CIS

Baseline readings

The CIS profiles collected over 8 months for both the 20 inch and 8 inch pipeline segments are shown in Figure 66 and Figure 67 below. The earlier (November 2006 and March 2007) readings were taken when all the segments for each respective size were electrically isolated from each other; the June 2007 profile was taken when the segments in each of the sections (4 ft deep, 2 ft deep, sand) were electrically connected, forming *three* continuous 'pipelines'.



Figure 66. CIS profile of 8 inch pipeline segments (potentials are in mV against copper/copper sulfate reference electrode).

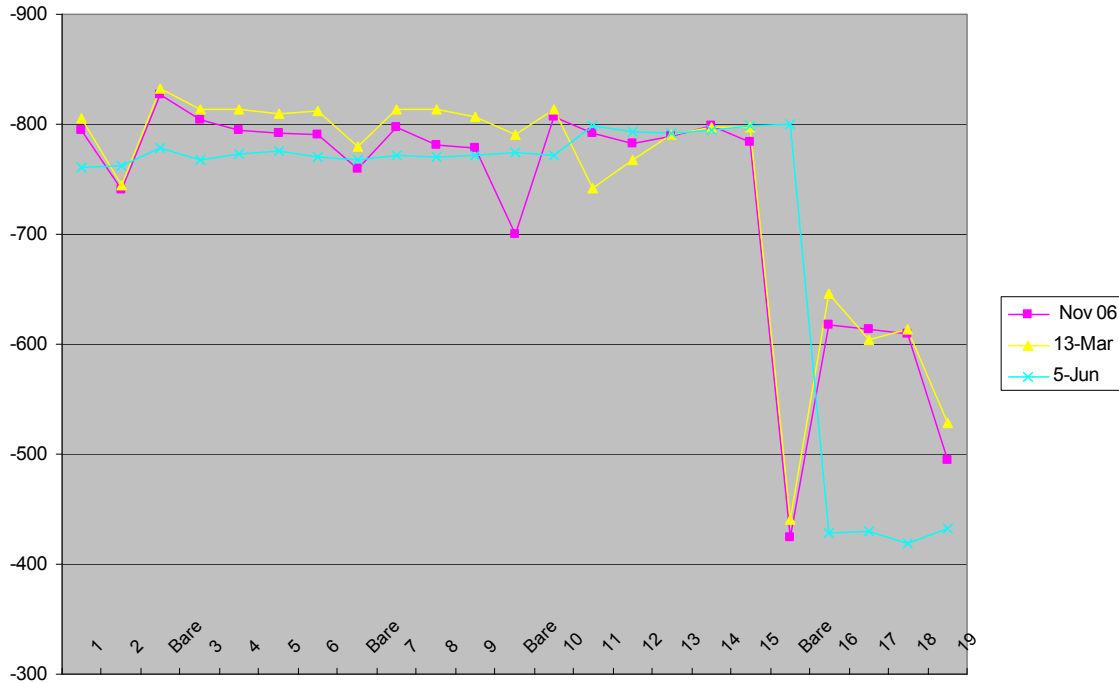


Figure 67. CIS profile of 20 inch pipeline segments (potentials are in mV against copper/copper sulfate reference electrode).

The charts show that the potentials are largely unchanged, which indicates the desired stability levels; the potentials of the pipeline buried in sand (Bare-19) have become more positive, which is likely the reflection of the lower moisture content due to warmer outside temperatures. Additionally, the operation of the sump pumps continuously removes the accumulated water from the sand backfill, this facilitating more positive potentials. Electrically linking the segments within each section together also, as expected, smoothed out the profile.

CIS under interference

The CIS profiles were taken under varying levels of AC interference. For these tests, all the segments were electrically connected and formed *one* continuous 'pipeline'. Several levels of interference were tested, with noise signal levels of 1 and 5V and three frequencies (10, 30, and 60Hz). Two devices were used to make measurements:

1. Allegro™ field computer.
2. In order to ascertain whether different equipment that would typically be used for CIS measurements would respond differently to the noise signal, in addition to the Allegro meter, the CIS profiles with 1V interference (10

and 60Hz) were also collected using a Fluke® multimeter (manual readings).

The summary of the tested conditions is summarized in Table 33.

Table 33. Summary of tested interference levels.

Voltage, V	1 V			5V		
Frequency, Hz	10	30	60	10	30	60
Fluke	x		x	x		x
Allegro	x	x	x	x	x	x

1. The potentials were measured without imposed cathodic protection current. Care was taken to ensure that the imposed AC interference signal continued a negligible level of direct current. The CIS plots were taken with approximately 1 ft intervals. The CIS profiles with and without interference that were collected with Allegro meter are shown in Figure 68 and Figure 69.

At a first glance, there is a considerable scatter in the data at all levels of interference and interference frequencies. The picture becomes clearer when the data is analyzed systematically.

The difference between the open-circuit (native) potentials and potentials collected under the influence of AC noise was tabulated and a histogram analysis of the magnitude of the difference at each CIS station was determined. The distribution of these values is shown in Figure 86 and Figure 87.

The charts indicate that the lower level of interference produced the distribution that is skewed to more negative values, with the peak between -30 and -50 mV, irrespective of the frequency of the noise. The higher interference level resulted in the distribution centered on approximately 0 mV of difference. The effect of frequency was also more pronounced. Thus, at 60Hz, the difference was confined to the narrowest band; lower frequencies produced a greater range of interferences. As seen in the CIS charts and distribution graphs, 5V 30Hz produced exerted the most influence on the measured potentials, with the excursions in the volt range.

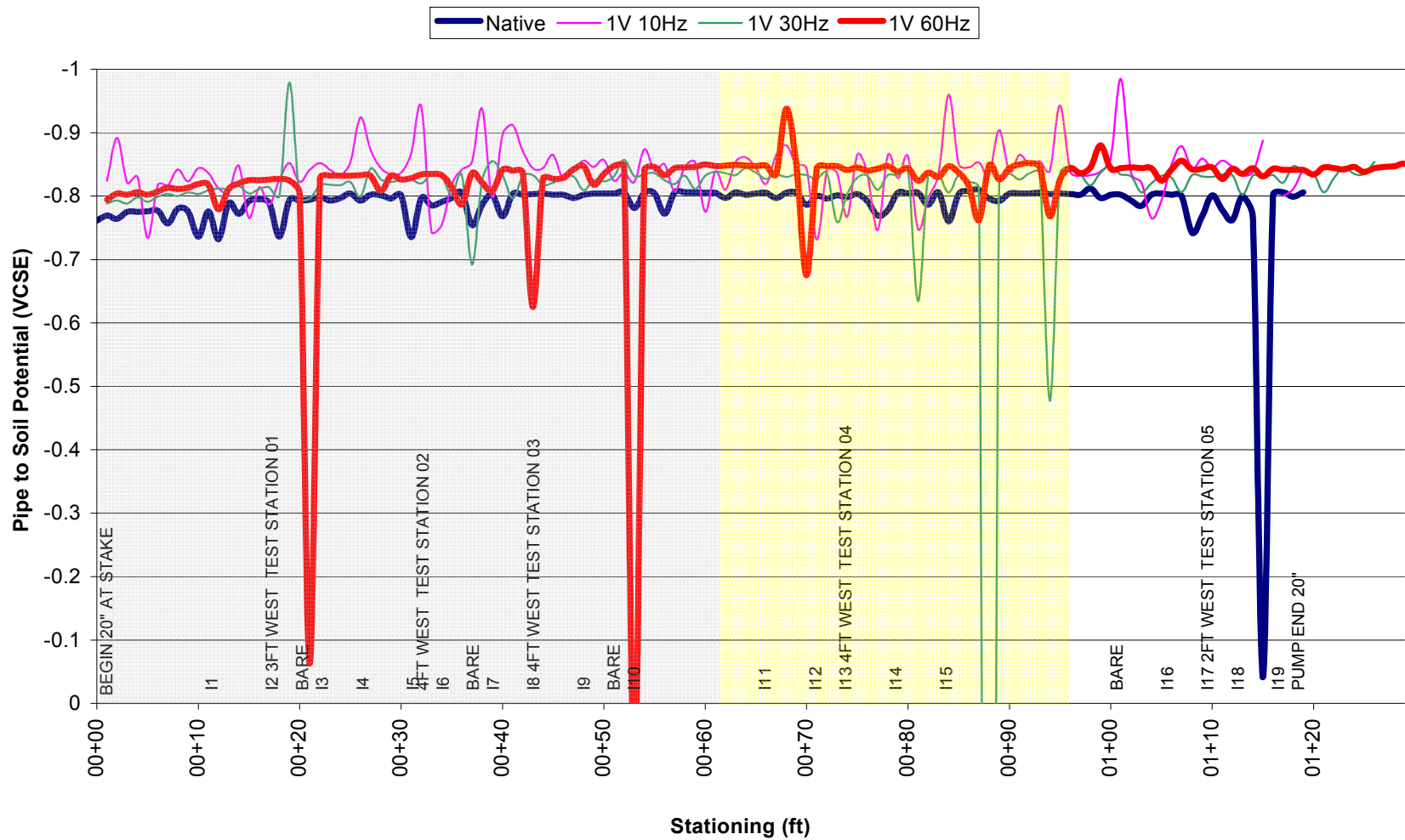


Figure 68. CIS profile (1V interference at three different frequencies). Gray shading – 4 ft depth of cover in soil; yellow shading – 2 ft depth of cover in soil; no shading – 4 ft depth of cover in sand. Allegro meter.

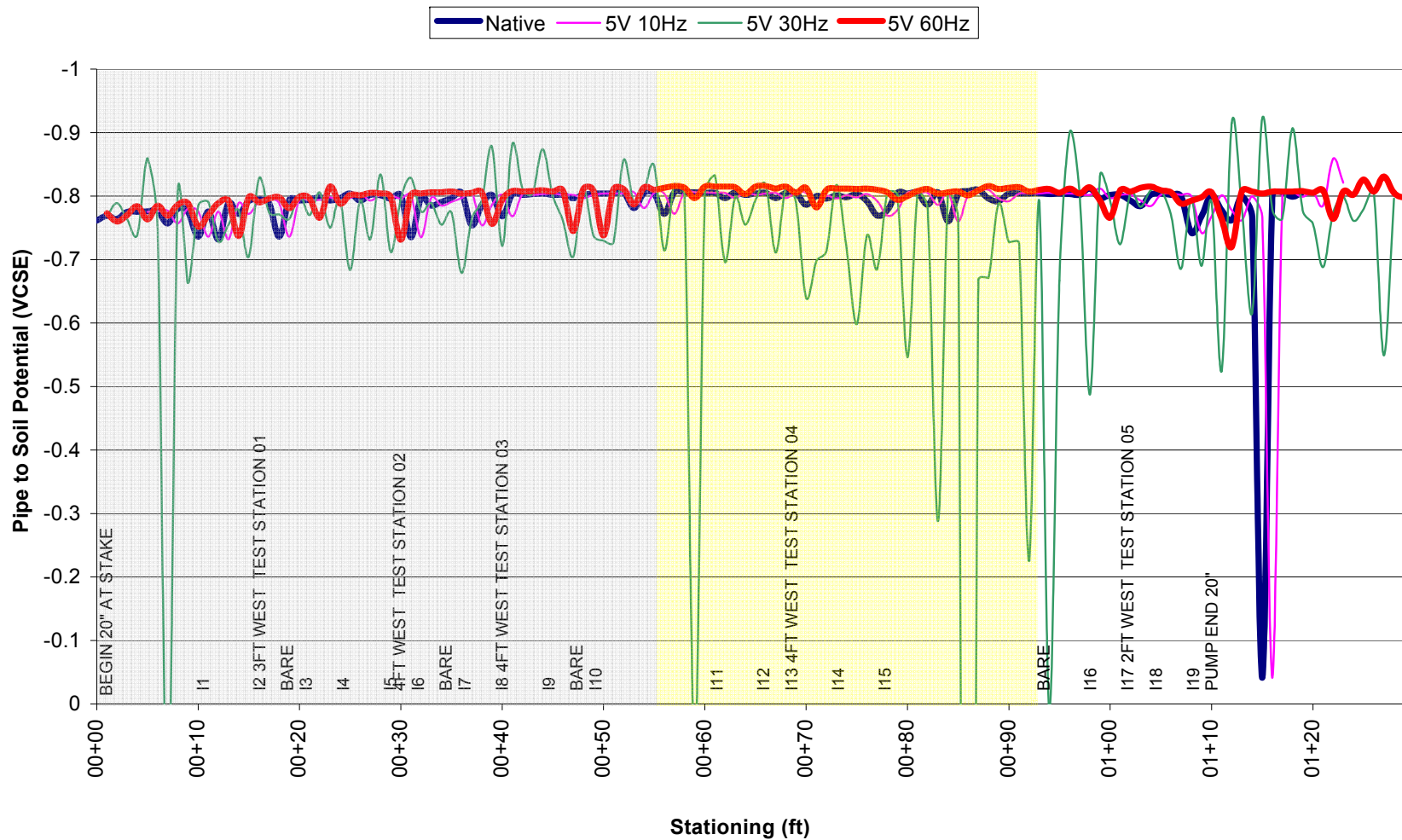


Figure 69. CIS profile (5V interference at three different frequencies). Gray shading – 4 ft depth of cover in soil; yellow shading – 2 ft depth of cover in soil; no shading – 4 ft depth of cover in sand. Allegro meter.

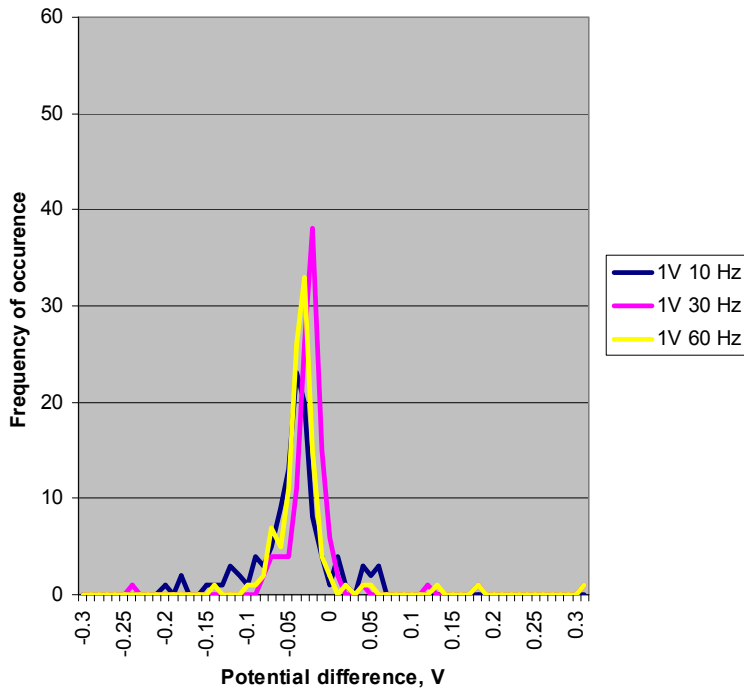


Figure 70. Distribution of potential difference between native potentials and potentials measured under AC interference (1V, different frequencies). Allegro meter.

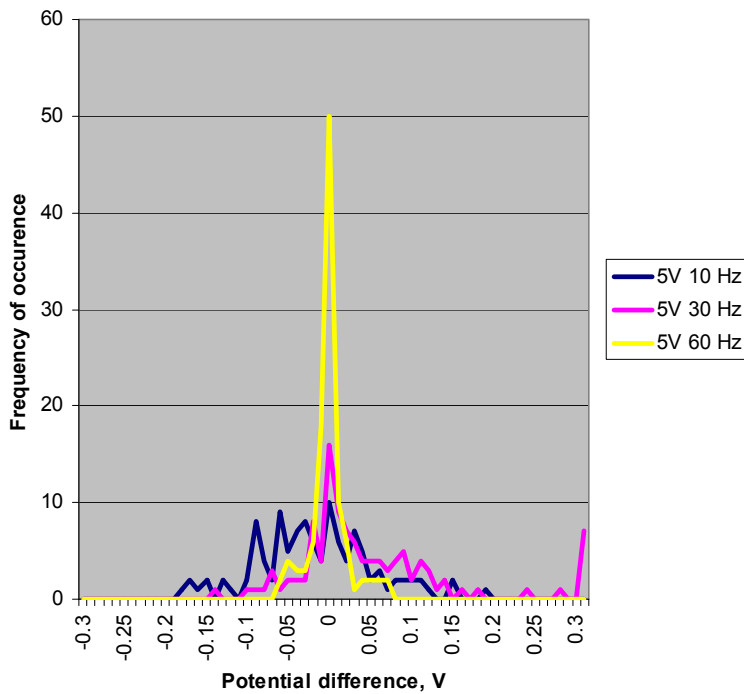


Figure 71. Distribution of potential difference between native potentials and potentials measured under AC interference (5V, different frequencies). Allegro meter.

With regard to the interference, one must keep the affected values in practical perspective. First, the whole set of CIS values would be considered unreliable if there is a suspicion of dynamic stray current interference. However, assuming that the CIS profiles are deemed acceptable, a value of positive 3.5V collected over a single CIS increment will still most likely be discarded as erroneous. In other words, it is expected to be filtered out from the decision-making with regard to the CP effectiveness.

In that sense, the surreptitious influence of the lower level of interference is more hazardous as it produced potential numbers that may not be considered overtly erroneous. There was a negative DC offset as well, which would have made the potentials appear more protective than in reality.

2. The CIS profiles taken with the Fluke multimeter are shown in Figure 72. The reaction time of the Fluke multimeter is longer than that of the Allegro unit. Therefore, as expected, most of the potential excursions seen in the Allegro charts, especially those at the higher frequency, were not registered. Both 10Hz and 60Hz profiles look relatively smooth; the charts have fewer peaks and valleys than the native potential profile.

The histogram analysis of the difference between the native and affected potentials yields distributions that are similar to those obtained for the Allegro meter (see Figure 73). The distributions of the magnitudes of the potential differences for both 10 and 60Hz are also skewed to the more negative values, with its peaks falling between -50 and -70 mV.

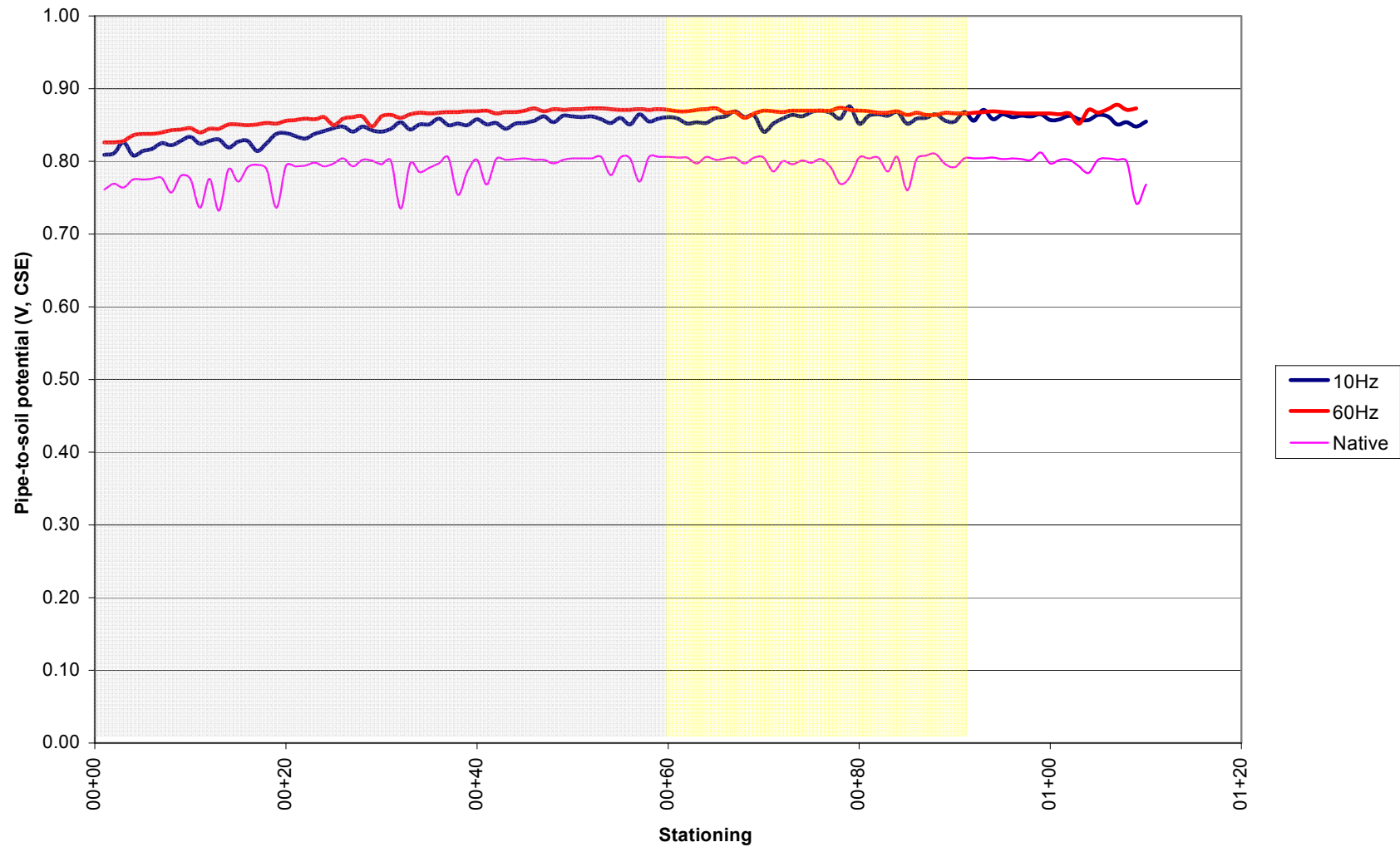


Figure 72. CIS profile (5V interference at two different frequencies). Gray shading – 4 ft depth of cover in soil; yellow shading – 2 ft depth of cover in soil; no shading – 4 ft depth of cover in sand. Fluke meter.

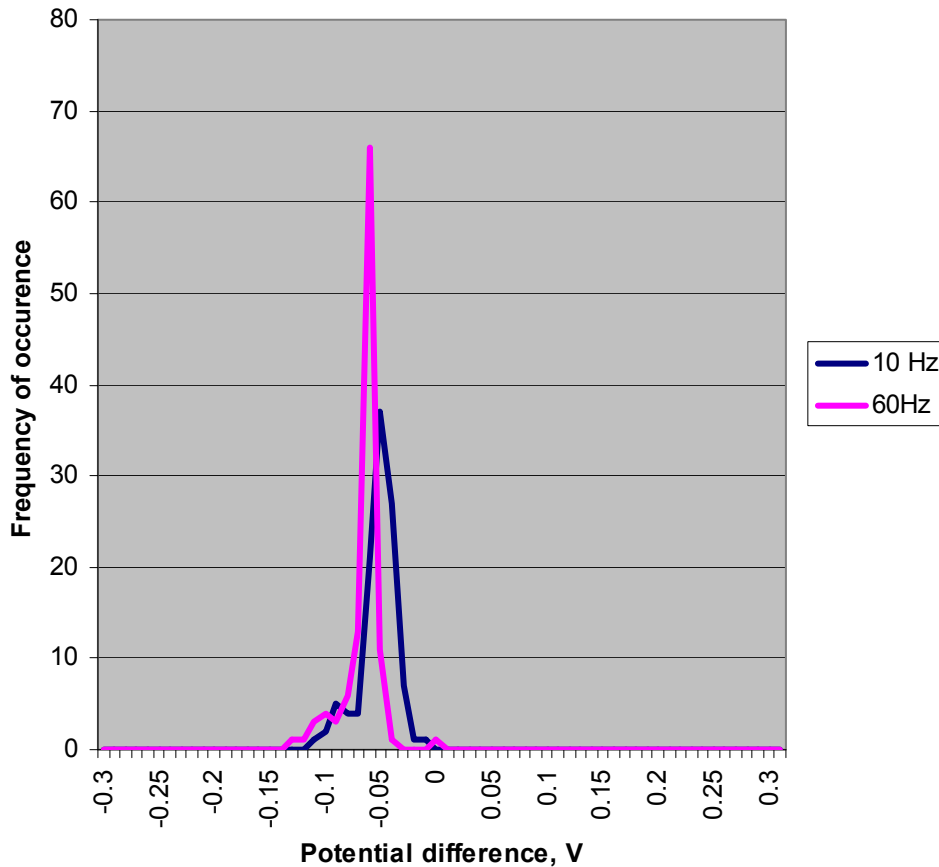


Figure 73. Distribution of potential difference between native potentials and potentials measured under AC interference (1V, different frequencies). Fluke meter.

If one adopts the criterion of 10 mV of the difference as the cutoff point for the 'acceptable' interference, then more than 70% of the values measured by the Allegro meter would fall out of compliance. The bar chart in Figure 74 shows that the best result was produced when the interference was produced by a 5V, 60Hz source.

With regard to the Fluke meter, due to the consistent DC offset registered by the unit, the picture is worse. Essentially, all of the measured values are outside the 10 mV range (Figure 75).

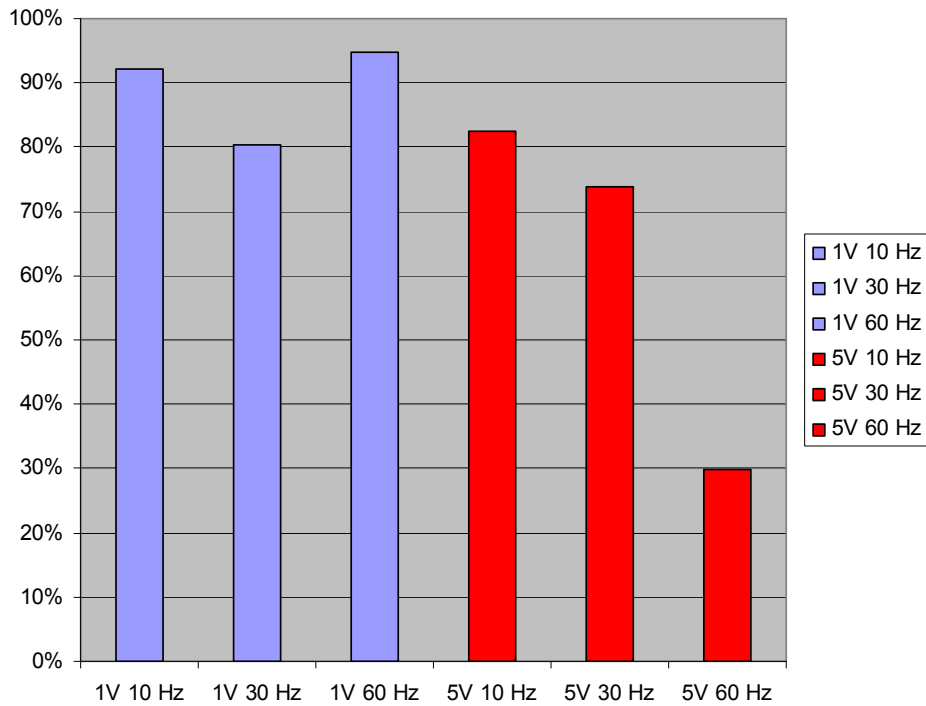


Figure 74. Percent of measurements affected by interference by more than 10 mV. Allegro meter.

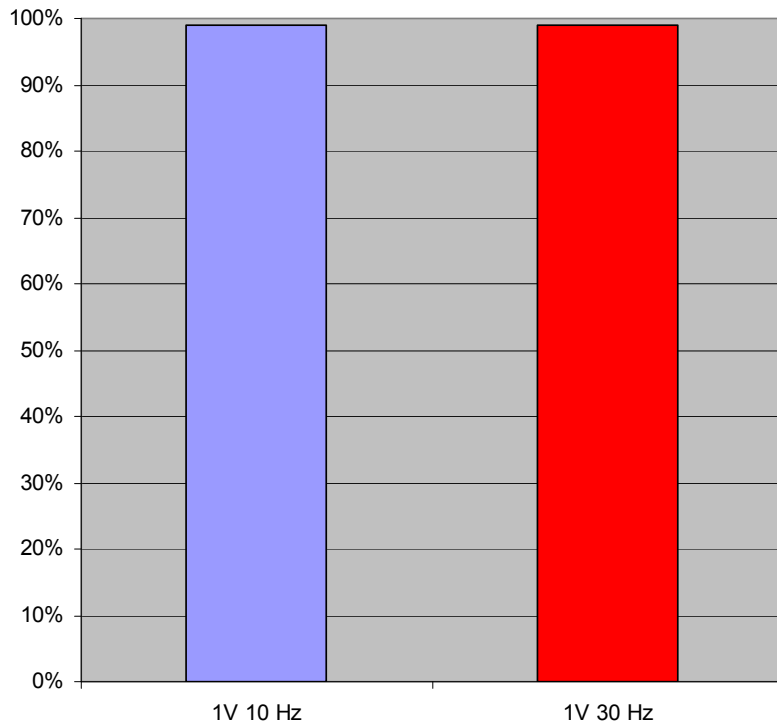


Figure 75. Percent of measurements affected by interference by more than 10 mV. Fluke meter.

Conclusions

Field measurements show that potential readings can be considerably affected by dynamic stray currents. Depending on the frequency of the stray current and whether it carries a DC component, the resulting CIS profile can produce skewed results.

The measurements indicate that even a relatively low level of interference (1V of AC current) can produce results that would, depending on the direction of the current (pick up vs. discharge) shift the measured potentials in or outside of the acceptance range, thus making the measurements more or less conservative. When the interference level is low, the primary challenge becomes the recognition that the readings contain an error.

The measurements are apparently affected by the type of the meter used to collect the readings. The devices with a lower response time are likely to be affected by the interference to a larger degree (especially at higher frequencies). However, the affected readings would act a flag and alert the operator that, unless noise is “filtered out”, the measurements are invalid. It is the devices with the higher response time that present the hazard of overlooking the presence of low-level, yet meaningful interference from stray currents.

The use of a stationary potential logging over time would be advisable if stray current interference is expected or suspected.

Dynamic (field) vs. static (laboratory) stray current interference measurements

Interference caused by the two different types of current has different ‘side effects’. Dynamic stray current, while producing errors in the CIS measurements, is nonetheless likely to be less detrimental than static DC current. Corrosion damage due to AC current is only a small fraction of the damage that would be caused by DC current of the same magnitude. Even if the static currents are relatively low, corrosion at the current discharge locations can be quite extensive. However, the important caveat is that AC corrosion can be equally as hazardous to underground structures if left unmitigated. [See a more detailed discussion on the field-based measurements to assess AC corrosion further.]

DCVG

Baseline readings

Direct Current Voltage Gradient (DCVG) survey of the buried sections was conducted to establish the accuracy with which the technique could locate the coating holidays. Additionally, the operator-related bias was assessed by having two surveyors with varying experience conduct the measurements. The results indicated that the operator bias was negligible. The table below shows the

results of the DCVG assessment; these results are compared to the actual locations of the holidays. In addition to defect locations, the holidays were sized in accordance with NACE RP0502.

The DCVG measurements also included assessment on ‘paired’ defects, i.e., measurements on two adjacent holidays electrically connected together. These preliminary trials indicated that the technique had no difficulty distinguishing between a small and a large holiday next to each other, or between two similarly sized holidays with a different circumferential position. Given this observation, the rest of the measurements were conducted with the pipeline segments electrically connected to form three individual ‘pipelines’.

As shown in the tables below, the DCVG measurements were able to pinpoint most anomaly locations with accuracy, with the deviation between the actual and the measured values being rather small regardless of the holiday size and circumferential position. Further, the defect sizing according to RP0502 correlates well with the actual holiday size.

Table 34. DCVG-based defect assessment (location).

DCVG Indication Station Comparison						
Segment	8-inch Pipe segments			20-inch Pipe segments		
	DCVG Indication Stationing (ft)	Actual Stationing (ft)	Difference, %	DCVG Indication Stationing (ft)	Actual Stationing (ft)	Difference, %
1	10.1	10.5	4%	12	12.9	8%
2	15.3	15.5	1%	20.6	18.65	-9%
Bare	17.5	17.5	0%	21.2	21.13	0%
3	19.7	20.5	4%	23	23.6	3%
4	25.2	25.5	1%	27.6	28.1	2%
5	30.2	30.5	1%	33.6	33.4	-1%
6	32.8	33	1%	36	36.3	1%
Bare	38	35	-8%	38.8	38.9	0%
7	41.7	42	1%	41	41.5	1%
8	46.8	47	0%	46	46.4	1%
9	51.8	52	0%	51	51.5	1%
Bare	54.6	54.5	0%	55.8	53.8	-4%
10	57.3	57	-1%	56	56.2	0%
11	73.5	73.7	0%	69.8	62.7	-10%
12	78.9	78.7	0%	70	67.7	-3%
13	80.8	81.2	0%	74.3	70.2	-6%
14	86	86.2	0%	74.6	75.2	1%
15	91.1	91.2	0%	79.6	80.2	1%
Bare	102	101.7	0%	92.2	91.7	-1%
16	105	105.2	0%	97	97.15	0%
17	110.6	110.2	0%	103	102.15	-1%

18	113	112.7	0%	105.9	104.65	-1%
19	118	117.7	0%	110	109.65	0%

The DCVG measurements were conducted on two adjacent defects, such as indication 12 and 13 electrically connected together (two 10 sq.in. holidays spaced about 3 feet apart). The method was not able to resolve between the two indications, but located one combined anomaly situated approximately in between the two actual holidays. When two distant indications (such as indication 2 and 15) were coupled together, DCVG surveyors were able to find both indications at their respective locations without difficulty. In view of this, the subsequent assessments were conducted on individual rather than combined pipe sections.

Table 35. DCVG-based defect assessment (defect size per NACE RP0502)

Indication	Defect size and orientation	Category Severity	
		8 inch segments	20 inch segments
1	Multiple small	3	3
2	1 sq. in @ 6	4	4
Bare		4	4
3	1 sq.in @ 3	1	1
4	1 sq. in @ 12	1	1
5	10 sq.in @ 12	1	1
6	10 sq.in @ 12	2	2
Bare		4	4
7	10 sq.in @ 3	2	2
8	10 sq. in @ 12	2	2
9	Ten 1 sq.in @ 12	1	2
Bare		4	4
10	10 sq.in @ 6	1	1
11	1 sq. in @ 12	1	1
12	10 sq. in @ 12	2	2
13	10 sq. in @ 12	2	2
14	10 sq.in @ 3	3	3
15	10 sq.in @ 6	2	2
Bare		4	4
16	1 sq. in @ 12	1	1
17	10 sq. in @ 12	2	2
18	10 sq. in @ 12	2	2
19	10 sq.in @ 6	2	1

The defect sizing, although still a controversial semi-quantitative procedure, shows that the larger holidays (such as bare sections) are found by DCVG to be the most severe. In one case, when the bare section is adjacent to a small

holiday, the latter registered as a severe indication. In general, the larger holidays (bare section and 10 sq. in. indications) fell in higher severity categories than the small 1 sq. in. ones. The results are consistent for both the 8- and 20-inch diameter pipeline segments.

DCVG readings under interference

Following the baseline readings, multiple experiments were carried out on various sections on both segments under different interference conditions. The laboratory experiments have demonstrated that DCVG is essentially immune to DC interference

The approach consisted on applying (directly to the pipe section) a sinewave signal to simulate dynamic stray currents. The interference levels applied to the pipe sections were 0, 1, 3, 5, and 15VAC. The overall magnitude of the interference was capped at 15VAC, with the reason being that this would be the highest level of AC permitted by NACE RP0177-2000, "Mitigation of Alternating Current and Lightning Effects on Metallic Structures and Corrosion Control Systems" as acceptable for personnel safety from shock hazard.

The operators were instructed to conduct DCVG in a manner that they would see as best way of locating the holiday despite the signs of interference. Therefore, in this regard, the degree to which an operator experience may contribute to the success of detecting an anomaly is not known.

The following anomalies were assessed:

Table 36. Anomalies (pipe sections) assessed under dynamic stray current interference.

Indication/Appurtenance Slack Chainage	Defect size and orientation	Anomalies tested	
		20 inch segments	8 inch segments
1	Multiple small		
2	1 sq. in @ 6	x	
Bare		x	x
3	1 sq.in @ 3	x	
4	1 sq. in @ 12	x	
5	10 sq.in @ 12	x	
6	10 sq.in @ 12		
Bare			
7	10 sq.in @ 3		
8	10 sq. in @ 12	x	
9	Ten 1 sq.in @ 12		
Bare			

10	10 sq.in @ 6	x	x
11	1 sq. in @ 12	x	x
12	10 sq. in @ 12		
13	10 sq. in @ 12		
14	10 sq.in @ 3		
15	10 sq.in @ 6	x	
Bare			
16	1 sq. in @ 12		
17	10 sq. in @ 12		
18	10 sq. in @ 12		
19	10 sq.in @ 6		

The chosen anomalies represent various flaw sizes, orientations, and pipeline segment diameters. The effect of stray currents was assessed using two parameters – distance to actual anomaly (from the spot identified by DCVG) and flaw sizing (using %IR method).

The level of interference was defined as Signal-to-Noise ratio (SNR), using the following formula:

$$SNR = 20 \log(\text{Amplitude of DCVG Signal} / \text{Amplitude of AC Noise Signal})$$

The DCVG and noise signals were input as voltage and as current to determine the effect of resistance.

The distance from the DCVG call to the actual anomaly was determined as length of the straight line connecting the two, using Archimedes formula for a right triangle. A schematic illustrating the calculation is shown in Figure 76.

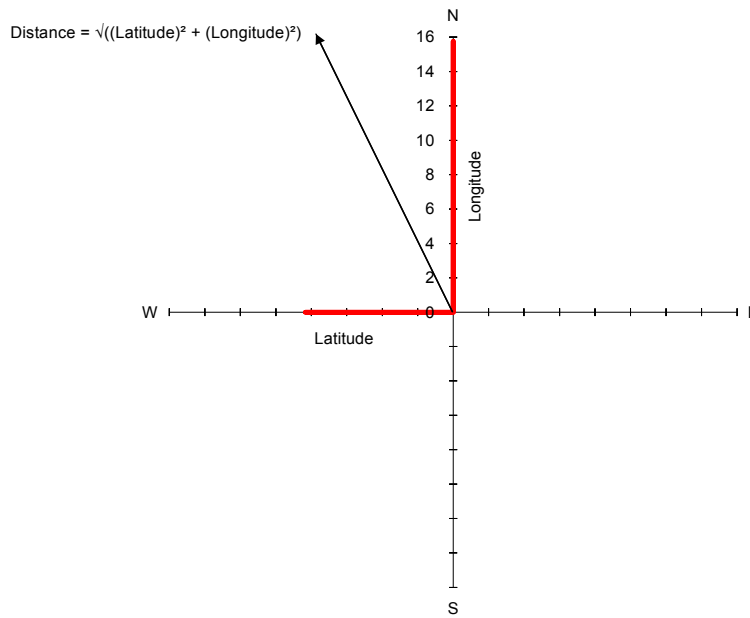


Figure 76. Schematic of calculation of absolute distance to anomaly.

The results of the experiments are summarized in Table 37 to Table 40 and in Figure 77 to Figure 84. There were several measurements per each interference level, using a different setting on the DCVG instrument. The values in the tables are therefore averages, which may be composed of a different number of actual measurements for each anomaly being tested. Further, because the voltage-based SNR is different from current-based SNR (due to impedance fluctuation during the field measurement), the averages for the same anomaly for the two types of SNR may be different. Note also, that because of the interference *voltage* being capped at 15VAC, due to soil/holiday impedance limitations, only half of the corresponding *current*-based interference levels could be categorized as “High”.

When considering the results, one needs to put them in the context of the DCVG field practice. For example, if the distance to the anomaly was found to be, e.g, 5 feet, whether or not this observation would be discarded as erroneous, would depend on the lateral distance from the located spot to the center of the pipe. If the supposed flaw is 5 feet off to the side from the pipe, the location would likely be considered an error and thus disregarded. However, if the located spot is inline with the pipe, then it is more likely to be judged as a legitimate indication. Certainly, if the distance is over, e.g., 10 feet, whether or not the DCVG call falls on or off the pipe would be (likely) treated as an error. The data that is highlighted in red in Table 37 to Table 40 has a lateral component (see Figure 76) that is less than 1 diameter of the pipe – the margins of error that could presumably be overlooked during the field measurements. However, these values are less than 2 feet, therefore the overall error is minimal and the anomaly will likely be found within the excavated site.

Table 37. Distance off from original indication location, ft. Interference is calculated as current SNR.

Anomaly		Interference Level		
(1")	Position	Low	Medium	High
		$0 \geq \text{dB} \geq -10$	$-10 > \text{dB} \geq -20$	$20 > \text{dB} \geq 30$
2	6 o'clock	0.083	2.51	-
3	3 o'clock	14	17	17
4	12 o'clock	2.1	1.2	-
11	12 o'clock	0.1	1.1	-
16	12 o'clock	-	3.8	-
(10")	Position	Low	Medium	High
		$0 \geq \text{dB} \geq -10$	$-10 > \text{dB} \geq -20$	$20 > \text{dB} \geq 30$
5	12 o'clock	8.9	8.8	8.5
8	12 o'clock	8	17	17
10	6 o'clock	0.4	1.5	-
10 (8" pipe)	6 o'clock	7.1	7.1	-
15	6 o'clock	0.5	0.6	-
Bare	-	-	1.1	0.083
Bare (8" pipe)	-	-	-	1.1

Table 38. Severity category, based on %IR under the influence of interference (current-based SNR).

Anomaly		Interference level		
(1''2)	Position	Low	Medium	High
		dB ≥ -4	-4 > dB ≥ -9.5	< -9.5
2	6 o'clock	-	1	1
3	3 o'clock	1	2	2
4	12 o'clock	1	1	1
11	12 o'clock	1	1	1
(10''2)	Position	Low	Medium	High
		dB ≥ -4	-4 > dB ≥ -9.5	< -9.5
5	12 o'clock	2	2	2
8	12 o'clock	1	1	1
10	6 o'clock	1	1	1
10 (8" pipe)	6 o'clock	-	1	1
15	6 o'clock	1	1	1
Bare	-	-	3	3
Bare (8" pipe)	-	-	-	2

Table 39. Distance off from original indication location, ft. Interference calculated as voltage SNR.

Anomaly		Interference Level		
(1")	Position	Low	Medium	High
		$0 \geq \text{dB} \geq -10$	$-10 > \text{dB} \geq -20$	$20 > \text{dB} \geq 30$
2	6 o'clock	-	0.08	1.25
3	3 o'clock	14.7	8.1	17.0
4	12 o'clock	0.5	3.2	3.2
11	12 o'clock	0.1	0.8	1.1
16	12 o'clock	-	3.8	-
(10")	Position	Low	Medium	High
		$0 \geq \text{dB} \geq -10$	$-10 > \text{dB} \geq -20$	$20 > \text{dB} \geq 30$
5	12 o'clock	8.7	9.0	8.8
8	12 o'clock	-	0.3	0.5
10	6 o'clock	0.32	0.42	1.13
10 (8" pipe)	6 o'clock	7.0	7.4	-
15	6 o'clock	0.4	0.7	1.1
Bare	-	-	-	0.08
Bare (8" pipe)	-	-	0.9	1.1

Table 40. Severity category, based on %IR under the influence of interference (voltage-based SNR).

Anomaly		Interference level		
(1")	Position	Low	Medium	High
		$\text{dB} \geq -4$	$-4 > \text{dB} \geq -9.5$	< -9.5
2	6 o'clock	1	1	1
3	3 o'clock	1	2	2
4	12 o'clock	1	1	1
11	12 o'clock	1	1	1
(10")	Position	Low	Medium	High
		$\text{dB} \geq -4$	$-4 > \text{dB} \geq -9.5$	< -9.5
5	12 o'clock	2	2	3
8	12 o'clock	1	1	1
10	6 o'clock	1	1	1
10 (8" pipe)	6 o'clock	1	1	1
15	6 o'clock	1	1	1
Bare	-		3	2
Bare (8" pipe)	-		2	2

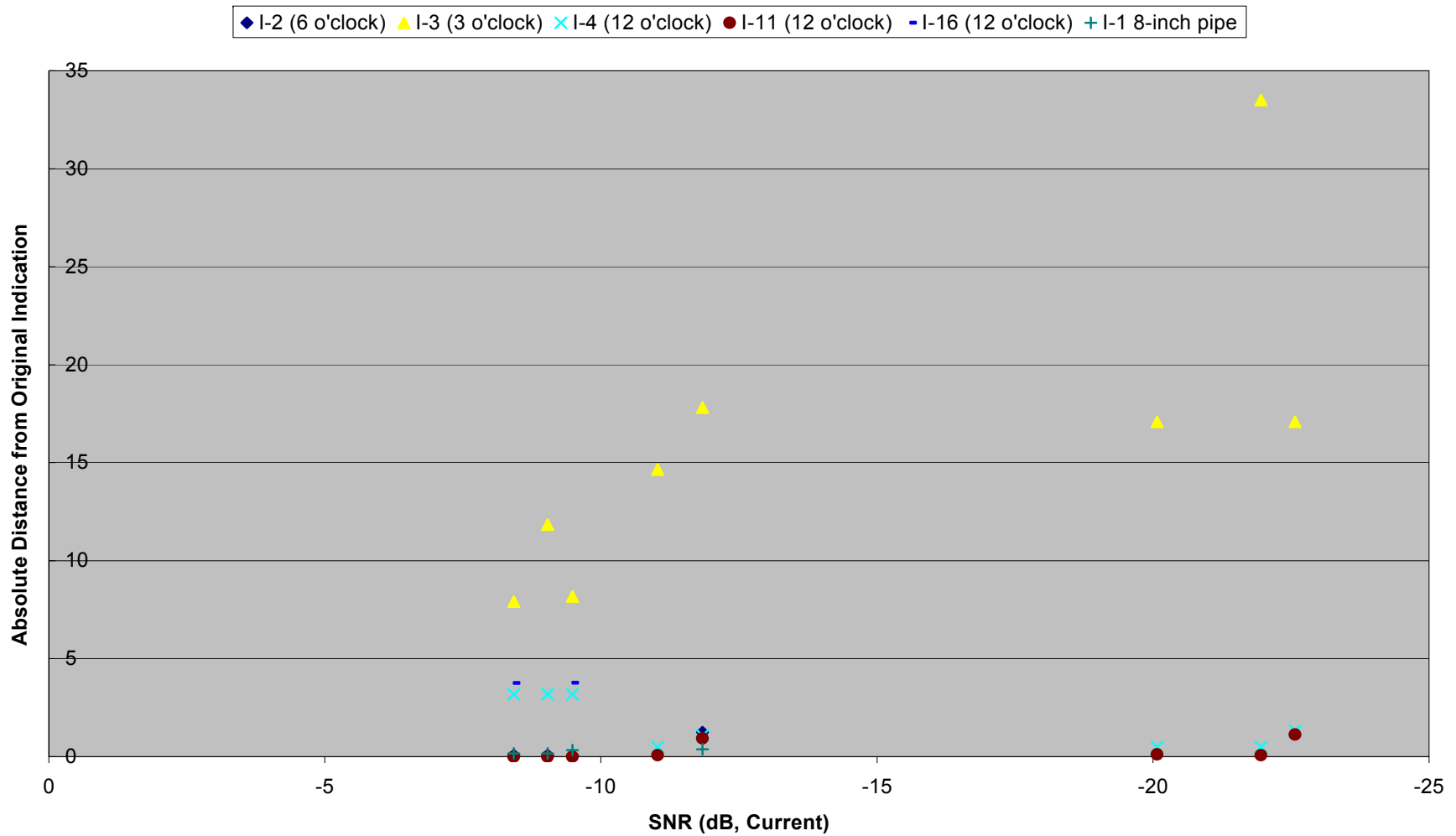


Figure 77. Effect of dynamic stray current interference on measurement accuracy for 1 sq.in. indications (all positions). Interference calculated as current SNR.

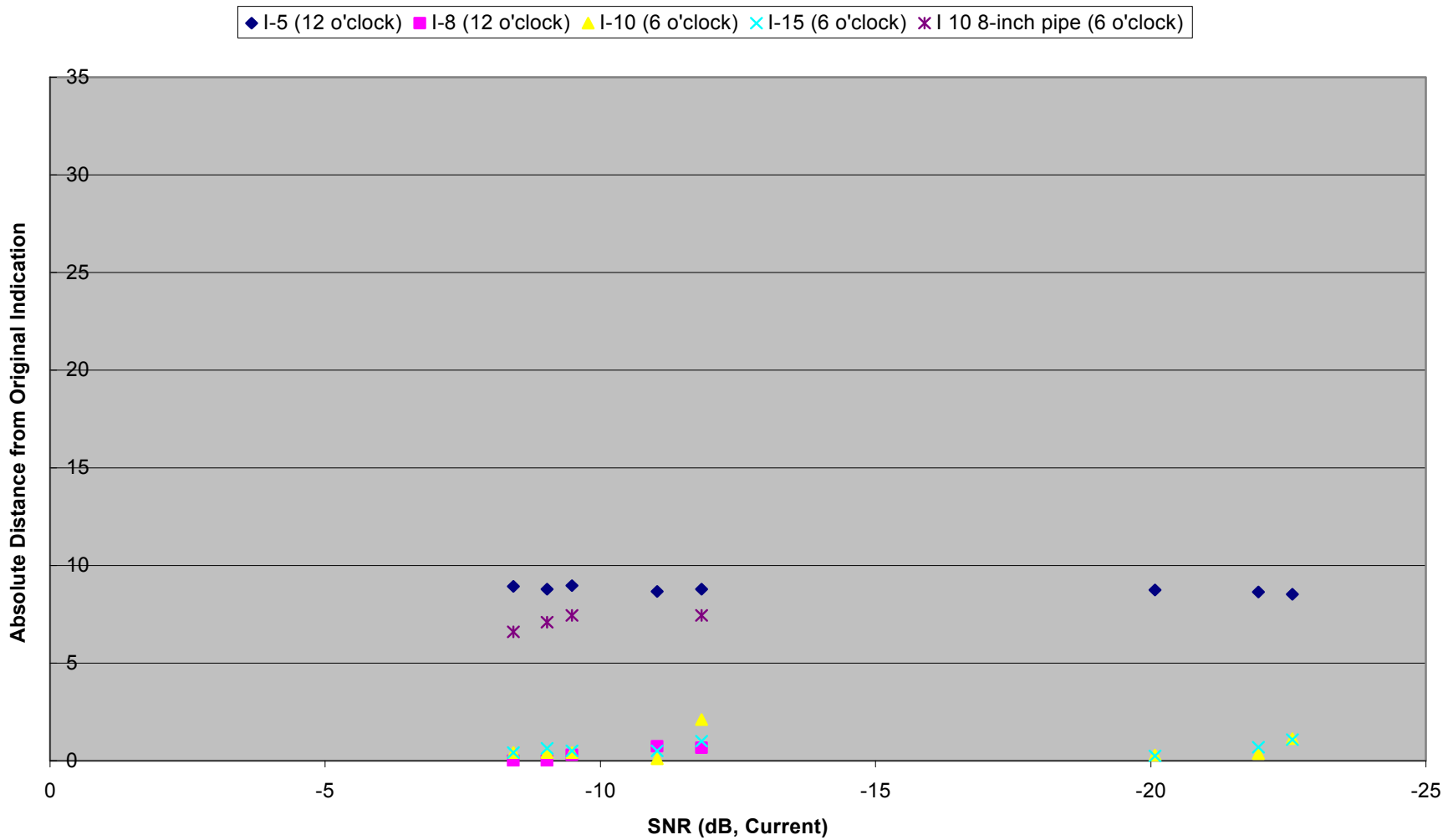


Figure 78. Effect of dynamic stray current interference on measurement accuracy for 10 sq.in. indications (all positions). Interference calculated as current SNR.

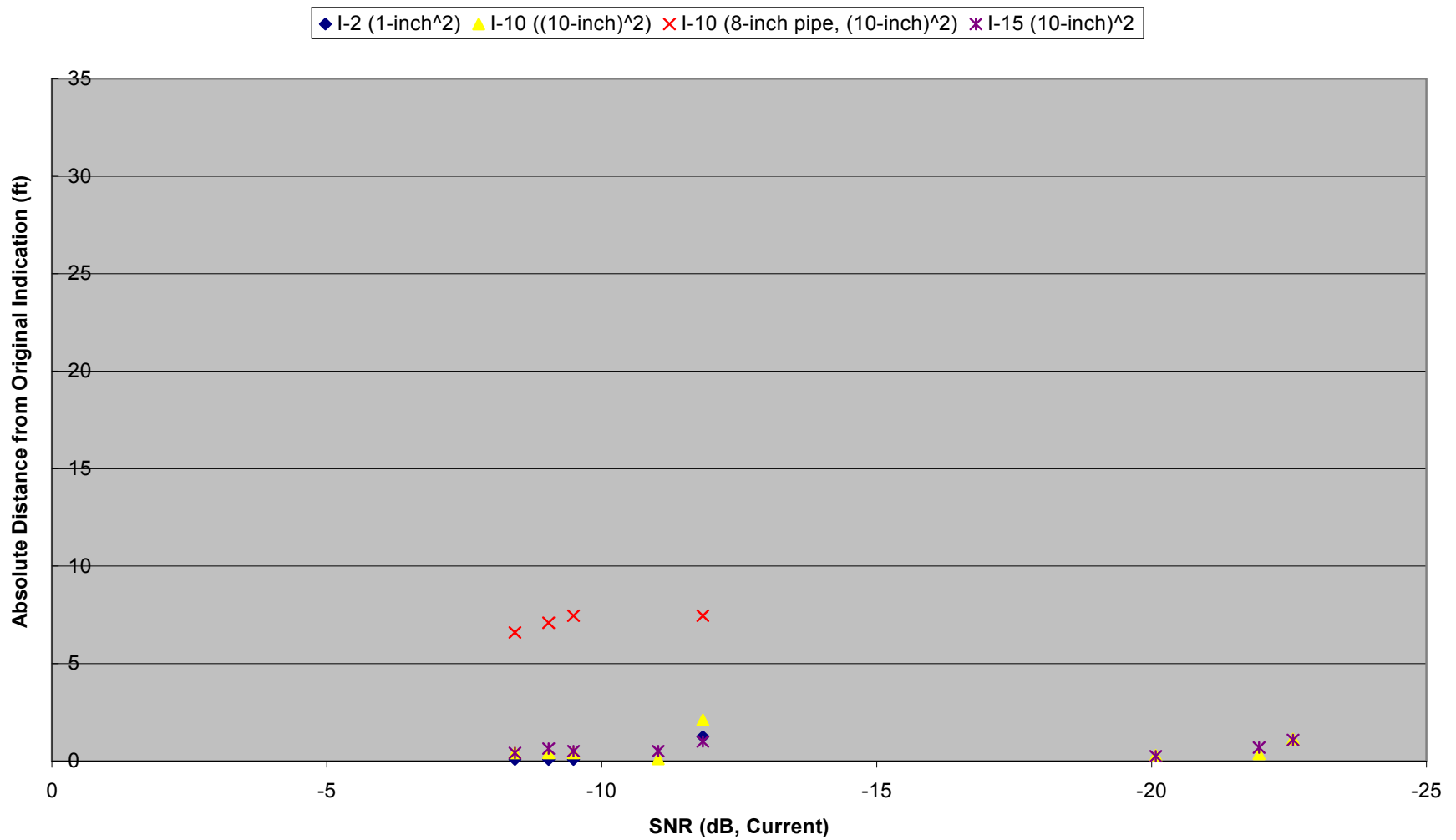


Figure 79. Effect of dynamic stray current interference on measurement accuracy for 6 o'clock positions (all indication sizes). Interference calculated as current SNR.

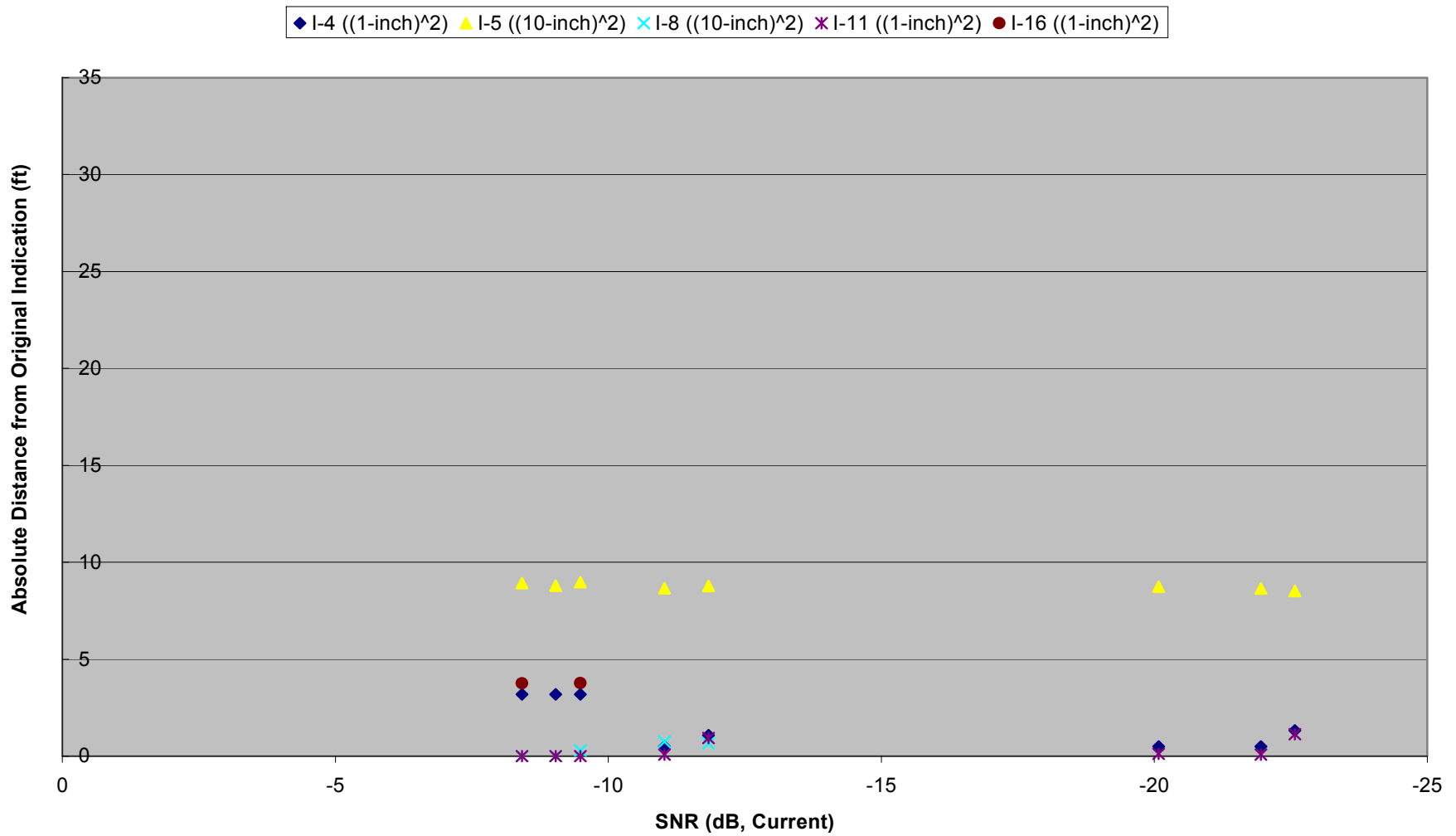


Figure 80. Effect of dynamic stray current interference on measurement accuracy for 12 o'clock positions (all indication sizes) Interference calculated as current SNR.

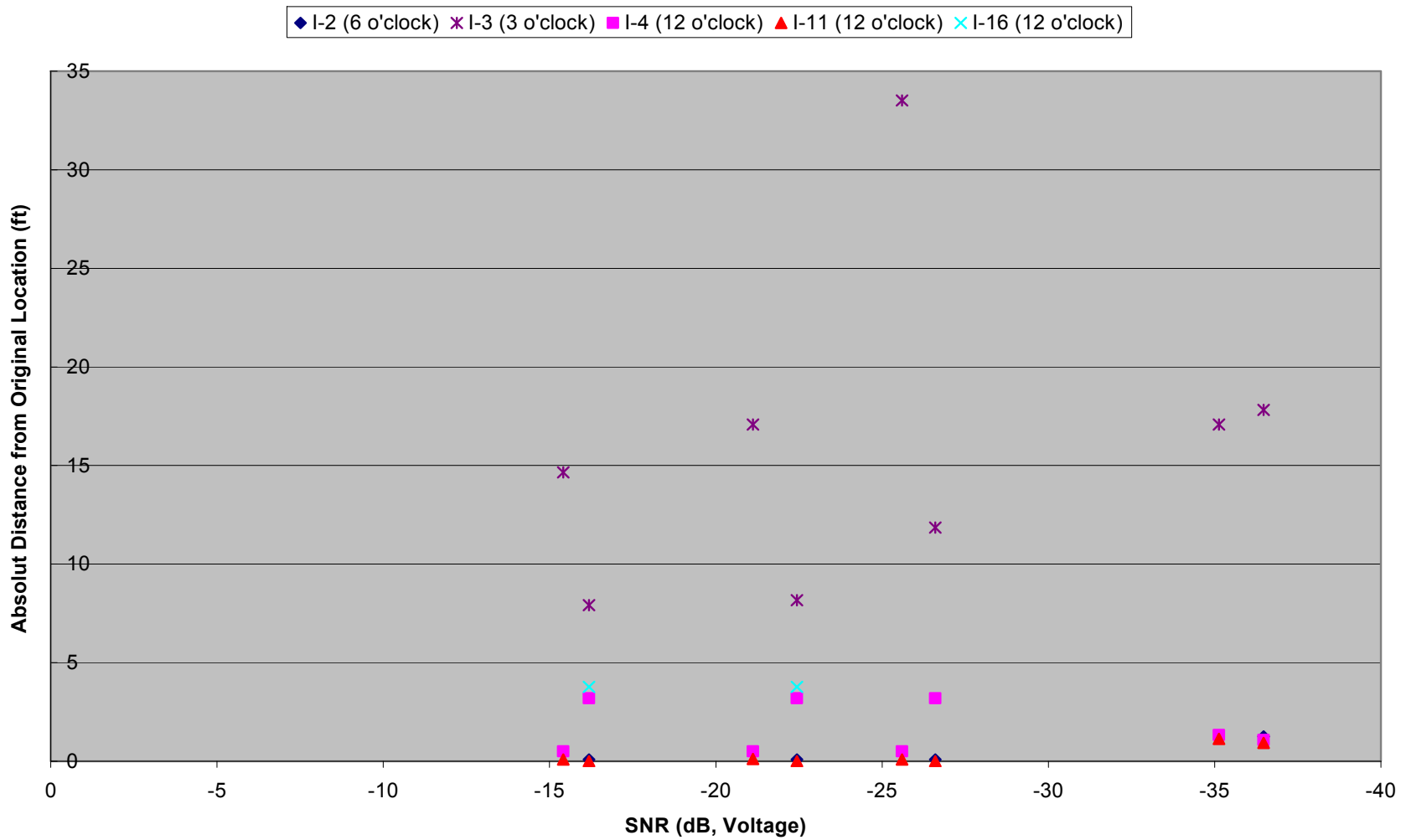


Figure 81. Effect of dynamic stray current interference on measurement accuracy for 1 sq.in. indications (all positions). Interference calculated as voltage SNR.

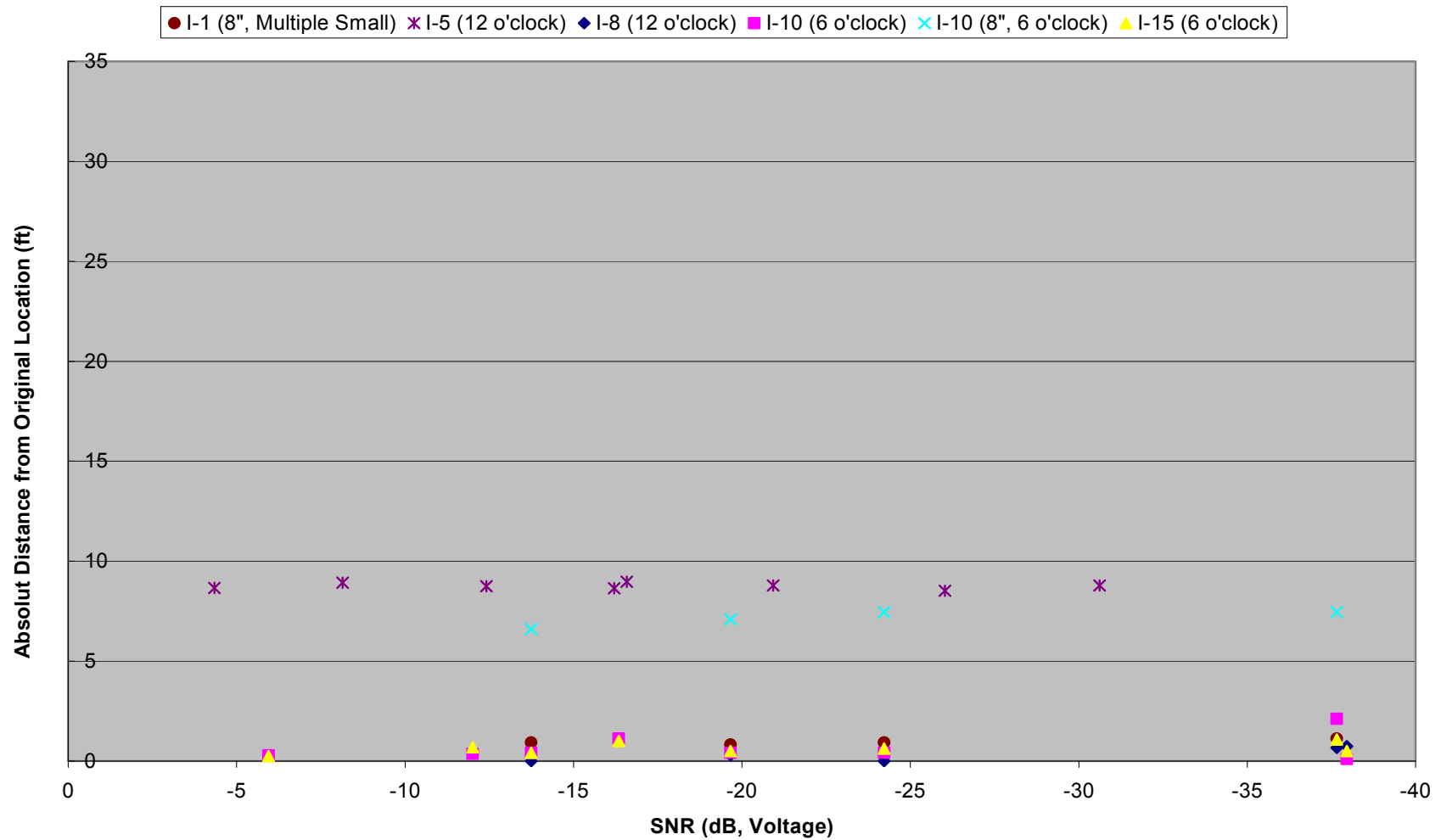


Figure 82. Effect of dynamic stray current interference on measurement accuracy for 10 sq.in. indications (all positions). Interference calculated as voltage SNR.

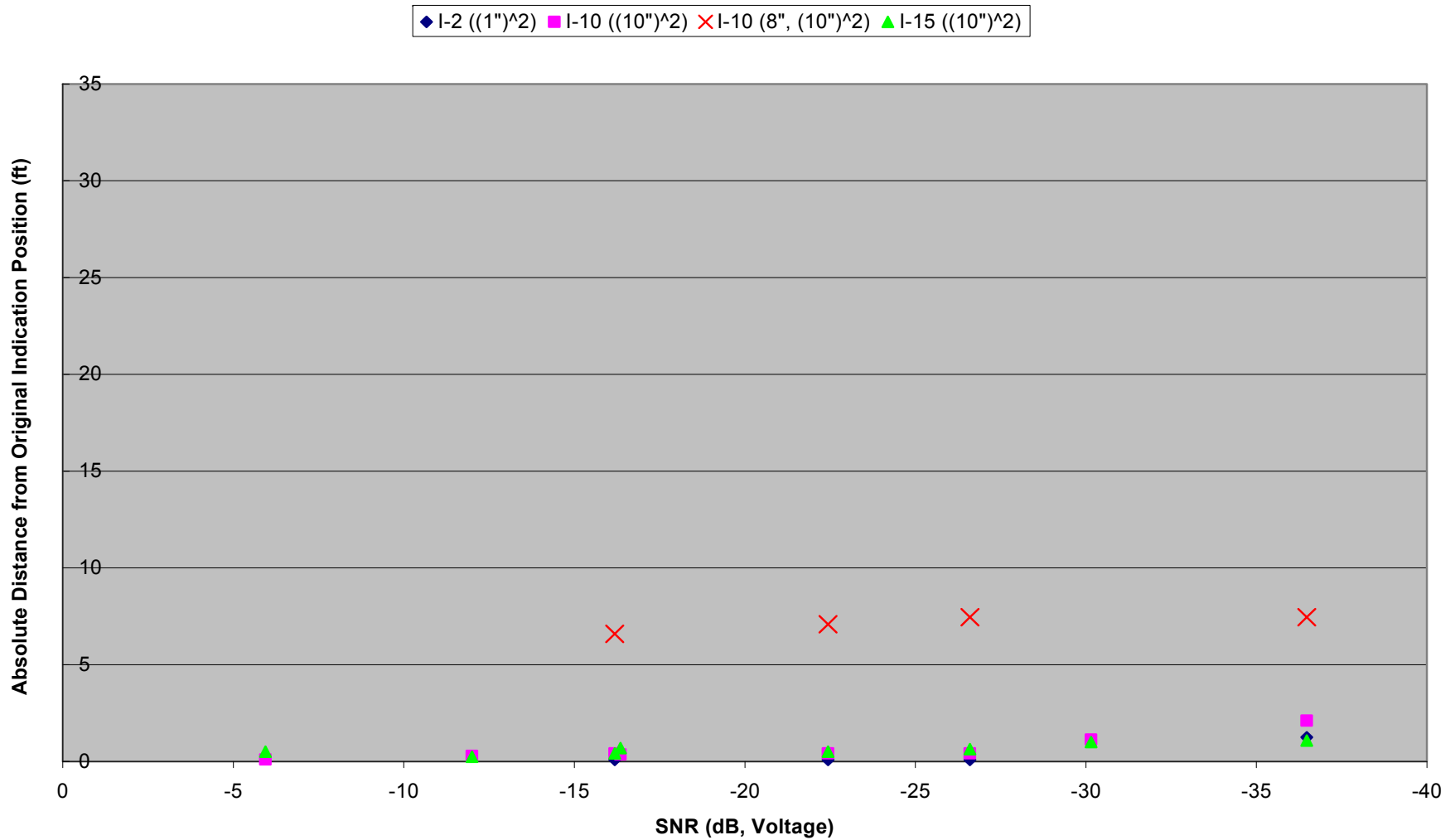


Figure 83. Effect of dynamic stray current interference on measurement accuracy for 6 o'clock positions (all indication sizes). Interference calculated as voltage SNR.

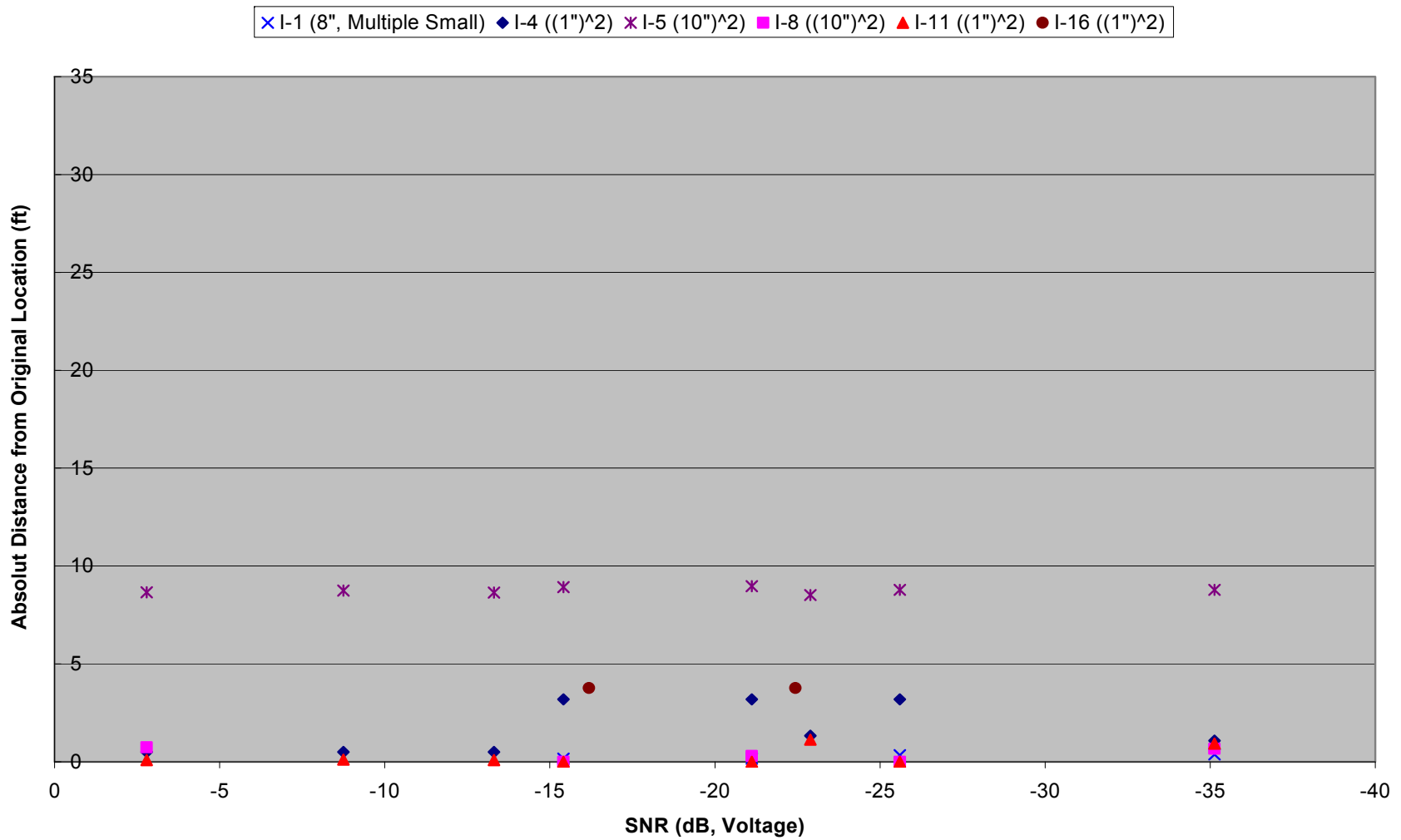


Figure 84. Effect of dynamic stray current interference on measurement accuracy for 12 o'clock positions (all indication sizes) Interference calculated as voltage SNR.

Conclusions

The field measurements point to a rather interesting observation. It appears that dynamic stray current interference with DCVG is a 'yes/no' issue, that is, if DCVG has difficulties with finding an indication (e.g., locates anomalies more than 5 feet off the pipeline), it has difficulties regardless of the signal-to-noise ratio. In fact, the error does not necessarily get any bigger as the SNR drops. This suggests that mitigation of dynamic stray currents, even if possible, would not be expected to improve the chances of the method's ability to locate the anomaly with precision.

The converse is true as well – if DCVG can accurately detect an anomaly at a low level dynamic SC, it is almost as accurate at a higher level of noise.

The findings suggest that the ability of the method to detect a small or a large defect under SC is about the same, ranging from about 40 to 75%. Similar pattern emerges when one considers the circumferential position – whether the holiday was at 6 or 12 o'clock, the method had approximately the same success rate.

The most consistently, DCVG was able to find bare pipe sections, which was expected.

Another conclusion with regard to the DCVG field trials is its capability to size the anomalies based on the percent IR drop method. Based on the measurements, most of small and large flaws were classified as Severity Category 1. Bare pipe sections were characterized as falling mostly in Category 2. The stray currents had no apparent effect on the outcome.

Pipeline Current Mapper

Pipeline current mapper ability to detect indications was briefly tested using the field facility. The primary challenge with regard to the mapper is that its resolution is not adequate for detecting small holidays. The PCM data is summarized in Figure 85; the chart includes baseline reading and the reading with 15VAC interference. As seen, the instrument's accuracy, which is marginal without interference, does not change when the noise is applied. Accurate detection of coating holidays was not possible.

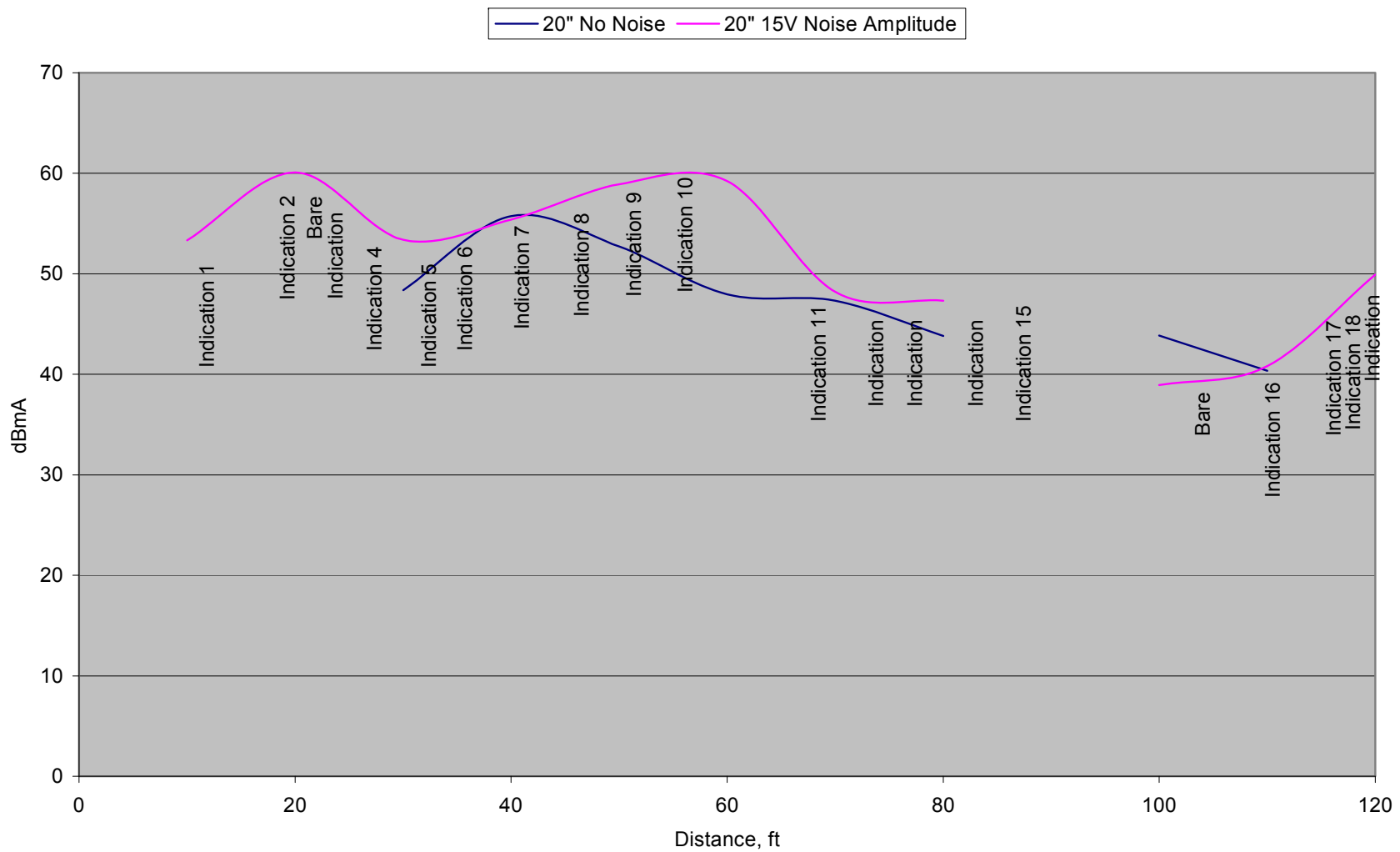


Figure 85. PCM data with and without interference.

AC Close Interval Survey as a means of AC Monitoring

The large-scale underground facility was used to evaluate the accuracy with which the alternating current density can be estimated using above-ground measurements of AC voltage (sometimes termed AC CIS).

In general, the following formula is used to estimate the current density based on the AC voltage

$$i = \frac{U}{R \times A}, \quad (1)$$

where:

i – AC current density (A/m²)

U – measured AC voltage (V)

R – resistance (ohm)

A – assumed or known area of bare metal (m²)

The value of resistance (R) is often referred to as a ‘spread resistance’; it is comprised of the resistance of the circular holiday with diameter d , and resistance of the coating (‘pore’ resistance). Algebraically, it can be presented as:

$$R = \frac{\rho_s}{2d} + \frac{4\rho_f h}{d^2 \pi}, \quad (2)$$

where

ρ_s and ρ_f – are soil and electrolyte resistance, respectively (ohm-m)

d – diameter of the holiday (m)

h – pore (coating) thickness (m)

It is reasonable to assume that $\rho_s = \rho_f$; at larger holiday sizes ($d \gg h$), the second term in equation (2) becomes negligible. Next, substituting in equation (1) and assuming the circular shape of the holiday, the calculated current density becomes:

$$i = \frac{8U}{\pi d \rho_s} \quad (3)$$

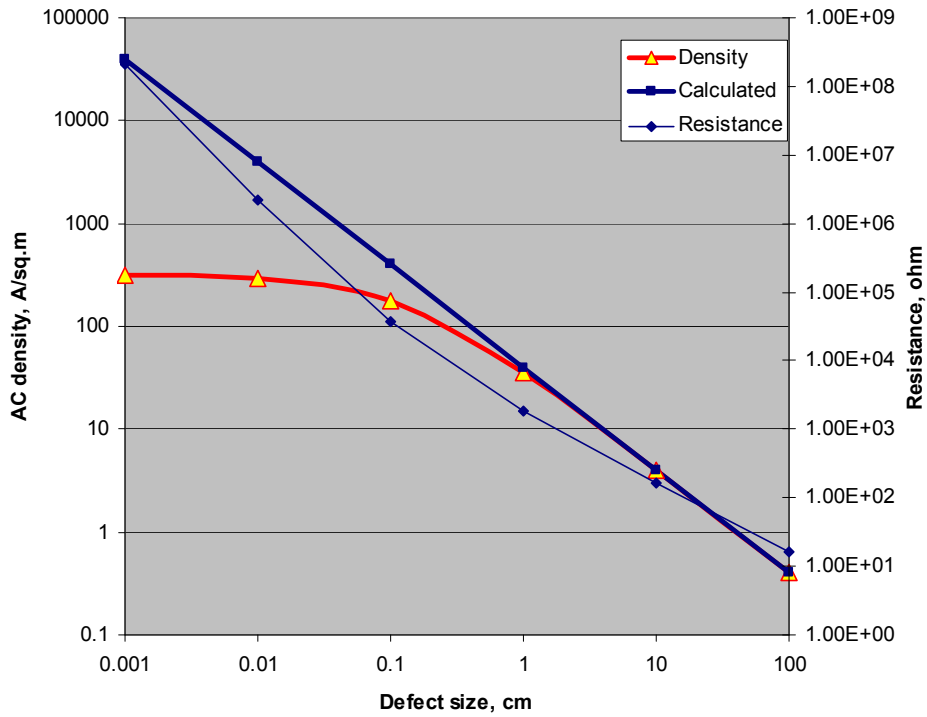
To determine whether this approach produces reasonable estimates of the AC current density in real conditions, AC signal was imposed on the sections of the buried 20 inch diameter pipeline. Various configurations of the defect sizes and orientations were tested. The current density calculated using equation (3) was then compared to the actual density determined using current measurements (vs. above-ground voltage survey) and known (actual) holiday size(s).

Table 41 shows soil resistivity values for the three segments of the 20 inch pipeline (buried in Dublin, OH soil at 4 feet, 2 feet, and in 4 feet of sand).

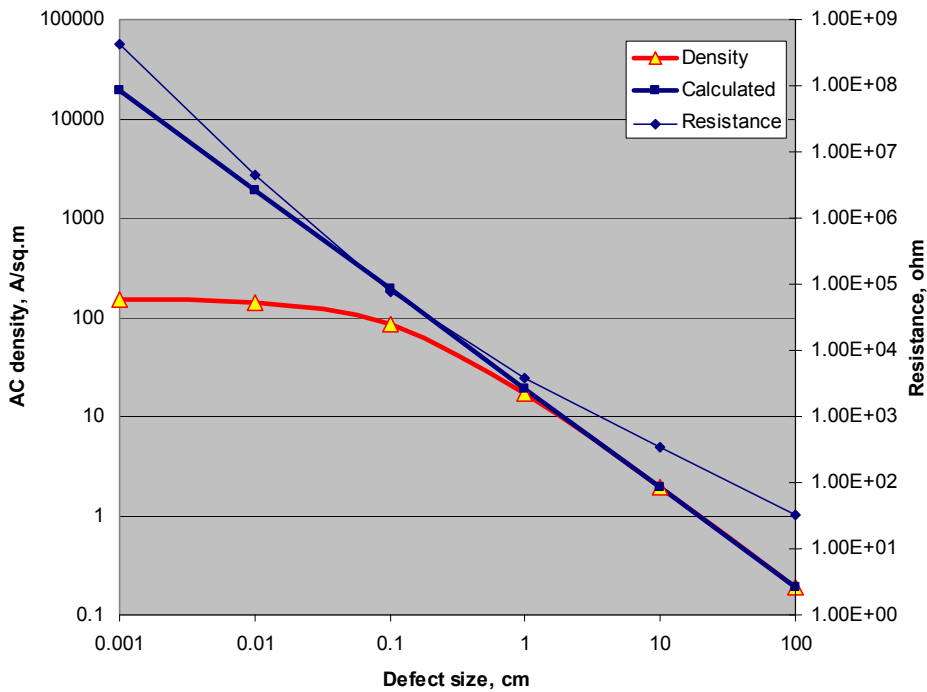
Table 41. Soil resistivity for the three pipeline segments.

Segment	Resistivity, ohm-cm
1	3200
2	3200
3	6600

The validity of the notion that holiday effects dominate pore effects on the resistivity above certain sizes is illustrated in the graphs below. The graphs in Figure 86 show dependence of current density and resistance on defect size (diameter) in soil (top) and sand (bottom). The red line shows actual current density calculated on the basis of equation (2); blue line shows current density calculated using equation (3); both calculations assume AC voltage of 5V.



Soil



Sand

Figure 86. Dependence of current density and spread resistance on defect diameter in soil (top graph) and sand (bottom graph). AC voltage is fixed at 5V.

As seen in the charts, at defect sizes greater than 1 cm, the spread resistance of the defect size dominates and becomes essentially equal to that estimated on the basis of (simplified) equation (3). Considering that the smallest size of the coating holidays on the buried pipeline segments is 1 inch (2.54 cm), the use of equation (3) to estimate the AC current density using AC CIS is justified.

Another trend analysis indicates that the influence of the soil resistivity on current density is diminished (from practical point of view) as the holiday size increases. Shown in Figure 87 is the dependence of the AC density on the soil resistivity for three different defect sizes – 0.1, 1, and 10 cm in diameter (AC voltage is 5V). The resistance calculations use equation (2); the coating thickness is approximately 20 mils (0.05 cm).

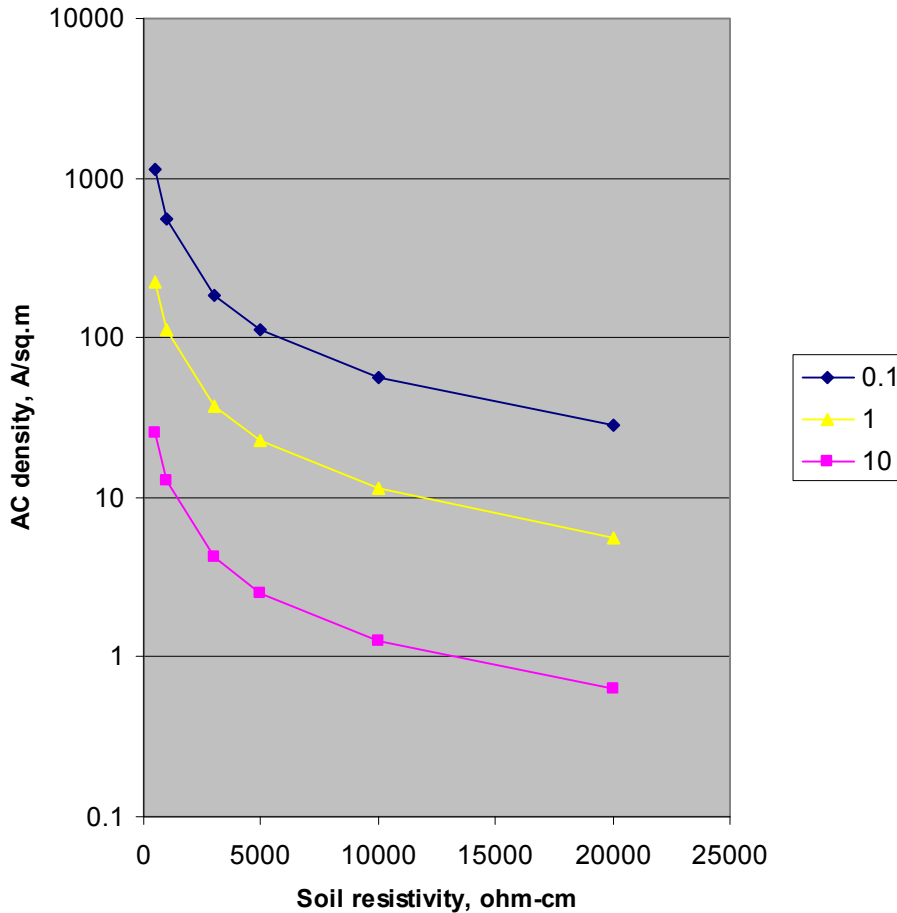


Figure 87. AC current density vs. soil resistivity (AC voltage fixed at 5V).

The lowest line (for the 10-cm diameter defect) is defined by substantially lower values than the lines for the smaller-sized defects. Whereas the difference in current densities for the soil resistivity of 20,000 ohm-cm and 500 ohm-cm is the

same for all three defects (40:1 as the dependence is linear), the density values for the 10 cm (4 inch) diameter defect remain under 10 A/m^2 for resistivities over 1000 ohm-cm. These densities are generally considered to be too low to be a cause of concern regarding AC corrosion.

The effect of voltage is direct (the voltage is in the numerator of equation (2)); hence, for the largest of the evaluated values of the holiday sizes (10 cm), the current density is greater than 50 A/m^2 for AC voltage of as small as 10V (soil resistivity is fixed at 5,000 ohm-cm). For the defect size of 1 cm, the current density is close to 50 A/m^2 for AC voltage as low as 1V.

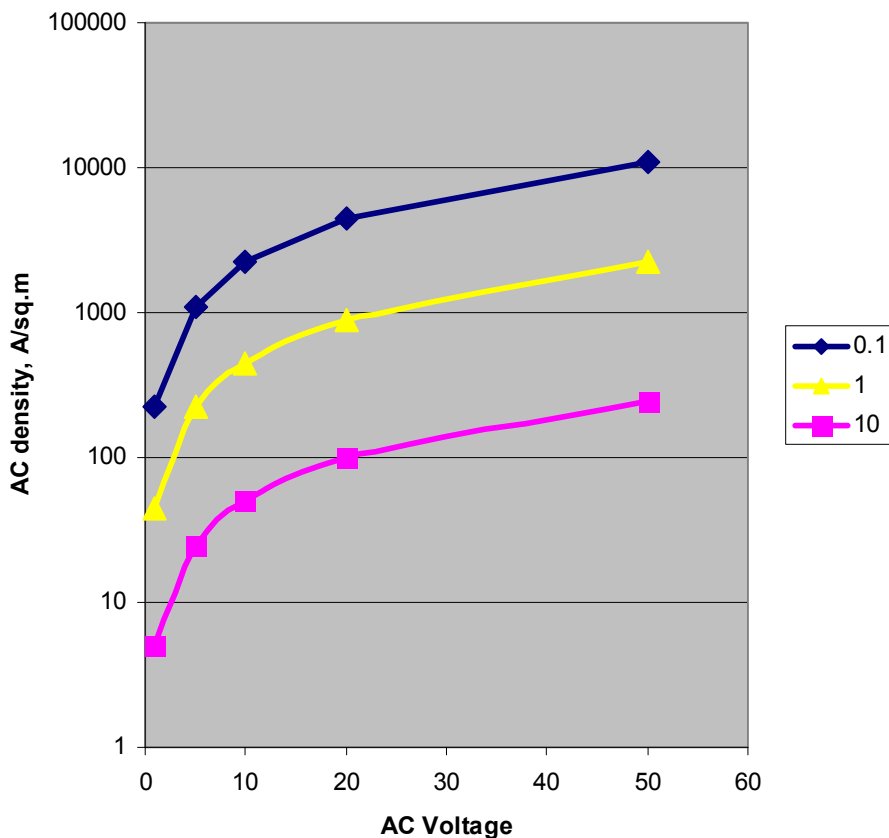


Figure 88. AC current density vs. AC voltage (soil resistivity fixed at 5,000 ohm-cm).

To establish the accuracy of the AC density calculations on the basis of the above ground AC CIS, AC voltage measurements were taken at intervals of 1 foot, directly above the buried pipeline segments. The AC signal was imposed directly on the buried structure using frequency generator.

The graph in Figure 89 shows AC CIS collected with and without the imposed interference signal; 10 pipeline sections comprising the first segment of the large-scale setup (buried in 4 feet of soil) were all electrically connected.

The graph shows that the values of AC voltage without the deliberately imposed interference are quite small. With the signal on, while the level of the interference would be considered low if it were detected on an actual pipeline, its magnitude is sufficient for the purposes of evaluation of the accuracy of the calculations for AC density.

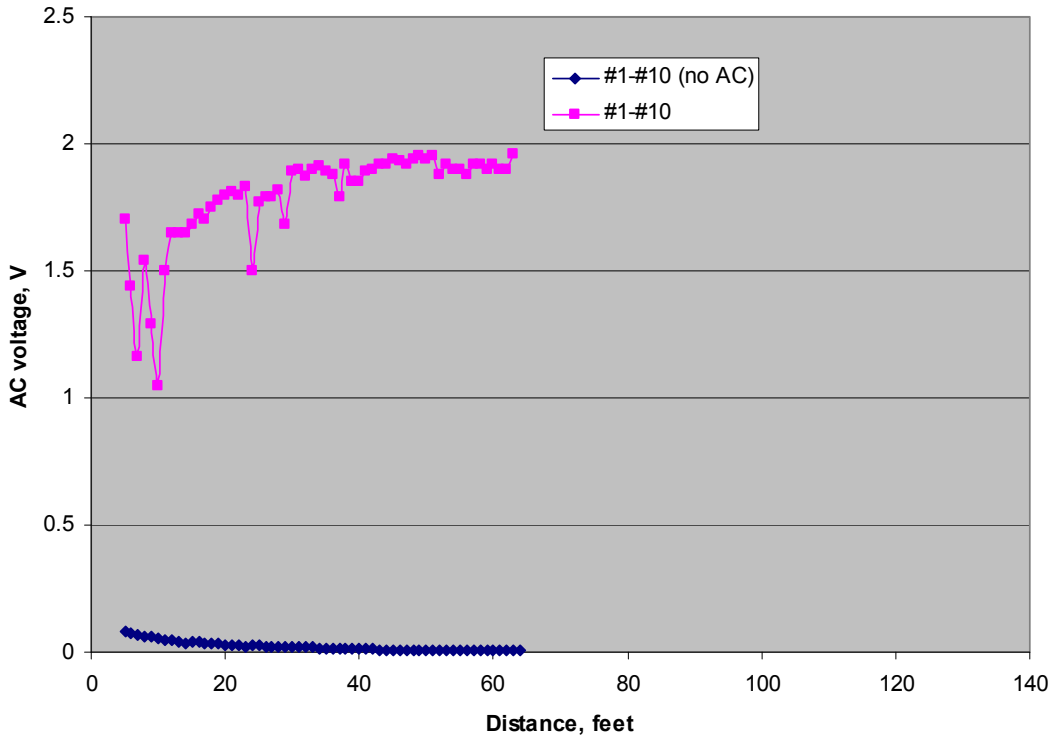


Figure 89. AC current density vs. distance (first pipeline segment, all sections connected).

Once the baseline interference was established, the AC CIS was taken with individual pipeline sections and various combinations thereof. The data was collected from all three pipeline segments. The details of the defect size and orientation for the surveyed sections are summarized in Table 42.

Table 42. Defect size and orientation.

Section	Defect size	Orientation	Section	Defect size	Orientation
1	Ten 1 in ²	12:00			
2	1 in ²	6:00	11	1 in ²	12:00
Bare			12	10 in ²	12:00
3	1 in ²	3:00	13	10 in ²	12:00
4	1 in ²	12:00	14	10 in ²	3:00
5	10 in ²	12:00	15	10 in ²	6:00
6	10 in ²	12:00			

Bare			Bare		
7	10 in ²	3:00	16	1 in ²	12:00
8	10 in ²	3:00	17	10 in ²	12:00
9	Ten 1 in ²	12:00	18	10 in ²	12:00
Bare			19	10 in ²	6:00
10	10 in ²	6:00			

The various AC CIS profiles are summarized in Figure 90. The general observation is that, in keeping with equation (3), the larger the holiday, the greater the AC voltage that could be imposed on the pipe section (due to the finite power of the frequency modulator) tended to be, with everything else being equal.

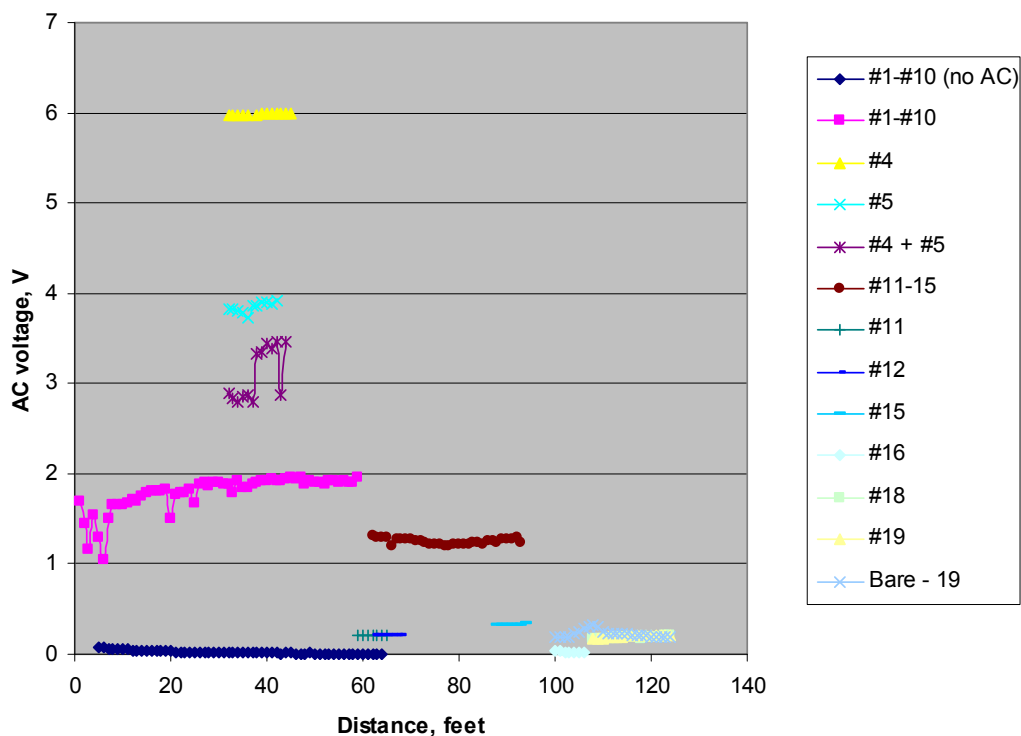


Figure 90. AC current density vs. distance for all surveyed combinations.

The graphs in Figure 91 and Figure 92 offer a comparison of the values AC densities calculated on the basis of the AC CIS profile and equation (3) versus the actual values, calculated using the known current supplied by the modulator and the area of the exposed defect. The AC CIS-based values use the averages for each CIS profile for each particular section or combination of sections.

The graph in Figure 91 plots the AC current density (actual and CIS average-based (calculated) against the effective defect size (total metal area converted was assumed to be of a circular shape and the effective diameter calculated).

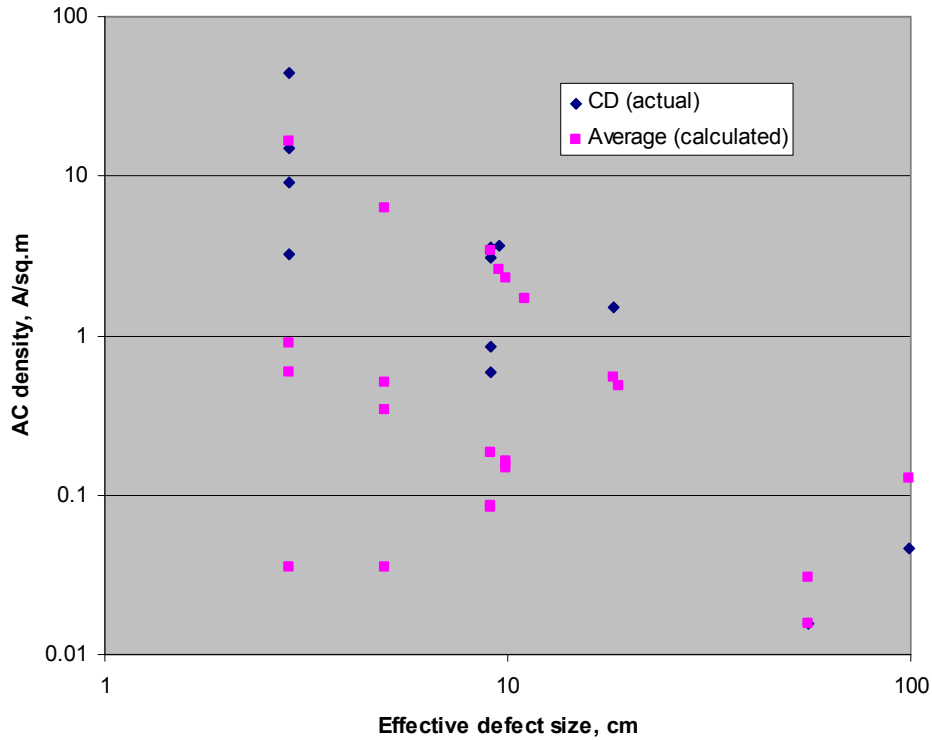


Figure 91. AC current density vs. effective defect size.

Although there is scatter in the data, the overall trend is similar to that shown in Figure 86 – i.e., the larger the defect, the smaller the AC density. The data in Figure 91 is plotted in Figure 92 to establish the correlation between the actual and the calculated density values.

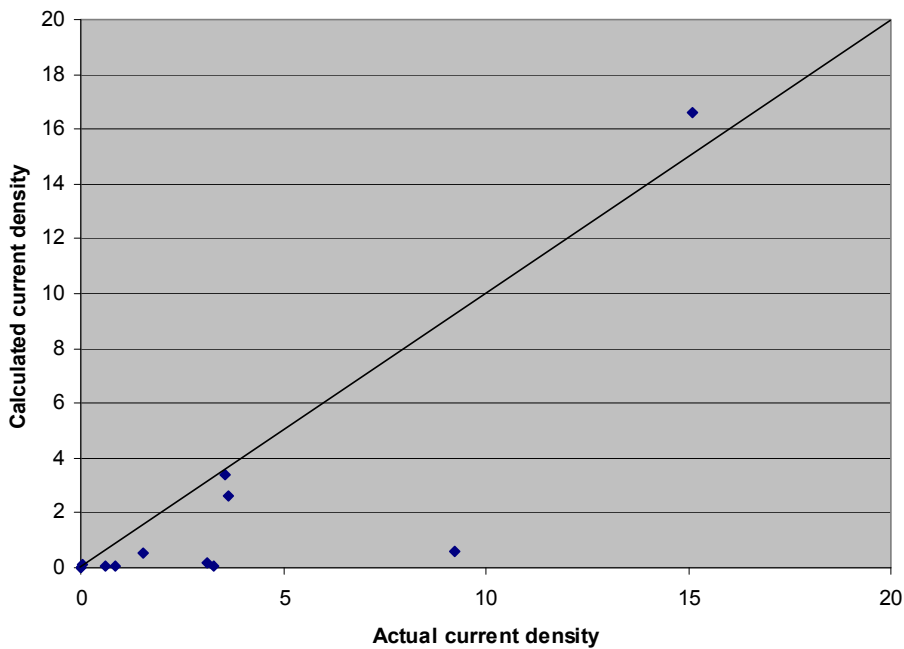


Figure 92. Actual current density vs. calculated current density.

The correlation is less than ideal; however, the general trend is reasonable. The numbers suggest that the estimates based on AC CIS are for the most part lower than the actual values. One possible explanation of this observation is that the value of resistance used in the calculation does not accurately reflect the actual resistance in the measured (electrical) circuit. From the practical standpoint, the values still can be used as estimates (as the difference, while there, is not tremendous).

Also, further analysis shows that the biggest difference between the actual and the calculated density values is associated with the lower-sized defects (which have higher current densities). This gives additional credence to the above argument that the defect-specific conditions (geometry and soil properties) may play a greater role in determining the current flow than ‘bulk’ soil resistivity.

Considering the above, Coupon Test Stations were used to estimate the current density using the CTS coupons, which were electrically connected to whatever section/section combination was being evaluated. The graph in Figure 93 shows two dependencies: (a) the ratio of the actual current density for the holiday only to that of the combined holiday and CTS coupon; (b) ratio of actual current density (for the combined area of the holiday(s) and the CTS coupon) to that calculated on the basis of equation (3) using AC potential of the CTS coupon.

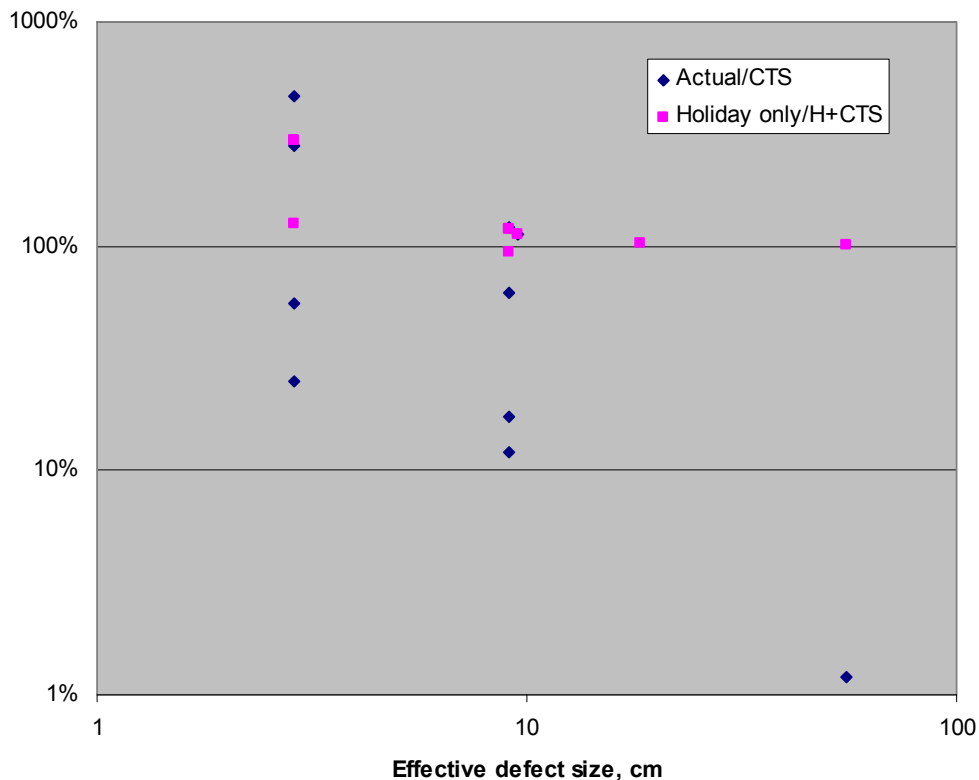


Figure 93. Actual current density vs. calculated current density.

The “Holiday only/H+CTS” ratio is a measure of whether switching in the CTS coupon caused the actual current density to change (by increasing the area and thus changing the resistance of the circuit). The primary conclusion is that if the holiday size is comparable to the size of the CTS coupon (approximately 1.4 in² (9 cm²)), the change of the area due to the addition of the CTS to the electrical circuit leads to the increase in the calculated current density relative to the actual (holiday only) value. Likewise, the addition of the coupon does not produce a material change in the calculated values if the area of the coupon is a smaller fraction of the actual holiday area.

Similarly, the “Actual/CTS” trend shows that the estimates calculated using the CTS coupon AC potential are much more conservative for the cases when CTS coupon is connected to a large(r) area of bare metal. For example, when the CTS coupon was connected to a section of bare pipe, the calculated value was two orders of magnitude higher than the actual one (calculated using the known current and bare metal area).

Conclusions

The field measurements show that assessments of the AC current density from the measured at-grade potential/voltage data can be attempted and provide the ‘order of magnitude’ estimates.

However, the equation that is used for this purpose (equation (3)) is based on the ‘bulk’ soil properties and requires a reasonably good estimate of the bare metal area. As such, the calculated values may be either too conservative or not conservative enough.

The use of CTS can be helpful in that it appears to provide a more accurate estimate of the current density. If CTS are used, it is critical to remember that the coupon size should be within the ‘ballpark’ of the area of the bare metal or the estimate will be considerably off the target.

It is therefore incumbent on the pipeline operators to make multiple estimates at several locations affected by the AC and to have some knowledge about the condition of the coating on the affected structure.

Field vs. laboratory findings

The above observations are in concert with the laboratory-based experiments. The small-scale measurements showed that the current estimates can be far off from the actual values if the resistivity of the soil is not known with accuracy. However, the bulk/soil resistivity is not the only factor controlling the AC current density; the impedance of each of the holidays is also significant. Whereas the

spread resistance of each of the holidays is not likely to have played the role in the measurements, the impedance of the soil/metal interface of each of the defects may be quite different, thus accounting for the difference in measured potentials and calculated current density.

GENERAL CONCLUSIONS

Experimental work

On the basis of extensive literature search and laboratory- and field-based investigations the following conclusions can be made:

1. Both forward and reverse model outputs were largely consistent in their broad trend assessments. The results point to the same factors that define the potential distribution above a buried pipeline, specifically, soil-related variables (soil resistivity, depth of cover) and pipe-related characteristics (flaw size and defect potential).
2. Laboratory experimental results showed that DCVG measurements can locate defects in the pipe with the same degree of accuracy both whether *static* (DC) interference currents are present or not. Under tested conditions, DCVG appeared to be a robust detection tool which was capable of identifying the presence of coating defects under static stray currents.

Based on the field measurements, *dynamic* stray current interference with DCVG appeared to be is a 'yes/no' issue, that is, if DCVG has difficulties with finding an indication (e.g., locates anomalies more than 5 feet off the pipeline), it has difficulties regardless of the signal-to-noise ratio. Therefore, mitigation of dynamic stray currents, even if possible, would not be expected to improve the chances of the method's ability to locate the anomaly with precision. If DCVG can accurately detect an anomaly at a low level dynamic SC, it is almost as accurate at a higher level of noise.

Under the tested conditions, the ability of the method to detect a small or a large defect under SC was about the same, ranging from about 40 to 75%. A similar pattern emerges when one considers the circumferential position – whether the holiday was at 6 or 12 o'clock, the method had approximately the same success rate. DCVG was the most consistent method able to find bare pipe sections, which was expected.

Another conclusion with regard to the DCVG field trials is its capability to size the anomalies based on the percent IR drop method. Based on the measurements, most small and large flaws were classified as Severity Category 1. Bare pipe sections were characterized as falling mostly in Category 2. This reinforces the notion that the sizing of anomalies using this approach produces only approximate results. The stray currents had no apparent effect on the outcome.

3. The existence of *static* DC current that is picked up and discharged by the structure may not be apparent to the CIS surveyor. The current, picked up/discharged by the holidays and not so much the interference voltage is what determines the extent of polarization caused by the stray current. Hence, if the resistance of soil is low, a considerably lower interference voltage can lead to the same effect.

Static stray currents present in the soils altered the actual (error-free) and as-measured OFF potentials along the pipe. Stray currents can lead to inaccurate CIS survey data, which in turn affects the ability to accurately discern the condition of the pipeline coating. For example, a location may show an OFF potential more negative than 1300 mV (which would suggest considerable overprotection) when in reality the OFF potential at that location is such that the defect is under-protected to the extent that damage is occurring.

4. The effect of *dynamic* stray current interference (AC currents of varying frequencies) on CIS was tested on the large-scale outdoor facility. Similar to the static currents, the impedance of the measured structure defined the magnitude of the measured potential and influenced the distribution of the CP and stray currents. Field measurements show that potential readings can be considerably affected by dynamic stray currents. Depending on the frequency of the stray current and whether it carries a DC component, the resulting CIS profile can produce skewed results.

The measurements indicate that even a relatively low level of interference (1V of AC current) can produce results that would, depending on the direction of the current (pick up vs. discharge) shift the measured potentials in or out of the acceptance range, thus making the measurements more or less conservative. When the interference level is low, the primary challenge becomes the recognition that the readings contain an error.

5. The field CIS measurements were affected by the type of the meter used to collect the readings. The devices with a lower response time are likely to be affected by the interference to a larger degree (especially at higher frequencies). However, such affected readings would act a flag and likely alert the operator that, unless noise is “filtered out”, the measurements are invalid. It is the devices with the higher response time that present the hazard of overlooking the presence of low-level, yet meaningful interference from stray currents.

The use of a stationary potential logging over time would be advisable if stray current interference is expected or suspected.

6. During the tests on the field site, pipeline current mapper (PCM) was found to have insufficient resolution to accurately determine the locations of the coating holidays even without dynamic stray current interference. Therefore, the imposition of noise did not appreciably degrade the already marginal instrument performance.
7. With regard to assessing AC corrosion likelihood through AC CIS, the experiments show that the knowledge of soil resistivity is absolutely critical if one attempts to estimate AC current densities using AC voltage measurements. The two adjacent soils (sand and clay) can have two drastically different resistivities. As was shown, in a highly conductive soil the margin of error between the estimated and the calculated values was minimal. In the higher resistance soil, the difference was found to be dramatically different.

The field measurements indicate that that the use of AC CIS for assessing the AC corrosion hazard even when the soil resistivity is known may lead to erroneous conclusions in high resistivity soils. The likely reason for such a difference is that the AC voltage measurements are subject to the same considerations as those involving the DC potentials. That is, each measured value may represent multiple 'sites' on the buried pipeline; depending on the impedance associated with each particular site, the AC voltage may be skewed more towards the voltage of some of the sites.

The field measurements show that assessments of the AC current density from the measured at-grade potential/voltage data can be attempted and provide the 'order of magnitude' estimates.

However, the equation that is typically used for this purpose is based on the 'bulk' soil properties and requires a reasonably good estimate of the bare metal area. As such, the calculated values may be either too conservative or not conservative enough.

The use of CTS can be helpful in that it appears to provide a more accurate estimate of the current density. If CTS are used, it is critical to remember that the coupon size should be within the 'ballpark' of the area of the bare metal or the estimate will be considerably off the target. It is therefore incumbent on the pipeline operators to make multiple estimates

at several locations affected by the AC and to have some knowledge about the condition of the coating on the affected structure.

Estimates also can be made using the software package made commercially available by PRCI. Using certain known input parameters (such as soil resistivity) and estimated values of coating quality and 'typical' holiday size, it was possible to make 'degree of magnitude' estimates of AC current density and relate it to AC corrosion likelihood, which correlated with the laboratory-based measurements using a scaled-down model of a pipeline.

Unique conditions

AC corrosion

The body of literature indicates that AC-corrosion or AC-enhanced corrosion is a bona fide phenomenon. Higher AC current densities are likely to result in accelerated corrosion of steel. There is an inverse relationship between the impact of AC current and its frequency; however, there appears to be a tacit agreement that at prevailing commercial current frequencies (such as 50 or 60Hz) corrosion is possible, even on the cathodically protected pipelines. General corrosion rates due to AC corrosion are not necessarily 'abnormally' high (much higher, naturally occurring rates of an existing pipeline which have been reported), but the rates are certainly multiples of the 'prevailing' corrosion rates of steel in soil in absence of AC.

With regard to the AC corrosion threat, some publications offer the following guidelines:

- · current density lower than 30 A/m^2 : no or low likelihood,
- · current density between 30 and 100 A/m^2 : medium likelihood,
- · current density higher than 100 A/m^2 : very high likelihood.

However, others studies concluded that AC current density discharge in the order of 10 or 20 A/m^2 can produce significant enhanced corrosion (higher rates of penetration and general attack). Therefore, there is an opinion that there likely was not a theoretical 'safe' AC current density, i.e., a threshold below which AC does not enhance corrosion; however, a practical one may exist for which the increase in corrosion due to AC is not appreciably greater than the free-corrosion rate for a particular soil condition.

Assessment of AC corrosion threat (and for that matter, AC mitigation) on the basis of AC voltage may be misleading. At present in the U.S., AC mitigation

is mostly driven by the safety considerations. The primary focus of these efforts is to reduce the induced AC voltage below the 15V to assure the compliance with the NACE Standard RP0177 “Mitigation of Alternating Current and Lightning Effects on Metallic Structures and Corrosion Control Systems”.

Considering that the primary factor in determining the possibility for the presence of AC corrosion is the AC current density, monitoring the current density rather than an AC voltage is crucial to assessing the AC current-related hazards to a buried pipeline. It is a very important departure from the prevailing practices of measuring (and mitigating) the AC voltages on the buried pipelines, notwithstanding the fact that the reduction of AC potentials is expected to reduce the AC current magnitude as well.

With regard to CP, the prevailing thought was that applying cathodic protection in accordance with industry standards could adequately control the AC-enhanced corrosion. However, multiple failures of pipelines under cathodic protection, primarily in Europe, have been attributed to AC corrosion. Additionally, case studies based on the investigations of failures of pipelines in the US have been presented recently.

A much more comprehensive treatise on the issue of AC corrosion can be found in Appendix A.

High CP (overprotection)

It is generally considered that the two possible hazards of overprotection are damages to external coating (cathodic disbonding) and hydrogen-related damage to the pipeline body.

Coating damage due to high CP potentials (overprotection) tends to be attributed to two primary causes: (1) formation of a high pH environment at the coating/steel interface, which weakens the chemical bonds leading to the loss of adhesion and cathodic disbondment and (2) evolution of gaseous hydrogen at the coating/steel interface, which may exacerbate coating disbondment.

Some published accounts contend that even pipelines with an FBE external coating that with evidence of blistering and disbondment are not in danger, because, as long as cathodic protection is operating on the pipeline, blistering and disbondment of FBE coating did not present an immediate integrity threat to the pipeline. The CP current was found to be able to penetrate under disbonded areas. Similar behavior was expected from some other types of

coatings such as asphalt and coal tar enamel which are regarded as “CP-compatible”, although there are no known published laboratory or field accounts. The CP-compatible coatings do not block CP current from reaching the underlying pipeline surface after “failing” (i.e., are not typically associated with shielding).

However, if disbondment progresses and extends to a large area, it is likely to put a strain on the CP system and lead to insufficient cathodic polarization levels thus creating conditions which may be harmful. Further, increased disbondment may expose steel regions that are more susceptible to hydrogen-related damage than the surrounding matrix. It is likely that different coatings respond differently to the same high CP potentials (i.e., exhibit different propensity to disbondment); the response is also likely to be the function of the pipeline surface preparation during coating application process.

The commonly used NACE recommended practice RP0169 (currently under review by NACE International) does not include any specific limit to avoid consequences of overprotection. To monitor the hazards of overprotection, a European standard, the ISO 15589-1 instructs to polarize a buried pipeline to potentials which are more negative than -850 mV and less negative than -1,200 mV (CSE). The limit of -1,200 mV is recommended to prevent cathodic disbondment. However, the reliance on the potential values alone may lead to underestimation of the hazards of overprotection. At high CP currents, the change in polarized potential can be relatively minor, compared to a significant (ten-fold) increase in applied CP current density. Therefore, when considering the limits for CP, both potential and current limits should be taken into account.

Some evidence exists that full-encirclement steel sleeves which are routinely used for onshore pipelines as a temporary or permanent repair of pipe anomalies could be linked to carrier pipe collapses. These collapses were attributed to hydrogen gas accumulation in the annular space between the sleeve and the carrier pipe due to excessive cathodic protection (CP) – associated with Type B sleeves and hydrogen stress cracking in hard spots under the sleeve repair due to corrosion (Type A sleeves).

In summary, coating damage at cathodically protected locations may not be an immediate threat to pipeline integrity because corrosion is mitigated. However, extensive areas of disbondment may be detrimental because of 1) increased current demand from the CP system (affecting current attenuation),

2) the possibility of corrosion occurring under disbonded coatings that CP might not protect, 3) inputting more hydrogen into the metal because of increased total current, and 4) exposing a hard spot that may be susceptible to hydrogen damage.

Excessive CP can accelerate hydrogen flux through the steel, which can potentially cause partial or complete collapse of the carrier pipe inside a full encirclement repair sleeve, as suggested by several accounts. Under certain conditions, pipelines with hard spots can be susceptible of hydrogen-related cracking.

As a general guideline, CP current density of 2 mA/ft² may be offered as a target upper limit for cathodic protection. The current density can be monitored through the use of Coupon Test Stations. The cathodic current criteria are preferred to the potential-based criteria when evaluating the overprotection conditions. Cathodic current densities specified in the ISO Standard 15589-1 are similar.

As a general guideline, polarized potentials more positive than -1,200 mV (CSE) can be used as an upper-limit criterion to minimize cathodic disbondment and hydrogen-related damage to the steel. The potential measurements with close interval surveys or using coupon test stations are the proper approaches to monitoring the hazards of overprotection.

ECDA methods under stray current interference

DCVG

DCVG measurements can locate defects in the pipe with the same degree of accuracy both whether *static* (DC) interference currents are present or not. Under tested conditions, DCVG appeared to be a robust detection tool which was capable of identifying the presence of coating defects under static stray currents. Based on the field measurements, *dynamic* stray current interference with DCVG appeared to be is a 'yes/no' issue, that is, if DCVG has difficulties with finding an indication (e.g., locates anomalies more than 5 feet off the pipeline), it has difficulties regardless of the signal-to-noise ratio. Therefore, mitigation of dynamic stray currents, even if possible, would not be expected to improve the chances of the method's ability to locate the anomaly with precision.

The method's capability to size the anomalies based on the percent IR drop method is marginal and produces only approximate results. The stray currents had no apparent effect on the outcome.

CIS

Static stray currents present in the soils altered the actual (error-free) and as-measured OFF potentials along the pipe. Stray currents can lead to inaccurate CIS survey data, which in turn affects the ability to accurately discern the condition of the pipeline coating. However, the existence of *static* DC current that is picked up and discharged by the structure may not be apparent to the surveyor. The current, picked up/discharged by the holidays and not so much the interference voltage is what determines the extent of polarization caused by the stray current. Hence, the resistance of soil is low, a considerably lower interference voltage can lead to the same effect.

The impedance of the measured structure defined the magnitude of the measured potential and influenced the distribution of the CP and stray currents, whether static or dynamic. Field measurements show that potential readings can be considerably affected by *dynamic* stray currents. Depending on the frequency of the stray current and whether it carries a DC component, the resulting CIS profile can produce skewed results.

The measurements indicate that even a relatively low level of interference (1V of AC current) can produce results that would shift the measured potentials in or outside of the acceptance range, thus making the measurements more or less conservative. When the interference level is low, the primary challenge becomes the recognition that the readings contain an error.

The field measurements were affected by the type of the meter used to collect the readings. The devices with a lower response time are likely to be affected by the interference to a larger degree (especially at higher frequencies). However, such affected readings would act a flag and likely alert the operator that, unless noise is “filtered out”, the measurements are invalid. It is the devices with the higher response time that present the hazard of overlooking the presence of low-level, yet meaningful interference from stray currents. The use of a stationary potential logging over time would be advisable if stray current interference is expected or suspected.

PCM

During the tests on the field site, pipeline current mapper (PCM) was found to have insufficient resolution to accurately determine the locations of the coating holidays even without dynamic stray current interference. Therefore, the imposition of noise did not appreciably degrade the already marginal instrument performance.

APPENDIX A
NACE INTERNATIONAL DOCUMENT
PRODUCED BY TG-327
NOT FOR FURTHER DISTRIBUTION WITHOUT APPROVAL FROM NACE
INTERNATIONAL



Date Prepared: 2006-11-20

TG 327

NOT APPROVED: This draft of a proposed NACE technical committee report is for committee use only and shall not

PROPOSED NACE TECHNICAL COMMITTEE REPORT

**“AC Corrosion State-of-the-Art: Corrosion Rate,
Mechanism, and Mitigation Requirements”**

Draft #1: Draft Prepared by the Task Group, Edited and Processed by Headquarters, and Distributed to STG 35 for Review and Comment and to the TCC RPC for Editorial Review—November 2006

NACE International
1440 South Creek Drive
Houston, Texas 77084-4906
+1 281/228-6200

© 2006, NACE International

NOT APPROVED: This draft of a proposed NACE technical committee report is for committee use only and shall not be duplicated in any form for publication or any use other than committee work.

This NACE International technical committee report represents a consensus of those individual members who have reviewed this document, its scope, and provisions. Its acceptance does not in any respect preclude anyone from manufacturing, marketing, purchasing, or using products, processes, or procedures not included in this report. Nothing contained in this NACE International report is to be construed as granting any right, by implication or otherwise, to manufacture, sell, or use in connection with any method, apparatus, or product covered by Letters Patent, or as indemnifying or protecting anyone against liability for infringement of Letters Patent. This report should in no way be interpreted as a restriction on the use of better procedures or materials not discussed herein. Neither is this report intended to apply in all cases relating to the subject. Unpredictable circumstances may negate the usefulness of this report in specific instances. NACE International assumes no responsibility for the interpretation or use of this report by other parties.

Users of this NACE International report are responsible for reviewing appropriate health, safety, environmental, and regulatory documents and for determining their applicability in relation to this report prior to its use. This NACE International report may not necessarily address all potential health and safety problems or environmental hazards associated with the use of materials, equipment, and/or operations detailed or referred to within this report. Users of this NACE International report are also responsible for establishing appropriate health, safety, and environmental protection practices, in consultation with appropriate regulatory authorities if necessary, to achieve compliance with any existing applicable regulatory requirements prior to the use of this report.

CAUTIONARY NOTICE: The user is cautioned to obtain the latest edition of this report. NACE International reports are subject to periodic review, and may be revised or withdrawn at any time without prior notice. NACE reports are automatically withdrawn if more than 10 years old. Purchasers of NACE International reports may receive current information on all NACE International publications by contacting the NACE International FirstService Department, 1440 South Creek Drive, Houston, Texas 77084-4906 (telephone +1[281]228-6200).

FOREWORD

This technical committee report represents the current understanding of the corrosion phenomenon associated with alternating current (AC) interference on buried steel pipelines. The state-of-the-art report's purpose is to set the stage for the subsequent step of developing corrosion protection criteria with regard to AC corrosion. In the past 20 years, AC corrosion has become recognized as a real threat to the integrity of underground structures, especially buried pipelines sharing the right-of-way with high-tension electrical lines.

Every attempt was made to incorporate as many published accounts as possible, including multiple international sources. However, given the increased awareness of AC corrosion by pipeline operators and the corrosion community at large, a considerable volume of literature on the subject exists, and some most recent publications may have been left out of the report. The report addresses AC corrosion characteristics and proposed mechanisms, and describes the currently used approaches to protection and monitoring. It is intended for use by pipeline operators and others concerned with control of AC corrosion. The report also identifies existing knowledge gaps and briefly outlines the path forward.

This technical committee report has been prepared by Task Group (TG) 327 on AC Corrosion State-of-the-Art: Corrosion Rate, Mechanism, and Mitigation Requirements. TG 327 is administered by Specific Technology Group (STG) 35 on Pipelines, Tanks, and Well Casings. This report is issued by NACE International under the auspices of STG 35.

NACE technical committee reports are intended to convey technical information or state-of-the-art knowledge regarding corrosion. In many cases, they discuss specific applications of corrosion mitigation technology, whether considered successful or not. Statements used to convey this information are factual and are provided to the reader as input and guidance for consideration when applying this technology in the future. However, these statements are not intended to be recommendations for general application of this technology, and must not be construed as such.

INTRODUCTION

The phenomenon of AC corrosion has been considered by many authors since the early 1900s. However, the mechanisms of AC corrosion are still not completely understood. The body of recent (post-1980) literature indicates that AC corrosion or AC-enhanced corrosion (ACEC) is a bona fide effect (reported corrosion rates up to 20 mpy (0.5 mm/y), with pitting rate considerably higher); there appears to be a tacit agreement that at prevailing commercial current frequencies (such as 50 or 60 Hz) corrosion is possible, even on cathodically protected pipelines.

AC corrosion on cathodically protected pipelines is not well understood, despite discussion about it dating back to the late 19th century. For many years, corrosion experts did not consider corrosion attributed to alternating currents on metallic structures very important. In 1891, Mengarini¹ concluded that corrosion ("chemical decomposition") by AC is (1) less than that caused by the equivalent direct current (DC), (2) it is proportional to the AC, (3) there exists a threshold AC density below which no "decomposition of electrolyte" occurs, and (4) the extent of corrosion decreases with increased AC frequency.

In 1916, McCollum et al² published a research paper that concluded iron does not suffer from attack when a limiting frequency of the current (somewhere between 15 and 60 Hz) is reached. AC corrosion was not well understood for two reasons: (1) the electrochemical phenomenon of corrosion is normally attributed to DC; and (2) the instruments normally used to measure the electric parameters in direct currents cannot correctly detect the presence of AC with frequencies between 50 and 100 Hz.³ Recently, there has been an increasing concern for AC corrosion mitigation because AC interference has been shown to affect cathodically protected underground structures and increase safety concerns

(i.e., high AC step-and-touch voltages). Factors that contribute to AC interference on pipelines include (1) the growing number of high-voltage power lines; (2) AC operated high-speed traction systems; (3) high isolation resistance of modern pipeline coatings; and (4) coating integrity.⁴

CHARACTERISTICS OF AC CORROSION

Corrosion Rate

There is a scarcity of data on the magnitude of the corrosion rate of steel in soils influenced by AC. The general understanding is that higher alternating currents lead to higher risk of AC corrosion. Ragault⁵ reiterates this notion and states that field investigations of conditions on a coated, cathodically protected pipeline with AC density ranging between 100 and 4,000 A/m² (with on-potentials between -2.0 and -2.5 V) did not show any clear relationship between AC density and corrosion rate (found to be between 8 and 13 mpy [0.2 and 0.3 mm/y]). Wakelin et al⁶ reports that three field studies and inspections found rates ranging from 17 to 55 mpy (0.4 to 1.4 mm/y) for AC densities between 75 and 200 A/m². A German field-based coupon study⁷ revealed rates scattered between 2 and 4 mpy (0.05 and 0.1 mm/y) at 100 A/m² and 12 mpy (0.3 mm/y) at 400 A/m²; the rate of pitting was more scattered—between 8 and 56 mpy (0.2 and 1.4 mm/y), and it showed much less pronounced dependence on the AC density.

A 1964 work by Bruckner⁸ (sponsored by the American Gas Association [AGA]⁽¹⁾) showed that in soils with pH between 6 and 7, the corrosion rate of steel is below 3 mpy (0.8 mm/y) at 155 A/m² and between 10 and 20 mpy (0.25 and 0.5 mm/y) at 775 A/m². A paper by Song et al⁹ reports corrosion rates as measured on coupons installed for 6 and 12 months next to a buried cathodically protected pipeline, which were exposed to AC with a carrier frequency of 60 Hz, but with an appreciable contribution of a 180 Hz harmonic. The rates were found to be linearly increasing with AC density (less than 10 mpy (0.25 mm/y) for densities below 100 A/m² and between 5 and 25 mpy (0.13 and 0.64 mm/y) for densities between 100 and 500 A/m²); on-potentials were generally over -0.9 V. The German field study⁷ observed pitting corrosion rates of 210 mpy (5.3 mm/y) associated with AC densities between 20 and 200 A/m².

A recent batch of publications presented the results of laboratory and field evaluation using coupons and probes. Short-term field testing by Nielsen and Galsgaard¹⁰ recorded peak AC corrosion rates as high as 10 mm/y (400 mpy); Gregoor and Pourbaix¹¹ reported short-term laboratory-based rates between 0.01 and 0.25 mm/y (0.4 and 9.9 mpy) per each A/m² of AC density, with actual observed rates falling between 0.65 and 3.4 mm/y (26 and 130 mpy). Shoeneich¹² reported corrosion rates from buried coupons exposed to 1 to 91 A/m² of AC density under cathodic protection (CP) potentials more negative than -0.95V (CSE); the observed rate did not exceed 0.02 mm/y (0.8 mpy).

A laboratory study by Yunovich and Thompson¹³ revealed that in the absence of CP, corrosion rates ranged from 3.5 to 8.2 mpy (0.09 to 0.21 mm/y).

Similarly to Song et al,⁹ Wakelin et al⁶ (and others) report that for a given AC density, the corrosion rate tends to decrease with time and suggests that there may even be an “incubation” period of one or more months, depending on the current density.

Morphological Characteristics

Goran¹⁴ studied AC in the field on steel test coupons. The test coupons were cathodically protected and exposed to different AC densities. The series of tests consisted of one with 10 V AC applied to the

⁽¹⁾ American Gas Association (AGA), 400 N. Capitol St. NW, Washington, DC 20001.

test coupons for approximately two years, and another one with 30 V AC during cathodic protection for 1.5 years. From the results and observations, he concluded the appearance of corrosion could be divided into three groups:

- Small point-shaped attacks evenly distributed across the surface (uneven surface);
- Large point-shaped attacks evenly distributed across the surface (rough surface); and
- A few large, deep local attacks on an otherwise uncorroded surface (“pocked” surface).

Nielsen and Cohn¹⁵ describe a distinct tubercle of “stone-hard soil” comprising a mixture of corrosion products and soil that is often observed to grow from the coating defect in connection with AC corrosion incidents. The specific resistivity of such a tubercle is expected to be significantly lower than the specific resistivity of the surrounding soil. In addition, the effective area of the tubercle is considerably greater than the original coating defect. Both processes tend to decrease the spreading resistance of the associated coating defect during the corrosion process, making the corrosion process autocatalytic in nature. Ragault⁵, while describing 31 AC corrosion cases on a polyethylene-coated gas transmission line, notes that corrosion product consisted mostly of magnetite mixed with soil. Williams¹⁶ also indicates that the corrosion product on steel under AC influence was mainly magnetite.

Some examples of the photographic evidence culled from the investigations of underground pipeline failures attributed to AC corrosion are reproduced in Figures 1 and 2.

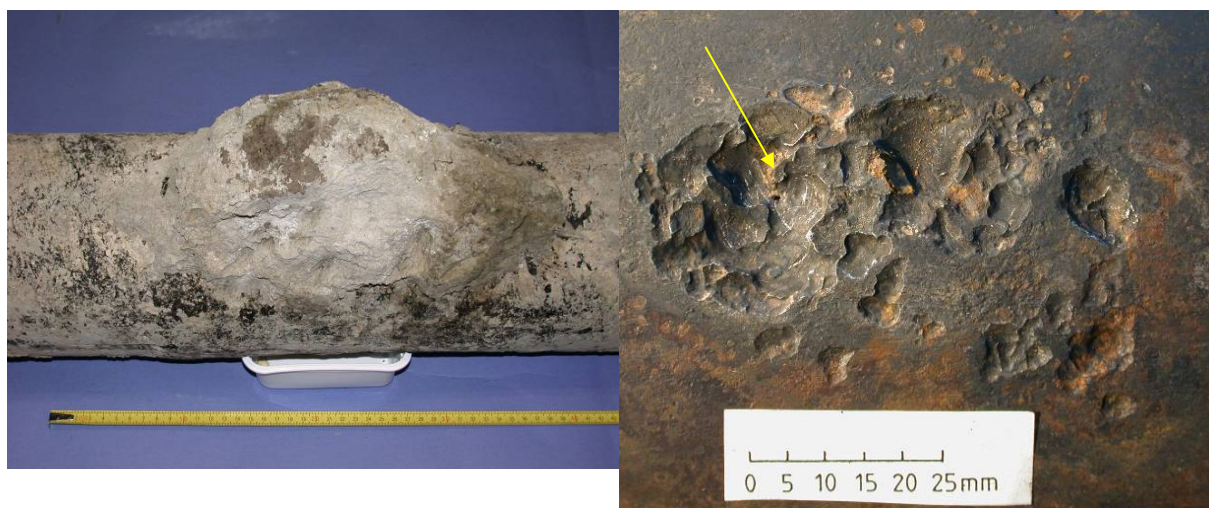


Figure 94. Leak site on underground natural gas transmission pipeline (attributed to AC corrosion) before and after cleaning. The arrow indicates the leak.¹⁷

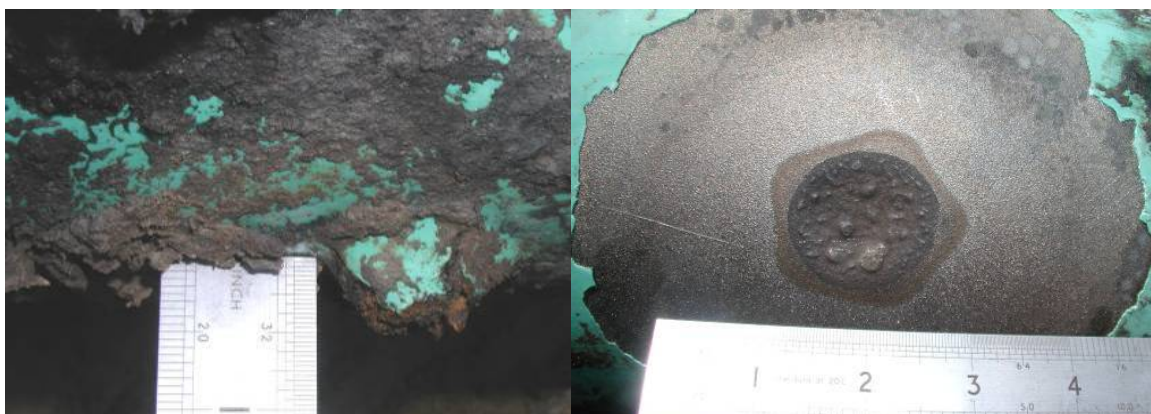


Figure 95. External corrosion site on a natural gas transmission pipeline (attributed to AC corrosion) before and after cleaning.¹⁸

Bolzoni et al¹⁹, who studied AC influence in solutions, report that the AC led to growth of thick but non-adhering corrosion products; the research results suggested that corrosion due to AC was likely to be localized.

If one follows the checklist presented in the 2000 CEOCOR proceedings³ to determine whether the corrosion attack is caused by AC based on the morphology of the damaged site, the picture becomes fuzzier. The questionnaire posts such questions as (1) Is there a coating defect, (2) Is the shape of corrosion damage a rounded pit, (3) Is the size of the pit much larger than the size of the associated coating defect, (4) Is the soil resistivity low/very low, and several others. Upon answering these and several other questions, the authors conclude that if “many” of the answers are “yes,” then it “probably” is an AC corrosion case. Wakelin et al⁶, while describing Canadian AC case histories, offers another, similar checklist to determine whether the cause of corrosion could be attributed to AC. The approach is to eliminate all other culprits (such as microbiologically influenced corrosion [MIC]) and evaluate the characteristics of the damaged region, paying particular attention to whether the pit has a rounded bottom and whether corrosion products had formed a hard dome over the pit.

AC Density

Studies performed in the 1950s and 1960s indicated that the AC-enhanced corrosion of steel is low, being in the range of 0.1 to 1% of a like amount of DC. Within this range (below 1%), Pookote and Chin²⁰ observed an increase in corrosion rate upon increasing AC density. Funk and Schoeneich²¹ reported the results of a two-year field study, which showed similar trends for both general corrosion rate and pitting. Gummow et al²² compiled an extensive literature survey on the subject of AC corrosion in 1998, when similar findings by many other researchers were presented. A 2005 study by Goidanich et al²³ reached a similar conclusion that DC equivalent percentage (defined as the ratio between observed corrosion rate to that expected for the DC of the same magnitude) for carbon steel in simulated soil solution is lower than 4%. The researchers also observed that this parameter tended to decrease with the increased current density.

In 1986, a corrosion failure on a high-pressure gas pipeline in Germany was attributed to AC corrosion. This failure initiated field and laboratory investigations that indicated induced AC-enhanced corrosion can occur on coated steel pipelines even when protection criteria are met. In addition, the investigations ascertained that above a minimum AC density, typically accepted levels of CP would not control AC-enhanced corrosion. The German AC corrosion investigators’ conclusions can be summarized as follows:²⁴

1. AC-induced corrosion does not occur at AC densities less than 20 A/m²;
2. AC-corrosion is unpredictable for AC densities between 20 to 100 A/m²;
3. AC corrosion occurs at current densities greater than 100 A/m²; and
4. The highest corrosion rates occur at holidays with a surface area between 100 and 300 mm².

(Note that these conclusions refer to steel structures that would be considered adequately protected in absence of AC; see European standard guidelines below for further discussion.)

Prinz et al²⁵ reported that since 1986 several cases of corrosion damage to cathodically protected pipelines have occurred in Germany and Switzerland due to alternating currents with a frequency of both 16-2/3 and 50 Hz.²⁵ In 1993, following a coating defects survey conducted in France, 31 cases of AC corrosion were found on a polyethylene-coated steel gas transmission pipeline (running parallel to a 400-kV high-voltage alternating current [HVAC] line) with relatively high (on-potentials in excess of -2.0 V CSE) levels of CP.⁵ The author of the study concluded the following factors increase AC corrosion risks: (1) a low level of CP (i.e., low DC density) with a high level of AC density, (2) small size of coating defects, and (3) low soil resistivity. Wakelin⁶ reported several corrosion anomalies occurring on pipelines exposed to induced AC interference in Canada. The above-cited literature survey²² concluded that corrosion rates in presence of AC:

- Increased in chloride-containing or deaerated environments;
- Increased with decreasing AC frequency (under 100 Hz);
- Increased with decreasing holiday surface area reaching a maximum for a holiday surface area of 645 mm²;
- Decreased with increasing CP current density; and
- Decreased with time.

Whereas many authors have concluded that there is a threshold AC density below which AC corrosion is not a factor, the magnitude of the threshold is being debated. Chin and Fu²⁶ studied mild steel exposed to a passivating sodium sulfate solution and observed that at 2,000 A/m² the passive layer appeared to be completely destroyed. In addition to the 20 A/m² cited above, the literature suggests that densities in excess of 30 A/m² may be detrimental to buried steel structures.²⁷

On the basis of laboratory tests, Pourbaix et al²⁸ concluded that AC corrosion is not related to any particular critical AC density value. In 1978, Jones²⁹ published the results of a study of low-alloy and carbon steel in sodium chloride solution, which observed an increase of corrosion rate of four to six times when the specimens in deaerated conditions were exposed to a 60-Hz current with a density of 300 A/m², but found no acceleration of corrosion under aerated conditions. A German standard, DIN 50925,³⁰ adopts a value of 30 A/m²; “Handbook of cathodic corrosion protection” by Baeckmann and Schwenk³¹ cites a value of 20 A/m².

European Standard CEN/TS 15280³² offers the following guidelines:

The pipeline is considered protected from AC corrosion if the root mean square (RMS) AC density is lower than 30 A/m².

In practice, the evaluation of AC corrosion likelihood is done on a broader basis:

- current density lower than 30 A/m²: no or low likelihood,
- current density between 30 and 100 A/m²: medium likelihood,
- current density higher than 100 A/m²: very high likelihood.

The standard also discusses the AC risk in terms of the ratio between AC and CP currents (assuming that the required protective CP potentials [see further discussion] are met):

- I_{AC}/I_{DC} is less than 5—AC corrosion likelihood is low,
- I_{AC}/I_{DC} is between 5 and 10—AC corrosion likelihood can exist and further investigation is typically necessary,
- I_{AC}/I_{DC} is greater than 10—AC corrosion likelihood is considered to be high and mitigation measures are normally taken (e.g., by using appropriate grounding).

Recent experimental studies by Yunovich and Thompson¹³ concluded that AC density discharge on the order of 20 A/m² can produce significantly enhanced corrosion (higher rates of penetration and general attack). Further, the authors stated that there likely was not a theoretical “safe” AC density, i.e., a threshold below which AC does not enhance corrosion; however, a practical one for which the increase in corrosion due to AC is not appreciably greater than the free-corrosion rate for a particular soil condition may exist.

The conclusions of the doctoral thesis by Goidanich³³ are similar in nature; the findings suggest that the current density of 10 A/m² may be hazardous, as it has increased the corrosion rate by two-fold in a simulated soil solution compared to the AC-free conditions (without CP).

AC Voltage

If one knows the soil resistivity and the pipeline’s AC voltage, by assuming the worst-case scenario of a 645 mm² holiday, the risk of AC corrosion can be determined using the following simple formula in Equation (1) to calculate AC density:

$$i = \frac{8V_{AC}}{\rho\pi d} \quad (1)$$

where:

i = AC density

V_{AC} = AC voltage of pipeline to remote earth

ρ = soil resistivity

d = diameter of a circular holiday having an area equal to that of the actual holiday

Thus, for the case of a 645-mm² holiday on a pipe in 1,000 ohm-cm soil, where the induced AC voltage on the pipeline is 10 V, the AC density at the holiday would be 225 A/m²; for the above-cited density of 100 A/m², the AC voltage would be 4.4 V.

This particular example has in fact been observed in a real-life case of pipeline failure investigation³⁴. The pipeline was buried in low-resistivity soil (200 to 600 ohm-cm); the AC voltage measurements showed values between 3 and 10 V. The AC density measurements using buried coupon test stations (CTS) indicated that, on several occasions, the density was in excess of 100 A/m². The plot in Figure 96 illustrates correlation between the actual observed pipe potential and current density.

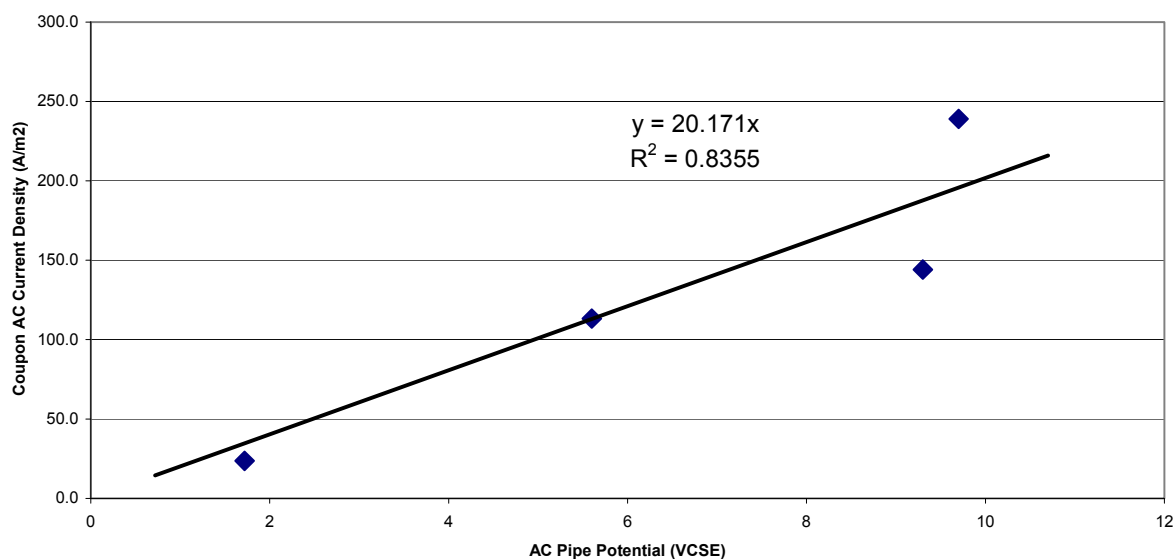


Figure 96. Relationship between measured AC pipe potential and measured coupon current density.³⁴

Some boundary conditions are often considered when assessing the “practical” risks of AC corrosion using the above estimates. For example, if one considers an AC density of 20 A/m² as the threshold, in 10 ohm-cm soil and a 645-mm² holiday, the typical maximum AC voltage estimated by this equation is 0.89 V. This magnitude of AC voltage is not uncommon on pipelines in non-AC interference areas. However, as illustrated in Figure 96, under certain conditions, the AC interference levels are often brought below 1.5 V AC in order to lower the AC densities to reduce the risk of AC corrosion.

This suggests that assessment of AC corrosion threat (and for that matter, AC mitigation) on the basis of AC voltage may be misleading. At present in the U.S., AC mitigation is mostly driven by safety considerations. The primary focus of these efforts is to reduce the induced AC voltage below 15 V with respect to local earth for steady-state conditions on above-grade portions, where personnel could readily come in contact with the pipeline or an appurtenance, to assure compliance with NACE Standard RP0177.³⁵

On the other hand, in Germany, the same threshold is 65 V.³⁶ Considering that the primary factor in determining the possibility for the presence of AC corrosion is the AC density, monitoring the current density rather than an AC voltage is used to assess the AC-related hazards to a buried pipeline.

This is a departure from the prevailing practices of measuring (and mitigating) the AC voltages on buried pipelines, notwithstanding the fact that the reduction of AC potentials is expected to reduce the AC magnitude as well.

The above-cited European standard suggests that to reduce the AC corrosion likelihood on a buried pipeline, the pipeline AC voltage should not exceed at any time 10 V over the entire pipeline or 4 V where the local soil resistivity measured along the pipeline is less than 25 ohm-m. However, these limits are sometimes considered overly restrictive for many pipelines influenced by overhead 50- and 60-Hz HVAC power systems without a history of corrosion failures. When pipeline systems run concurrently with electrical transmission lines for significant lengths at close separation distances, especially in high-resistivity areas with complex electromagnetic fields and conductor geometries, even the 15-V AC limit results in extensive and expensive mitigation.

Frequency Effects

As mentioned earlier, published accounts^{20,26,37,38,39,40,41,42} indicate that there is an inverse relationship between AC-induced corrosion and the frequency of the signal—corrosion rate decreases with increasing frequency. While one can assume that at very high frequencies AC is not expected to influence the corrosion process, as evidenced by the published case studies, AC at commercial frequencies of 50 or 60 Hz can cause corrosion of affected structures (see further discussion in the next section). Also, the magnitude of the potentials shifts due to the AC signal decrease with the frequency.

The frequency also affects the pit morphology, the pit density, and passivity current density (decrease with increasing frequency^{26,39,41}).

The following example (taken from the Yunovich and Thompson study⁴³) shows estimated current flow through the steel specimen exposed to soil using an equivalent analog circuit (Randle’s model), shown in Figure 97. The circuit consists of a double layer capacitance (C_1), solution resistance (R_s), and “effective resistance” (R_{eff}) representing the combination of the charge-transfer and Warburg (diffusion-related) impedances. The circuit also incorporates an AC power source (V_1). (See more on this subject in the AC corrosion mechanism section.)

The analysis used a commercial electrical circuit modeling software that can simulate electric circuitry behavior and calculate (over a range of imposed AC voltage frequencies) the current passing through each component of an electrical circuit for given parametric values. The circuit in Figure 97 uses actual experimentally observed values (24 V AC was imposed on the specimen to achieve the AC density of approximately 400 A/m²).

The results of the simulation for the case illustrated in Figure 97 are shown in Figure 5, which shows the current passing through R_{eff} (related to corrosion process) and the current passing through R_s (the total current in the circuit). As seen, there is a sharp drop-off in the R_{eff} current as the impedance of the capacitor in series with R_{eff} diminishes with increasing frequency, thus “short-circuiting” the R_{eff} resistance connected in parallel. However, although most of the current at 60 Hz passes through the capacitance and thus does not affect corrosion reactions, there is a non-trivial amount of AC (119 microamperes, approximately 0.3% of the total) that still passes through the R_{eff} at 60 Hz.

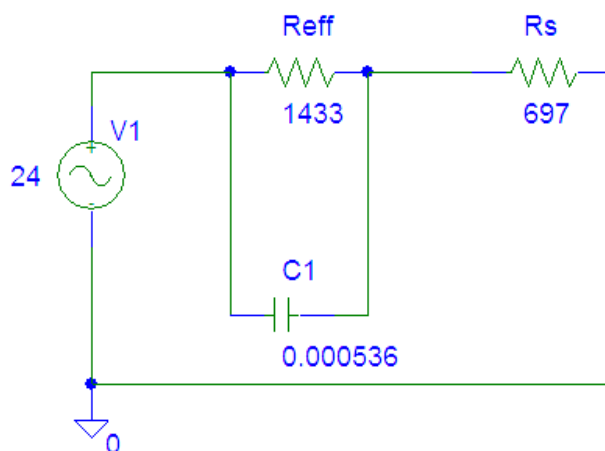


Figure 97. Electrical equivalent circuit.⁴³

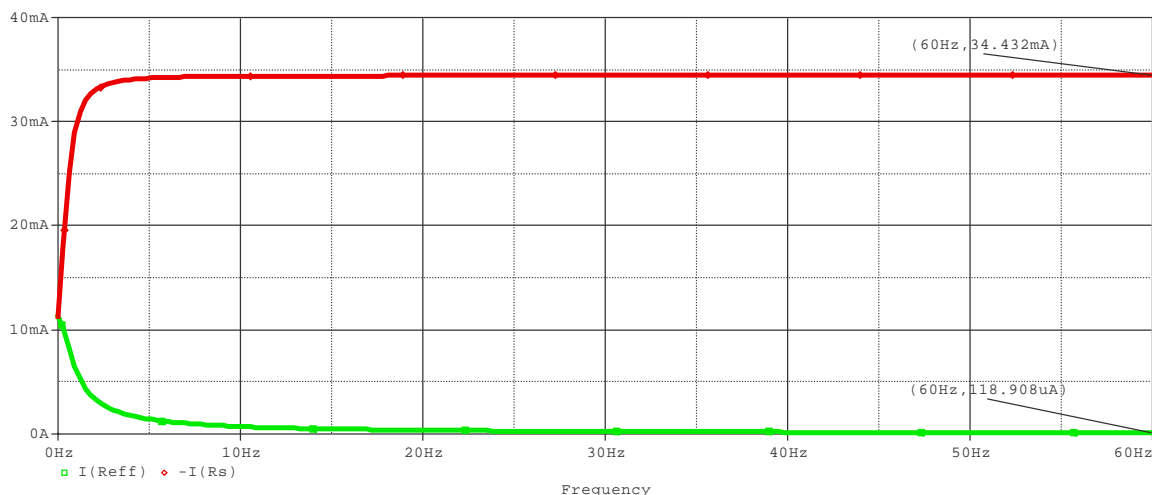


Figure 98. An illustration of a simulation run (red line shows total AC in the circuit; green line shows current passing through R_{eff}).⁴³

AC CORROSION MECHANISM

Given the often present differences in conclusions published on the subject of AC corrosion, there is no agreed-on mechanism for the phenomenon, particularly as it applies to corrosion in soils. There is a controversy about the direction of AC polarization of metal—to more negative or positive potentials (see e.g., Pookote and Chin²⁰ and Hamlin⁴⁴). There appears to be a consensus on one aspect of AC corrosion: the corrosion rate associated with a particular AC density is less than 1% of that caused by DC of similar magnitude (a dissenting study by Radeka et al⁴⁵ suggests that in seawater the AC “efficiency” is between 6 and 14% for 60 Hz densities between 20 and 150 A/m²). An early work by Williams¹⁶ (1966) dismissed the notion that AC corrosion is the result of the waveform rectification at the steel surface and suggested that the mechanism of the attack is essentially that of DC corrosion. A study by Juetner et al⁴⁶ on a ring-disk (mild steel-Pt) electrode in water-based solutions of sulfates, carbonates, and chlorides at AC densities up to 200 A/m² concludes that there were no indications of a change in the anodic or cathodic reaction mechanism. Gummow et al²² presents summaries of several of the quoted studies; the proposed explanations focus on the effect of AC corrosion current passing through the resistive components of the corrosion circuit on the anodic and cathodic reactions.

Several publications with regard to the AC corrosion mechanism are discussed in further detail.

Electrical Equivalent Circuit Analysis

Nielsen and Cohn¹⁵ offer a more extensive discussion of the aspects of the AC corrosion model; an extended summary of the article is presented below.

Pipelines with highly resistant coatings are susceptible to induction of AC voltage from high-voltage power lines. The AC voltage may be a source of corrosion at coating defects where the AC discharges from the pipe. Equivalent circuits modeling AC corrosion can be helpful in understanding the corrosion process and underlying mechanisms.

Figure 99 shows a schematic of an equivalent AC corrosion circuit suggested by Nielsen. The AC and DC sources impose a DC and AC voltage in between the pipeline and remote earth at a specific location or coating defect. The AC source represents AC induction, whereas the DC source represents the CP system.

The corrosion reaction in this example consists of the non-equilibrium reaction sequence of the oxidation of iron (VB1) and the reduction of one of the three VB2 equilibrium reactions (see Equations [2] through [5]).



The equilibrium potentials for such two electrochemical reaction schemes are represented by E_{o1} and E_{o2} in Figure 99, being additional electrochemical or electromotive forces defining the open-circuit DC potential.

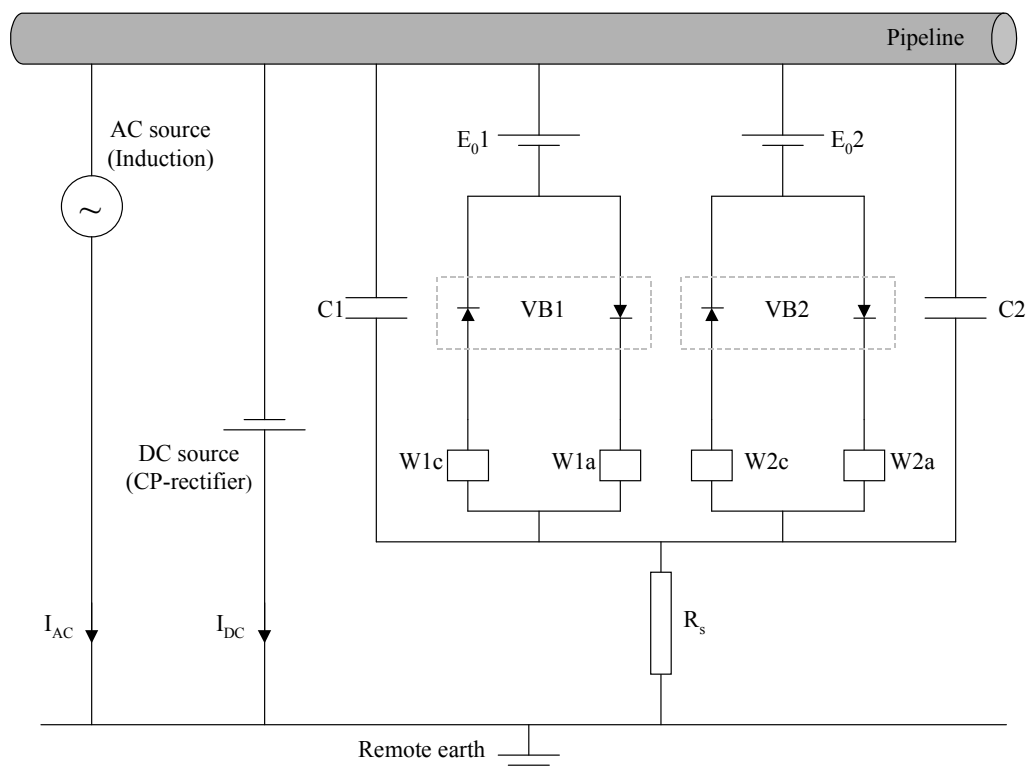


Figure 99. Schematic of a proposed AC corrosion equivalent circuit.²⁵

Electrochemical equilibrium processes existing at the steel surface are associated with an equilibrium potential (E_o). The equilibrium potential can be calculated using the Nernst equation, Equation (6):

$$E_0 = E^0 + \frac{RT}{nF} \cdot \ln \frac{a_B^b}{a_A^a} \quad (6)$$

where:

E^0 = standard equilibrium potential;

R = gas constant;

T = absolute temperature;

n = number of valence electrons;

F = Faraday's constant; and

a_x = activity or concentration of the species X of equilibrium equation [$a_A = bB + ne^-$].

Hence, E01 and E02 represent the equilibrium potentials of two Volmer-Butler reaction schemes (VB1 and VB2) occurring at the corrosion interface, such as (1) iron dissolution (oxidation)—1a and iron re-deposition (reduction)—1c and (2) water/oxygen/hydrogen oxidation—2a and water/oxygen/hydrogen reduction—2c.

In a simpler Randle's circuit (similar to the one shown in Figure 97), polarization resistance represents the charge transfer resistance of the slowest process. In the proposed circuit, there are individual charge transfer resistances for each single process and illustrated as a diode element in the equivalent diagram, Figure 99. At potentials different from the equilibrium potential, the process proceeds with a rate that can be described by the Faradaic current according to the Volmer-Butler equation (Equations [7a] and [7b]). The Volmer-Butler equations relate to a single electrode process, consisting of anodic and cathodic current-potential characteristics.

$$I_{F,a} = I_0 \left[\frac{C_{A,surface}}{C_{A,bulk}} \cdot \exp\left(\frac{E - E_0}{\beta_a}\right) \right] \quad (7a)$$

$$I_{F,c} = I_0 \left[-\frac{C_{B,surface}}{C_{B,bulk}} \cdot \exp\left(\frac{E - E_0}{\beta_c}\right) \right] \quad (7b)$$

where:

I_F = Faradaic current related to the process;

I_0 = Exchange current related to the process;

$C_{i,surface}$ = Surface concentration of species i;

$C_{i,bulk}$ = Bulk concentration of species i;

E = Polarized potential (off-potential);

E_0 = Equilibrium potential of the process as given by Equation (6); and

β_a, β_c = Tafel slope related to the anodic and cathodic reactions.

To each of the individual processes, a diffusion impedance or diffusion element is attached and symbolized by W (for Warburg impedance). This impedance restricts the rate by which the reactions can occur due to diffusion limitations of reactants (and products for that matter). It is noted that this

impedance is frequency dependent. The Faradaic current passing through the circuit is determined by the sum of the Volmer-Butler impedance and the Warburg diffusion impedance. These describe, so to speak, the degree to which the electrochemical reactions are fast enough to occur at the relevant frequency.

The Volmer-Butler theory only applies to the current passing through the polarization resistance component of the interface and does not apply to the current that passes through the capacitive component. The capacitive nature of the electrochemical interface imparts frequency dependence to the portion of current that passes through the polarization impedance/resistance.

Nielsen et al⁴⁸ attribute the AC corrosion process to the Volmer-Butler element represented as VB1 and VB2 in Figure 99. AC corrosion occurs if the charge during the anodic half-cycle exceeds the cathodic charge (Equation 8). However, if the opposite occurs, corrosion does not take place. This is possibly an overly simplified statement of an AC corrosion mechanism.

$$I_a (\Delta t) > I_c (\Delta t) \quad (8)$$

The last element, R_s , the spread resistance, is controlled by factors relating to the resistance of the soil solution, porosity, and geometric factors at the interface between the soil and the coating defect. An ohmic resistance or IR drop develops when current flows from remote earth to a coating defect of the pipeline through the soil.

Figure 100 shows the effect of the defect configuration on the pipe-to-soil resistance. Thus, a bare surface (Figure 7a) results in only a soil resistance. However, a coated surface with a holiday gives rise to both soil resistance and spread resistance. A large IR drop develops near the vicinity of the pipe-to-soil interface where the coating defect is present. A geometric spread effect is produced as a result of concentrated current flux lines allowed by the defect geometry to spread out from the narrow coating defect. When the area of the defect is taken into account, small defects have smaller spread resistances (per unit area) compared with larger coating defects.

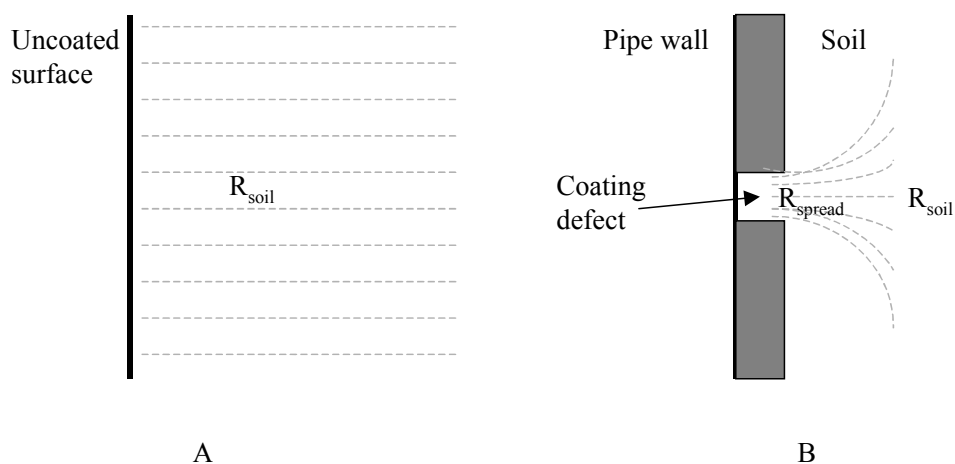


Figure 100. Illustration of geometrical effects on pipe to soil resistance.²⁵

Due to the low impedance of the capacitance, the spread resistance, R_s , is the dominating (greatest) impedance element at 50/60 Hz in the current path between a coating defect and remote earth, thus controlling the AC magnitude.

AC effect on corrosion process in absence of CP

Using extensive laboratory work, Yunovich and Thompson⁴³ used a conventional electrochemistry approach (modified Randle’s equivalent analog circuit depicted in Figure 97 and described earlier) to develop an AC corrosion model in the absence of CP. As discussed, only a small amount of the 60-Hz AC discharge passes through the resistive component of the equivalent circuit, which results in corrosion (metal-loss) reactions. The AC passing through this resistive component produces both anodic and cathodic polarization shifts (sinewave-dependent) resulting in a net increase in the average corrosion rate compared to the free corrosion rate.

The proposed model for AC corrosion does not invoke any new electrochemical concepts and is based on the conventional (DC) treatment of the corrosion processes. AC corrosion is characterized by the rapid formation of a diffusion controlled (Warburg) process for corrosion in soils. Although diffusion controlled, the overall impedance decreases as the total AC increases.

In this analysis, it is assumed that the metal loss reactions are non-reversible, and the reduction reaction is the conventional oxygen-water reduction. Likewise, it is assumed that metal loss is the only available oxidation reaction. Prior work indicates that the application of CP results in possible non-metal-loss oxidation reactions. For the following example, no CP is assumed. It is realized that each reaction sequence has a specific time constant associated with that specific reaction. Therefore, the above assumption implies that the time constant is sufficiently fast that the reaction sequence is applicable at 60 Hz.

An example of a corrosion process under the influence of AC signal is illustrated in the schematic in Figure 101. The graph is based on realistic potential and current values; the assumed E_{corr} is -700 mV (SCE) and i_{corr} is 4.7 mA (which corresponds to a corrosion rate of 3 mpy (0.08 mm/y) for a 4,580-mm² specimen). As seen from the graph, the imposition of an AC signal results (shown by the “AB0CA” sinewave) in the potential shifts in anodic (positive) and cathodic (negative) direction of the corroding metal during the respective halves of the sinusoid; the absolute value of the potential shift is 150 mV.

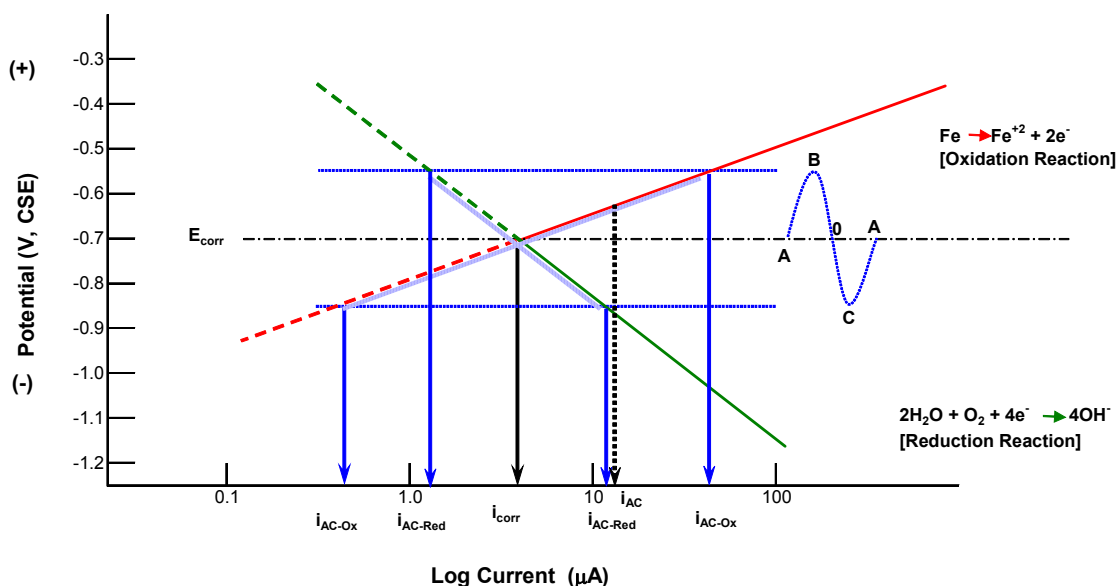


Figure 101. Schematic of proposed mechanism of AC-enhanced corrosion.

The relationship between potential (E) and current (i) is semi-logarithmic. The dependence of the anodic potentials (E_a) can be approximated with a linear equation of the type $E_a = \beta \log(i_a) + b$, where β is the Tafel slope of the anodic process, and i_a is the anodic reaction current. During the anodic part of a single period of the sinewave (AB0), the anodic current density increases to the value denoted i_{AC-Ox}^a ; during the cathodic part, the anodic current density decreases to the value denoted i_{AC-Ox}^c . During the semi-log dependence between potential and current, the average anodic current for a single AC sinewave period (i_{AC}) is greater than the i_{corr} value for freely corroding conditions in the absence of AC. Therefore, in this example, the presence of the AC signal equivalent to a ± 150 -mV peak polarization shift produced an increase in the oxidation current from 4.7 μ A to 13 μ A, which corresponds to an increase in corrosion rate from 3 to 8.5 mpy (0.08 to 0.22 mm/y).

The above example illustrates the proposed underlying principle for the ACEC mechanism: polarization of the metal sample by the imposed AC produces a net anodic (oxidation) current greater than the free-corrosion current, thus leading to accelerated corrosion attack. A more rigorous analysis of the proposed model follows below. The example is still based on the realistic values assumed above.

Assume that the $E = f(i)$ relationship is defined by Equation (9):

$$E = \beta_a \log(i) + b \quad (9)$$

where β_a is the Tafel slope for a corroding metal in soil (assumed to be 150 mV per decade of current).

In order to determine the value of the free member b , two more values are needed (E and i). Following the above example, the value of E is assumed to be -700 mV; the value of i is assumed to be equal to the magnitude necessary to produce a "typical" corrosion rate. Equation (10) yields the value of i :

$$r(\text{mpy}) = 0.129 \times \frac{i \times a}{A \times n \times D} \quad (10)$$

where

r = corrosion rate in mil per year

0.129 = conversion factor

i = corrosion current, mA

A = specimen area, cm^2

a = atomic weight of iron (55.8 g)

n = the valence of the dissolving iron (2)

D = density (7.87 g/cm^3)

1 cm = 10 mm

For the average corrosion rate of 3 mpy (0.08 mm/y), substituting the values in Equation (10) yields the corrosion current value of 4.7 mA (based on the area of a sample of 4,580 mm^2).

Next, the value of b is calculated by substituting -700 mV and 4.7 mA into equation (9) to produce the answer (99.8 mV).

Further assume that the potential shift due to the AC signal is defined by Equation (11):

$$E_{AC} = E_o \sin(2\pi ft) \quad (11)$$

where:

E_{AC} = potential at time t due to the AC signal

E_o = amplitude of potential shift of corroding metal due to AC (assumed to be 150 mV)

f = frequency of the signal (60 Hz or 0.0167 seconds)

Rearranging Equation (9) and substituting the assumed and calculated values, one arrives at the relationship between current i and potential E_{AC} as shown in Equation (12):

$$i = 10 \frac{E_{corr} + E_{AC} - b}{\beta_a} = 10 \frac{E_{corr} + E_o \sin(2\pi ft) - b}{\beta_a} \quad (12)$$

The graph in Figure 102 illustrates an example of the change in E_{AC} and the resultant current for a single period of a sinewave. As seen during the anodic semi-cycle, the current exhibits shifts to considerable magnitudes, much greater than the free corrosion current. During the cathodic semi-cycle, the oxidation current decreases compared to the free corrosion current, but not to the same degree as the increase during the anodic semi-cycle. Therefore, the complete AC cycle results in a net positive increase in the oxidation current. This is consistent with the illustration shown in Figure 101.

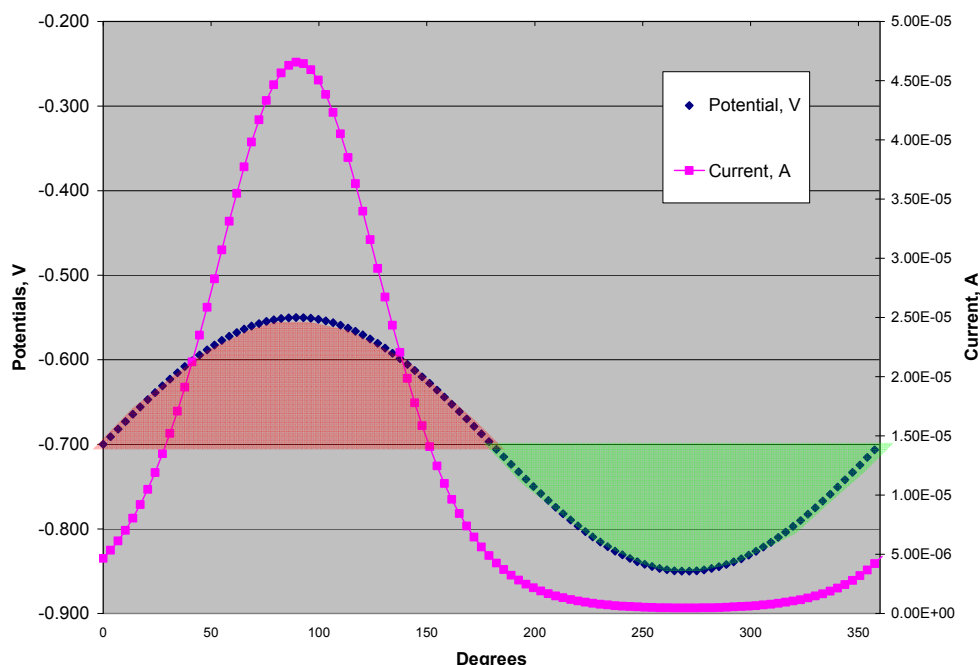


Figure 102. Potential and current shifts for a single period of 60-Hz current producing 150 mV of potential shift.

As the current distribution in time has been determined, it is possible to calculate the metal loss associated with each current and determine the corrosion rate. The graph in Figure 103 shows the calculated metal loss versus time for a single period of imposed AC and also depicts the cumulative metal loss for the same time. Based on the graphed data, estimated AC corrosion rate produced by the imposed AC signal with the assumed characteristics is 8.5 mpy (0.22 mm/y).

In the preceding example, conventional polarization analysis was used to estimate the increase in corrosion rate due to an applied AC voltage. Furthermore, this analysis predicts the parameters that have the most significant effect on ACEC are those that determine the amount of current that passes through the effective resistance of the equivalent circuit.

The model suggests that alternating currents (60 Hz) cause anodic (positive) polarization shifts during the positive portion of the imposed AC sinewave along with cathodic polarization shifts in the negative portion of the AC sinewave; the net result is an increase in the average oxidation (metal-loss) current compared to the free corrosion condition. The proposed model for the AC mechanism showed excellent correlation with the experimental results.

Earth Alkaline Versus Alkaline Cations

In accordance with the above, Stalder⁴⁷ proposes that AC corrosion may be affected by the chemical composition of the environment at the steel-soil interface and its impact on the spread resistance. This theory considers the concentration ratio between earth alkaline cations (such as Ca^{2+} and Mg^{2+}) and alkaline cations present in the soil (such as Na^+ , K^+ , or Li^+). Alkaline cations such as calcium and magnesium form hydroxides [$\text{Ca}(\text{OH})_2$, $\text{Mg}(\text{OH})_2$] caused by the surplus of hydroxide ions in the environment produced by the CP reactions. Hydroxides may be converted into carbonates (CaCO_3 , MgCO_3) in the presence of carbon dioxide CO_2 . Hydroxides and carbonates of earth alkaline cations produce solid precipitates with low solubility. In comparison, hydroxides and carbonates formed with cations such as sodium and potassium (NaOH , KOH , Na_2CO_3) are soluble. The resistive solid deposits

act to increase the spread resistance (R_s) associated with the coating holidays. Therefore, Stalder suggests that earth alkaline cations in the soil (which promote the formation of high resistive deposits) may lead to a higher spread resistance and a correspondingly lower magnitude of AC at the coating holiday (lower risk of AC corrosion).

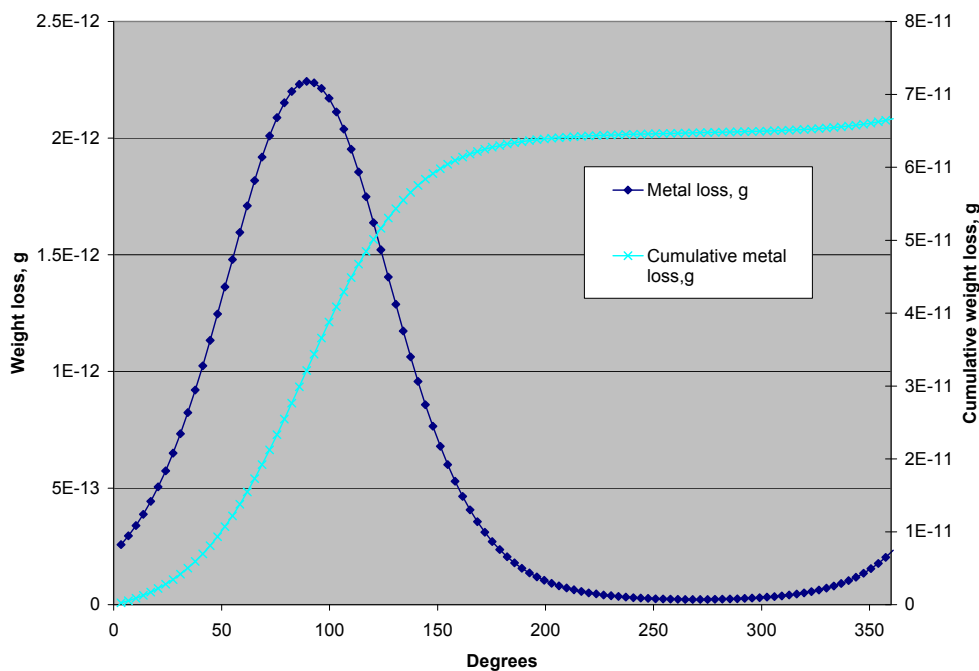


Figure 103. Instant and cumulative metal loss for a single period of a 60-Hz AC producing 150 mV of potential shift.

In addition to the greater spread resistance produced by the earth alkaline cations, earth alkaline cations have been shown to passivate the anodic branch of the metal dissolution (VB1) process at pH values as low as 6. This would also have the effect of decreasing AC corrosion caused by a Volmer-Butler anodic dissolution mechanism. Thereby, Stalder proposed that the ratio of earth alkaline cations to alkaline cations is critical to identifying areas where AC corrosion is most probable.

Alkalinization Mechanism

The above theories by Stalder on earth alkaline versus alkaline cations provided the basis for the alkalinization theory. Nielsen et al^{48,49,50,51,52,53} further develop this theory.

In brief, this mechanism proceeds when hydroxide (OH^-) produced by CP current accumulates in the near surroundings of the coating defect (Figure 104). The combined action of potential vibration caused by the AC and adequately high pH induces corrosion attacks. Potential fluctuations between the immunity and passivity regions of the Pourbaix diagram (Figure 105) may cause corrosion due to different time constants associated with iron dissolution (fast) and subsequent formation of passive film (slower). At very alkaline pH (14), the formation of dissolved HFeO_2^- may stabilize corrosion at a very high penetration rate.

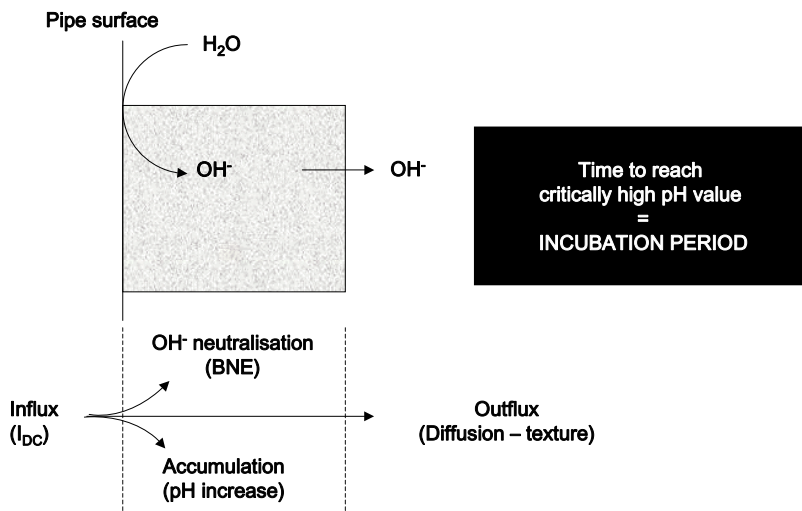


Figure 104. Mass balance schematics for OH^- ions produced by CP at a coating defect.

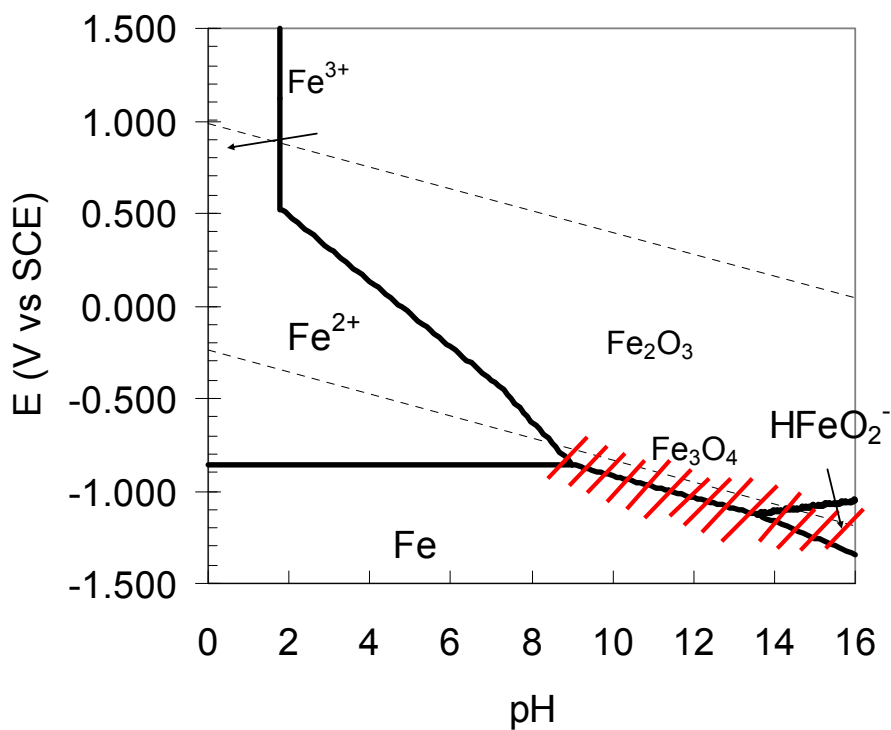


Figure 105. Pourbaix diagram showing unsafe region with respect to AC corrosion.

Further, it has been illustrated by laboratory soil box experiments as well as field investigations that the DC density has a significant effect on the spread resistance and accordingly on the AC density and corrosion rate.

Soil box experiments were run over three weeks each and were performed in alkaline pore solution in inert quartz sand.⁵² In all experiments, the AC voltage was controlled at 15 V. Six experiments were conducted, and the electrical parameters and corrosion rate were monitored using an electrical resistance probe.¹⁰ The test duration was over two to three weeks each, and the experiments differed by the applied polarization (ON) potential (-850, -950, -1,100, -1,200, -1,250, and -1,300 mV CSE, respectively).

Figure 106 through Figure 16 show some results from these studies. All data from the six experiments have been merged into the graphs. Figure 106 shows that AC density increases as the DC density is increased. Data in Figure 107 suggest that the spread resistance is inversely proportional to the DC density. Figure 108 and Figure 16 show that the corrosion rate increases as a function of not only AC density (Figure 108) but also DC density (Figure 109). The researchers attribute the latter trend to the alkalization at the steel interface due to accumulation of hydroxide ions. As such, the authors theorize that DC may influence the AC corrosion process, and that excessive CP should therefore be avoided. These conclusions were adopted by the European standard.³²

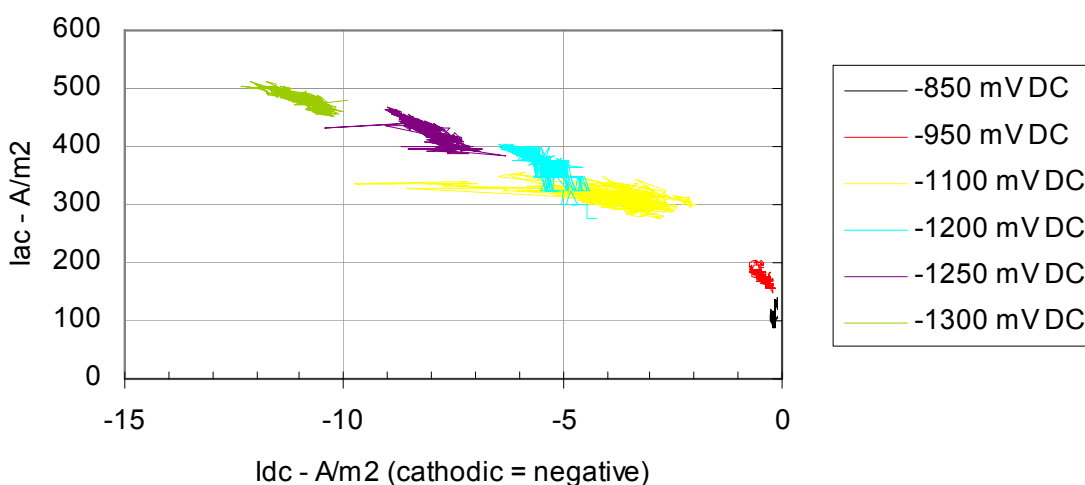


Figure 106. Correlation between AC and DC—NaOH soil box.

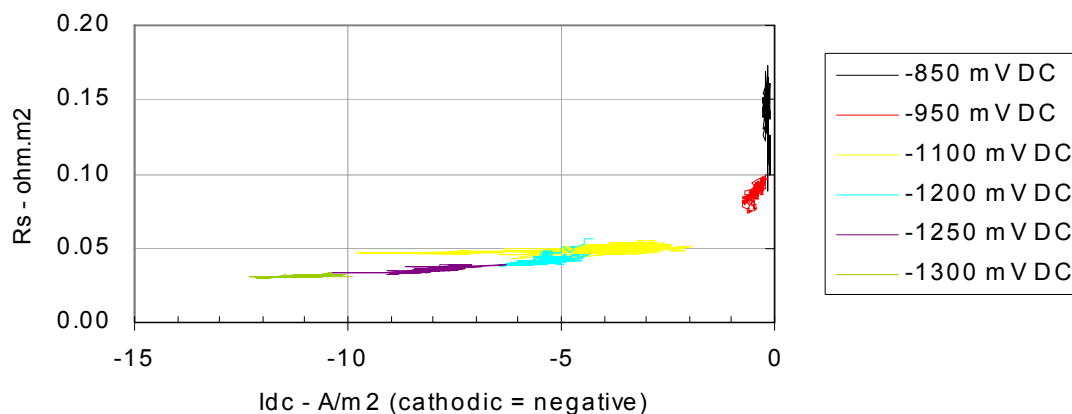


Figure 107. Correlation between DC and spread resistance—NaOH soil box.

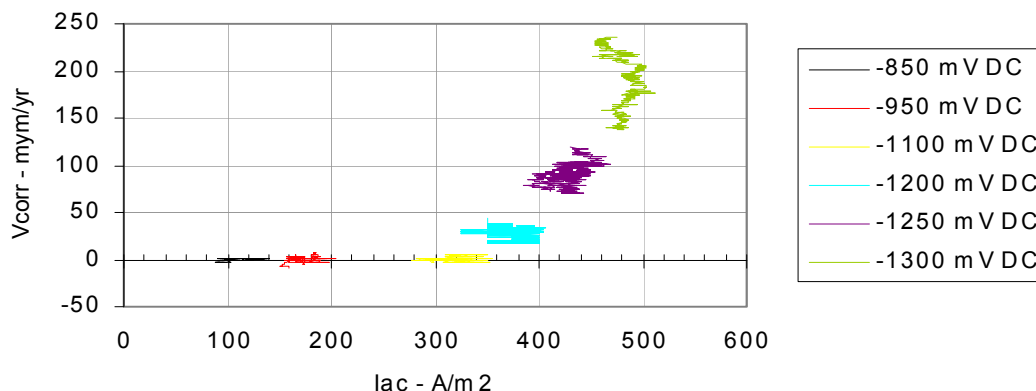


Figure 108. Correlation between AC and corrosion rate—NaOH soil box.

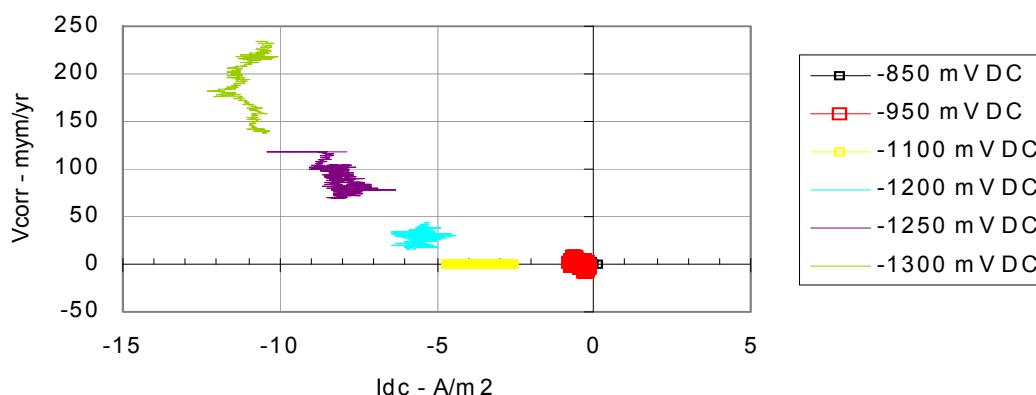


Figure 109. Correlation between DC and corrosion rate—NaOH soil box.

Effects of AC on overpotential

As discussed earlier, there is empirical evidence that AC may cause polarization (potential shift) of the affected structure. Bockris⁵⁴ suggested that some degree of AC “current rectification” may take place at the steel interface, and the difference in the anodic and cathodic Tafel slopes of the corrosion process results in the net positive or negative potential shift.

Other authors^{26,40,55,56,57,58} also pointed out that the ratio of the anodic and cathodic Tafel slopes determines the sensitivity of the corroding system with regard to the AC caused polarization. If the potential shift is asymmetrical ($r = \beta_a/\beta_c \neq 1$), when an external sinusoidal potential excitation is applied, a net DC (rectification current) results. However, regardless of the ratio, if the corrosion

process is controlled by activation polarization, under AC influence, corrosion (or exchange) current density would be expected to increase, which could lead to corrosion.

The acceleration of the corrosion rates in the presence of AC has been attributed by some authors^{20,29} to reduction of polarization of both the anodic and cathodic areas, as well as the passivation^{26,59,60} of the affected material. Authors observed that the corrosion potential is shifted in the negative direction^{26,59} and that the exchange current density increases and the Tafel slopes decrease correspondingly.^{20,29}

Lazzari et al⁶¹ suggest that more than one of the theories proposed in literature should be considered, thus proposing a “mixed” mechanism. The authors discuss the issue of reversibility of cathodic and anodic processes and state that the process occurring during the anodic half-cycle of the AC signal may not be completely reversed during the cathodic half-cycle. As a result, the double-layer chemistry may be affected, which in turn would influence the corrosion kinetics, leading to changes in the polarization behavior and shifts of corrosion (or equilibrium) potential.

Therefore, considering that in most cases the principal anodic process during the anodic half-cycle is metal dissolution and the principal cathodic one during the cathodic half-cycle is either oxygen reduction or hydrogen evolution, similarly to Yunovich and Thompson¹³ and Nielsen and Cohn,¹⁵ the authors conclude that the charge during the anodic cycle (metal dissolution) is greater than the charge during the cathodic cycle (metal deposition).

CATHODIC PROTECTION

The issue regarding what level of CP should be applied to mitigate AC corrosion is not without controversy.

Historically, the thought advocated by some was that applying CP in accordance with industry standards could adequately control AC-enhanced corrosion. However, as mentioned above, multiple failures of pipelines under CP, primarily in Europe, have been attributed to AC corrosion. The 1986 German investigation of an AC corrosion failure reported a high pitting rate despite CP current density of 1.5 to 2 A/m² and on-potentials of -1.8 to -2.0 V (CSE).⁷ The literature survey by Gummow et al²² cites the follow-up investigation to the failure; it was found that increasing the CP current density to 5 A/m² reduced the corrosion rate at 50 A/m² AC by a factor of two. The survey also cites another German work that demonstrated that AC corrosion could be mitigated at CP current densities of 4 A/m²; another quoted publication shows that even at 10 A/m² of DC density, AC corrosion remained considerable at AC densities of 100 to 200 A/m².

A report by Frazier⁶² indicated that the coupons immersed in a simulated ground electrolyte and exposed to intermittent application of AC and CP were found to be adequately protected by 100 mV of cathodic polarization.

The German standard³⁰ requires limiting current density while maintaining about 1 A/m² of DC density on coated pipelines. A 1986 study by Hamlin⁴⁴ states that metals (including pipeline steel) under the influence of AC could be protected but “usually at higher initial current densities.”

Several recent published accounts warrant a further discussion. Hosokawa et al⁶³ present the results of a study that found AC corrosion could be mitigated to a corrosion rate of 0.4 mpy (0.01 mm/y) if AC density is below 70 A/m², but the AC related attack remained probable if the AC density was over the threshold value. The study, carried out on two cathodically protected buried pipelines, used buried 100-mm² coupons to monitor the efficiency of impressed current CP and the level of AC reduction (using decoupling devices and magnesium anodes as grounding devices); without actually reporting on the findings, the study shows the following diagram (Figure 17) to illustrate the adopted criteria for DC and AC.

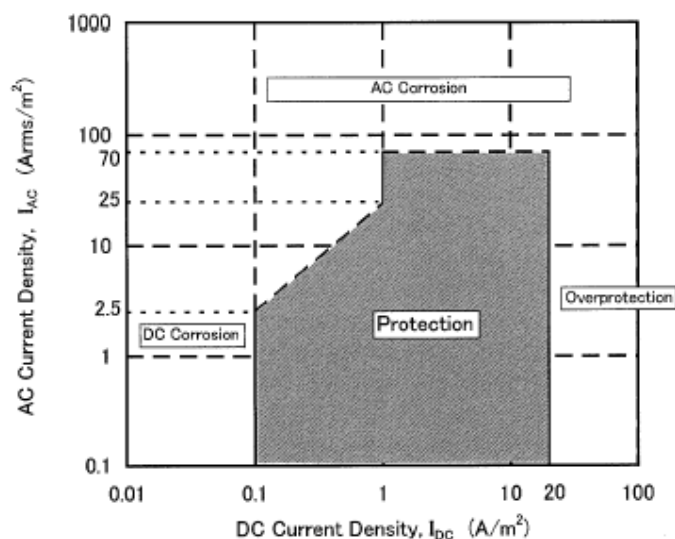


Figure 110. AC and DC density relationship to achieve protection⁶³

The above diagram brings forth the notion of a CP “effectiveness threshold” in the presence of alternating currents, i.e., it suggests that if AC density is in excess of a certain value (70 A/m² as proposed by the quoted study), CP is not likely to have an effect unless the AC levels are reduced below the “threshold” at which CP can mitigate corrosion.

The authors also set the upper limit on CP current at 20 A/m² due to concerns of overprotection. Thus, the paper offers the following combination of AC and CP criteria for AC corrosion mitigation (which, according to the specific field evaluations, was proved to be adequate):

Protection achievable if:

- (a) for $0.1 \text{ A/m}^2 \leq I_{CP} \leq 1.0 \text{ A/m}^2$, limit $I_{AC}(\text{rms}) < 25 I_{CP}$
- (b) $1.0 \text{ A/m}^2 \leq I_{CP} \leq 20 \text{ A/m}^2$, limit $I_{AC}(\text{rms}) < 70 \text{ A/m}^2$

As discussed earlier, following the notion that alkalization at the steel interface has an impact on AC corrosion, Nielsen⁴⁹ presents the results of field tests and proposes that “the CP level has a dramatic influence on the AC corrosion process” and that “excessive” CP can exacerbate AC attack and thus should be avoided. The values reported in the article show that at direct currents about 10 A/m² and off-potentials of approximately -1,100 mV (CSE), corrosion rates gradually increased to as high as 10 mm/y (400 mpy) (as measured by electrical resistance probes over a two-week period).

These results were incorporated in European Standard CEN/TS 15280,³² which states that “it is recommended to lower the pH at the steel/electrolyte interface by adjusting the CP ‘E_{on}’ to obtain a CP ‘E_{off}’ more negative than, but as close as possible to, the limiting critical potential indicated in EN 12954⁶⁴ (-850 mV [CSE] for iron or steel in aerobic or -950 mV [CSE] in anaerobic soil containing sulfate reducing bacteria).”

Gregoor and Pourbaix¹¹ posit in contrast that, based on a large number of short-term laboratory tests, protection from AC corrosion is only achievable when the potential of steel is within the “immunity” region of the Pourbaix diagram. In the tests, this corresponded to the imposed CP potentials more negative than -1,150 mV (CSE). Using Pourbaix diagram considerations, the authors postulate that, given the highly alkaline environment at the coating defects on the CP protected steel in soil, it is imperative to keep the “true” CP potentials more negative than the offered criterion. The authors

comment that the proposed AC corrosion protection criterion may not be practical, and advocate the use of mitigation measures (grounding) to prevent AC. No consideration was given to the effect of such low potentials on coating adhesion and hydrogen induced cracking in steel.

Another publication⁶⁵ discusses the results of a laboratory study. The paper concludes that, based on weight loss and electrochemical measurements, CP of carbon steel can be achieved at potentials more negative than -1,150 mV (CSE). Corrosion protection is considered in terms of DC and AC density ratio (i_{DC}/i_{AC}); according to the conclusions, the ratio should be higher than $3 \text{ mA}_{DC}/\text{A}_{AC}$. Using the empirically derived relationship, the following correlation between the required CP current density for bare steel, i_{prot} (mA/m^2), is given in Equation (13) for the conditions when known AC density is above $30 \text{ A}/\text{m}^2$:

$$i_{prot} = i_L + K_{AC} i_{AC} \quad (13)$$

Where:

i_L is oxygen limiting current density (mA/m^2),

i_{AC} is AC density (A/m^2), and

K_{AC} is a constant, estimated in the range 2 to 5;

The paper also notes that the “conventional” -0.85 V (CSE) CP criterion is not adequate in the presence of AC interference.

While there is an apparent contradiction between the proposed polarization potential values between the European standard and the two publications described above, it can be argued that these positions have the same goal. The notion of reducing both the CP levels and the concomitant pH values is aimed at ensuring that the potential fluctuations of steel caused by the AC are “contained” within the passivity/immunity region of the Pourbaix diagram (see hatched region in Figure 105 for an illustration).

Similarly, the position advocating much lower (more negative) polarization potentials seeks the same—ensuring that the steel potentials fall within the immunity region at all times, albeit at what are likely to be high(er) pH values. However, given the slope of the $\text{Fe}/\text{HFeO}_2^-$ equilibrium at high pH, the latter position requires more stringent control of potentials in the presence of AC influence. Also, besides the practical considerations with regard to maintaining such negative polarization (which may not be achievable in some conditions), the impact on coating disbondment and hydrogen induced cracking becomes a concern.

With regard to the alkalization theory, it should also be pointed out that elevated pH is likely to be present in conditions in which soil moisture content is limited. In such soils, the abundance of oxygen supply to the steel surface and constraints on the outward migration of the hydroxide ions due to low moisture content lead to hydroxide concentration build-up at the surface. It has been demonstrated in laboratory studies⁶⁶ and observed in the field that relatively low CP potentials (off-potentials of approximately -850 mV [CSE]) give rise to pH values in excess of 12 at the steel surface. If the applied potentials are kept at the levels suggested on the basis of alkalization’s impact on AC corrosion, according to the Pourbaix diagram-based reasoning, the steel would be in the potential-pH region where AC corrosion may be likely.

One other aspect of the CP requirements for AC corrosion protection that has not been adequately addressed in the published literature is the polarization shift. Yunovich and Thompson¹³ have demonstrated that at low ($20 \text{ A}/\text{m}^2$) AC densities, steel specimens exposed to soil have achieved protection under 100 mV of polarization shift. The contour plot of AC density-CP polarization shift-

depth of penetration (normalized to the control specimens) is shown in Figure 18. However, the plot is based on a limited number of tests and should not be taken as the definitive guideline.

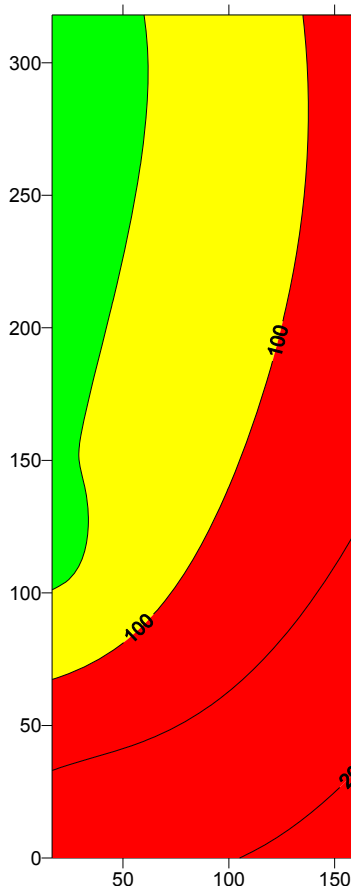


Figure 111. Contour plot of AC density (A/m^2 , horizontal axis)—CP polarization shift (mV, vertical axis)—Depth of penetration relative to control (%).

AC MITIGATION METHODS

AC mitigation in conjunction with CP is frequently used to minimize any effect of AC interference. Historically, several methods, such as installation of decoupling or grounding devices, were used to reduce AC interference. As shown above, although increasing the CP current density is reported to reduce AC corrosion, AC corrosion can ostensibly remain significant even when “conventional” CP criteria are being met. Further, it is being argued that increasing CP to control AC corrosion may result in the opposite effect due to increased pH and reduced spread resistance at the defect in the coating.

Therefore, the typical means of controlling AC corrosion is to provide grounding at critical locations to transfer the discharge point of the AC from the pipeline to the grounding conductors. Computer modeling has shown that properly located earthing conductors reduce the pipe leakage current density by an order of magnitude or more.⁶⁷ The induced current in the pipe is likely to increase after mitigation is installed; however, the discharge density is normally reduced, and the grounding conductors discharge the bulk of the current if properly designed. Although the major industry

emphasis for AC mitigation has been for touch voltage considerations, it is thought that in locations where adequate mitigation (i.e., grounding) has been installed to reduce the coating stress voltage during faults to under 5 kV, and a touch voltage is maintained below 15 V at above-grade portions and appurtenances, and step-and-touch voltages during faults comply with the criteria in IEEE Standard 80,⁶⁸ AC corrosion may not be of great concern.

Certainly, because of the above, mitigation installed for electrical safety considerations has a beneficial effect on controlling AC corrosion. However, the mitigation measures are installed at regularly spaced intervals along the affected pipeline section. In addition to personnel safety, the criteria for successful AC/voltage mitigation normally include considerations for reducing AC corrosion likelihood. In many cases, the effectiveness of the mitigation measures is only evaluated with regard to steady-state touch voltage conditions, which may not be sufficient for AC corrosion control. Mitigation is also often installed for fault (inductive and conductive) conditions, as fault conditions make mitigation significantly more difficult than simply reducing steady-state voltages.

As the literature survey indicates, AC voltages are not necessarily related to the probability of corrosion, and AC density is a more reliable metric for assessing AC-enhanced corrosion risk. Furthermore, there is no definitive agreed-on threshold of AC density.

One experimental observation that is relevant to AC mitigation is that the efficiency (the ratio of the observed weight loss to the theoretical one) of sacrificial anodes, which are routinely used for AC mitigation, apparently decreases as AC interference increases. Recent research⁶⁵ suggested the consumption rate of Mg anodes increased about 10 times at AC density above 7 A/m².

AC CORROSION MONITORING

Considering that it is relatively simple to measure AC voltage on a buried pipeline, AC potential measurements (such as AC close interval survey [CIS]) have been the primary parameter for characterizing the AC level on pipelines. However, measuring AC voltage is primarily a measure of IR drop in the ground and has all of the problems of dealing with IR drop in pipe-to-soil potential measurements. That is, the IR drop (and therefore AC voltage measurement) is dependent on several factors including soil resistance, spread resistance, holiday size, holiday distribution, overall coating condition, etc. Although AC voltage is an appropriate measure for safety concerns (step-and-touch voltages), AC voltage is not a good parameter to assess the likelihood of AC corrosion. On the other hand, once relationships have been established between AC density and AC voltage measurements at local sites, AC voltage surveys are sometimes used to apply those relationships along that right-of-way. Whereas estimates of the AC density are sometimes made using the AC voltage (assuming that information is available with regard to the coating defect size and soil resistivity), some argue that caution should be exercised while making calculations—in very low-resistivity soils, potentials as low as 1 V AC would yield AC density “sufficiently high” to be considered hazardous, which seemingly runs contrary to field experience.

The measure that is typically used is the polarized potential (off-potential). Unfortunately, prior studies have specifically addressed the problems of making “fast” (in this case somewhere around 300 measurements per second to characterize a 60-Hz signal) off-potential measurements, especially on pipelines. Inductive effects (spiking) requires 100 to 500 ms to make a measurement of most pipelines compared to the 17 ms of a single 60-Hz cycle. Further, potential measurement alone does not “fix” the conditions at the steel/soil interface; as discussed earlier, knowledge of pH is a component of determining whether the potentials fall in the immunity region on the Pourbaix diagram.

As such, for AC monitoring, AC density appears to be a reliable measurable parameter related to AC corrosion. Because the current density and not just current flow in the ground is typically measured, the use of CTS has been suggested by many.

The CTS-based approach is capable of determining the AC discharge on the fixed area coupon(s), and thus provides a means to estimate the AC density and, with the proper criterion, the probability of AC corrosion at a defect of similar size to the coupon area. Furthermore, the CTS coupons also register the changes in the currents and potentials (both AC and DC) due to the operation (or lack) of AC mitigation measures such as individual Mg anodes or Zn ribbon anodes.

One question associated with the use of the CTS coupons for the purposes of assessing the probability of AC corrosion is the choice of coupon sizes. Gummow et al²² presents a brief discussion on this subject, noting that the published literature strongly suggests that the preferred size for the coupon is 100 mm², as several field studies had found that this is the size of the holiday for which the most AC corrosion took place. The cited publications also have indicated that the holidays smaller than 3 mm² did not suffer from AC corrosion.

Funk and Schoeneich⁷ also commented on the use of buried coupons for AC corrosion; the authors concluded that, due to the temporal dependence of the corrosion rate, the coupons should be buried for at least one year. It should be noted that the primary purpose for the coupons in this study was determination of the corrosion rate via weight loss measurements, as opposed to the use of the CTS coupons for monitoring.

Another presented conclusion (and the current practice of Ruhrgas AG, Germany) is that multiple coupons (at least three) should be installed in each location known or suspected to have AC corrosion problems such that the probability of encountering the worst case is increased.

As an alternative to coupons, electrical resistance probes are sometimes used; these are still subject to the sensor size considerations. A number of publications reported on field and laboratory studies based on this approach. The end users typically consider the costs and benefits of each of the technologies.

One important aspect of monitoring (whether CTS or resistance probe-based) is the duration of data logging. The following two charts in Figure 112 and 20 are taken from a CORROSION/2007 paper,⁶⁹ the paper discusses field data collected from CTS located near the pipelines sharing the right-of-way with HVAC transmission lines.

As seen in both charts, there are significant variations in the induced AC density on collocated pipelines due to HVAC line loading changes. Figure 112 is a plot of AC density (calculated using the area of a CTS coupon) over a 20-day period taken at 1-hour intervals (average) during July and August 2006. Figure 113 is a plot of the measured coupon AC density over a 3-day period taken at 1-minute intervals (average current during the recorded minute) at the same coupon.

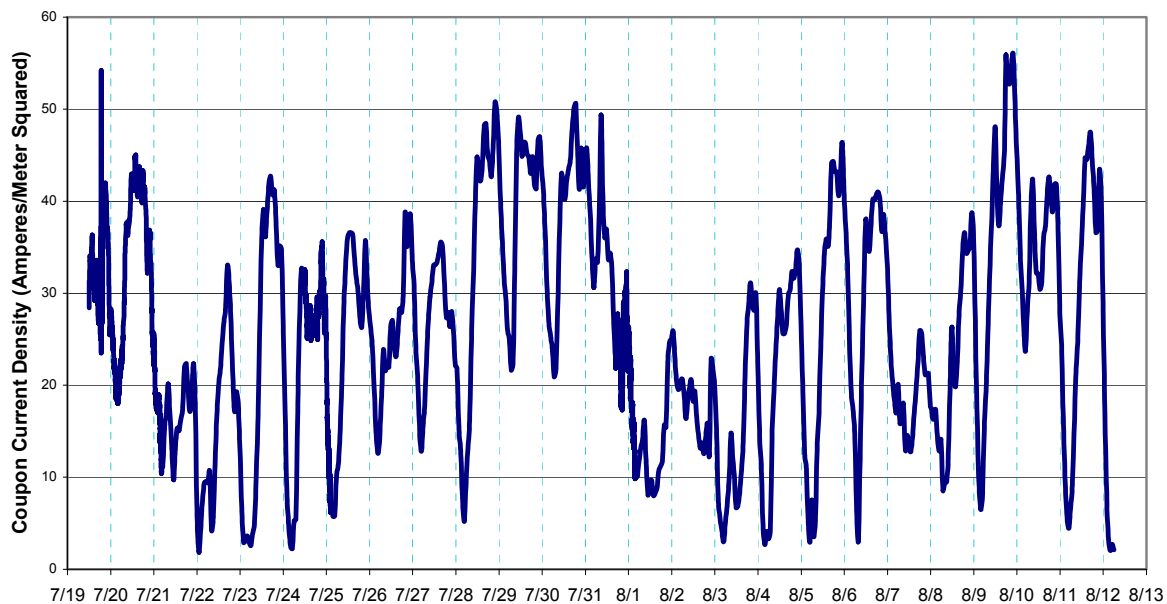


Figure 112. AC density at a coupon over 20 days July/August 2006.

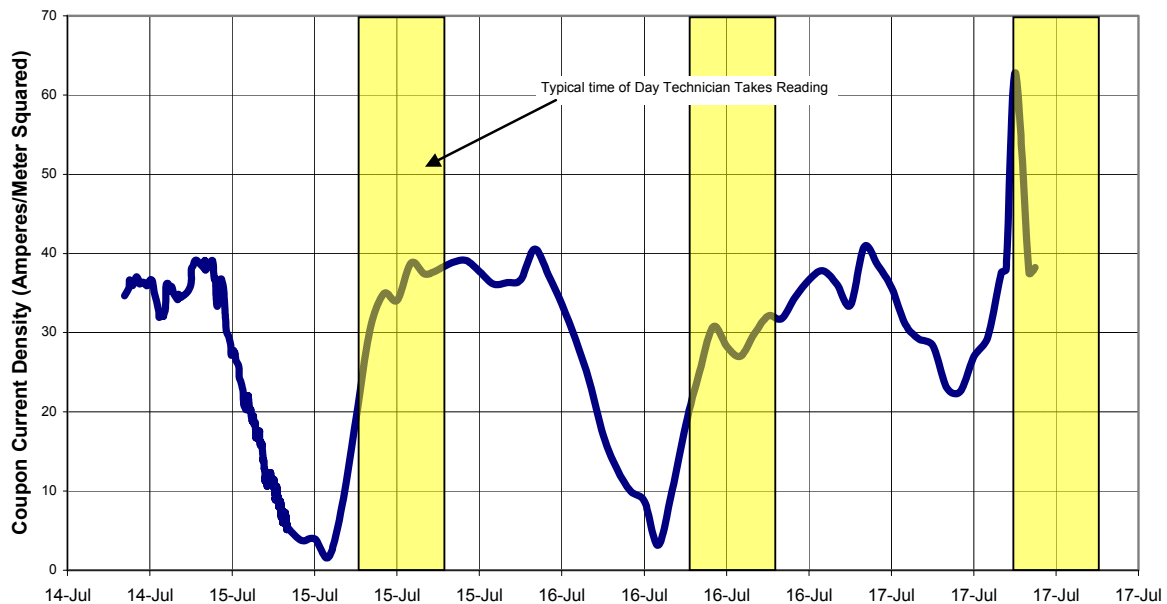


Figure 113. AC density at a coupon over 3-day period in July 2006.

The author comments that the highest induced AC potentials are typically found during the daytime when the readings taken by corrosion technicians (as opposed to the data gathered over a longer period of time by acquisition devices) are typically collected. The primary conclusion is that the duration of monitoring could play a major role in deciding the likelihood of AC corrosion attack.

SUMMARY

The body of literature indicates that AC corrosion or AC-enhanced corrosion has become accepted as a bona fide phenomenon, which constitutes a shift from the earlier paradigm. Probabilistically, higher AC densities are likely to result in accelerated corrosion of steel. There is an inverse relationship between the impact of AC and its frequency; however, there appears to be a consensus that at prevailing commercial current frequencies (such as 50 or 60 Hz) corrosion is possible, even on cathodically protected pipelines.

General corrosion rates due to AC corrosion are not necessarily “abnormally” high (much higher naturally occurring rates of an existing pipeline have been reported), but the rates are certainly multiples of the “prevailing” corrosion rates of steel in soil in the absence of AC.

Although there have been investigators who have attempted to explain mechanisms of AC corrosion, there is a lack of technical consensus on the mechanism and the extent of the effect of AC on underground metallic structures. The published data possess a great deal of scatter; in many cases testing environments were not necessarily representative of conditions existing on buried pipelines, or the results are only applicable to a specific situation.

Inasmuch as there is still debate as to how AC affects corrosion rate and when there is a high likelihood of AC corrosion (conflicting accounts on whether there is a “safe” threshold value of AC density below which AC corrosion is not likely to be a concern), there are no agreed-on criteria for AC corrosion protection. As discussed, the European standard advocates judicious use of CP current in order to avoid alkalization, which, according to the theory, reduces the resistance at the steel interface and promotes corrosion. Other publications propose the use of very negative (-1,100 mV [CSE]) polarization potentials to protect from AC corrosion; both practical and technical issues make this approach less attractive.

There is also an opinion that AC corrosion control may only be feasible when AC corrosion current density is brought below a certain value.

Discussion of AC mitigation indicates that while the use of 15 V (currently used as the personnel safety threshold value in the U.S.) as the criterion for low AC corrosion likelihood may lead to underestimating AC corrosion threats in some instances, it is still used as a target, as the reduction of AC voltage leads to the attendant reduction of AC discharging from the pipeline. However, while AC voltage is an appropriate measure for safety concerns (step-and-touch voltages), it is not a reliable metric to assess the likelihood of AC corrosion.

Therefore, the choice of AC monitoring approach typically involves methodologies that permit the measurement of current density. The most forward application of such an approach is the use of CTS; alternatively, temporarily installed electrical resistance probes are often used for periodic monitoring of conditions. Duration of monitoring sometimes plays a role in determination of the AC corrosion threat; longer duration times are typically employed to capture periods of both high and low AC interference.

PATH FORWARD

The primary conclusion stemming from the state-of-the-art literature review is that there are sizeable knowledge gaps in both the fundamental understanding of AC corrosion phenomenon and the practical aspects regarding the approach to AC corrosion monitoring, mitigation, and control.

In particular, more experimental and field-based work might establish the protection criteria for AC corrosion by determining whether *all* expected AC interference conditions can be controlled by CP or whether some threshold level of AC would control the impact. The published accounts with regard to appropriate CP levels in the presence of AC interference are seemingly contradictory. There are no known published accounts with regard to the polarization shift criterion.

Certain commonly used means of AC mitigation are likely topics for further investigation. Recent research suggests that the current efficiency of galvanic anodes employed to reduce AC interference levels may be substantially lower in service due to increased corrosion rates.

The expanded body of evidence addressing the above gaps would enable undertaking the next logical step—development of a standard for AC corrosion monitoring, mitigation, and control. The European corrosion community has already taken this step by adopting a standard approved in 2006 (CEN/TS 15280:2006).³² CEOCOR, a Belgium-based association of corrosion professionals and experts comprising 14 member countries, publishes a booklet with guidelines for AC corrosion risk assessment. Both publications were cited in this report; the criteria and recommendations in these documents are based on the existing understanding of AC corrosion and thus have the same knowledge gaps.

REFERENCES

1. G. Mengarini, *Electrical World* 16, 6 (1891): p. 96.
2. B. McCollum, G. Ahlborn, "Influence of frequency of alternating or infrequently reversed current on electrolytic corrosion," *Technologic papers of the Bureau of Standards*, No. 72, August 15, 1916.
3. L. Diabiase, "Corrosion due to alternating current on metallic buried pipelines: background and perspectives," *Committee on the Study of Pipe Corrosion and Protection, CEOCOR, 5th International Congress, Bruxelles, Belgium, 2000*.
4. Summary, *ibid*.
5. I. Ragault, "AC Corrosion Induced by V.H.V Electrical Lines on Polyethylene Coated Steel Gas Pipelines," *CORROSION/98*, paper no. 98557 (Houston, TX: NACE, 1998).
6. R. Wakelin, R. Gummow, S. Segall, "AC Corrosion—Case Histories, Test Procedures, and Mitigation," *CORROSION/98*, paper no. 98565 (Houston, TX: NACE, 1998).
7. D. Funk, H.G. Schoeneich, "Problems with Coupons when Assessing the AC-Corrosion Risk of Pipelines," *3R International, Special Steel Pipelines* 41, (2002): p. 54.
8. W. Bruckner, "The Effects of 60 Cycle Alternating Current on the Corrosion of Steels and Other Metals Buried in Soils," *University of Illinois, Technical Bulletin No. 470*, November 1964.
9. H. Song, Y. Kim, S. Lee, Y. Kho, Y. Park, "Competition of AC and DC Current in AC Corrosion Under Cathodic Protection," *CORROSION/2002*, paper no. 02117 (Houston, TX: NACE, 2002).
10. L.V. Nielsen, F. Galsgaard, "Sensor Technology for On-Line Monitoring of AC Induced Corrosion Along Pipelines," *CORROSION/2005*, paper no. 05375 (Houston, TX: NACE, 2005).
11. R. Gregoor, A. Pourbaix, "Detection of AC Corrosion," *3R International* 42, 6 (2003): pp. 289-395.
12. H.G. Shoeneich, "Research Addresses High Voltage Interference, AC Corrosion Risk for Cathodically Protected Pipelines," *Oil and Gas Journal* 2 (2004): pp. 56-63.
13. M. Yunovich, N.G. Thompson, "AC Corrosion: Corrosion Rate and Mitigation Requirements," *CORROSION/2004*, paper no. 04206 (Houston, TX: NACE, 2004).
14. C. Goran, "Alternating current corrosion on cathodically protected steel in soil—A long term field investigation," *5th International Congress, Bruxelles, Belgium, 2000*.

15. L.V. Nielsen, P. Cohn, "AC corrosion and electrical equivalent diagrams," CEOCOR, Committee on the Study of Pipe Corrosion and Protection, 5th International Congress, Bruxelles, Belgium, 2000.
16. J. Williams, "Corrosion of Metals Under the Influence of Alternating Current," *Materials Protection* 5, 2 (1966): p. 52.
17. P. Linhardt, G. Ball, "AC Corrosion: Results from Laboratory Investigations and from a Failure Analysis," CORROSION/2006, paper no. 06160 (Houston, TX: NACE, 2006).
18. CC Technologies, internal data archives, 2003.
19. F. Bolzoni, S. Goidanich, L. Lazzari, M. Ormellese, M.P. Pedferri, "Laboratory Testing on the Influence of Alternated Current on Steel Corrosion," CORROSION/2004, paper no. 04208 (Houston, TX: NACE, 2004).
20. S. Pookote, D.T. Chin, "Effect of Alternating Current on the Underground Corrosion of Steels," *Materials Performance* 17, 3 (1978): p. 9.
21. D. Funk, H.G. Schoeneich, "Problems with Coupons when Assessing the AC-Corrosion Risk of Pipelines," 3R International, *Special Steel Pipelines* 41 (2002): p. 54.
22. R. Gummow, R. Wakelin, S. Segall, "AC Corrosion—A New Challenge to Pipeline Integrity," CORROSION/98, paper no. 98566 (Houston, TX: NACE, 1998).
23. S. Goidanich, L. Lazzari, M. Ormellese, M.P. Pedferri, "Influence of AC on carbon steel corrosion in simulated soil conditions," 16th ICC, paper 04-03, held September 19-24, Beijing, China, 2005.
24. G. Helm, T. Helm, H. Heinzen, W. Schwenk, "Investigation of Corrosion of Cathodically Protected Steel Subjected to Alternating Currents," 3R International 32 (1993): p. 246.
25. W. Prinz et al, "Alternating Current Corrosion of Cathodically Protected Pipelines," 1992 International Gas Research conference, Orlando, Florida., held November 16-19, 1992.
26. D.T. Chin, T.W. Fu, "Corrosion by Alternating Current: A Study of the Anodic Polarization of Mild Steel in Na₂SO₄ Solution," *Corrosion* 35, 11 (1979): p. 514.
27. F. Stalder, "AC corrosion of cathodically protected pipelines. Guidelines for risk assessment and mitigation measures, Annex N.5-4," CEOCOR, 5th International Congress, Bruxelles, Belgium, 2000.
28. A. Pourbaix, P. Carpentiers, R. Gregoor, "Detection and Assessment of Alternating Current Corrosion," *Materials Performance* 38, 3 (2000): pp. 34-39.
29. D. Jones, "Effect of Alternating Current on Corrosion of Low Alloy and Carbon Steels," *Corrosion* 24, 12 (1978): p. 428.
30. DIN 50925 *Korrosion der Metalle; Nachweis der Wirksamkeit des kathodischen Korrosionsschutzes erdverlegter Anlagen*, 1992.
31. W. von Baeckmann, W. Schwenk (eds.), *Handbuch des Kathodischen Korrosionsschutzes*, Wiley-VCH, Weinheim, 1999.
32. CEN/TS 15280:2006, *Evaluation of A.C. Corrosion Likelihood of Buried Pipelines—Application to Cathodically Protected Pipelines*.
33. S. Goidanich, "Influence of alternating current on metals (sic) corrosion," PhD thesis, Politecnico di Milano, 2005.

34. R.D. Floyd, "Testing and Mitigation of AC Corrosion on 8" Line: A Field Study," CORROSION/2004, paper no. 04210 (Houston, TX: NACE, 2004).
35. NACE Standard RP0177 (latest revision), "Mitigation of Alternating Current and Lightning Effects on Metallic Structures and Corrosion Control Systems" (Houston, TX: NACE).
36. Technical Recommendation No. 7, "Measures for the installation and operation of pipelines in the vicinity of three-phase high-voltage systems and single-line traction systems," Verlags - und Wirtschaftsgesellschaft der Elektrizitätswerke mbH, WVEW, Frankfurt Main, 1985.
37. S.Z. Fernandes, S.G. Mehendale, S. Venkatachalam, "Influence of Frequency of Alternating Current on the Electrochemical Dissolution of Mild Steel and Nickel," Journal of Applied Electrochemistry 10, (1980): pp. 649-654.
38. M.L. Mateo, T. Fernandez Otero, D.J. Schiffrin, "Mechanism of Enhancement of the Corrosion of Steel by Alternating Currents and Electrocatalytic Properties of Cycled Steel Surfaces," Journal of Applied Electrochemistry 20, (1990): pp. 26-31.
39. W. Qiu, M. Pagano, G. Zhang, S.B. Lalvani, "A Periodic Voltage Modulation Effect on the Corrosion of Cu-Ni Alloy," Corrosion Science 37, 1 (1995): pp. 97-110.
40. D-T. Chin, S. Venkatesh, "A Study of Alternating Voltage Modulation on the Polarization of Mild Steel," Journal of Electrochemical Society 126, (1979): pp. 1908-1913.
41. K.V. Quang, F. Brindel, G. Laslaz, R. Buttoudin, "Pitting Mechanism of Aluminium in Hydrochloric Acid Under Alternating Current," Journal of Electrochemical Society 130, 6 (1983): pp. 12481-252.
42. R.L. Ruedisueli, H.E. Hager, C.J. Sandwith, "An Application of a State-of-the-Art Corrosion Measurement System to a Study of the Effects of Alternating Current on Corrosion," Corrosion 43, 6 (1987): pp. 331-338.
43. M. Yunovich, N.G. Thompson, "AC corrosion: mechanism and proposed model," paper no. IPC04-0574, Proceedings of IPC 2004 International Pipeline Conference, held October 4-8, 2004, Calgary, Alberta, Canada.
44. A.W. Hamlin, "Alternating Current Corrosion," Materials Performance 25, 1 (1986): p. 55.
45. R. Radeka, D. Zorovic, D. Barisin, "Influence of frequency of alternating current on corrosion of steel in seawater," Anti-Corrosion Methods 27, 4 (1980): p. 13.
46. K. Juetner, M. Reitz, S. Schaefer, H. Schoeneich, "Rotating ring-disk studies on the impact of superimposed large signal AC currents on the cathodic protection of steel," Electrochemical Methods in Corrosion Research VI, Materials Science Forum, Vol. 289-292, 1998, p. 107.
47. F. Stalder, "Influence of soil composition on the spread resistance and of ac corrosion on cathodically protected coupons," CEOCOR, Committee on the Study of Pipe Corrosion and Protection, 5th International Congress, Bruxelles, Belgium, 2000.
48. L.V. Nielsen, K.V. Nielsen, B. Baumgarten, H. Breuning-Madsen, P. Cohn, H. Rosenberg, "Induced Corrosion in Pipelines: Detection, Characterization and Mitigation," CORROSION/2004, paper no. 04211 (Houston, TX: NACE, 2004).
49. L.V. Nielsen, "Role of Alkalization in AC Induced Corrosion of Pipelines and Consequences Hereof in Relation to CP Requirements," CORROSION/2005, paper no. 05188 (Houston, TX: NACE, 2005).

50. L.V. Nielsen, P. Cohn, "AC corrosion in pipelines. Field experiences from a highly corrosive test site using ER corrosivity probes," CEOCOR 2003.
51. L.V. Nielsen, B. Baumgarten, P. Cohn, "On-Site measurements of AC induced corrosion: effects of AC and DC parameters," CEOCOR, 7th International Congress, 2004.
52. L.V. Nielsen, B. Baumgarten, P. Cohn, "Investigating AC and DC stray current corrosion," CEOCOR, 7th International Congress, 2005.
53. L.V. Nielsen, B. Baumgarten, P. Cohn, "A field study of line currents and corrosion rate measurements in a pipeline critically interfered with AC and DC stray currents," CEOCOR 2006.
54. J.O'M. Bokris, A.K.N. Reddy, Modern electrochemistry – An Introduction to an Interdisciplinary Area, Vol. 2 (New York, NY: Plenum Press, 1970).
55. S.B. Lalvani, X.A. Lin, "A Theoretical Approach for Predicting AC-Induced Corrosion," Corrosion Science 36, 6 (1994): pp. 1039-1046.
56. U. Bertocci, "AC Induced Corrosion. The Effect of an Alternating Voltage on Electrodes Under Charge-Transfer Control," Corrosion 35, 5 (1979): pp. 211-215.
57. R.W. Bosh, W.F. Bogaerts, "A Theoretical Study of AC-Induced Corrosion Considering Diffusion Phenomena," Corrosion Science 40, 2/3 (1998): pp. 323-336.
58. S.B. Lalvani, X. Lin, "A Revised Model for Predicting Corrosion of Materials Induced by Alternating Voltages," Corrosion Science 38, 10 (1996): pp. 1709-1719.
59. D.T. Chin, P.Sachdev, "Corrosion by Alternating Current: Polarization of Mild Steel in Neutral Electrolytes," Journal of Electrochemical Society 130, (1983): pp. 1714-1718.
60. T.C. Tan, D.T. Chin, "Effect of Alternating Voltage on the Pitting of Aluminium in Nitrate, Sulfate and Chloride Solutions," Corrosion 45, 12 (1989): pp. 984-989.
61. L. Lazzari, S. Goidanich, M. Ormellese, M.P. Pedferri, "Influence of AC on Corrosion Kinetics for Carbon Steel, Zinc and Copper," CORROSION/2005, paper no. 05189 (Houston, TX: NACE, 2005).
62. M.J. Frazier, "Induced AC Influence on Pipeline Corrosion and Coating Disbondment," GRI, Project No. A381, December 1994.
63. Y. Hosokawa, F. Kajiyama, Y. Nakamura, "New CP Criteria for Elimination the Risks of AC Corrosion and Overprotection on Cathodically Protected Pipelines," CORROSION/2002, paper no. 02111 (Houston, TX: NACE, 2002).
64. Cathodic protection of buried or immersed metallic structures - General principles and application for pipelines; English version of DIN EN 12954 (Kathodischer Korrosionsschutz von metallischen Anlagen in Boeden und Waessern - Grundlagen und Anwendung fuer Rohrleitungen; Deutsche Fassung EN 12954:2001, Deutsches Institut Fur Normung E.V.; Publication Date:Apr 1, 2001).
65. S. Goidanich, L. Lazzari, M. Ormellese, M.-P. Pedferri, "Effect of AC on cathodic protection of carbon steel in simulated soil conditions," EUROCORR 2006, Maastricht, Netherlands, held September 25-28, 2006.
66. L.I. Freiman, M. Yunovich, "Special Behavior of Steel Cathode in Soil and Protection Assessment of Underground Pipe with a Buried Coupon," Protection of Metals 27, 3 (1991): pp. 437-447.

67. D.E. Gilroy, "AC interference—Important Issues for Cross Country Pipelines," CORROSION/2003, paper no. 03699 (Houston, TX: NACE 2003).

68. ANSI/IEEE Std 80 (latest revision), "IEEE Guide for Safety in AC Substation Grounding" (New York, NY: IEEE).

69. P.D. Simon, "Dynamic Nature of HVAC Induced Current Density on Collocated Pipelines," CORROSION/2007, paper no. 07650 (Houston, TX: NACE, 2007).

APPENDIX A

CASE STUDIES

CASE STUDY 1 (ADAPTED FROM REFERENCE 34)

Background

On August 29, 2002, a pipeline operator experienced an in-service leak on a section of a liquid butane pipeline in Rockwall County, Texas. The pipeline is an 8-in. (203-mm) diameter by 0.19-in. (4.8-mm) nominal wall thickness API⁽²⁾ 5L X52 pipe and was installed in 1999. The external coating on the line is a mill-applied fusion-bonded epoxy at a nominal 16-mil (0.41-mm) thickness. The girth welds are coated with heat-shrink sleeves. CP is supplied by impressed current deep anode systems.

The leak resulted from an external corrosion pit containing a through-wall pinhole penetration (see Figure A1). The outside dimensions of the corrosion pit were approximately 1 x 2 in. (25 x 51 mm).



Figure A1. Location of external through-wall corrosion pit.

The company performed an in-line inspection (ILI) using a magnetic flux leakage tool to detect and characterize corrosion-caused metal loss on this section. Based on the results of the inspection, several locations were identified for excavation and direct examination. A service company was retained by the pipeline operator to collect information during the excavations, to evaluate the effectiveness of the CP system, and to provide information as to the cause of the defects.

The testing performed at each excavation site consisted of:

- Visual observation of the pipe line right-of-way
- Pipe-to-soil potential measurements

⁽²⁾ American Petroleum Institute (API), 1220 L St. NW, Washington, DC 20005.

- Soil resistivity measurements
- Linear polarization resistance
- Microbiologically influenced corrosion (MIC) investigation
- Supporting analysis
 1. Qualitative testing for chemical species
 2. Electrolyte pH
 3. Pipe conditions
 4. Coating conditions

Anomaly Investigation Results

Several areas were excavated and the anomalies in the pipe evaluated using the above detailed examination. These sites consisted of flat terrain. Initial observations revealed a soil profile consisting of three distinct layers.

The top layer, the organic layer, was very thin (about 6 in. [152 mm]). The second layer (going down in depth) consisted of a 10-ft (3-m) layer of black moist clay material. The third layer, which encased the pipeline 2 ft (6 m) above and below, consisted of a brown moist clay soil with little to no gravel in the soil matrix. The soil samples were tested for soluble cations, soluble anions, moisture content, MIC, electrical resistivity, pH, and corrosion rate (using linear polarization resistance). The results are shown in Table A1. The soils can be classified as clay with high moisture content, rich in bacteria and falling into a highly corrosive category.

Initial observations of the area surrounding the anomaly revealed a black granular deposit approximately 2 in. (51 mm) in diameter located at the 12 o'clock orientation. This deposit was collected and used to determine the detection of problem-causing bacteria involved in microbiologically influenced corrosion. On-site qualitative testing for chemical species within the corrosion product produced the following results:

- | | |
|---|----------|
| • pH | >10 |
| • Carbonate (CO ₃ ⁻) | Positive |
| • Sulfide (S ²⁻) | Negative |
| • Ferrous Iron (Fe ²⁺) | Positive |
| • Ferric Iron (Fe ³⁺) | Positive |
| • Calcium (Ca ²⁺) | Negative |

The presence of an elevated pH and a positive reaction to carbonate indicate the presence of CP. The positive tests for ferrous and ferric ions, however, and the corrosion anomaly itself indicate that either the CP film formed after the corrosion had occurred or another corrosion mechanism was contributing to the problem. No sulfides (often observed in corrosion products resulting from MIC) were found.

Inspection of the defects revealed an isolated smooth, round corrosion morphology that was uncharacteristic of either MIC or conventional direct stray current corrosion. A corrosion rate of 60 mpy (1.5 mm/y) in the presence of CP cannot be easily explained, absent some accelerating factor such as MIC or stray current interference. Testing of the corrosion products showed no evidence of any bacteria related by-products, and the corrosion morphology was not typical of these bacteria related corrosion mechanisms.

In DC stray current interference, the corrosion products are soluble due to the low pH at the discharge location, and the pitting is generally found to be free of corrosion products. In the observations made during this study, the corrosion products were present in the pits, and the pH was found to be indicative of effective CP. These discrepancies led to the possibility of a nontraditional corrosion mechanism such as AC corrosion.

Nothing in the review of the CP history suggests a plausible explanation for the rapid rate of corrosion experienced on this pipeline. In addition, the records indicate that the CP rectifiers have been maintained in continuous operation and that, when necessary, repairs to rectifier components have been carried out in a timely manner to minimize rectifier outages.

Various attempts were made at correlating anomaly location, CIS data, and the physical location of the power lines, especially in the areas where HVAC lines and pipelines shared the right-of-way. A plot was developed and overlays measured pipe-to-soil AC potentials with the number of ILI corrosion anomalies per linear foot of pipe in a given segment. Twenty-seven external coupon stations were installed on the pipeline, at 1-mile (1.6-km) intervals, to measure the DC potentials, AC potentials, and current densities. The plot of the AC potentials and defect distribution (in number of anomalies per linear foot of pipe) are shown in Figure A2.

These data indicate that the highest population of ILI corrosion anomalies is located in the first 5 miles (8 km) where the AC potentials typically exceeded 4.0 V.

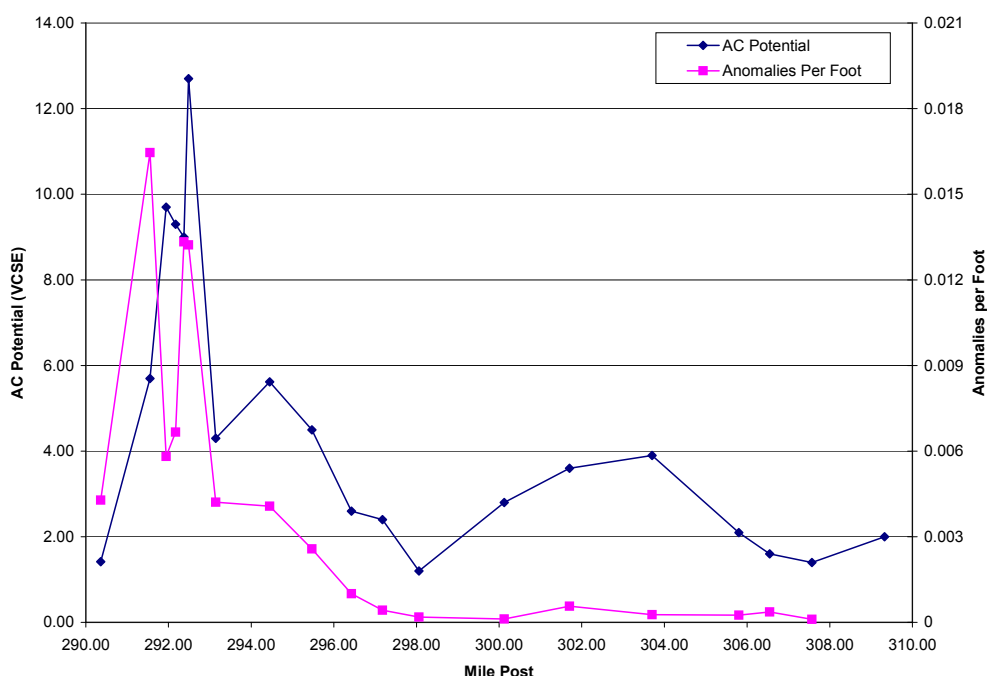


Figure A2. AC potentials and “defect density” (anomalies per linear foot of pipe).
1 ft = 0.3048 meter

Coupon test stations (CTS) provide an alternative to conventional off-potential measurement for evaluating the effectiveness of a CP system.

Following the installation of the CTS, initial measurements and CIS data were collected at each station. The pertinent data collected at the four stations in the most affected area are listed in Table A1 and discussed in further detail.

Table A1. Summary of pertinent CTS data.

Location	AC Density (A/m ²)	Possible Corrosive Effect

Nevada Booster	23.7	AC corrosion unpredictable
Rustic Meadows	239.1	AC corrosion likely
Highway 66	144.1	AC corrosion likely
Parker Road	113.3	AC corrosion likely

Nevada Booster Station

The Nevada Booster Station CTS is located adjacent to the perimeter fence over the line heading south from the station. At this location, measurements on both the pipe and coupon indicated that from a CP standpoint, the piping is well protected with off-potentials of -1.291 V (CSE) and -1.265 V (CSE) on the pipe and coupon, respectively. The native (unpolarized coupon) at this site had a free corrosion potential of -0.858 V (CSE). The CIS collected upstream and downstream from the CTS showed adequate DC potentials and generally flat (neither increasing nor decreasing) AC potentials. The coupon was also collecting DC from the CP system at a current density of 3.00 A/m². The AC potential recorded at this site was 1.73 V, and the coupon was found to have an AC density of 23.68 A/m².

Rustic Meadows

This CTS is located one mile south of Nevada Booster. At this location, measurements on both the pipe and coupon indicated that from a CP standpoint, the piping is well protected with off-potentials of -1.242 V (CSE) and -1.173 V (CSE) on the pipe and coupon, respectively. The native (unpolarized coupon) at this site had a free corrosion potential of -0.868 V (CSE). The CIS data collected upstream and downstream from the CTS showed adequate DC potentials and increasing AC potentials as the survey proceeded south toward the Highway 66 test station. The coupon was also collecting DC from the CP system at a current density of 8.32 A/m². The AC potential recorded at this site was 9.7 V, and the coupon was found to have an AC density of 239.08 A/m².

Highway 66

The Highway 66 CTS was installed on the north end of the Highway 66 crossing, across the street from the electric power substation. At this location, measurements on both the pipe and coupon indicated that from a CP standpoint, the piping is well protected with off-potentials of -1.230 V (CSE) and -1.056 V (CSE) on the pipe and coupon, respectively. The native (unpolarized coupon) at this site had a free corrosion potential of -0.832 V (CSE). The CIS data collected upstream and downstream from the CTS showed adequate DC potentials and a generally flat (neither increasing nor decreasing) AC potential profile of nearly 8 to 10 V (zinc grounding cells on versus grounding cells off). The coupon was also collecting a high DC density from the CP system at 4.80 A/m². The A/C potential recorded at this site was 9.30 V, and the coupon AC density was found to be 144.13 A/m².

Parker Road

The Parker Road CTS was installed on the north side of the Parker Road crossing. At this location, measurements on both the pipe and the coupon indicated that from a CP standpoint, the location was well protected with off-potentials of -1.224 V (CSE) and -1.220 V (CSE) on the pipe and coupon, respectively. The native (unpolarized coupon) at this site had a free corrosion potential of -0.806 V (CSE). The CIS data collected upstream and downstream from the CTS showed adequate DC potentials and generally a flat AC voltage profile (neither increasing nor decreasing). The coupon was also collecting a high DC density from the CP system at 3.42 A/m². The AC potential recorded at this site was 5.50 V, and the coupon AC density was found to be 113.31 A/m².

Corrosion Morphology

Inspection of the corrosion pits on the failed piece of pipe and at the five anomaly investigations revealed an isolated smooth, round corrosion morphology that was uncharacteristic of either microbially influenced corrosion or conventional DC stray current corrosion. All five anomaly locations investigated were found to be the result of external corrosion pitting with a similar morphology to that of the leak site.

Corrosion products collected from four of the five locations were black, moist, and granulated (paste), and the underlying pipe substrate was shiny. The depth of the five anomalies ranged from 53 to 120 mil (1.3 to 3 mm), and all were located in FBE-coated pipe. The coating in the area surrounding the pits was brittle and had poor adhesion.

Mitigation Methods

The installation of zinc grounding cells at selected locations on the pipeline was chosen as the appropriate method to mitigate the alternating currents on the pipe. The line had two existing zinc grounding cells, Nevada Booster and the railroad near the substation. Table A2 summarizes the AC potential and AC density relief provided, while the cells are bonded to the structure. The reduction in AC potential was observed to be greatest at Highway 66, which is within approximately 600 ft (180 m) of the railroad zinc cell installation. At the Highway 66 location, the coupon AC density was similarly reduced by over 22%, while the zinc cells were connected. It should be noted that few effects are recognized for the zinc cells installed at Nevada Booster. This is due to the fact that the cells at the booster station are installed across an insulating flange for the purpose of eliminating the chance of an AC arc across the insulator.

Table A2. Summary of effects of zinc grounding cells on AC potentials and current density

Location	Pipe AC Potential, V (CSE)		Coupon AC Density, A/m ²	
	Zinc On	Zinc Off	Zinc On	Zinc Off
Parker Road	5.6	6.4	113.3	130.3
Highway 66	9.3	11.3	144.1	176.1
Rustic Meadows	9.7	10.8	239.1	269.7
Nevada Booster	1.72	1.76	23.7	24.4

Conclusions

The following conclusions have been drawn based on review of the information:

1. The excessive AC densities observed on the CTS and the physical and chemical analysis indicate that the likely cause of the observed corrosion anomalies is AC corrosion. This conclusion is supported by the correlation of higher defect occurrences within areas of higher AC potentials.
2. The CP system is and has been operating at levels that should be able to protect the pipeline adequately in the absence of severe AC discharge(s).
3. The existing AC mitigation system (2 zinc grounding cells) reduces the AC potential to maintain safe step-and-touch potentials, but has not sufficiently reduced the AC discharges (at

the locations tested) to a level that would permit the CP system to overcome the detrimental effects. The installation of additional grounding cells mitigates the AC discharges to acceptable levels.

4. The recently installed CTS provide a means of measuring AC.

CASE STUDY 2 (ADAPTED FROM REFERENCE 17)

Background

During routine inspection of a natural gas transmission line (25 bar [2,500 kPa], 150-mm inner diameter, 4.5-mm wall thickness, 45 years in service), a leak was identified by discoloration of plants. The area was excavated (Figure A3), and the leaking section of the pipe (1.5 m long) was transferred to the laboratory for examination, together with samples from the surrounding soil. The backfill was original soil of silty clay texture. The leak was located in the 6 o'clock position and was covered by a large cap (approximately 200-mm diameter) of hard, agglomerated soil.



Figure A3—Excavation site.

The pipeline runs in parallel to a railway (16 $\frac{2}{3}$ -Hz system) for approximately 10 km, and the leak occurred at the end of this section. The pipe is coated with bitumen, and the CP is checked every three years by extensive measurements. The protection criterion was met at all times, and the last check did not indicate an existing defect. The influence of AC was known for some time, but was not considered to be critical. Measurements after the failure indicated peak AC voltages of 20 to 30 V_{rms} in the affected region (Figure A4).

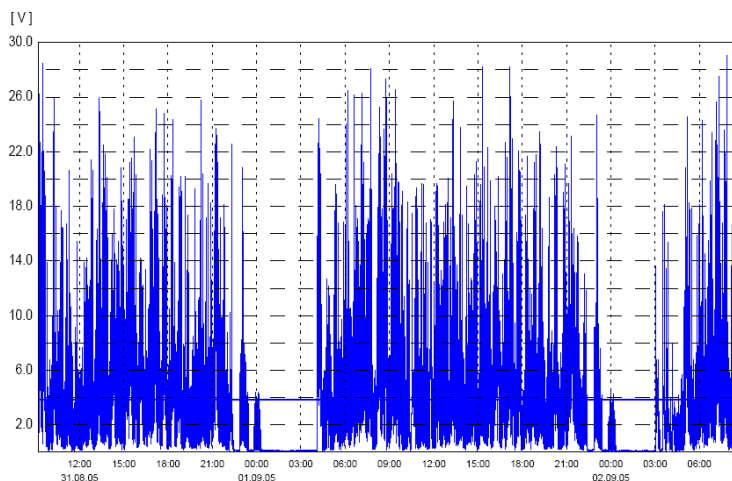


Figure A4—Record of AC voltage over 2 days.

Visual Examination

Figure A5 shows the hard cap of soil adhering to the pipe and covering the leak. Polyester resin was used to impregnate the surface of the cap to stabilize its structure.



Figure A5—The pipe with a cap of solidified soil covering the leak.

After hardening of the resin, the bituminous coating around the cap was peeled off, and the whole cap was carefully removed from the pipe; see Figure A6.



Figure A6—Cap removed. The leak is located in the center of the black spot.

It was found that the bituminous coating had delaminated in all areas of the pipe and had become brittle. However, in the area surrounding the leak, i.e., under the cap, it was rather soft and sticky, adhering well to the steel. The area above and around the leak was covered by bituminous material with regions of shiny appearance (Figure A7).

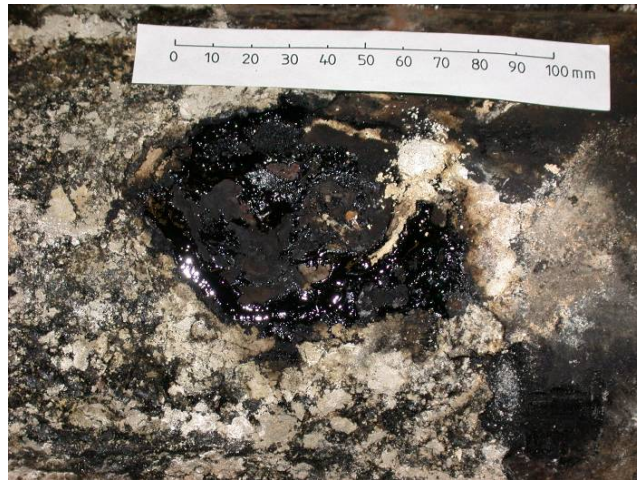


Figure A7—Shiny appearance of the bitumen above the leak.

After removal of this material and cleaning, localized attack with deep cavities in a generally passive surface and a pinhole-size penetration were found; see Figures A8 and A9.



Figure A8—Pipe surface after removal of the coating.



Figure A9—The corroded area after cleaning. The arrow indicates the leak.

The cap was cut perpendicular to the pipe's axis, in the plane of the leak position. Figure A10 presents a view of the cross section. Above the corroded area, the original layer of the coating is no longer visible. Instead, the bitumen has spread out and formed a bubble-like structure (black material, denoted A in Figure A10). Embedded we find regions of soil material (grey material, B) and a white substance (material C), well separated by thin layers of material A.

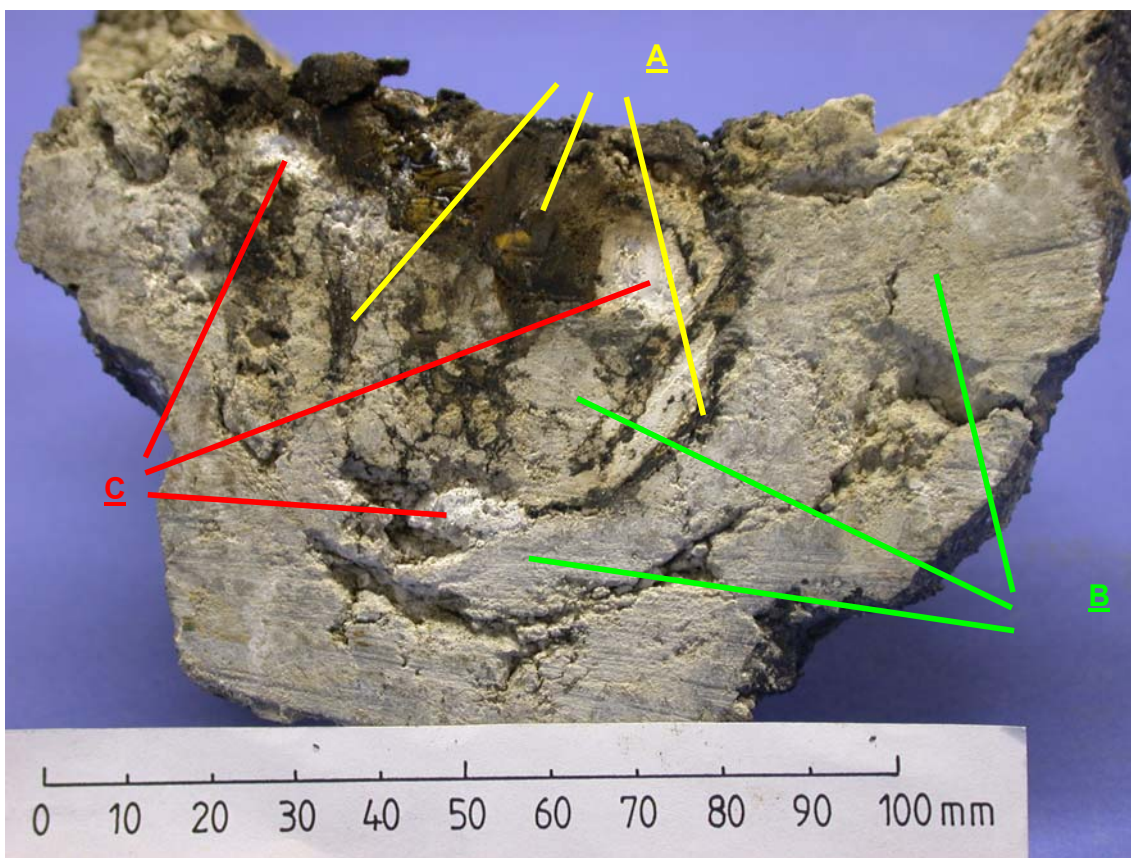


Figure A10—View of the cross section of the soil cap, in direction of the pipe’s axis. The letters indicate different types of material.

Chemical Analyses

Multiple samples of materials A, B, and C were characterized by wet chemical analysis and by energy dispersive X-ray analysis (EDX) in the scanning electron microscope (SEM), operated at 20 kV. The results are summarized as follows:

Material A

All black material was based on bitumen with varying amounts of iron oxide (mainly magnetite) and a sodium compound, presumably carbonate. The inorganic components are finely dispersed in the bituminous matrix.

The bituminous material was removed by extracting with an organic solvent, and the solid residual was separated into magnetic and non-magnetic portions. Figures A11a and A11b present the corresponding EDX spectra. The element sulfur is believed to originate from the bitumen as it was also identified in a sample of the bitumen of remelted appearance visible in Figure A7; see EDX analysis in Figure A12.

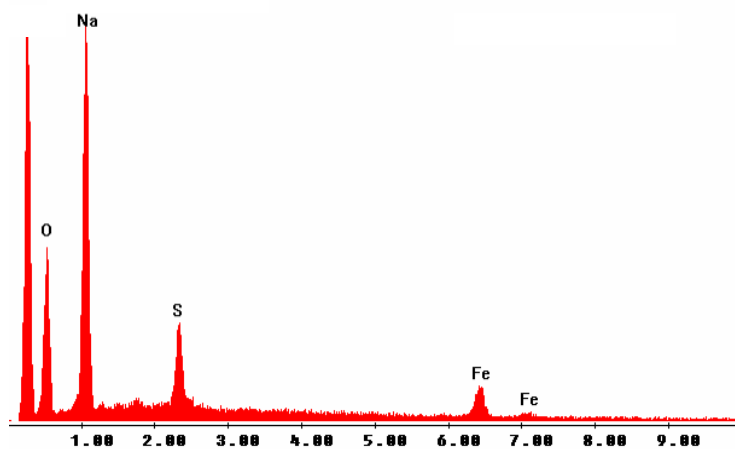


Figure A11a—EDX spectrum of the non magnetic fraction of material A.

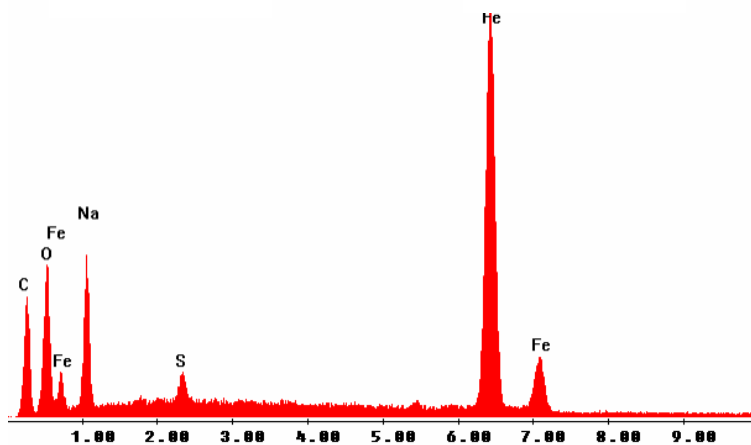


Figure A11b—EDX spectrum of the magnetic fraction of material A.

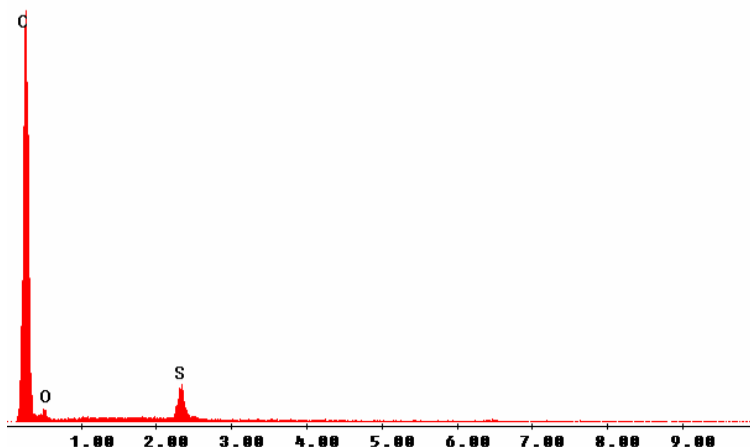


Figure A12—EDX spectrum of the shiny bitumen visible in Figure A7.

Material B

This grey material is based on the soil material, i.e., it is a silicate incorporating minor amounts of alkali (Na, K) and earth alkali (Ca, Mg) ions; see EDX analysis in Figure A13. Based on the analysis of an aqueous eluate of the soil (ratio 1 g solid/10 mL distilled water) sampled far from the corrosion site, the Na ions are soluble (110 mg Na/kg soil), and a pH of 8.2 was found. The content of soluble Na increases with decreasing distance from the corrosion site and was found as high as 12,500 mg/kg in material from inside the cap. The EDX spectrum in Figure A14 was obtained from material sampled inside the cap.

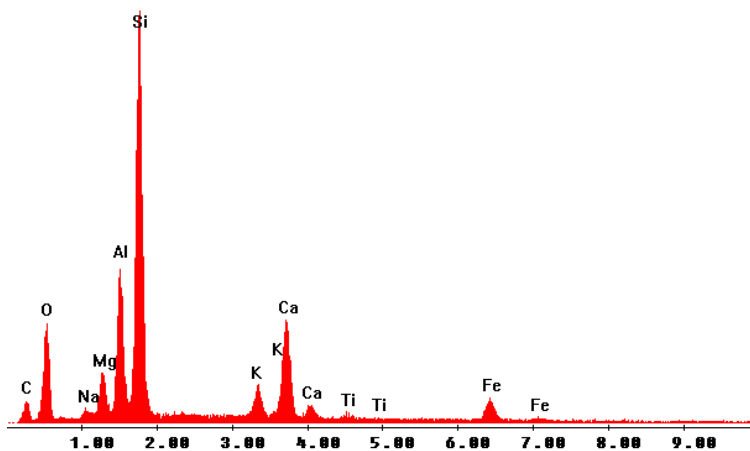


Figure A13—EDX spectrum of the soil far from the corrosion site.

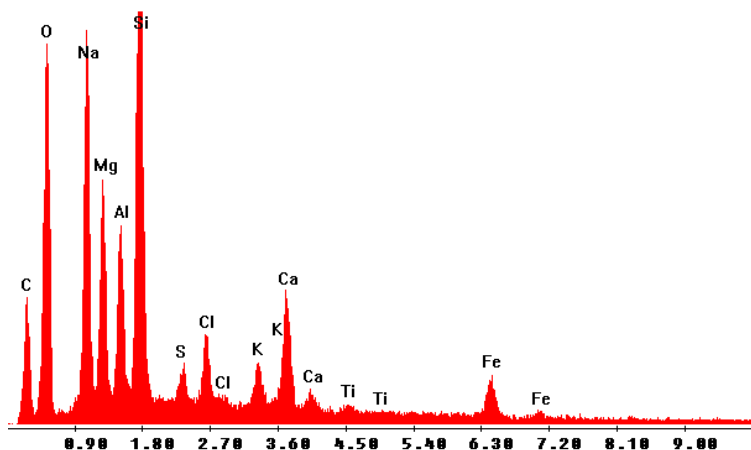


Figure A14—EDX spectrum of material B.

Material C

This white substance was identified as a mixture of NaHCO_3 and Na_2CO_3 in a molar ratio of 1:1, without any significant impurities, its EDX analysis is presented in Figure A15. A solution of 1 g in 10 mL water resulted in pH of 9.6.

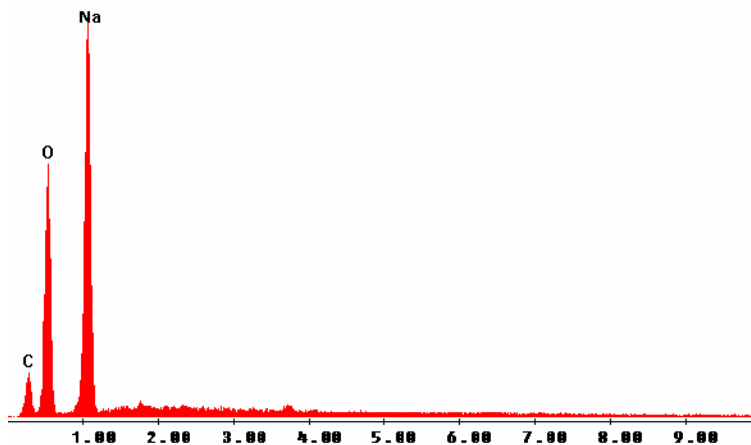


Figure A15—EDX Spectrum of material C.

Summary and Discussion

This case of pipeline corrosion is characterized by localized attack similar to pitting. Surprisingly, the bituminous coating was found to be deformed like a bubble. Its appearance gives the impression of being remelted. Such thermal influence could also explain the good adherence of the coating in the vicinity of the corrosion site, while it was found generally delaminated in all other areas, which should be considered normal, given its age. Magnetite was found to be the major corrosion product; however, it could not form a protective layer and was dispersed in the bituminous material. High cathodic activity is indicated by large volumes of pure sodium carbonate embedded in the bubble.

The findings from the failure analysis indicate that processes that can hardly be explained by normal corrosion and appear compatible with AC-influenced corrosion have taken place. These specific features are (1) strongly localized, pitting-like attack, (2) finely dispersed magnetite as the predominant corrosion product, (3) accumulation of large amounts of sodium carbonate, (4) indications of local temperature excursions to values softening bitumen, and (5) influence of mechanical forces mixing soil, bitumen, and sodium carbonate as could be achieved by slowly evolving gas bubbles.